Universitat Autònoma de Barcelona

Escola Tècnica Superior d'Enginyeria

Departament d'Enginyeria Química

OPERATION, MODELING AND AUTOMATIC CONTROL OF COMPLETE AND PARTIAL NITRIFICATION OF HIGHLY CONCENTRATED AMMONIUM WASTEWATER

PhD Thesis

Supervised by

Juan Antonio Baeza Labat and Julián Carrera Muyo

IRENE JUBANY GÜELL

Bellaterra – March 2007

JUAN ANTONIO BAEZA LABAT i JULIÁN CARRERA MUYO, professors agregats del Departament d'Enginyeria Química de la Universitat Autònoma de Barcelona,

CERTIFIQUEM:

Que l'enginyera química IRENE JUBANY i GÜELL ha realitzat sota la nostra direcció, el treball que amb títol "Operation, modeling and automatic control of complete and partial nitrification of highly concentrated ammonium wastewater", es presenta en aquesta memòria, i que constitueix la seva Tesi per a optar al Grau de Doctor per la Universitat Autònoma de Barcelona.

I perquè en prengueu coneixement i consti als efectes oportuns, presentem a l'Escola Tècnica Superior d'Enginyeria de la Universitat Autònoma de Barcelona l'esmentada Tesi, signant el present certificat a

Bellaterra, març 2007

Dr. Juan Antonio Baeza Labat

Dr. Julián Carrera Muyo

al Joan

ACKNOWLEDGEMENTS / AGRAÏMENTS

Aquesta tesi és el resultat de cinc anys al grup de “Depuradores” del Departament d’Enginyeria Química de la UAB. Aquestes ratlles són per agrair l’ajuda i suport que he rebut de totes les persones que han fet possible que avui pugui presentar aquesta memòria de tesi.

En primer lloc, vull agrair al Juan i al Julián, els meus directors, la gran ajuda i suport que sempre m’han donat. He après molt de vosaltres i amb vosaltres. Us complementeu molt bé i crec que hem fet un gran equip. No podia haver tingut uns directors millors. Us vull donar les gràcies especialment per a confiar en mi per a defensar els nostres treballs en congressos nacionals i internacionals. Ha estat una experiència molt enriquidora.

En segon lloc, vull donar les gràcies al Javier, la persona que està darrera del grup, fent que tot funcioni. És una llàstima que els càrrecs t’hagin impedit poder participar més del dia a dia d’aquest treball, ho he trobat a faltar. Gràcies per haver-me donat l’oportunitat de fer la tesi amb vosaltres i per a preocupar per mi en tot moment, fins hi tot quan vaig decidir no continuar en el món de la recerca. Espero que puguem continuar en contacte.

Un agraïment especial als companys de grup amb els quals vaig començar aquesta aventura: Maria, Albert G, Maite, Gladys i Lorena C; i als companys amb els quals l’he acabada: Mar, Albert B, Marcos, Josep, Maria Eugénia, Vinicius i Julio. Amb companys com vosaltres és fàcil treballar-hi. També un moltes gràcies a la Lorena F, l’Anna i la Noelia que m’han ajudat molt en les tasques diàries del laboratori. També als companys del grup de gasos: David, Juan Pedro, Guillermo, Marc, Jero, Rosa, Oscar, Xavi, Maria i Toni. I finalment al Carles C, el nostre biòleg de capçalera. Gràcies per ajudar-me amb el FISH, en els meus intents de comptar els “bitxos”.

També vull mencionar a tots els amics, companys de despatx, companys de “classe”... que he anat guanyant durant aquest cinc anys i amb els quals hem fet una bona pinya: Nuria CC, Sandra, Anna S, Jaume, Anna M, Paqui, Ramon, Tri, Anna U, David, Cristina, Núria CB, Oriol, Fernando, Kristin, Ernest MU, Lucía, Inés, Eduard, Núria M, Laura H, Engràcia, Marcel, Juan Miguel, Carol, Enric, Martí, Juli, Albert S, Tere, Estela, Vane, Luis Felipe, Bea, Belén i a tu també (si és que me n’he oblidat).

També vull agrair el suport a tots els titulars i catedràtics del departament, a les secretàries, especialment a la Nati i a la Montse, i als tècnics de laboratori: Manuel, Rosi i Pepi.

També a la Mercè i la Mònica del Servei de Microscòpia, per la seva paciència davant els meus problemes amb el confocal.

No puc deixar d’agrair als meus companys de viatges per les hores que hem passat junts al cotxe fent quilòmetres, fent caravana, escoltant la ràdio, explicant-nos els problemes i/o les

aventures, comentant les notícies, dormint, aprenent geologia, química analítica, cuina, música... Els viatges s'han fet curts amb vosaltres: Alba E, Enric, Alba S, Josep, Engràcia, Anna T, Cristina. Us trobaré molt a faltar.

On summer 2005 I had a nice time in Denmark. I would like thank Barth for the opportunity he gave me to work with him and his group. I learnt a lot from you and I felt very comfortable in your team. You also gave me the opportunity to come back to Denmark for a week the following year and to go to Leipzig for a conference. I'm very grateful for all this. It was a pleasure to work with Akihiko, Susanne, Arnaud, Sanin, Mona, Axel, Aurelie and Julien. It was not also working together; it was also traveling, having fun, living together… I also thank Manuel, Patricia, Anders, Larisa, Axel, Jose and Roza for their friendship, help and support. I will always have you in my heart.

També vull mencionar el suport econòmic en forma de beca predoctoral del Ministerio de Educación y Ciencia que m'ha permès estar aquí durant aquests anys.

Per acabar, vull agrair el suport dels meus pares i de la Júlia.

I finalment, el suport incondicional del Joan, que malgrat els caps de setmana amb excursió a la UAB, la mala lluna pels experiments i els mesos de tortura d'escriptura de la memòria, sempre m'ha fet costat i m'ha animat a seguir endavant i a aprofitar totes les oportunitats. Amb tu al meu costat tot ha estat més fàcil i agradable.

SUMMARY

Biological nitrogen removal of high-strength ammonium wastewater was studied in this thesis, particularly, the nitrification process (the oxidation of ammonium to nitrate). This two-step reaction, catalyzed by two kinds of bacteria (AOB and NOB), can suffer serious inhibition problems due to ammonia and nitrous acid when dealing with highly concentrated ammonium wastewater and therefore it requires adequate process control. However, these inhibitions can be used to achieve partial nitrification (the oxidation of ammonium to nitrite), which coupled to a denitrifying process leads to significant benefits in terms of use of resources.

A mathematical model describing the kinetics and the stoichiometry of the nitrification process was developed and calibrated. It considered the aforementioned inhibitions and took into account both kinds of nitrifying bacteria and also heterotrophic bacteria. Specific experiments were designed for parameter estimation and parameter identifiability tools were used to analyze and improve them. Optimal experimental designs were used to calibrate most of the model parameters and the obtained values were compared with values found in the literature. Affinity constants for substrate and substrate inhibition coefficients were estimated twice using different sludges and, as a result, different values were found indicating that they change depending on the biomass acclimation. This model was coupled to the hydraulic model of the experimental system (pilot plant) and was implemented in Matlab ®.

Fluorescence *in situ* hybridization (FISH) was used for bacterial fractions detection and quantification. Several equipments were used for fluorescence detection: an epifluorescence microscope, a confocal microscope and a flow cytometer. Previously, several procedures and steps were optimized: the area-based quantification method, the sonication step, the in-solution FISH protocol and the flow cytometric analysis. Biomass fractions were determined with each of the equipment and also with simulations. Obtained results were compared and the advantages and disadvantages of the tested methodologies were discussed considering the accuracy of the results, the speed of the analysis and the availability of the equipment. FISH combined with confocal microscopy turned out to be the best technique for nitrifying biomass quantification although flow cytometry could not be extensively investigated.

The start-up of a complete nitrification system was optimized by means of mathematical simulation using the previously developed and calibrated method. Two automatic control strategies were optimized and implemented in the experimental system by using sludge from a municipal wastewater treatment plant as inoculum. The controller was based on the measurement of the oxygen uptake rate (OUR) in the last reactor of the system and actuated over the nitrogen loading rate. Results were compared with a start-up performed with manual control and it was demonstrated that automatic control decreased the length of the start-up and increased its stability. Then, experimental results were simulated with the nitrification model. Model predictions agreed well with experimental data only after modifying two of the model

parameters. The final model was useful for both long- and short-term prediction. The sludge enrichment in nitrifying bacteria was checked with FISH and confocal microcopy.

The nitrifying sludge obtained after the last start-up contained both AOB an NOB and was used to achieve partial nitrification. Some environmental conditions and the automatic control strategy were changed in order to inhibit NOB and wash them out of the system. Partial nitrification with an effluent devoid of nitrate was achieved at 25 ºC, 1.1 mg O_2 L^{-1} and pH of 8.3 using the appropriate OUR set point for the automatic controller. Steady partial nitrification was run for 120 days with an averaged nitrogen loading rate of 0.5 g N g^{-1} VSS d^{-1}. FISH analysis demonstrated that NOB were completely washed out. The control strategy was improved by the addition of two expert rules and stable operation was maintained even when external disturbances were provoked. Finally, a model-based study was performed to test the partial nitrification start-up strategy under different conditions and system configurations.

RESUM

El tema d'estudi d'aquesta tesi és l'eliminació biològica de nitrogen d'aigües amb alta càrrega d'amoníac, més concretament, el procés de nitrificació (l'oxidació de l'amoni a nitrat). Aquesta reacció en dos passos, catalitzada per dos tipus de microorganismes (AOB i NOB), pot patir greus problemes d'inhibicions per amoníac i àcid nitrós. Això és especialment important quan es tracta aigua amb alta concentració d'amoni i per tant, es necessita un control del procés adequat. Tot i així, aquestes inhibicions es poden utilitzar per a aconseguir nitrificació parcial (l'oxidació de l'amoni a nitrit), la qual combinada amb el procés de desnitrificació, aporta beneficis importants pel què fa a la utilització dels recursos.

En aquesta tesi es mostra el desenvolupament i calibratge d'un model matemàtic per a descriure la cinètica i l'estequiometria de la nitrificació. El model considera les inhibicions mencionades anteriorment i té en compte els dos tipus de bacteris nitrificants i també els bacteris heteròtrofs. Es varen dissenyar experiments específics per a l'optimització dels paràmetres del model i amb l'ajuda d'eines d'identificabilitat de paràmetres, aquests experiments es van analitzar i millorar. Els dissenys d'experiments òptims van ser utilitzats per al calibratge de la majoria dels paràmetres del model i els paràmetres obtinguts es van comparar amb valors trobats a la bibliografia. Les constants d'afinitat pel substrat i els coeficients d'inhibició per substrat es van determinar dues vegades utilitzant biomasses diferents i es van obtenir resultats diferents. Això indicà que aquests paràmetres són variables i depenen de l'aclimatació de la biomassa. El model final es va introduir en el model hidràulic del sistema experimental (planta pilot) i es va implementar en Matlab.

Es va utilitzar la tècnica d'hibridació fluorescent *in situ* (FISH) per a la detecció i quantificació de les fraccions bacterianes. Per a la detecció de la fluorescència, es van utilitzar diferents equips: un microscopi d'epifluorescència, un microscopi confocal i un citòmetre de flux. En primer lloc, es varen optimitzar alguns dels passos i procediments com el mètode de quantificació basat en l'àrea, el temps de sonicació, el protocol pel FISH en solució i la citometria de flux. En segon lloc, es van determinar les fraccions bacterianes amb cadascun dels mètodes i també amb simulació. Els resultats obtinguts es van comparar entre ells i es van discutir els seus avantatges i inconvenients tenint en compte la precisió dels resultats, la velocitat de l'anàlisi i la disponibilitat de l'equip. La millor metodologia va resultar ser l'observació del FISH amb el microscopi confocal encara que la citometria de flux no es va poder investigar prou a fons.

El model matemàtic desenvolupat i calibrat en aquesta tesi es va utilitzar per a l'optimització de la posada en marxa d'un sistema de nitrificació completa. En realitat es van optimitzar dues estratègies de control que posteriorment es van implementar experimentalment partint d'un inòcul procedent dels llots d'una estació de tractament d'aigües residuals urbanes. El controlador dissenyat es basava en la mesura de la velocitat del consum d'oxigen (OUR) en

l'últim reactor del sistema i actuava sobre la càrrega d'entrada de nitrogen. Els resultats obtinguts es van comparar amb els resultats d'una posada en marxa amb control manual i es va demostrar que el control automàtic permet disminuir el temps de posada en marxa i augmentar l'estabilitat del procés. Posteriorment, els resultats experimentals es van simular amb el model matemàtic. El model s'ajustà molt bé a les dades experimentals després de modificar només dos dels seus paràmetres. Finalment, el nou model es va utilitzar per a fer prediccions del comportament del sistema a curt i llarg termini. L'enriquiment de la biomassa en microorganismes nitrificants es va comprovar mitjançant el FISH i la microscòpia confocal.

La biomassa que es va obtenir després de la última posada en marxa del sistema contenia AOB i NOB i va ser la biomassa que es va fer servir per a aconseguir la nitrificació parcial. Per a fer-ho, es van canviar algunes de les condicions ambientals i l'estratègia del control automàtic, concretament, per a inhibir el creixement dels NOB i eliminar-los del sistema. La nitrificació parcial amb una sortida sense nitrats es va aconseguir a 25 ºC, 1.1 mg O_2 L^{-1}, pH de 8.3 i amb un *set point* d'OUR apropiat en el control automàtic. La nitrificació parcial es va mantenir de forma estable durant uns 120 dies amb una càrrega mitjana de 0.5 g N g^{-1} SSV d^{-1}. L'anàlisi microbiològic amb FISH va demostrar que la població de NOB havia estat eliminada del sistema. Posteriorment, el sistema de control es va millorar amb l'adició de dues regles de control expert que van permetre l'operació estable del sistema davant de pertorbacions externes provocades. Finalment es va realitzar un estudi basat en simulacions per a provar l'estratègia de posada en marxa del sistema de nitrificació parcial en diferents condicions ambientals i amb diferents configuracions.

CONTENTS

PART I - Chapter 1

INTRODUCTION

1. WATER, NITROGEN CYCLE AND HUMAN ACTIVITY

Water availability for human population

Water is an essential life-sustaining element. Although about 70 % of the Earth is covered with water, 97.5 % of that is part of salty oceans, and therefore, only 2.5 % is freshwater. Freshwater has a global volume of 35.2 million cubic kilometers, from which, 69.5 % is in glaciers, 30.1 % is groundwater and 0.4 % is surface and atmospheric water. Surface and atmospheric water can be found in freshwater lakes (67.4 %), soil moisture (12.2 %), atmosphere (9.5 %), plant and animals (0.8 %), rivers (1.6 %) and other wetlands (8.5 %) (UNESCO 2006). Therefore, only a small portion of the world water is available for life.

These water resources are very deficiently distributed among human population, being one of the main causes of poverty. It has been estimated that in order to ensure the basic needs, every individual needs 20 to 50 liters per day of water free from harmful contaminants (UNESCO 2006). However, while the poorest fraction of population consume about 20 to 70 L d^{-1} per person, the water consumption in Catalunya per person is about 250 L d^{-1} and in the United States is about 400 L d^{-1} (Poch 1999).

In addition, the growing world's population is not in accordance with water availability. The global climate change is favoring the combination of lower precipitation and higher evaporation in many regions increasing the unbalanced distribution. This diminishes the water quantities in rivers, lakes and groundwater storage while the water pollution increases. Nowadays, warming of the climate system is unequivocal, as it is now evident from observation of increases in global average air and ocean temperatures, widespread melting of snow and ice, and rising global means see level (Alley et al. 2007). Therefore, the wise use of water, the water recycle and the wastewater treatment are becoming more and more vital aspects in water management.

With respect to freshwater, the main pollutants are organic matter, pathogens and microbial contaminants, nutrients (nitrogen and phosphorus), salinization, acidification (precipitation and runoff), heavy metals, toxic organic compounds and micro-organic pollutants, thermal, silt and suspended particles and others like radioactivity, fluoride and selenium. Although, natural systems have high intrinsic capacity to remove some of these pollutants it is not enough for the high load of these contaminants going into the environment. Consequently, a number of wastewater treatment processes are being developed.

The nitrogen cycle

Nitrogen, specifically in the ammonia form, is the pollutant studied in this thesis. Nitrogen actively cycles through the atmosphere, the continental land mass and the world's oceans, and

represents a critical nutrient upon which plant, microbial, and animal life depend. The biological transformations in the nitrogen cycle are depicted in Figure 1.1.

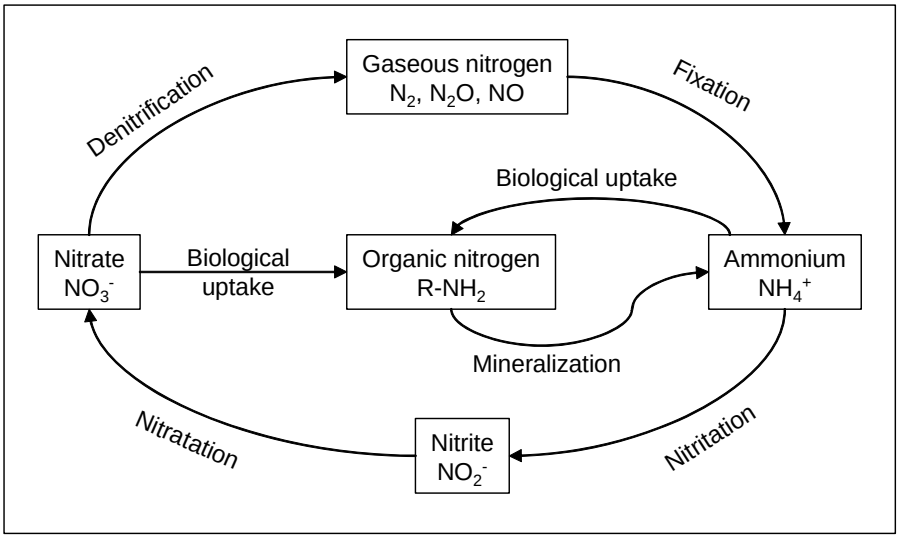

Figure 1.1 Overview of the biological transformations in the nitrogen cycle.

Fixation is the process in which dinitrogen gas is converted to ammonium, the only way that organisms can attain nitrogen directly from the atmosphere. Considering that the nitrogen stored in the atmosphere is about one million times larger than the total nitrogen contained in living organisms, this process is of great importance. It is carried out by certain bacteria which, in some cases, form symbiotic relationships with host plants. High-energy natural events such as lightning, forest fires and even hot lava flows can cause the fixation of smaller but significant amounts of nitrogen. Biological uptake is the incorporation of ammonium and nitrate into protein and other organic nitrogen by plants, bacteria or other soil organisms. The mineralization process (or decomposition) produces inorganic nitrogen (ammonium) from dead organisms. It is carried out by bacteria and fungi. Bacteria are the responsible for the rest of the biological transformations: nitrification (biological oxidation of ammonium to nitrate via nitrite) and denitrification (biological reduction of nitrate to dinitrogen gas).

The human activity has severely altered the nitrogen fluxes of the natural cycle. Some of the major processes in this alteration include the chemical fixation of nitrogen into fertilizers and their application to crops. It causes increasing rates of denitrification and leaching of nitrate into groundwater that eventually flows into streams, rivers, lakes and estuaries. The nitrogen cycle is also modified due to the fossil fuel combustion and forest burning increasing the global concentration of N_2O and NO in the atmosphere. This favors the climate warming and the deposition of nitrogen from atmospheric sources. On the other hand, livestock ranching, that releases a large amount of ammonia into the environment from their wastes, sewage waste and septic tanks increase the ammonia content of soil and hydrologic systems through leaching, groundwater flow and runoff. Figure 1.2 shows the predominant sources of nitrogen around the world (UNESCO 2006). Fixation is the primary source throughout South America, Africa,

Australia, and the northernmost reaches of Asia and North America. Atmospheric pollution and subsequent nitrogen deposition plays a dominant role throughout the industrialized northern temperate zones of Europe, Asia and North America. Fertilizers are the predominant source across major food producing regions. Livestock constitutes the most important source in Eastern Europe and India. Urban sewage loads create localized 'hotspots' for pollution. Understanding the patterns of such loadings is critical to the design of management interventions to protect society and well-functioning ecosystems (UNESCO 2006).

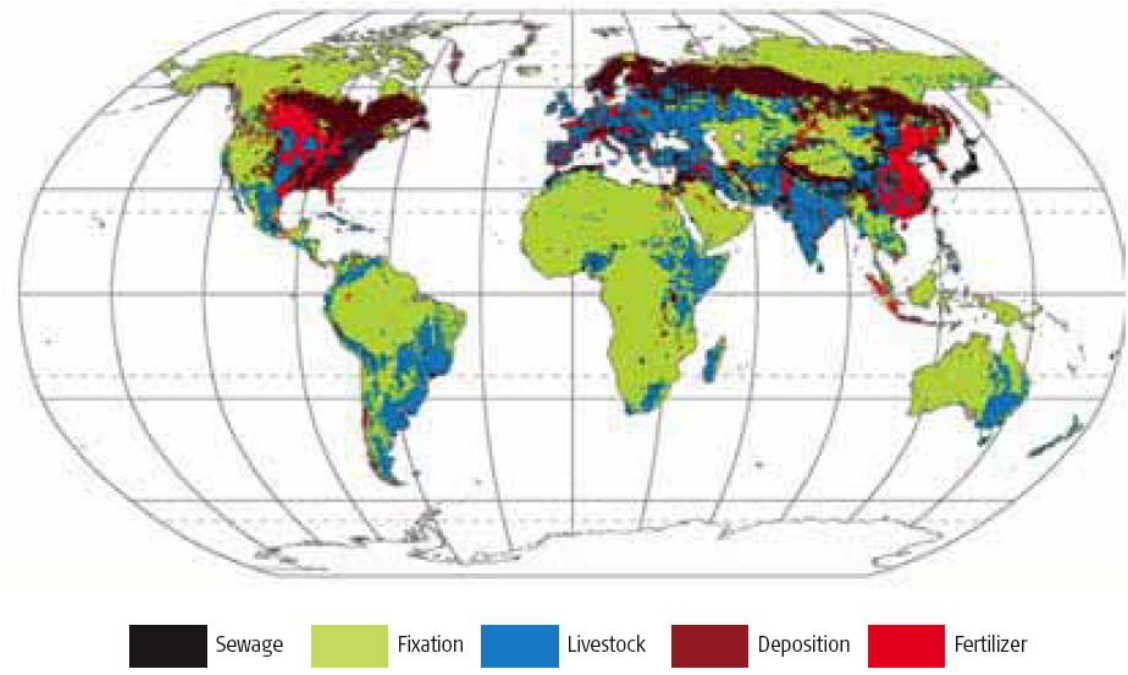

Figure 1.2 Predominant sources of contemporary nitrogen loading. From UNESCO (2006), data from the Water systems analysis group at University of New Hampshire.

In aquatic systems, nitrogen pollution can lead to eutrophication, a nutrient over-enrichment that produces harmful algal blooms, fish-kill events and species shifts. Moreover, nitrate and nitrite in drinking water can be a health danger. Nitrate is converted by bacteria into nitrite which then oxidizes the blood's hemoglobin, impeding the transport of oxygen and producing a drastic reduction of oxygenation known as cyanosis. This is especially problematic for babies causing the "blue baby" syndrome. Moreover, it seams that high nitrate levels could be correlated with cancer (Cantor 1997).

Regulation regarding nitrogen

In Europe, the nitrogen content of wastewater is regulated by the European Union, in particular by the Council Directive 91/271/EEC of 21 May that concerns the collection, treatment and discharge of urban wastewater and the treatment and discharge of wastewater from certain industrial sectors. The requirements of nitrogen for discharges from urban wastewater treatment plants (WWTP) to sensitive areas are depicted in Table 1.1.

Table 1.1 Discharges requirements of nitrogen from urban WWTPs to sensitive areas.

Population equivalent (p.e.)*	Concentration (mg N L^{-1})	Reduction (%)
10^4 - 10^5	15	80
> 10^5	10	70-80

*1 p.e. (population equivalent) means the organic biodegradable load having a five-day biological oxygen demand (BOD_5) of 60 g O_2 d^{-1}.

Based on this directive, the *Real Decreto* 509/1996 of 15 May fixed the nitrogen restrictions in Spanish urban WWTPs. With respect to industrial wastewater, the *Generalitat de Catalunya*, in the *Decret* 130/2003 of 13 May, set the nitrogen discharges limits at 100 mg NO_3^- L^{-1}, 60 mg NH_4^+ L^{-1} and 90 mg N L^{-1} of organic nitrogen according to the *Real Decreto* 995/2000 of 2 June and the Council Directive 91/271/EEC of 21 May.

2. NITRIFICATION AND WASTEWATER SOURCES

Nitrogen removal from wastewater is mainly performed biologically in wastewater treatment plants by enhancing the natural nitrification and denitrification processes. Nitrification is the conversion of ammonium to nitrate in a two-step process: ammonium is first oxidized to nitrite (nitritation process) by ammonium oxidizing bacteria (AOB) and then, nitrite is oxidized to nitrate (nitratation) by nitrite oxidizing bacteria (NOB). Denitrification is the conversion of nitrate to dinitrogen gas by denitrifying bacteria.

Optimum conditions for ammonium removal from urban wastewater are widely known and applied by using different systems and configurations (EPA 1993). However, research on high-strength ammonium wastewater treatment is still a “hot-spot”. This kind of ammonium-rich wastewater is produced by several human activities: petrochemical, pharmaceutical, fertilizer and food industries, urban solid waste disposal, pig farms or sludge dewatering; and most of them have the particularity to have a very low content of biodegradable chemical oxygen demand (COD), i.e., low BOD. Table 1.2 shows some examples of high-strength ammonium wastewaters. Examples from other industries can be found in Wiesmann (1994).

Reject water from activated sludge dewatering has been the wastewater source for a number of works in the recent literature because of their existence in all WWTPs, its specific characteristics (ammonium, COD and alkalinity concentration, pH and temperature) and the finding of a new bacterial group (anammox bacteria). However, the optimal treatment for this kind of wastewater could not be optimal for other wastewaters with different characteristics; and therefore, they should be specifically investigated.

This thesis looks at the treatment of highly concentrated ammonium wastewater (≈ 3000 mg L^{-1}) with very low biodegradable COD content. The research was performed with synthetic

wastewater at pilot scale focusing only on the nitrification process and working under mild conditions (20-25 ºC).

Table 1.2 High-strength ammonium wastewaters with their composition of ammonium and COD.

Wastewater	NH_4^+ (mg N L^{-1})	COD (mg COD L^{-1})	BOD_5/COD	Reference
Piggery wastewater	4400-15200	20000-153000	0.3-0.5	Eum and Choi (2002)
Urine from separate collection	1800-3800	1580-3350	-	Udert et al. (2003)
Swine liquid waste discharged from a process separating urine	3000	4500*	-	Terada et al. (2003)
Reject water of digested sludge	1100	6000	-	Teichgräber (1993)
Reject water of digested sludge	1000	810	0.3	Hellinga et al. (1998)
Reject water of digested sludge	880	571	-	Pynaert et al. (2004)
Supernatant of anaerobic digestion of the organic fraction of municipal wastes	200-2600	3000-35000	0.25-0.45	Mace et al. (2006)
Landfill leachate	< 2000	-	-	Shiskowski and Mavinic (1998)
Landfill leachate	880-1500	1100	0.05	Doyle et al. (2001)
Wastewater from potato starch production after anaerobic pre-treatment	1050	3000	0.3	Abeling and Seyfried (1992)
Wastewater from bottle frost	4000-6000	0	0	Carrera et al. (2003a)
Wastewater from pharmaceutical industry	150-500	1600-15000	-	Torrijos et al. (2004)

* Total organic carbon (TOC) in mg C L^{-1}.

3. THE MICROBIOLOGY OF NITRIFICATION

Ammonium oxidizing bacteria, AOB

AOB are obligately chemoautotrophic Gram-negative bacteria that utilize ammonia as a source of electrons for the immobilization of inorganic carbon into biomass. This sole energy source drives carbon fixation, the assimilation of monomers into precursor metabolites and the subsequent polymerization of building blocks and macromolecules. They are aerobic, employing oxygen as the final or terminal electron accepter. Figure 1.3 shows a diagram of the involved process, where Y_A is the growth yield.

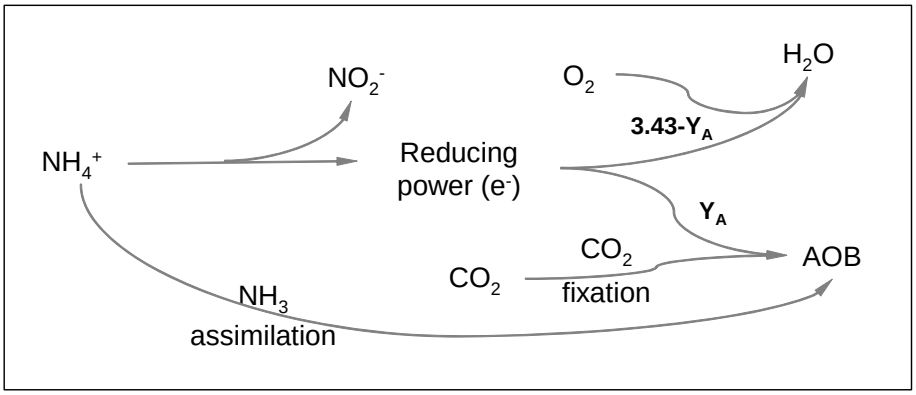

Figure 1.3 Diagram of chemical reactions for ammonium oxidation and AOB growth.

The stoichiometric equation for the oxidation of ammonium to nitrite is (EPA 1993):

$$NH_4^+ + 1.5\ O_2 \rightarrow NO_2^- + 2\ H^+ + H_2O + (70\ kcal\ mol^{-1}) \quad (1.1)$$

And the equation for the synthesis of new bacteria, assuming that the empirical formulation of bacterial cells is $C_5H_7NO_2$, is (EPA 1993):

$$13\ NH_4^+ + 15\ CO_2 \rightarrow 10\ NO_2^- + 3\ C_5H_7NO_2 + 23\ H^+ + 4\ H_2O \quad (1.2)$$

The stoichiometry of the equation for ammonium oxidation and biomass growth, coupling equations 1.1 and 1.2, depends on the Y_A value.

AOB can grow at temperatures of 5-35 ºC with the optimum around 25-35 ºC. With respect to pH, the range is smaller, around 5.8-9.0 with 7.8 as the optimum (Blackall and Burrell 1999).

On the basis of phenotypic characteristics, AOB have been divided into the five genera *Nitrosomonas*, *Nitrosolobus*, *Nitrosovibrio*, *Nitrosococcus* and *Nitrosospira* (Watson et al. 1989). Based on the comparative 16S rRNA sequence analysis, cultured AOB comprise two monophyletic groups within the *Proteobacteria. Nitrosococcus oceanus* and *Nitrosococcus halophilus* belong to the gamma subclass of the class *Proteobacteria* (Woese et al. 1985), while the members of the genera *Nitrosomonas*, *Nitrosospira*, *Nitrosovibrio* and *Nitrosolobus*, as well as *Nitrosococcus mobilis* (actually a member of the genus *Nitrosomonas*) constitute a closely related assemblage within the beta subclass of *Proteobacteria* (Head et al. 1993; Pommerening-Röser et al. 1996; Teske et al. 1994). Figure 1.4 shows the maximum parsimony tree of nitrifying bacteria based on comparative analysis of 16S rRNA sequences.

Nitrite oxidizing bacteria, NOB

NOB are chemoautotrophic bacteria with the ability to use nitrite as their energy source and to assimilate CO_2 as the carbon source for cell growth. They are not all obligate chemoautotrophs. In fact, many strains of *Nitrobacter* can grow as heterotrophs, where both energy and carbon are obtained from organic carbon sources, or mixotrophically (Watson et al. 1989). These

bacteria are collectively known as facultative chemoautotrophs or lithoautotrophs. They are also aerobic although some of them can also grow anaerobicaly and heterotrophicaly (Bock et al. 1988). Figure 1.5 shows a diagram of the processes involved in the chemoautotrophic and aerobic growth of NOB, where Y_N is their growth yield.

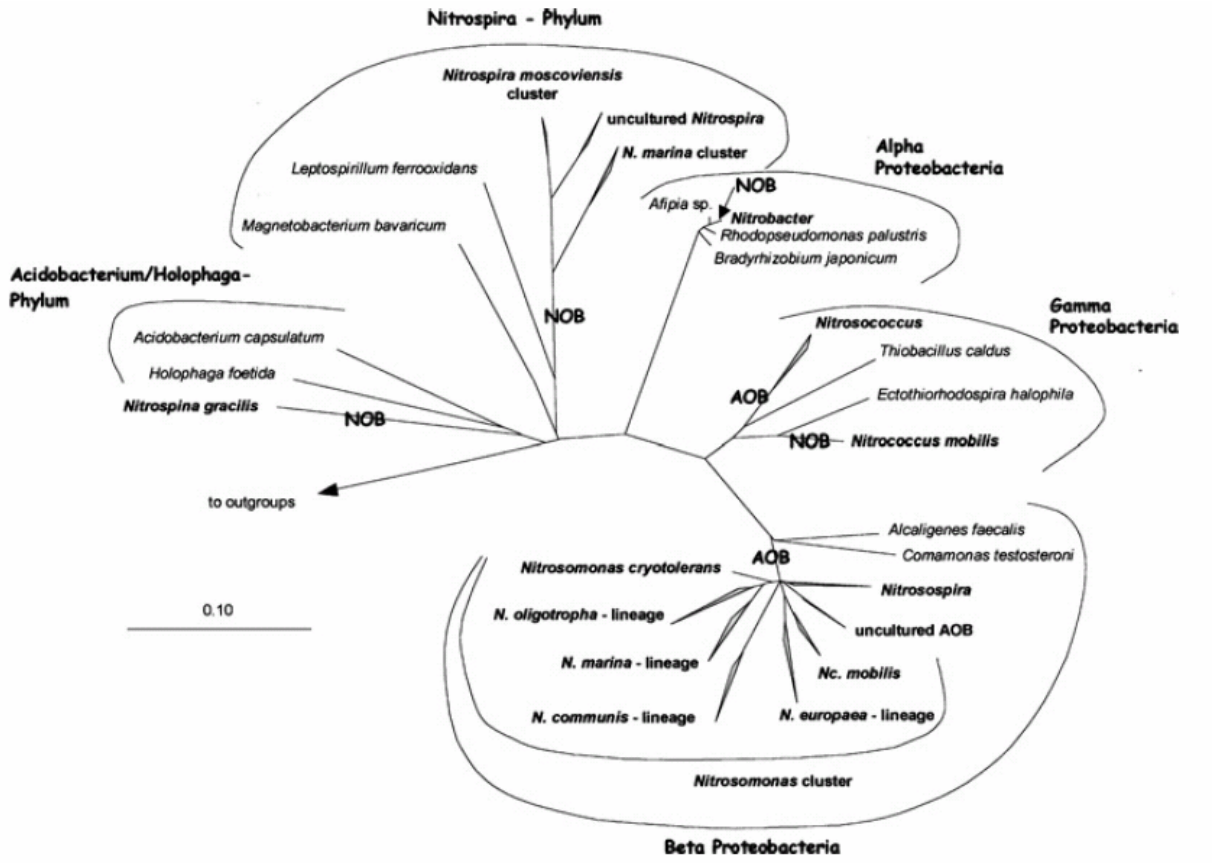

Figure 1.4 Maximum parsimony tree of nitrifying bacteria based on comparative analysis of 16S rRNA sequences. Groups of nitrifying bacteria are displayed in bold; Branches in the tree leading to ammonia or nitrite oxidizing bacteria are labeled AOB or NOB, respectively. The scale bar indicates 0.1 estimated change per nucleotide. From Schramm (2003).

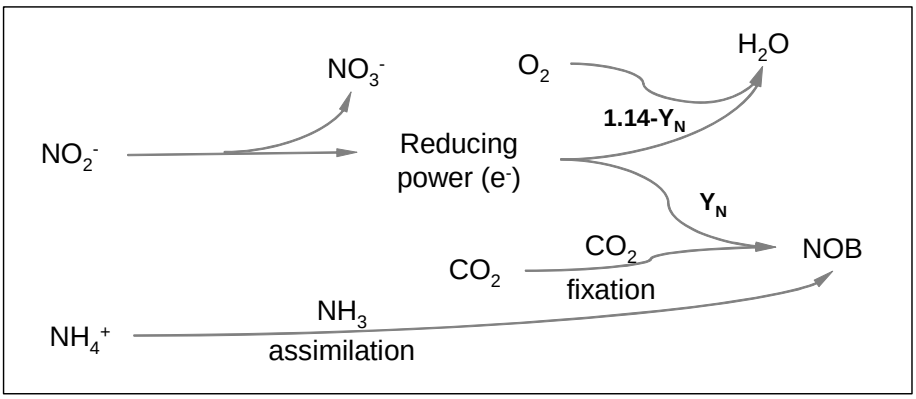

Figure 1.5 Diagram of chemical reactions for nitrite oxidation and NOB growth.

The stoichiometric equation for the oxidation of nitrite to nitrate is (EPA 1993):

$$NO_2^- + 0.5\ O_2 \rightarrow NO_3^- + (18\ kcal\ mol^{-1}) \quad (1.3)$$

And the equation for the synthesis of new bacteria, assuming that the empirical formulation of bacterial cells is $C_5H_7NO_2$, is (EPA 1993):

$$10\ NO_2^- + 5\ CO_2 + NH_4^+ + 2\ H_2O \rightarrow 10\ NO_3^- + C_5H_7NO_2 + H^+ \quad (1.4)$$

The stoichiometry of the equation for nitrite oxidation and biomass growth, coupling equations 1.3 and 1.4, depends on the Y_N value.

The optimal growth conditions for NOB are at neutral to alkaline pH values (7.6 - 8.0) but they can grow in the range 6.5-8.6. Growth will occur at temperatures between 5 ºC and 37 ºC, and optimally at temperatures between 25 and 30 ºC, in suitably aerated environments (Watson et al. 1989).

Based on ultrastructural properties, cultivated NOB have been assigned to the four recognized genera *Nitrobacter*, *Nitrococcus*, *Nitrospira* and *Nitrospina*. While the first two affiliate with the alpha and gamma subclasses of *Proteobacteria*, respectively (Teske et al. 1994), the genus *Nitrospira* belongs to the separate phylum *Nitrospira* (Ehrich et al. 1995). The phylogenetic affiliation of *Nitrospina* is less clear. Although originally grouped with the delta *Proteobacteria* (Teske et al. 1994) more recent phylogenetic analyses (Schramm 2003) indicate that *Nitrospina* is quite distinct from delta *Proteobacteria* and might represent a separate group close to the *Acidobacterium/Holophaga* phylum (see Figure 1.4).

Inhibitions

Anthonisen et al. (1976) observed and quantified the inhibitory effect of nitrogenous compounds to nitrifying bacteria. They also postulated that the inhibition was related to concentrations of un-ionized forms, i.e. ammonia and nitrous acid. Figure 1.6 shows a diagram of the inhibitions reported by Anthonisen et al. (1976). Although they did not observe AOB inhibition by nitrous acid it was detected by other authors (Carrera 2001; Van Hulle et al. 2004) and therefore it was added in the figure.

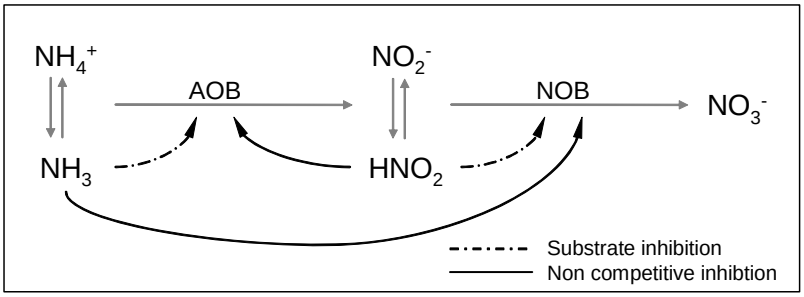

Figure 1.6 AOB and NOB inhibitions due to ammonia and nitrous acid.

These inhibitions are only significant when dealing with high-strength ammonium wastewater because the inhibitory concentrations are much higher than ammonia and nitrous acid concentrations of urban wastewater. In fact, they are key points in the design and implementation of processes for high-strength ammonium wastewater: either to avoid them or to use them for nitratation suppression.

Apart from ammonia and nitrous acid, nitrifying organisms are susceptible to a wide array of organic and inorganic inhibitors: aniline, p-phenilendiamine, phenol, chloroform, sodium azide, perchlorate, copper, fluoride, zinc, nickel, cadmium, mercury and cobalt among others (Carrera et al. 2003b; EPA 1993; Guisasola et al. 2003; Hu et al. 2002; López-Fiuza et al. 2002). However, they can adapt to many inhibitory compounds when inhibitors are constantly present in the wastewater (Turk and Mavinic 1989; Villaverde et al. 2000).

4. NOVEL BIOLOGICAL NITROGEN REMOVAL PROCESSES

Typically biological ammonium removal (i.e. nitrification and denitrification) have been performed with several different configurations: Wuhrmann, Ludzack-Ettinger, Bardenpho, A^2O, SBR, etc. (WEF 1992; WPCF 1983). However, the need of high-strength ammonium wastewater treatment motivated the research of new processes and more optimal configurations. These novel treatments are briefly described in this section, however, more information can be found in Schmidt et al. (2003), Khin and Annachhatre (2004) and Manipura et al. (2005). Figure 1.7 shows the flux diagrams of these processes.

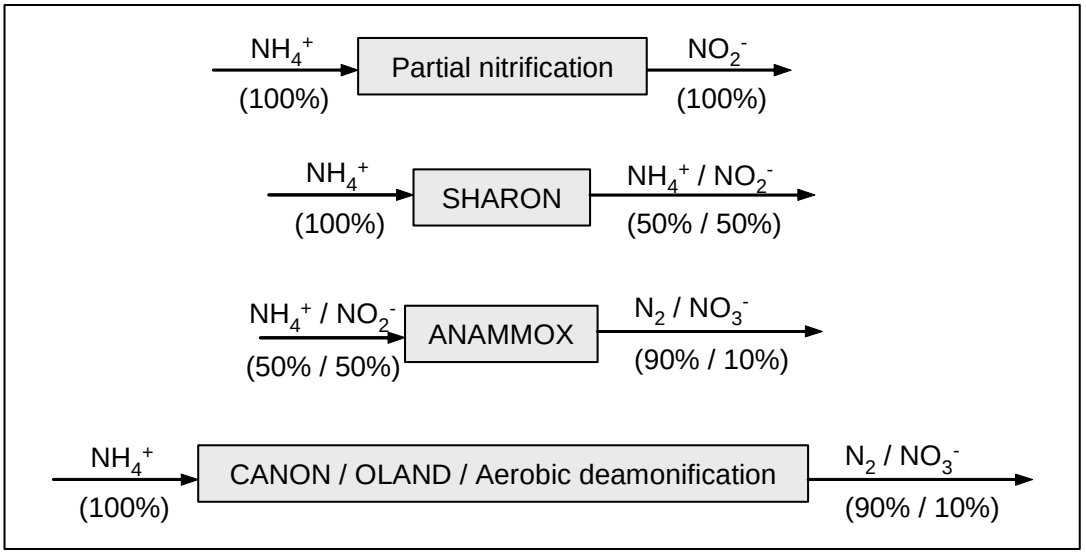

Figure 1.7 Flux diagrams of partial nitrification, SHARON, ANAMMOX, CANON, OLAND and aerobic deamonification processes. In brackets: percentages of nitrogenous compounds in the flow.

Partial nitrification process

Partial nitrification is the oxidation of ammonium to nitrite, but not to nitrate. To achieve partial nitrification, the subsequent oxidation of nitrite must be prevented. This process can be combined with the ANAMMOX process (see below) or with the conventional denitrification (the so called 'nitrite route') obtaining significant benefit in terms of use of resources (Turk and Mavinic 1987). The process needs less aeration and the subsequent denitrification consumes less COD because nitrite and not nitrate has to be reduced to dinitrogen gas. There exist several ways of preventing the oxidation of nitrite, all of them making use of the different response of AOB and NOB in front of specific conditions or compounds concentration: temperature, DO, pH, ammonia, free-hydroxylamine, etc. A comprehensive review can be found in Chapter 7.

An example of partial nitrification is the SHARON (single reactor high activity ammonia removal over nitrite) process, which makes use of the different growth rates of AOB and NOB at temperatures of around 35 ºC (Hellinga et al. 1998). It works as a chemostat at a hydraulic retention time (HRT) higher than the growth rate of NOB but lower than that of AOB (around 1day). Because this process has no sludge retention, NOB are not able to remain in the reactor and are easily washed out of the system. Another consequence of the no sludge retention is the low biomass concentration in the reactor. Moreover, the temperature dependency of this process is a disadvantage for the treatment of all kinds of wastewaters; however, sludge reject water has the optimal characteristics to be treated with this process.

ANAMMOX process

The ANAMMOX (anaerobic ammonia oxidation) process is the denitrification of nitrite with ammonia as the electron donor (Jetten et al. 1998). Anaerobic ammonia oxidation is carried out by a group of planctomycete bacteria (Strous et al. 1999), two of which have been named provisionally ('*Candidatus* Brocadia anammoxidans' (Jetten et al. 2001) and "*Candidatus* Kuenenia stuttgartiensis' (Schmid et al. 2000)). The main characteristics are the high doubling time (11 days), the low biomass yield (0.13 g dry weight g^{-1} $N\text{-}NH_3$) and the requirement of ammonia:nitrite ratio of 1:1.3 (Schmidt et al. 2003). Therefore, this process needs a preceding partial nitrification step that converts approximately half of the wastewater ammonium to nitrite. The low growth rate and biomass yield makes the start-up of this process very difficult, especially for full-scale systems. The effluent of the SHARON process ideally suits as influent of the ANAMMOX process for the treatment of reject sludge wastewater (Van Dongen et al. 2001; Volcke et al. 2005).

CANON, OLAND and aerobic deamonification processes

CANON (completely autotrophic nitrogen removal over nitrite) (Sliekers et al. 2002), OLAND (oxygen-limited autotrophic nitrification-denitrification) (Kuai and Verstraete 1998) and

aerobic deamonification (Hippen et al. 2001) are different terms to design similar processes with similar nitrogen removal stoichiometry and microbial composition. They are based on the combination of partial nitrification and ANAMMOX in a single aerated reactor. The basic principle of these processes is based on supplying oxygen to the process such that nitrification only proceeds up to the nitrite step. Then, due to the lack of an electron acceptor, nitrite is consumed to oxidize the remaining ammonium. These processes require precise process control to prevent nitrite build-up by oxygen excess and long time for the start-up.

5. ESSENTIAL TOOLS FOR RESEARCH

Modeling

Models are used in the areas of science and engineering and they are of special interest also in wastewater treatment for several purposes (Jeppsson 1996):

Design. Models allow the exploration of the impact of changing system parameters and development of systems designed to meet the desired process objectives at minimal cost.

Research. Models serve as a tool to develop and test hypotheses and thereby gaining new knowledge about the process.

Process control. Models allow for the development of new control strategies by investigating the system response to a wide range of inputs without endangering the actual system.

Forecasting. Models are used to predict future system performance when exposed to foreseen input changes and provide a framework for testing appropriate counteractions.

Performance analysis. Models allow for analysis of system performance over time when compared with laws and regulations and what the impact effluent requirements on system design and operational costs will be.

The most important matter is that models allow the study of processes of great complexity such as biological nitrogen removal, where there are several bacterial populations and several compounds affecting the performance of the system, having long time responses and non-linear behavior. Therefore, they are essential for design, research, process control, forecasting and performance analysis. Nevertheless, appropriate models with appropriate parameters should be used to get accurate outputs. This implies, in most cases, parameter calibration.

With respect to the nitrification modeling, Activated Sludge Models ASM1, ASM2, ASM2d and ASM3 (Henze et al. 2000) are accepted models for the simulation of urban WWTP systems, however they may not be accurate for high-strength ammonium wastewater treatment

systems. In the last cases, two-step nitrification models should be used (Chandran and Smets 2000).

Microbiological characterization

Fluorescence *in situ* hybridization (FISH) is a microbiological technique for bacteria identification and quantification that allows better understanding of the microbiology of the processes. This tool, applied to the biological nitrogen removal process, allows the identification of the species involved in each step (nitritation, nitratation and denitrification) and helps in the study of the optimal conditions for their growth. FISH is becoming more and more essential in the research of this topic, even for chemical engineers, because the comprehensive understanding of any chemical reaction can not be accomplished without the accurate characterization of their catalysts (although they are bacteria).

6. RESEARCH MOTIVATIONS AND THESIS OVERVIEW

This thesis was framed in one of the research lines of the GENOCOV group (liquid and gas effluents treatment group: nutrients, odors and volatile organic compounds removal) in the Department of Chemical Engineering at the Universitat Autònoma de Barcelona. This group was born in the 1990s with the aim to conduct research on improving the current biological wastewater treatment systems. Three theses were defended around year 2000 which are the antecedent of this thesis. Firstly, Juan Baeza developed a supervisory control system to improve the operation of a biological nutrient removal pilot plant (Baeza 1999). Secondly, David Gabriel examined and modified the ASM2d model to monitor the activated sludge process on a pilot plant (Gabriel 2000). Finally, Julián Carrera investigated the biological treatment of an industrial high-strength ammonium wastewater (Carrera 2001). This last work established the starting point for this thesis. Then, the research group put its efforts on the separate study of the phosphorous removal process and the nitrogen removal process. Maite Pijuan studied the effect of different carbon sources and continuous aeration on the enhanced biological phosphorus removal process (Pijuan 2004). On the other hand, Albert Guisasola developed respirometric and titrimetric tools for modeling biological organic matter removal and nutrient removal processes from wastewater (Guisasola 2005) which were also helpful for the progress of this thesis. Around 2004 the group started a new research line in gas treatment and also diversified the existing research lines by focusing on more specific topics as modeling, benchmarking and combined phosphorous and nitrogen removal. This thesis was performed in the research line of high-strength ammonium wastewater treatment.

Research motivations

Highly concentrated ammonium wastewater needs specific treatment before discharging it into the sewage system or recycling it to the conventional WWTPs. Partial nitrification is one of the most appropriate processes for the biological treatment of this kind of wastewater; however there was still a lack of knowledge about the most appropriate configurations and conditions. A proof of the interest that this topic generated on the research community is the enormous amount of recently published articles on the topic. The achievement of partial nitrification treating high-strength ammonium wastewater at lower temperatures than reject water was one of the main incentives since reject water was being extensively studied by other researchers. The background and knowledge about process control of the research group motivated the incorporation of control strategies in the operation of the experimental system in order to improve its performance. On the other hand, essential tools like modeling could not be avoided because of its usefulness for process and control optimization. This fact motivated the development and calibration of an appropriate model for nitrification. Moreover, the FISH technique, that was already used in the research group for PAOs (polyphosphate accumulating organisms) quantification and was used in the literature for nitrifying community analysis, was also applied to the nitrification studies of this thesis to increase the comprehension of the studied biological system.

Thesis overview

This document is divided into five parts. The first part (*General introduction*), in which this section is included, is the introduction to the topic and the statement of the objectives of this thesis. The second part (*Modeling*) shows the description of the mathematical model of a two-step nitrification process and the calibration of some of the model parameters. This part also includes the description of the experimental system (pilot plant) and its modeling equations. The third part (*Nitrifying community analysis*) shows the use of the FISH technique for nitrifying fractions determination and quantification. Part of this chapter was carried out during a stay at the Technical University of Denmark (DTU). The fourth part (*Simulation, operation and automatic control*) is divided into two chapters and shows the operation of the pilot plant; first as a complete nitrification system and then as a partial nitrification system. The previously described model and the biomass quantification method developed in the previous section are applied in these chapters. Moreover, process control (conventional strategies and supervisory control) is also developed and applied. The last part (*Conclusions*) gives an overview of the main achievements of this thesis and points out the topics for future research derived from this thesis.

The format and length of this document have the aim to extensively describe and discuss the experiments and simulations performed through the research period in order to get a worthy document for the following researchers in the group. Therefore, the main motivation during the

writing was that other PhD students could be able to use it as a handbook, a reference book or a compilation of protocols for techniques and experiments. I wish someone will find it useful.

7. REFERENCES

Abeling U, Seyfried CF. 1992. Anaerobic-aerobic treatment of high-strength ammonium wastewater - Nitrogen removal via nitrite. *Water Science and Technology* 26(5-6):1007-1015.

Alley R, Berntsen T, Bindoff NL, Chen Z, Chidthaisong A, Friedlingstein P, Gregory J, Hegerl G, Heimann M, Hewitson B and others. 2007. Climate change 2007: The physical science basis. Summary for policymakers. *Fourth Assessment Report of the Intergovernmental Panel on Climate Change*.

Anthonisen AC, Loehr RC, Prakasam TBS, Srinath EG. 1976. Inhibition of nitrification by ammonia and nitrous acid. *Journal of the Water Pollution Control Federation* 48(5):835-852.

Baeza JA. 1999. Development and implementation of a supervisory system for the management and control of WWTPs (in Spanish). PhD Thesis. Bellaterra: Universitat Autònoma de Barcelona.

Blackall LL, Burrell PC. 1999. The microbiology of nitrogen removal in activated sludge systems. In: Seviour RJ, Blackall LL, editors. *The microbiology of activated sludge*. Dordrecht: Kluwer Academic Publishers. p 203-226.

Bock E, Wilderer PA, Freitag A. 1988. Growth of Nitrobacter in the Absence of Dissolved-Oxygen. *Water Research* 22(2):245-250.

Cantor KP. 1997. Drinking water and cancer. *Cancer Causes & Control* 8(3):292-308.

Carrera J. 2001. Biological ammonium removal from high-strength ammonium wastewater. Process parameters study and design of a full-scale industrial WWTP (in Spanish). PhD Thesis. Bellaterra: Universitat Autònoma de Barcelona.

Carrera J, Baeza JA, Vicent T, Lafuente J. 2003a. Biological nitrogen removal of high-strength ammonium industrial wastewater with two-sludge system. *Water Research* 37(17):4211-4221.

Carrera J, Torrijos M, Baeza JA, Lafuente J, Vicent T. 2003b. Inhibition of nitrification by fluoride in high-strength ammonium wastewater in activated sludge. *Process Biochemistry* 39(1):73-79.

Chandran K, Smets BF. 2000. Single-step nitrification models erroneously describe batch ammonia oxidation profiles when nitrite oxidation becomes rate limiting. *Biotechnology and Bioengineering* 68(4):396-406.

Doyle J, Watts S, Solley D, Keller J. 2001. Exceptionally high-rate nitrification in sequencing batch reactors treating high ammonia landfill leachate. *Water Science and Technology* 43(3):315-322.

Ehrich S, Behrens D, Lebedeva E, Ludwig W, Bock E. 1995. A New Obligately Chemolithoautotrophic, Nitrite-Oxidizing Bacterium, *Nitrospira moscoviensis sp*.nov and Its Phylogenetic Relationship. *Archives of Microbiology* 164(1):16-23.

EPA. 1993. Manual of Nitrogen Control. Washington, DC, USA: US Environmental Protection Agency.

Eum Y, Choi E. 2002. Optimization of nitrogen removal from piggery waste by nitrite nitrification. *Water Science and Technology* 45(12):89-96.

Gabriel D. 2000. Monitoring and modelling applied to the control of a pilot wastewater treatment plant with nutrient removal (in Catalan). PhD Thesis. Bellaterra: Universitat Autònoma de Barcelona.

Guisasola A. 2005. Modelling biological organic matter and nutrient removal processes from wastewater using respirometric and titrimetric techniques. PhD Thesis. Bellaterra: Universitat Autònoma de Barcelona.

Guisasola A, Baeza JA, Carrera J, Casas C, Lafuente J. 2003. An off-line respirometric procedure to determine inhibition and toxicity of biodegradable compounds in biomass from an industrial WWTP. *Water Science and Technology* 48(11-12):267-275.

Head IM, Hiorns WD, Embley TM, McCarthy AJ, Saunders JR. 1993. The Phylogeny of Autotrophic Ammonia-Oxidizing Bacteria as Determined by Analysis of 16s Ribosomal-Rna Gene-Sequences. *Journal of General Microbiology* 139:1147-1153.

Hellinga C, Schellen AAJC, Mulder JW, Van Loosdrecht MCM, Heijnen JJ. 1998. The SHARON process: An innovative method for nitrogen removal from ammonium-rich waste water. *Water Science and Technology* 37(9):135-142.

Henze M, Gujer W, Mino T, Van Loosdrecht M. 2000. Activated sludge models ASM1, ASM2, ASM2D and ASM3. Scientific and technical report no. 9. London: IWA Publishing.

Hippen A, Helmer C, Kunst S, Rosenwinkel KH, Seyfried CF. 2001. Six years' practical experience with aerobic/anoxic deammonification in biofilm systems. *Water Science and Technology* 44(2-3):39-48.

Hu Z, Chandran K, Grasso D, Smets BF. 2002. Effect of nickel and cadmium speciation on nitrification inhibition. *Environmental Science and Technology* 36(14):3074-3078.

Jeppsson U. 1996. Modelling aspects of wastewater treatment processes. PhD Thesis. Lund: Lund Institute of Technology (LTH).

Jetten MSM, Strous M, van de Pas-Schoonen KT, Schalk J, van Dongen UGJM, van de Graaf AA, Logemann S, Muyzer G, van Loosdrecht MCM, Kuenen JG. 1998. The anaerobic oxidation of ammonium. *FEMS Microbiology Reviews* 22(5):421-437.

Jetten MSM, Wagner M, Fuerst J, van Loosdrecht M, Kuenen G, Strous M. 2001. Microbiology and application of the anaerobic ammonium oxidation ('anammox') process. *Current Opinion in Biotechnology* 12(3):283-288.

Khin T, Annachhatre AP. 2004. Novel microbial nitrogen removal processes. *Biotechnology Advances* 22(7):519-532.

Kuai LP, Verstraete W. 1998. Ammonium removal by the oxygen-limited autotrophic nitrification-denitrification system. *Applied and Environmental Microbiology* 64(11):4500-4506.

López-Fiuza J, Buys B, Mosquera-Corral A, Omil F, Méndez R. 2002. Toxic effects exerted on methanogenic, nitrifying and denitrifying bacteria by chemicals used in a milk analysis laboratory. *Enzyme and Microbial Technology* 31(7):976-985.

Mace S, Dosta J, Gali A, Mata-Alvarez J. 2006. Optimization of biological nitrogen removal via nitrite in a SBR treating supernatant from the anaerobic digestion of municipal solid wastes. *Industrial and Engineering Chemistry Research* 45(8):2787-2792.

Manipura A, Duncan JR, Roman HJ, Burgess JE. 2005. Potential biological processes available for removal of nitrogenous compounds from metal industry wastewater. *Process Safety and Environmental Protection. ICHEME* 83(B5):474-480.

Pijuan M. 2004. Effect of different carbon sources and continous aeration on the EBPR process. PhD Thesis. Bellaterra: Universitat Autònoma de Barcelona.

Poch M. 1999. Les qualitats de l'aigua. Barcelona: Departament de Medi Ambient. Generalitat de Catalunya.

Pommerening-Röser A, Rath G, Koops HP. 1996. Phylogenetic diversity within the genus Nitrosomonas. *Systematic and Applied Microbiology* 19(3):344-351.

Pynaert K, Smets BF, Beheydt D, Verstraete W. 2004. Start-up of Autotrophic Nitrogen Removal Reactors via Sequential Biocatalyst Addition. *Environmental Science and Technology* 38(4):1228-1235.

Schmid M, Twachtmann U, Klein M, Strous M, Juretschko S, Jetten M, Metzger JW, Schleifer KH, Wagner M. 2000. Molecular evidence for genus level diversity of bacteria capable of catalyzing anaerobic ammonium oxidation. *Systematic and Applied Microbiology* 23(1):93-106.

Schmidt I, Sliekers O, Schmid M, Bock E, Fuerst J, Kuenen JG, Jetten MSM, Strous M. 2003. New concepts of microbial treatment processes for the nitrogen removal in wastewater. *FEMS Microbiology Reviews* 27(4):481-492.

Schramm A. 2003. In situ analysis of structure and activity of the nitrifying community in biofilms, aggregates, and sediments. *Geomicrobiology Journal* 20(4):313-333.

Shiskowski DM, Mavinic DS. 1998. Biological treatment of a high ammonia leachate: Influence of external carbon during initial startup. *Water Research* 32(8):2533-2541.

Sliekers AO, Derwort N, Gomez JLC, Strous M, Kuenen JG, Jetten MSM. 2002. Completely autotrophic nitrogen removal over nitrite in one single reactor. *Water Research* 36(10):2475-2482.

Strous M, Fuerst JA, Kramer EHM, Logemann S, Muyzer G, van de Pas-Schoonen KT, Webb R, Kuenen JG, Jetten MSM. 1999. Missing lithotroph identified as new planctomycete. *Nature* 400(6743):446-449.

Teichgräber B. 1993. Control strategies for a highly loaded biological ammonia elimination process. *Water Science and Technology* 28(11-12):531-538.

Terada A, Hibiya K, Nagai J, Tsuneda S, Hirata A. 2003. Nitrogen removal characteristics and biofilm analysis of a membrane-aerated biofilm reactor applicable to high-strength nitrogenous wastewater treatment. *Journal of Bioscience and Bioengineering* 95(2):170-178.

Teske A, Alm E, Regan JM, Toze S, Rittmann BE, Stahl DA. 1994. Evolutionary Relationships among Ammonia-Oxidizing and Nitrite-Oxidizing Bacteria. *Journal of Bacteriology* 176(21):6623-6630.

Torrijos M, Carrera J, Lafuente J. 2004. Improving the biological nitrogen removal process in pharmaceutical wastewater treatment plants: a case study. *Environmental Technology* 25:423-431.

Turk O, Mavinic DS. 1987. Benefits of using selective inhibition to remove nitrogen from highly nitrogenous wastes. *Environmental Technology Letters* 8(9):419-426.

Turk O, Mavinic DS. 1989. Maintaining nitrite build-up in a system acclimated to free ammonia. *Water Research* 23(11):1383-1388.

Udert KM, Fux C, Münster M, Larsen TA, Siegrist H, Gujer W. 2003. Nitrification and autotrophic denitrification of source-separated urine. *Water Science and Technology* 48(1):119-130.

UNESCO. 2006. Water, a shared responsibility. The United Nations World Water Development Report 2. Paris, France: UNESCO.

Van Dongen U, Jetten MSM, Van Loosdrecht MCM. 2001. The SHARON®-Anammox® process for treatment of ammonium rich wastewater. *Water Science and Technology* 44(1):153-160.

Van Hulle SWH, Volcke EIP, López Teruel J, Donckels BMR, Van Loosdrecht MCM, Vanrolleghem P. Influence of temperature and pH on the kinetics of the SHARON nitritation process. *In: Proceedings of 4th IWA World Water Congress and Exhibition* 2004; Marrakech, Morocco. IWA Publishing.

Villaverde S, Fdz-Polanco F, García PA. 2000. Nitrifying biofilm acclimation to free ammonia in submerged biofilters. Start-up influence. *Water Research* 34(2):602-610.

Volcke EIP, Van Hulle SWH, Donckels BMR, van Loosdrecht MCM, Vanrolleghem PA. 2005. Coupling the SHARON process with Anammox: Model-based scenario analysis with focus on operating costs. *Water Science and Technology* 52(4):107-115.

Watson SW, Bock E, Harms H, Koops HP, Hooper A. 1989. Nitrifying bacteria. In: Staley JT, Bryant MP, Pfennig N, Holt JG, editors. *Bergey's manual of systematic bacteriology, vol 3*. Baltimore: The Willians & Wilkins Co. p 1808-1834.

WEF. 1992. Design of municipal wastewater treatments plants. Water Environment Federation. Alexandria, USA: Water Environment Federation.

Wiesmann U. 1994. Biological nitrogen removal from wastewater. *Advances in biochemical engineering/biotechnology* 51:113-154.

Woese CR, Weisburg WG, Hahn CM, Paster BJ, Zablen LB, Lewis BJ, Macke TJ, Ludwig W, Stackebrandt E. 1985. The Phylogeny of Purple Bacteria - the Gamma-Subdivision. *Systematic and Applied Microbiology* 6(1):25-33.

WPCF. 1983. Nutrient control. Manual of practice FD-7. Washington: The Water Pollution Control Federation.

PART I - Chapter 2

OBJECTIVES

The main objective of this thesis is the partial nitrification of highly concentrated ammonium wastewater using automatic control to achieve stable and robust operation. This objective includes the study of this process from different points of view and using different tools (modeling, respirometry and microbiology techniques) in order to improve the knowledge of the process.

Other goals to be achieved during this thesis are:

- The development and calibration of a nitrification model considering: (1) the nitrification as a two-step process; (2) the inhibitions due to ammonia and nitrous acid and (3) the growth of nitrifiers and heterotrophs.

- The development of the hydraulic model of the experimental system (reactors and settler) to be used together with the nitrification model to be able to simulate the behavior of the system.

- The development and study of the best methodology for biomass fractions determination using microbiological tools.

- The development and application of the best strategy to start up a complete nitrification system from an urban WWTP sludge.

- The development and application of the best strategy to start up a partial nitrification system from an enriched nitrification population (complete nitrification) and its stable operation in the long term.

PART II - Chapter 3

NITRIFICATION MODEL: DEVELOPMENT AND CALIBRATION

Part of this chapter was presented as oral presentation:

Jubany I, Carrera J, Baeza JA, Lafuente J. Modeling biological nitrite oxidation including biomass growth and substrate inhibition using only oxygen uptake rate measurements. 4th IWA World Water Congress and Exhibition. Marrakech, Marocco September 2004.

Parts of this chapter were published as:

Carrera J, **Jubany I**, Carvallo L, Chamy R, Lafuente J. (2004) Kinetic models for nitrification inhibition by ammonium and nitrite in a suspended and an immobilized biomass systems. Process Biochemistry. 39 1159-1165.

Guisasola A, **Jubany I**, Baeza JA, Carrera J, Lafuente J. (2005) Respirometric estimation of the oxygen affinity constants for biological ammonium and nitrite oxidation. Journal of Chemical Technology and Biotechnology. 80 388-396

Jubany I, Baeza JA, Carrera J, Lafuente J. (2005) Respirometric calibration and validation of a biological nitrite oxidation model including biomass growth and substrate inhibition. Water Research. 39(18) 4574-4584.

Part of this chapter is in preparation for publication as:

Jubany I, Baeza JA, Carrera J, Lafuente, J. Respirometric determination of NOB inhibition coefficient for free ammonia. Environmental Technology.

A mathematical model to describe a nitrifying activated sludge system was developed. It considered nitrification as a two-step process and took into account the heterotrophic bacteria and their related processes. Free ammonia and free nitrous acid were considered the real substrates and inhibitors for nitrifying bacteria. Temperature and pH effects on the model parameters were also included. Specific experiments were designed for parameter estimation and parameter identifiability tools were used to analyze and improve them. Optimal experimental designs were used to calibrate most of the model parameters and the values obtained were compared with values found in the literature. It was demonstrated that although the values in the literature are quite scattered, the estimated values were in accordance with those previously reported. Affinity constants for substrate and substrate inhibition coefficients were estimated twice using different sludges and, as a result, different values were found indicating that they can change depending on the biomass acclimation.

1. INTRODUCTION

Several models have been used to describe the nitrification. Most of them consider the ammonium oxidation as a one-step process and are based on the Activated Sludge Model no.1, ASM1 (Henze et al. 2000). Chandran and Smets (2000a; 2000b) demonstrated that two-step models are needed to describe nitrification batch experiments when nitritation and nitratation rates are similar or when the nitratation process is the limiting process. There are some conditions under which this behavior is observed: high temperature (Hellinga et al. 1998), low dissolved oxygen (Chung et al. 2007) and existence of inhibitors (Kim and Seo 2006). Therefore, several studies have been published using two-step models for the description of the nitrification process (Gee et al. 1990; Hao et al. 2002b; Nowak et al. 1995; Sheintuch et al. 1995; Wett and Rauch 2003; Wyffels et al. 2004).

The use of two-step models is specially required when dealing with high-strength ammonium wastewater because ammonium oxidizing bacteria (AOB) and nitrite oxidizing bacteria (NOB) can be easily inhibited by ammonium and nitrite. Anthonisen et al. (1976) already demonstrated the existence of substrate inhibition of AOB and NOB and the inhibition of NOB due to ammonium. In fact, they postulated and demonstrated that free ammonia (FA) and free nitrous acid (FNA) concentrations, rather than ammonium or nitrite ion concentrations, inhibit nitrification. They performed several experiments under different conditions and with different systems which allowed them to draw a chart in which the degree of inhibition of nitritation and nitratation processes can be determined depending on the pH. Other authors have also found inhibition of AOB due to FNA (Carrera 2001; Van Hulle et al. 2004). Inhibition of AOB and/or NOB due to nitrate is not usually included in the available models since the authors did

not detect it. Only a reference was found where *Nitrobacter agilis* activity was negatively affected by nitrate (Hunik et al. 1994a).

Usually substrate inhibition is modeled with a Haldane-type of equation (Carvallo et al. 2002; Picioreanu et al. 1997; Sheintuch et al. 1995) as shown in equation 3.1. However, other type of equation has also been used. For example, in Wett and Rauch. (2003), a non competitive inhibition was used whereas in Gee et al. (1990) a modification of the Haldane expression including ammonium inhibition was considered in the nitratation expression.

$$r = r_{max} \cdot \frac{S}{K_S + S + \frac{S^2}{K_I}} \tag{3.1}$$

In equation 3.1, r and r_{max} are the current and maximum process rates, S is the substrate concentration, K_S is the substrate affinity coefficient and K_I is the substrate inhibition coefficient.

With respect to ammonium inhibition to NOB and nitrite inhibition to AOB, they are usually modeled as non competitive inhibitions (Gee et al. 1990; Pambrun et al. 2006) with an expression like equation 3.2, where K_I is the non-competitive inhibition coefficient and S_I is the inhibitory compound concentration. Nevertheless, recently, Vadivelu et al. (2006a) found that this was not the appropriate expression for the description of FNA effect on a *Nitrosomonas* culture.

$$r = r_{max} \cdot \frac{K_I}{K_I + S_I} \tag{3.2}$$

A complete model to accurately describe the existing biological reactions occurring in a basically nitrifying system should evidently consider the processes related to AOB and NOB (growth and decay) but also the processes related to heterotrophic bacteria. It has been demonstrated that the fraction of heterotrophic bacteria in a system with very low chemical oxygen demand (COD) concentration in the influent is high enough to be taken into account. For example, Vadivelu et al. (2006b) found 82 % of *Nitrosomonas* sp. and no NOB in a sequencing batch reactor (SBR) reactor which was fed with synthetic wastewater devoid of COD and Vadivelu et al. (2006d) found 73 % of *Nitrobacter* in a SBR reactor fed with only nitrite and trace elements. They considered that the remaining fractions (18 % and 27 % respectively) were heterotrophs. Heterotrophs always exist in the nitrification mixed cultures because they grow from the decay products of the nitrifiers. Liebig et al. (2001) reported 50 % of bacteria other than nitrifiers in a membrane-assisted bioreactor and concluded that they could not had grown only from the influent COD of the reject water. This result showed that the COD resulting from nitrifier decay had to be accounted for as a significant carbon source in that system. Therefore an extensive model should include, at least, the growth and decay of

heterotrophs and the processes related to the decay products (hydrolysis, ammonification, etc.). However, these processes are not needed if only the nitrogenous compounds are to be studied (Bernet et al. 2005; Gee et al. 1990; Nowak et al. 1995). In this thesis, all these processes were indeed considered since the total biomass concentration and the biomass fractions were also modeled.

Once the mathematical model is defined, a value for each model parameter must be assigned. Usually, all the parameters are taken from literature, especially when performing theoretical studies which do not compare the results obtained by simulation with experimental data (Coelho et al. 2000; Hao et al. 2002b). In other cases, only some of the parameters are calibrated with specific experiments in order to fit the experimental data to the model prediction (Moussa et al. 2005; Wyffels et al. 2004). However, the widely scattered values found in the literature for each parameter makes it difficult to choose the appropriate ones to describe a specific system, especially if it is taken into account that they were usually estimated with different methods and under different conditions. Furthermore, it has been demonstrated that the population in a nitrifying sludge can vary significantly from one system to another (Egli et al. 2003), which implies that the proper values for the model parameters can also be different.

Respirometry is the measurement and interpretation of the biological oxygen consumption rate under well-defined experimental conditions (Spanjers et al. 1997). This technique is widely used in the calibration of biological models since it can be easily implemented and it allows obtaining a high frequency of measurements and increasing the data information content of an experiment. Therefore, batch respirometric experiments are frequently used to calibrate nitrification models (Brouwer et al. 1998; Spanjers and Vanrolleghem 1995). All these studies are based on short-term batch experiments with low initial substrate concentration, where the growth and decay kinetics can be neglected. In order to estimate the maximum specific growth rate of AOB and NOB ($\mu_{max,A}$, $\mu_{max,N}$), the value of the growth yields (Y_A and Y_N) and the populations concentration are required (X_A and X_N). The difficulties in the estimation of each specific bacterial group concentration led to the estimation of parameters combinations such us $\mu_{max,A} \cdot X_A$ and $\mu_{max,N} \cdot X_N$ or even $\mu_{max,A} \cdot X$ and $\mu_{max,N} \cdot X$, where X is the total biomass concentration provided that the growth yields are known (Chandran and Smets 2005; Gernaey et al. 2001; Gernaey et al. 1998). In Novák et al. (1994), autotrophic and heterotrophic bacteria concentrations ($X_{autotrophic}$ and X_H) were calculated with the simulation of the experimental continuous system and then, they were used in the estimation of maximum specific growth rates of nitrifiers (as one-step process) and heterotrophs with batch respirometric experiments. Therefore the estimated maximum growth rates were dependent on the parameters used in the simulation, basically the growth yields and the decay rates. Other works use the total biomass concentration and the growth yields to determine X_A and X_N but without taking into account the heterotrophic bacteria (Chandran and Smets 2000a; Gee et al. 1990). Copp and Murphy (1995) developed an in situ nitrifier mass estimation technique to determine the nitrifier

population within an activated sludge sample using dominant cultures of nitrifying organisms (*Nitrosomonas europaea* and *Nitrobacter agilis*). They used the obtained fraction to estimate some model parameters of the mixed population and of the NOB population. Other methods for the estimation of the maximum specific growth rate involve monitoring the nitrogenous compounds (ammonia, nitrite and nitrate) instead of the oxygen uptake rate (OUR) in batch or continuous experiments but assuming some simplifications in the mathematical description (Antoniou et al. 1990; Sözen et al. 1996; Yuan et al. 1999). However, these methods are only adequate for the determination of the global maximum specific growth rate of nitrifiers.

The most common technique used for the determination of the bacterial decay rate is the measurement of the decrease of the respiration activity (usually with short respirometric batch tests) over time when bacteria are kept under starvation conditions (Copp and Murphy 1995; Spanjers and Vanrolleghem 1995). The plot of the natural logarithm of the respiration rate versus time gives a straight line with a slope of minus decay rate (–b). However, Dold et al. (2005) pointed out that this technique does not accurately estimate the decay rate because it does not consider the autotrophic growth on organic nitrogen lysed from heterotrophs. Furthermore, they demonstrated that the correct estimation of the decay rate is important for the following determination of the maximum specific growth rate in most of the available methods. On the other hand, Vadivelu et a. (2006b; 2006d) determined decay rates of enriched *Nitrosomonas* and *Nitrobacter* cultures with a respirometric in-situ method considering the heterotrophs.

With respect to the inhibition coefficients and affinity constant for substrate, they can easily be obtained with respirometric experiments in which the bacterial activity is measured at different concentrations of substrate or inhibitory compound (Carvallo et al. 2002; Picioreanu et al. 1997; Sheintuch et al. 1995; Van Hulle et al. 2004). However, these kinetic coefficients depend on the sludge adaptation to different levels of the inhibitory compound or substrate concentration (Antileo et al. 2002) and therefore they should be evaluated for each specific sludge and conditions.

It is noticeable that the estimation of most of the model parameters is not a trivial issue and that it often require the previous determination of other model parameters and the biomass concentration. Another difficulty, particularly when calibrating parameters using only OUR data, is the possible correlation between the parameters that makes it impossible to give a unique value to each one. In order to study this phenomenon, some tools were developed. On the one hand, the structural identifiability analysis is a mathematical tool to determine the identifiable parameters or combination of parameters of a model, and it depends only on the model structure. Some examples of this analysis can be found in Petersen et al. (2003) and Dochain and Vanrolleghem (2001). On the other hand, the practical identifiability analysis shows whether a structurally identifiable model is practically identifiable with the available experimental data. In addition, this analysis can be used for parameter uncertainty evaluation and optimal experimental design (Vanrolleghem et al. 1995).

Selective inhibitors of nitritation and nitratation processes are often required in calibration experiments in order to uncouple these processes. The most used nitritation inhibitor is allylthiourea (ATU: CH_2=$CHCH_2NHCSNH_2$). It was used for example, in Surmacz-Gorska (1996) and Nowak et al. (1994) to distinguish the OUR due to nitrification from the endogenous OUR, because it selectively inhibits nitritation probably by chelating the copper of the ammonia monooxygenase active site (Ginestet et al. 1998). Ginestet et al. (1998) studied the effect of ATU on nitritation, nitratation, heterotrophic growth and endogenous decay of a mixed population. They found that at 86 μM (10 mg L^{-1}), it selectively, instantaneously and completely inhibited nitritation without affecting the other processes. Chandran and Smets (2000b) achieved successful inhibition of nitritation by biomass incubation with 2 mg L^{-1} ATU and 2 mg $N\text{-}NH_4^+$ L^{-1} for 60 min without affecting nitratation.

With respect to the nitratation inhibition, there exist two compounds which are usually used. One of them is chlorate (ClO_3^-). It was also used in Surmacz-Gorska et al. (1996) and Nowak et al. (1994). Belser and Mays (1980) studied the effect of this compound to pure strains of AOB and NOB and also to soils and sediments. They concluded that 10 mM of chlorate was the appropriate concentration to selectively inhibit pure cultures of NOB even though using mixed cultures the inhibition was not always complete. The effect on AOB was negligible. However, deeper studies using *Nitrosomonas europaea* and *Nitrobacter winogradskyi* showed that the latter organism reduces chlorate to chlorite (ClO_2^-) which then inhibits both nitritation and nitratation processes (Hynes and Knowles 1983). Thus, when working with mixed cultures, inhibition tests should be previously performed. The other widely used inhibitory compound for nitratation is azide (sodium azide: NaN_3), which is a selective bacteriostatic agent that is active against gram-negative (Ginestet et al. 1998). It was successfully used in Sánchez et al. (2001) and Chandran and Smets (2000b). Ginestet et al. (1998) demonstrated that it can be used as a selective inhibitor of nitratation because at a concentration of 24 μM (1.56 mg L^{-1}) it does not affect the endogenous, ammonia-dependent, acetate-dependent respiration rates of mixed cultures but does instantaneously and completely inhibit nitrite oxidation. They also demonstrated that the inhibition is reversible. It must be stated that higher concentrations (>100 μM) also affects nitritation.

2. OBJECTIVES

The first objective is to develop a mathematical model considering the nitrification as a two-step process, taking into account the heterotrophic biomass and their related processes and considering the temperature and pH effect on the model parameters. The second objective is to calibrate the nitritation and nitratation parameters with well-designed specific experiments. The final model and its parameters should be appropriate to describe the performance of the nitrifying activated sludge system shown in the following chapters.

3. MATERIALS AND METHODS

This section includes the description of the two respirometers (named respirometer and reactor) and the two respirometric techniques used for parameter determination. In fact, different methods were used for similar purposes, but since these experiments were carried out along the thesis, the methods were being improved as new experience and knowledge were gained. This section also gives the main ideas for optimal experimental design for parameter estimation and for the assessment of the parameter estimation confidence intervals using the FIM (Fisher Information Matrix). In the last part, a brief description of the used chemical analyses is pointed out. All the experiments in this chapter were performed with biomass from a nitrifying activated sludge system that was running in a pilot plant (described in Chapter 4).

3.1 RESPIROMETER DESCRIPTION

The respirometer consisted of a magnetically stirred vessel of 1 L capacity. Aeration was supplied from the bottom through a microdiffuser which ensured small air bubbles and good oxygen transfer from the gas phase to liquid phase. Figures 3.1 and 3.2 show a schematic representation and an overview photograph of the whole experimental setup. A massflow controller was used to provide the steady and specific air flow required for an accurate OUR calculation. The respirometer vessel was thermally controlled by submerging it into a bath. The pH was continuously measured with a pH probe (WTW-Sentix 81) and controlled by the automatic addition of acid or base by a microdispenser. Dissolved oxygen (DO) was measured with a WTW-CellOx 325 probe. These pH and DO probes were connected to a multiparametric reception equipment (WTW-Inolab 3). This multiparametric equipment was connected via RS232 to a PC that monitored the data and stored it in a Microsoft Excel sheet through a Visual Basic 6.0 software. This respirometer and the software were set up and programmed by Albert Guisasola during his PhD thesis (Guisasola 2005).

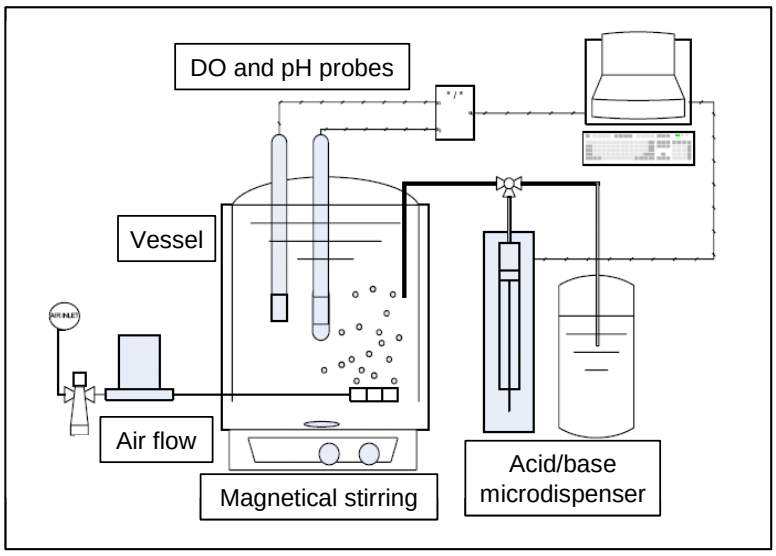

Figure 3.1 Schematic representation of the respirometer. Adapted from Guisasola (2005).

Figure 3.2 Respirometer picture. Obtained from Guisasola (2005).

3.2 LFS RESPIROMETRY IN THE RESPIROMETER

LFS respirometry refers to the respirometric technique in which the DO is measured in the liquid phase (L), the gas is flowing (F) and the liquid is static (S) according to the classification described in Spanjers et al. (1997). This technique was used to test the inhibitory concentration of the used specific inhibitors (ATU and azide) and to estimate the Y_A and Y_N and the NOB inhibition coefficient for FA ($K_{I,FA,N}$).

The DO balance in the liquid phase of an LFS respirometer considering constant volume and dividing the OUR into endogenous OUR (OUR_{end}) and exogenous OUR (OUR_{ex}) is shown in equation 3.3.

$$\frac{dS_O}{dt} = k_L a \cdot \left[S_O^* - S_O(t)\right] - OUR_{end} - OUR_{ex} \qquad (3.3)$$

where S_O is the DO concentration, k_La is the global oxygen transfer coefficient, S_O^* is the DO saturation concentration, OUR_{end} is the OUR in the absence of substrate from external sources and OUR_{ex} is the OUR in presence of external substrate (in this work, ammonium and/or nitrite).

The experimental procedure is as follows. First, biomass from the third reactor of the pilot plant (where total ammonium nitrogen (TAN) and total nitrite nitrogen (TNN) concentrations were usually low) was withdrawn and placed into the respirometer with the aeration and the temperature and pH controls on. If the biomass was already under endogenous conditions or it had been left for some hours without substrate, a substrate pulse was added before the start of the experiment. This pulse aimed to “wake up” the biomass because it was observed that after a long period under starvation conditions, the substrate consumption mechanisms were slowly activated and this could have negative effect on the obtained results (Marsili-Libelli and Tabani

2002; Vanrolleghem et al. 1998). When this substrate pulse was depleted, the aeration was stopped to calculate OUR_{end}. When the DO had dropped approximately 1 mg O_2 L^{-1}, the aeration was started again and the DO curve until the DO concentration reached the equilibrium value (S_{OE}) was used to calculate k_La. Equations 3.4 and 3.5 show the DO balance for the determination of OUR_{end} and k_La respectively,

$$\frac{dS_O}{dt} = -OUR_{end} \tag{3.4}$$

$$S_O(t) = (S_O(0) - S_{OE}) \cdot \exp(-k_L a \cdot t) + S_{OE} \tag{3.5}$$

where $S_O(0)$ is the DO concentration at time t = 0. It is important to determine k_La and S_{OE} before every experiment because they depend on environmental conditions such as temperature and barometric pressure and also on the properties of the liquid.

After k_La determination, the amount of substrate needed for the experiment was injected into the respirometer and the OUR_{ex} was calculated as shown in equation 3.6. It is important to note that although the OUR due to the external substrate should be named OUR_{ex}, it is usually named OUR. Therefore, when OUR is mentioned anyplace in this thesis, we actually mean OUR_{ex}. Endogenous OUR is always named OUR_{end}.

$$OUR_{ex} = k_L a \cdot [S_{OE} - S_O(t)] - \frac{dS_O}{dt} \tag{3.6}$$

Figure 3.3 shows an example of the DO profile of a "wake up" pulse, the DO profile for OUR_{end} and k_La determination and the DO profile of a first experimental pulse.

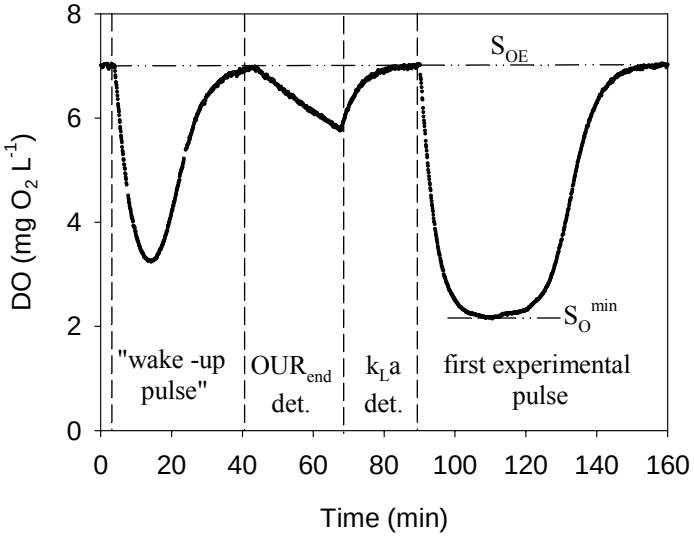

Figure 3.3 DO profile of a "wake up" pulse, OUR_{end} and k_La determination and first experimental pulse with LFS respirometry in the respirometer. S_{OE} and S_O^{min} are indicated.

It is important to previously test the experimental conditions such as biomass concentration, air flow and substrate pulse concentration because the DO drop and the experiment length depend on these conditions. The DO drop due to the substrate pulse must be high enough to clearly differentiate the S_{OE} to the reached minimum DO (S_O^{min}) to minimize the error in the OUR estimation; but it can not reach very low S_O^{min} to avoid high DO limitations. In addition, the time required for the pulse depletion should not be very long in order to be able to perform several pulses in one day. High biomass concentration, low air flow and high substrate concentration lead to low S_O^{min}. On the contrary, low biomass concentration, low air flow and high substrate concentration cause long experiments. The optimal solution must be tested for each different biomass and different experiment.

For an easier comprehension, the experimental pulses series and inhibitors addition for each specific parameter determination are detailed in section 4.

3.3 LSS RESPIROMETRY IN THE RESPIROMETER

LSS respirometry, following the classification in Spanjers et al. (1997), is the respirometric technique in which the DO is measured in the liquid phase (L) and both gas and liquid are static (SS). This technique was used here for the determination of the affinity constants for DO of AOB and NOB ($K_{O,A}$, $K_{O,N}$), for the determination of the inhibition coefficient and affinity constant for FA of AOB ($K_{S,FA,A}$ and $K_{I,FA,A}$) and for the determination of the inhibition coefficient for FNA of AOB ($K_{I,FNA,A}$). Two different methodologies were used in these experiments.

3.3.1 METHOD A: DO vs TIME

In this methodology, the experimental DO profile obtained due to the biological activity without air supply is fitted to the DO mass balance equation and the parameters are estimated. $K_{O,A}$ and $K_{O,N}$ were determined with this method.

Biomass from the pilot plant was withdrawn and placed in the respirometer vessel with air supply. When steady conditions of pH and temperature where reached and the “wake-up” pulse was depleted, the experimental amount of substrate was injected. Its concentration was chosen to be high enough to avoid substrate limitation but low enough to avoid substrate inhibition. When the maximum substrate consumption rate was achieved, the aeration was stopped and the DO drop was monitored until it reached ≈ 0 mg O_2 L^{-1}. The DO profile was then fitted to the corresponding DO mass balance equation in order to estimate the affinity constant for oxygen. In the $K_{O,A}$ estimation experiment, sodium azide was used to get rid of the nitratation process.

3.3.2 METHOD B: OUR vs SUBSTRATE/INHIBITOR CONCENTRATION

This methodology consists of the OUR measurement at different substrate or inhibitor concentrations. It was used to determine $K_{S,FA,A}$, $K_{I,FA,A}$ and $K_{I,FNA,A}$.

In the $K_{S,FA,A}$ and $K_{I,FA,A}$ determination, the procedure was as follows. First of all, biomass from the pilot plant was withdrawn and placed in the respirometer vessel with air supply under steady conditions of pH and temperature. After the "wake up" pulse depletion, the air supply was stopped and the DO was monitored until it reached 1.5 mg O_2 L^{-1} to calculate OUR_{end} as the slope of the DO profile between 2.5 and 1.5 mg O_2 L^{-1}. Then, the air supply was started again and a small amount of substrate was added. The air was stopped and a sample of the liquid was taken to analyze substrate concentration. DO was monitored until it again reached 1.5 mg O_2 L^{-1} and the air supply was started again until the DO surpassed 2.5 mg O_2 L^{-1}. Then it was stopped and started at least three times more in order to be able to estimate OUR in quadruplicate (see Figure 3.4 for an example of this methodology when there is exogenous substrate in the medium). Afterwards, the substrate concentration in the liquid was increased by the addition of more concentrated substrate pulses and the procedure was repeated as many times as experimental data were required. OUR_{ex} was calculated with the averaged value of the slopes of the DO drops and with OUR_{end} as shown in equation 3.7, where n is the number of OUR estimations with exogenous substrate under the same conditions.

$$OUR_{ex} = \frac{\sum_{i}^{n}\left(-\frac{dS_O}{dt}\right)_i}{n} - \left(-\frac{dS_O}{dt}\right)_{end} \qquad (3.7)$$

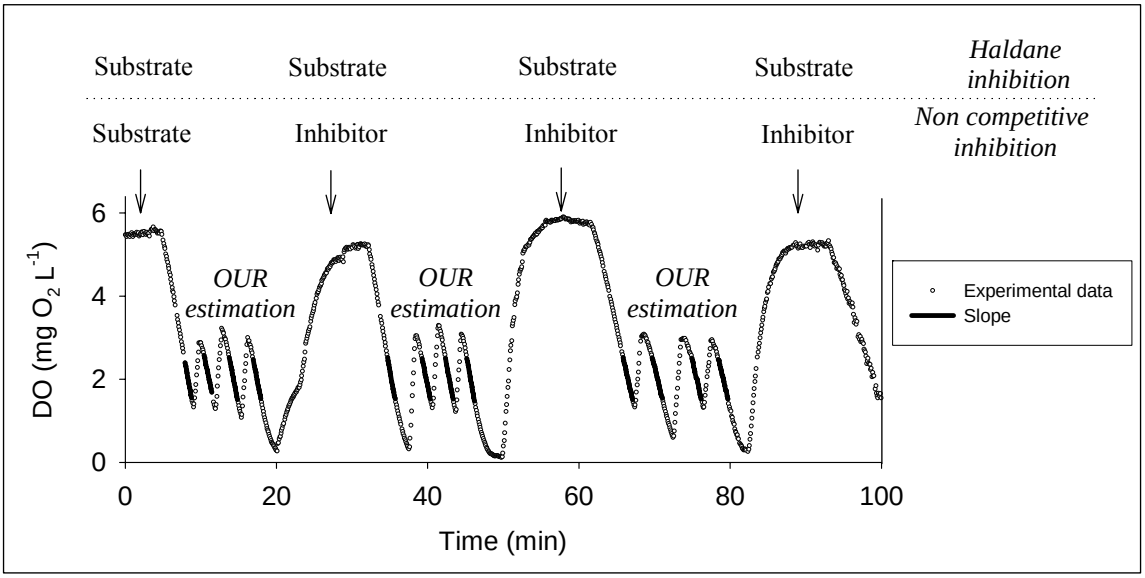

Figure 3.4 DO profile of a LSS respirometric experiment in the respirometer using method B. Experimental procedures are depicted for the determination of the parameters of substrate inhibition (Haldane equation) and non competitive inhibition.

This methodology was slightly modified when $K_{I,FNA,A}$ was determined because the substrate and the inhibitor were different compounds. The first pulse was a substrate pulse (TAN) of the appropriate concentration to avoid both substrate limitation and substrate inhibition. After four OUR estimations, some inhibitor (TNN) was added and a sample was taken to analyze both

substrate and inhibitor concentrations. Then, four OUR estimations were again monitored. This was repeated for several inhibitor concentrations. This procedure is also depicted in Figure 3.4.

It was important to maintain the environmental conditions (temperature, pH and range of DO) at least when the DO drops were taking place because the only parameter that should change was the substrate or inhibitor concentration.

3.4 PILOT PLANT REACTOR AS A RESPIROMETER

The other respirometer used for the determination of model parameters was one of the reactors of the pilot plant. Although the whole pilot plant is described in Chapter 4, one of the reactors is described here with the focus on its use as a respirometer for batch experiments.

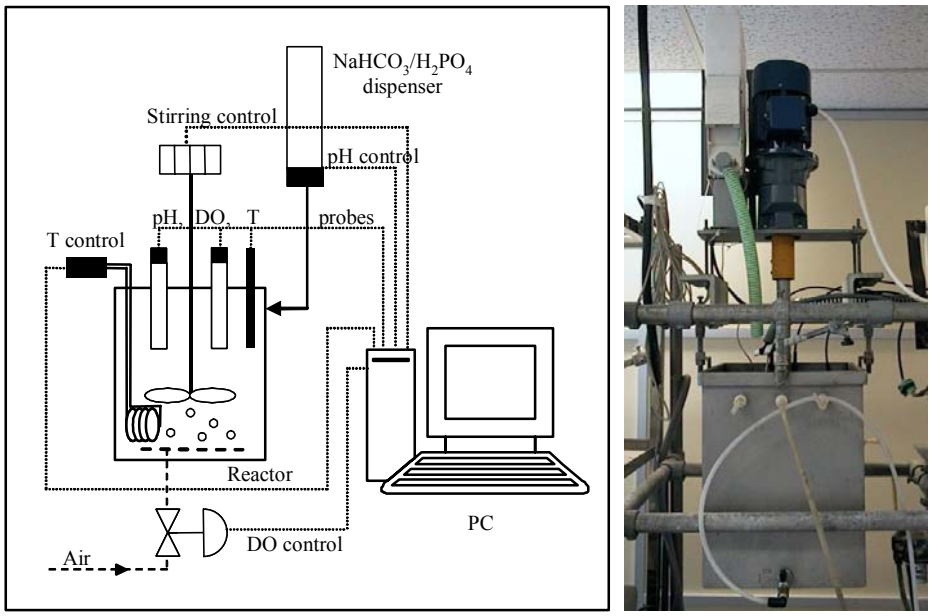

Figure 3.5 Schematic representation (left) and photograph (right) of the reactor used as a respirometer.

It consisted of a 26 L reactor with mechanical stirring and an air diffuser. DO, temperature and pH were measured in the liquid with a DO probe (WTW-Cellox 325), a pH probe (Crison-pHrocon18 controller) and a temperature probe (Pt100). Figure 3.5 shows a schematic diagram of this respirometer and a photograph of it. The pH was automatically controlled by the addition of solid $NaHCO_3$ or KH_2PO_4 depending on the experiment. The DO was maintained at a pre-selected set point with a control loop based on a digital PID algorithm. Temperature was also controlled using an electric device. When this reactor was used as a respirometer for parameter determination, the pilot plant had to be stopped. This was the main drawback of this methodology; however, some advantages were also obtained: (1) the high volume of the reactor enabled that high sample volume could be withdrawn with a high frequency; (2) steady experimental conditions (pH, temperature and DO concentration) could be easily maintained even during long experiments thanks to the implemented controllers. It must also be explained

that specific inhibitors were not used in the reactor because at least one third of the available biomass would had been wasted in the experiment.

3.5 LSS RESPIROMETRY IN THE REACTOR

Automatic OUR determination was already implemented in the reactor (Baeza et al. 2002). It was LSS respirometry since the OUR was calculated as the slope of the DO drop when the air supply was stopped. Each OUR measurement (performed every 5 minutes) began with the deactivation of the PID controller over aeration. Then, the aeration valve was shut down and the stirring speed reduced from normal operation (200 rpm) to 100 rpm to minimize surface oxygen transfer. Next, DO measurements were acquired every 4 seconds until the DO decreased by 1.5 mg O_2 L^{-1} or during a maximum period of 4 minutes. At this point, the stirring speed was increased to normal operation. Finally, the acquired measurements were fitted to a linear regression to calculate the OUR value. The dynamics of the sensor was not taken into account because the first DO measurements were not used in the regression analysis (Baeza et al. 2002).

Two different methodologies were used for parameter estimation. In method C, OUR vs time was measured and in method D, OUR vs substrate concentration was used.

3.5.1 METHOD C: OUR vs TIME

This methodology was used to estimate most of the kinetic parameters of NOB with a sole experiment. Fist of all, the influent and recycling pumps of the pilot plant were stopped and the connections within reactors were disconnected to avoid liquid circulation. The reactor used as respirometer was left under steady environmental conditions until all the accumulated TAN and TNN were completely removed and then OUR_{end} was estimated. Afterward, a pulse of substrate was added and the OUR was monitored. It was extremely important to maintain the environment conditions steady during the whole experiment. Finally, OUR_{end} was subtracted from each OUR measurement and the obtained OUR profile was fitted to the model that described the substrate depletion and biomass growth in order to calibrate the model parameters.

3.5.2 METHOD D: OUR vs SUBSTRATE CONCENTRATION

This methodology was the same than that explained in method B. It was used to determine the inhibition coefficient and affinity constant for FNA of NOB ($K_{S,FNA,N}$, $K_{I,FNA,N}$), $K_{S,FA,A}$ and $K_{I,FA,A}$.

First of all, the pilot plant pumps and inflow were stopped and the reactors isolated. The desired conditions of pH and temperature were set in the controllers. When endogenous conditions were reached, OUR_{end} was estimated in duplicate and then a substrate pulse (either TAN or TNN) was added. After two automatic OUR determinations more substrate was added.

Before each OUR determination, a sample was withdrawn to analyze the substrate concentration. This procedure was repeated as many times as experimental data were required. In order to obtain OUR_{ex}, OUR_{end} was subtracted from each OUR data.

Unlike in method C, where it is so important to keep the environmental conditions steady during the whole experiment, in method D, it is only important that these conditions are steady and equal during the OUR determinations but not the rest of the time. The reason is that each of the experimental point in method D is not related to the rest of the data points. On the contrary, in method C, all the points are connected by the time course.

3.6 CORRECTION TO DO MEASUREMENT

The high salt content of the activated sludge system (see Chapter 6) influenced the saturation oxygen concentration in the liquid since it decreases when the salt content increases. This phenomenon was taken into account in the oxygen probes calibration of the respirometers. Otherwise, OUR would have been overestimated and it would have led to erroneous parameter assessment.

3.7 THEORETICAL FRAMEWORK FOR OPTIMAL EXPERIMENTAL DESIGN FOR PARAMETER ESTIMATION (OEP/PE)

Optimal experimental design for parameter estimation (OED/PE) was used to compare the practical identifiability of the parameters obtained with different experimental procedures. It is based on the Fisher Information Matrix (FIM) (Dochain and Vanrolleghem 2001), which summarizes the information content of the experimental data because it considers the output sensitivity functions and the measurement errors of experimental data (i.e., precision of an experiment). In the present study, the FIM was estimated as detailed in equation 3.8:

$$FIM = \sum_{i=1}^{n} \left(\frac{\partial OUR}{\partial p}(t_i) \right)^T Q_i \left(\frac{\partial OUR}{\partial p}(t_i) \right) \tag{3.8}$$

where OUR is a vector of n values predicted by the model at times t_i (i = 1 to n), p is a vector containing all the estimated parameters and Q is a measurement error covariance matrix. In fact, in this case, Q is a 1x1 matrix because only OUR data were used and the error was considered the same along the time. The value for Q can be estimated as:

$$Q = \left(s^2\right)^{-1} = \left(\frac{SSE}{N - np} \right)^{-1} \tag{3.9}$$

where s is the measurement error, SSE is the squared sum errors of N measured values and np is the number of estimated parameters.

Different OED/PE criteria can be obtained using scalar measures of the FIM and its inverse (Dochain and Vanrolleghem 2001): determinant (det), trace (tr) and the smallest and largest eigenvalues (λ_{min} and λ_{max}) of the matrix. These criteria are summarized in Table 3.1.

Table 3.1 Criteria for OED/PE

Criterion name	Criterion	Optimal
A	$tr(FIM^{-1})$	Min
Modified A	tr(FIM)	Max
D	det(FIM)	Max
E	$\lambda_{min}(FIM)$	Max
Modified E	$\lambda_{max}(FIM)$ /$\lambda_{min}(FIM)$	Min

3.8 ASSESSMENT OF THE PARAMETER ESTIMATION CONFIDENCE INTERVALS

Assuming white measurement noise (i.e. independent and normally distributed with zero mean), no model mismatch, no data autocorrelation and uncorrelated errors, the inverse of the FIM provides the lower bound of the parameter estimation error covariance matrix, which can be used for assessing the estimation uncertainty of the optimal estimated parameters. In case only a single variable is measured, parameter confidence can be estimated as shown in equation 3.10 (Dochain and Vanrolleghem 2001):

$$\sigma(\theta_i) = \sqrt{\frac{J_{opt}(\theta)}{N - np} \cdot FIM_{ii}^{-1}} \qquad (3.10)$$

where $\sigma(\theta_i)$ is the estimated uncertainty of parameter θ_i, J_{opt} is the objective function value for the optimal parameters, N is the number of data and np is the number of parameters. This procedure was used in some of the parameters estimated in this chapter.

A comprehensive analysis of the influence of the quality and quantity of experimental data on the estimated parameters and the obtained standard errors can be found in Guisasola et al. (2006), where Haldane inhibition model is used as a case study.

3.9 PARAMETER ESTIMATION, MODELING AND SIMULATION

Parameter estimation and model prediction were performed with Matlab 6.5® (2002) when differential equations had to be solved. Differential equations were solved using an explicit Runge-Kutta formula (ode45). Parameter estimation was carried out by using the Nelder-Mead Simplex search method. Otherwise, the Regression tool of Sigmaplot® (2002) was used, which also calculates the confidence interval of the estimated parameters.

3.10 ANALYSES

TAN was analyzed by means of a continuous flow analyzer (CFA) based on potentiometric determination of ammonia (Baeza et al. 1999). TNN and nitrate were measured with capillary electrophoresis using a WATERS Quanta 4000E CE. The used electrolyte solution was a WATERS commercial solution and the conditions of the analyses were 20ºC, 15 kV from a negative source, indirect UV detection at 254 nm and 6 min of analysis (Carrera et al. 2003). Volatile suspended solids (VSS) were determined according to Standard Methods (APHA 1995).

4. RESULTS AND DISCUSSION

In this section, the development of the two-step nitrification model considering also heterotrophic biomass is firstly presented. Then, the calibration experiments are described starting with the parameters of NOB kinetics and ending with the parameters of AOB kinetics. This section also includes the discussion of the results, basically the comparison of the obtained results with parameters found in the literature and the examination of the better methods and experimental design for parameter estimation.

4.1 NITRIFICATION MODEL DEVELOPMENT AND DESCRIPTION

Nitrification was modeled as a two-step process which considered AOB and NOB populations because it was then used for the simulation of high-strength ammonium wastewater treatment. Heterotrophic bacteria were also included to be able to describe the total biomass concentration and the specific bacterial fractions. Table 3.2 shows the kinetics for each of the processes considered: growth and decay of each kind of bacteria, ammonification of soluble organic nitrogen, hydrolysis of entrapped organics and hydrolysis of entrapped organic nitrogen.

The process stoichiometry for this model is shown in Table 3.3. Six soluble compounds were considered (as concentration in the bulk liquid): total ammonia nitrogen (S_{TAN}), total nitrite nitrogen (S_{TNN}), nitrate (S_{NO3}), soluble biodegradable organic nitrogen (S_{ND}), dissolved oxygen (S_O) and readily biodegradable substrate (S_S). Inorganic carbon concentration (CO_2 or HCO_3^-) was not considered because it was always in excess due to the pH control and therefore it never limited the biomass growth. With respect to the particulate compounds, AOB (X_A), NOB (X_N), heterotrophic bacteria (X_H), inert products arising from biomass decay (X_P), slowly biodegradable substrate (X_S) and particulate biodegradable organic nitrogen (X_{ND}) were considered.

Table 3.2 Process kinetics for the two-step nitrification model including heterotrophic bacteria.

Process	Process rate (d^{-1})
1. Growth of X_A	$\mu_{max,A} \cdot \frac{S_O}{K_{O,A}+S_O} \cdot \frac{S_{TAN}}{K_{S,TAN,A}+S_{TAN}+\frac{S_{TAN}^2}{K_{I,TAN,A}}} \cdot \frac{K_{I,TNN,A}}{K_{I,TNN,A}+S_{TNN}} \cdot X_A$
2. Growth of X_N	$\mu_{max,N} \cdot \frac{S_O}{K_{O,N}+S_O} \cdot \frac{S_{TNN}}{K_{S,TNN,N}+S_{TNN}+\frac{S_{TNN}^2}{K_{I,TNN,N}}} \cdot \frac{K_{I,TAN,N}}{K_{I,TAN,N}+S_{TAN}} \cdot X_N$
3. Growth of X_H	$\mu_{max,H} \cdot \frac{S_O}{K_{O,H}+S_O} \cdot \frac{S_S}{K_{S,H}+S_S} \cdot X_H$
4. Decay of X_A	$b_A \cdot X_A$
5. Decay of X_N	$b_N \cdot X_N$
6. Decay of X_H	$b_H \cdot X_H$
7. Ammonification of S_{ND}	$k_a \cdot S_{ND} \cdot X_H$
8. Hydrolysis of X_S	$k_h \cdot \frac{X_S/X_H}{K_X+X_S/X_H} \cdot \frac{S_O}{K_{O,H}+S_O} \cdot X_H$
9. Hydrolysis of X_{ND}	$k_h \cdot \frac{X_S/X_H}{K_X+X_S/X_H} \cdot \frac{S_O}{K_{O,H}+S_O} \cdot X_H \cdot \frac{X_{ND}}{X_S}$

Table 3.3 Process stoichiometry for the two-step nitrification model including heterotrophic bacteria.

Compounds →	S_{TAN}	S_{TNN}	S_{NO3}	S_{ND}	S_O	S_S	X_A	X_N	X_H	X_P	X_S	X_{ND}
Process ↓	(mg N L^{-1})				(mg O_2 L^{-1})		(mg COD L^{-1})					(mg N L^{-1})
1. Growth of X_A	$-\frac{1}{Y_A} - i_{XB}$	$\frac{1}{Y_A}$	0	0	$-\frac{3.43 - Y_A}{Y_A}$	0	1	0	0	0	0	0
2. Growth of X_N	$-i_{XB}$	$-\frac{1}{Y_N}$	$\frac{1}{Y_N}$	0	$-\frac{1.14 - Y_N}{Y_N}$	0	0	1	0	0	0	0
3. Growth of X_H	$-i_{XB}$	0	0	0	$-\frac{1 - Y_H}{Y_H}$	$-\frac{1}{Y_H}$	0	0	1	0	0	0
4. Decay of X_A	0	0	0	0	0	0	-1	0	0	f_P	$1-f_P$	$i_{XB}-f_P \cdot i_{XP}$
5. Decay of X_N	0	0	0	0	0	0	0	-1	0	f_P	$1-f_P$	$i_{XB}-f_P \cdot i_{XP}$
6. Decay of X_H	0	0	0	0	0	0	0	0	-1	f_P	$1-f_P$	$i_{XB}-f_P \cdot i_{XP}$
7 Ammonification of S_{ND}	1	0	0	-1	0	0	0	0	0	0	0	0
8. Hydrolysis of X_S	0	0	0	0	0	1	0	0	0	0	-1	0
9. Hydrolysis of X_{ND}	0	0	0	1	0	0	0	0	0	0	0	-1

The terms TAN ($N\text{-}NH_4^+ + N\text{-}NH_3$) and TNN ($N\text{-}NO_2^- + N\text{-}HNO_2$) were used instead of ammonium and nitrite because they are the true compounds analyzed in the chemical analyses. Equations 3.11 and 3.12 were used for the calculation of the FA (NH_3) and the FNA (HNO_2) concentrations in equilibrium with TAN and TNN respectively. They are derived from the acid-base equilibrium of these compounds.

$$FA = \frac{TAN \cdot 10^{pH}}{\left(K_b / K_w + 10^{pH} \right)} \cdot \frac{17}{14} \tag{3.11}$$

$$FNA = \frac{TNN}{\left(K_a \cdot 10^{pH} + 1 \right)} \cdot \frac{47}{14} \tag{3.12}$$

In the entire thesis, FA is expressed in terms of mg NH_3 L^{-1}, FNA in mg HNO_2 L^{-1} and TAN and TNN in mg $N\text{-}NH_4^+$ L^{-1} and mg $N\text{-}NO_2^-$ L^{-1} respectively. The ratio between the ionization constant of the ammonia equilibrium (K_b) and the ionization constant of water (K_w) is related to the temperature as shown in equation 3.13, and the temperature effect on the ionization constant of the nitrous acid equilibrium (K_a) is shown in equation 3.14 (Anthonisen et al. 1976).

$$K_b / K_w = \exp\left(\frac{6344}{273 + T} \right) \tag{3.13}$$

$$K_a = \exp\left(\frac{-2300}{273 + T} \right) \tag{3.14}$$

It is important to differentiate TAN from NH_4^+ because at the working pH range (7-8.5) the NH_3 fraction can be large (the pK_a of the equilibrium at 25ºC is 9.2) and thus TAN is quite different from NH_4^+. With respect to TNN and NO_2^-, this difference is very small because the working pH range is quite far from the pK_a of the nitrite/nitrous acid equilibrium (at 25 ºC pK_a is 3.4) and thus, if NO_2^- was considered instead of TNN, the error would be minimal.

It is quite accepted that FA and FNA are the preferred substrates of AOB and NOB and also the inhibitory species (Anthonisen et al. 1976). If these statements are taken into account, the affinity constants for substrate and the inhibition coefficients used in this model should be considered constants in terms of FA and FNA ($K_{S,FA,A}$, $K_{S,FNA,N}$, $K_{I,FA,A}$, $K_{I,FNA,A}$, $K_{I,FNA,N}$, $K_{I,FA,N}$) and dependent on pH and temperature in terms of TAN and TNN ($K_{S,TAN,A}$, $K_{S,TNN,N}$, $K_{I,TAN,A}$, $K_{I,TNN,A}$, $K_{I,TNN,N}$, $K_{I,TAN,N}$). Therefore, equations 3.11 to 3.14 were included in the model.

In the AOB and NOB growth processes, a Monod expression was used to describe the kinetic dependence on the DO concentration. Affinity constants for oxygen ($K_{O,A}$ and $K_{O,N}$)

represented the DO concentration at which the nitritation or nitratation rates were half the maximum values. The substrate (TAN or TNN) effect on the growth process was considered with a Haldane expression since both AOB and NOB were inhibited by their own nitrogenous substrates. With respect to AOB, the affinity constant for TAN ($K_{S,TAN,A}$) and the inhibition coefficient for TAN ($K_{I,TAN,A}$) represented the TAN concentration at which the nitritation rate was half the maximum value due to substrate limitation and substrate inhibition respectively. In the same way, the affinity constant for TNN ($K_{S,TNN,N}$) and the inhibition coefficient for TNN ($K_{I,TNN,N}$) of NOB, represented the TNN concentration at which the nitratation rate was half the maximum value due to substrate limitation and substrate inhibition respectively. Moreover, a non competitive expression was also included in both AOB and NOB growth processes to consider the inhibition of AOB for TNN and the inhibition of NOB for TAN. Again, the value of the inhibition coefficients, $K_{I,TNN,A}$ and $K_{I,TAN,N}$, represented the TNN and TAN concentrations at which the growth rates were half the maximum values and were considered constant in terms of FNA and FA.

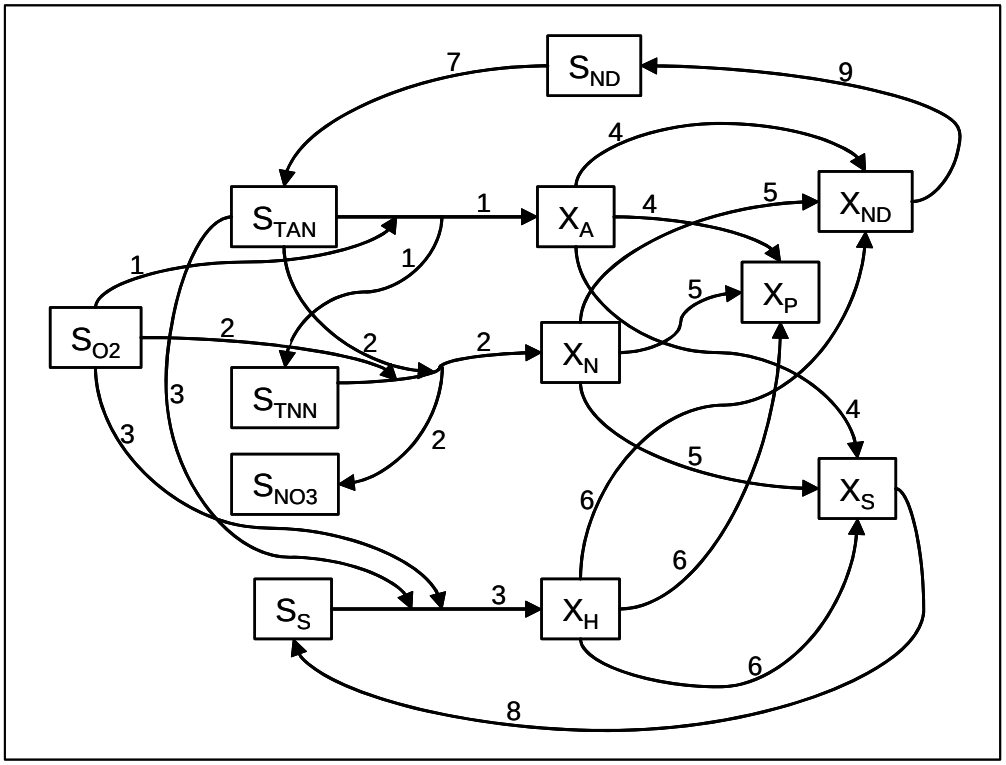

Figure 3.6 Diagram of the two-step nitrification model including heterotrophic bacteria. Numbers indicate processes according to Tables 3.2 and 3.3.

Nitratation inhibition by nitrate was reported in Hunik et al. (1994a). They found that high nitrate concentration produced a significant effect on a pure culture of Nitrobacter agilis (about 10 % reduction of the maximum nitratation rate at 250 mg $N\text{-}NO_3$ L^{-1}). However, this inhibition was not detected with the biomass used in this work. The absence of inhibition was tested with a specific experiment where the maximum OUR due to nitratation process was determined at several nitrate concentrations. The results showed no decrease of the maximum

OUR at the nitrate concentrations tested (up to 1000 mg $N\text{-}NO_3^-$ L^{-1}). Consequently, nitratation inhibition by product was not taken into account in the model.

Decay rates of AOB and NOB were modeled as first order processes with respect to X_A and X_N. The rest of the processes are related to the heterotrophic growth and were needed for the modeling of the total biomass concentration. The kinetic expressions were taken from ASM1 (Henze et al. 2000). Figure 3.6 shows a diagram that describes the interactions between the model compounds and the involved processes. Neither anoxic nor anaerobic growth was considered because the entire pilot plant was working under completely aerobic conditions.

4.2 SELECTIVE INHIBITORS FOR AOB AND NOB: ATU AND AZIDE

Selective inhibitors of nitritation and nitratation processes were required in some of the experiments. After studying the literature review shown in the introduction, ATU (10 mg L^{-1}) and azide (1.56 mg L^{-1}) were chosen. The reported inhibitory concentrations were tested with biomass from the pilot plant and LFS respirometry. Temperature and pH were kept constant around 25ºC and 7.5 respectively along the experiment. After OUR_{end} and k_La were determined, a pulse of TAN (25 mg N L^{-1}) was added to the medium and the DO was recorded. In order to check the effect of azide on the nitritation process, another pulse with both TAN (25 mg N L^{-1}) and azide was added. Finally, the biomass was changed and then a new pulse of TAN (25 mg N L^{-1}) was injected. Before TAN was totally consumed, ATU was added to test its effect on the nitritation process. OUR profile of each pulse was calculated from the DO profile. Figure 3.7.A shows that the two nitrification steps were clearly observed in the first pulse since the nitratation step was slower than the nitritation one under these experimental conditions. The total oxygen consumption (OC) related to this pulse (corresponding to the area under the OUR profile) was 108.4 mg O_2. If the second pulse is considered, it can be seen that the second shoulder, corresponding to the nitratation step, was not observed, which could indicate the occurrence of nitratation inhibition. Moreover, the OC in this second pulse was 81.8 mg O_2. The ratio of this value and the OC in the first pulse (0.755) is in agreement with the stoichiometric ratio of OC between nitritation and full nitrification: 0.75 (=3.43/4.57). This, together with the fact that the maximum OUR in both pulses was similar, clearly indicated that nitritation was not affected by the added amount of azide. However, nitratation was completely inhibited. The last pulse showed that nitritation inhibition by ATU was total and immediate and that it apparently did not have effect on nitratation.

The same experimental scheme was used to test these compounds on NOB. First, a pulse of TNN (60 mg N L^{-1}) was added. When it was depleted, a second pulse of TNN (60 mg N L^{-1}) and ATU was supplied. Finally, TNN was added again and when the maximum consumption rate was reached, azide was added. Figure 3.7.B shows the OUR profiles obtained for each pulse. If the first and second pulses are compared, the reached maximum OURs were the same and the calculated total OCs were almost equal: 63.4 and 63.8 mg O_2 respectively. This demonstrated that ATU did not inhibited nitratation. On the contrary, azide inhibited this

process just after addition as the third pulse shows. Therefore, both ATU and sodium azide could be used with biomass from the pilot plant as selective inhibitors for nitritation and nitratation process respectively at the tested concentrations.

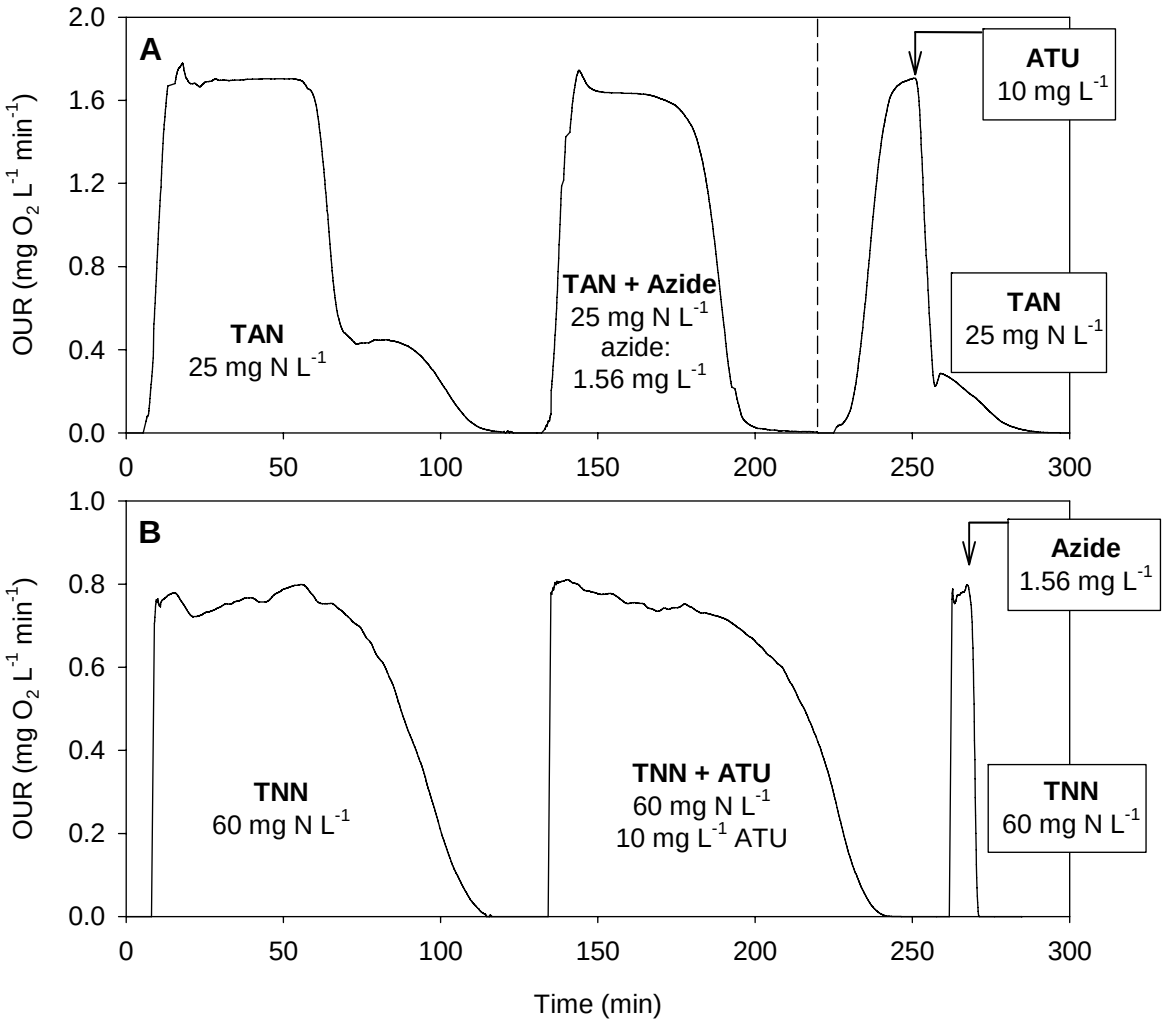

Figure 3.7 Assessment of nitritation and nitratation inhibition with ATU (10 mg L^{-1}) and sodium azide (1.56 mg L^{-1}). **A.** TAN pulses of 25 mg N L^{-1} without inhibitor, with sodium azide and with ATU. Dashed line indicates the use of new biomass. **B.** TNN pulses of 60 mg N L^{-1} without inhibitor, with ATU and with sodium azide.

4.3 GROWTH YIELD DETERMINATION OF AOB AND NOB (Y_A AND Y_N)

In this study, the growth yield is defined as the biomass produced as COD per oxidized nitrogen. This definition must be taken into account for the parameter determination and model development.

Dochain et al. (1995) and Petersen et al. (2003) studied the structural indentifiability of Monod-based activated sludge models and found that only some parameter combinations were identifiable when only OUR measurements were available. Most of these combinations

contained the biomass growth yield and the initial substrate concentration. In order to avoid identifiability problems in this thesis, the growth yields were determined with specific experiments and then they were used in the respirometric determination of other parameters such as maximum specific growth rate, affinity constants for substrate or inhibition coefficients.

First of all, Y_N was estimated using LFS respirometry in the respirometer. Several TNN pulses were performed with different known initial TNN concentration (TNN_{pulse} = 5, 10, 15 and 20 mg N L^{-1}). Actually, it could be done with only one pulse because only total OC and TNN_{pulse} concentration are required. However, it would result in too much uncertainty on the yield calculation because of the high sensitivity of this parameter to the OC and TNN_{pulse} values. Figure 3.8.A shows the results from the batch tests at 25 ºC and pH of 7.5 with biomass taken from the pilot plant.

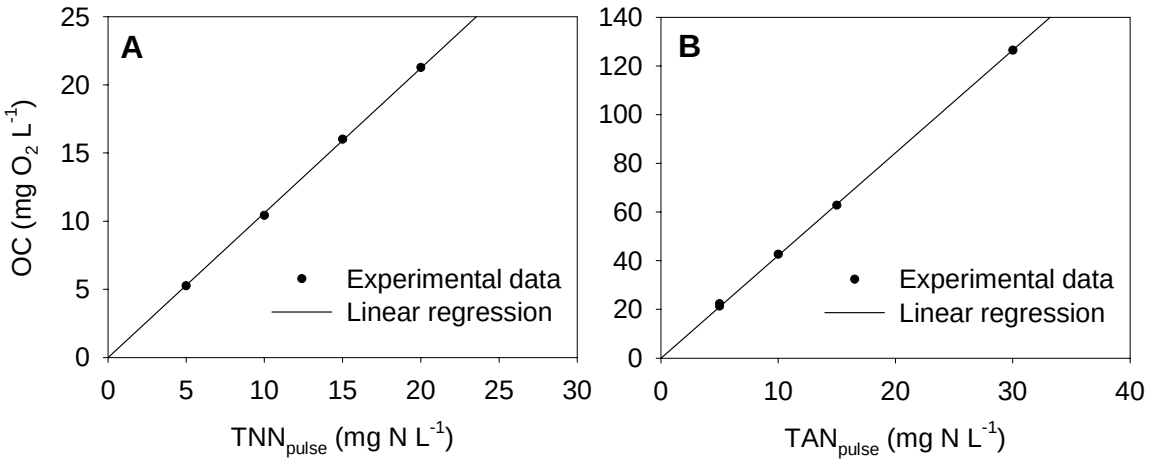

Figure 3.8 Biomass yields determination: OC as a function of the initial nitrogen concentration. **A.** TNN pulses for Y_N determination. **B.** TAN pulses for Y_A determination.

OC was calculated as the area under the exogenous OUR which was obtained from the DO profile of each batch experiment. Y_N was calculated from the slope of the linear regression of the experimental data and using equation 3.16. This equation is the compact form of equation 3.15 which was directly obtained from Table 3.3. Expression in the numerator is the OC per unit of produced X_N (stoichiometric coefficient of DO in the NOB growth process) and the expression in the denominator is the oxidized TNN per unit of produced X_N (stoichiometric coefficient of TNN in the NOB growth process).

$$\frac{OC}{TNN_{pulse}} = \frac{\dfrac{1.14 - Y_N}{Y_N}}{\dfrac{1}{Y_N}} \qquad \left[\frac{\dfrac{gO2_{sto,2} - gO2_{NOB}}{gO2_{NOB}}}{\dfrac{gN_{ox,2}}{gO2_{NOB}}} \right] \tag{3.15}$$

$$\frac{OC}{TNN_{pulse}} = 1.14 - Y_N \qquad \left[\frac{gO2_{sto,2} - gO2_{NOB}}{gN_{ox,2}}\right] \tag{3.16}$$

The units of these equations are detailed inside square brackets, where $O2_{sto,2}$ is the stoichiometric OC in the 2nd step of the nitrification process (nitratation), $O2_{NOB}$ is the COD produced in the NOB growth and $N_{ox,2}$ is the N-TNN oxidized to nitrate.

The slope obtained from the linear regression was 1.06 mg O_2 mg^{-1} N, and Y_N was calculated as 0.08 ± 0.01 g COD g^{-1} N (0.056 ± 0.007 g VSS g^{-1} N considering biomass as $C_5H_7NO_2$).

Y_A was calculated with a similar methodology: a set of experiments with different initial TAN concentration (TAN_{pulse} = 5, 5, 10, 15, 30 mg N L^{-1}) was performed at a temperature of 25ºC and a pH of 7.5. The experimental data and the linear regression for these respirometric experiments are shown in Figure 3.8.B. As already stated in Chandran and Smets (2000b), the assimilated TAN by AOB can not be ignored in the Y_A determination with respirometric experiments. In this study, TAN assimilated by NOB was also considered. Therefore, it was considered that some of the added TAN_{pulse} was oxidized to TNN (and then to nitrate), some was assimilated by AOB for growing and some was assimilated by NOB for growing. Equation 3.17 describes the relation between OC and TAN_{pulse} considering TAN assimilation for biomass growth by both nitrifying populations. This equation consists of two main terms: the OC due to nitritation (first term) and the OC due to nitratation (second term). These terms were basically obtained from Table 3.3. The first term includes the stoichiometric coefficients of DO and TAN for AOB growth and a conversion factor to account for the TAN assimilated for NOB growth. This conversion factor was needed because the stoichiometric coefficient of TAN for AOB growth (i.e. $1/Y_A+i_{XB}$) does not consider the amount of TAN assimilated for NOB growth, which TAN_{pulse} indeed includes. The second term was obtained from the stoichiometric coefficients of DO, TAN and TNN for NOB growth and was also corrected with a conversion factor. In this case, the conversion factor was needed to consider the TAN assimilated in the AOB growth process, which was not included in the expression $1/Y_N+i_{XB}$. Equation 3.18 is the compact form of equation 3.17.

$$\frac{OC}{TAN_{pulse}} = \frac{\frac{3.43 - Y_A}{Y_A}}{\frac{1}{Y_A} + i_{XB}} \cdot \frac{1 + Y_A \cdot i_{XB}}{1 + i_{XB} \cdot (Y_A + Y_N)} + \frac{\frac{1.14 - Y_N}{Y_N}}{\frac{1}{Y_N} + i_{XB}} \cdot \frac{1 + Y_N \cdot i_{XB}}{1 + i_{XB} \cdot (Y_A + Y_N)} \tag{3.17}$$

$$\left[\frac{\frac{gO2_{sto,1} - gO2_{AOB}}{gO2_{AOB}}}{\frac{gN_{ox,1} + gN_{AOB}}{gO2_{AOB}}} \cdot \frac{gN_{ox,1} + gN_{AOB}}{gN_{ox,1} + gN_{AOB} + gN_{NOB}} + \frac{\frac{gO2_{sto,2} - gO2_{NOB}}{gO2_{NOB}}}{\frac{gN_{ox,2} + gN_{NOB}}{gO2_{NOB}}} \cdot \frac{gN_{ox,2} + gN_{NOB}}{gN_{ox,2} + gN_{AOB} + gN_{NOB}}\right]$$

$$\frac{OC}{TAN_{pulse}} = \frac{4.57 - Y_A - Y_N}{1 + i_{XB} \cdot (Y_A + Y_N)} \qquad \left[\frac{gO2_{sto,1+2} - gO2_{AOB} - gO2_{NOB}}{gN_{ox,1} + gN_{AOB} + gN_{NOB}} \right] \tag{3.18}$$

The units of these equations are detailed inside square brackets following this nomenclature:

$O2_{sto,1}$: stoichiometric OC in the 1st step of nitrification (nitritation)
$O2_{sto,2}$: stoichiometric OC in the 2nd step of nitrification (nitratation)
$O2_{sto,1+2}$: stoichiometric OC in the whole nitrification process (nitritation+nitratation)
$O2_{AOB}$: COD produced in the AOB growth process
$O2_{NOB}$: COD produced in the NOB growth process
$N_{ox,1}$: N-TAN oxidized to nitrite
$N_{ox,2}$: N-TNN oxidized to nitrate (= $N_{ox,1}$ if nitrate was the only final product)
N_{AOB}: N-TAN assimilated due to AOB to grow
N_{NOB}: N-TAN assimilated due to NOB to grow

The nitrogen content of nitrifiers (i_{XB}) was previously determined by Guisasola (2005) with biomass from the pilot plant as 0.08 g N g^{-1} COD. Using this value, equation 3.18, the previously obtained Y_N and the slope of the linear regression on Figure 3.8.B (slope = 4.22), Y_A was calculated as 0.18 ± 0.01 g COD g^{-1} N (0.127 ± 0.007 g VSS g^{-1} N considering biomass as $C_5H_7NO_2$).

Table 3.4 Growth yields of AOB and NOB calculated in this work and values obtained from literature.

Y_A	Y_N	Methodology	Pure/mixed culture	Reference
(g VSS g^{-1} N)				
0.127	0.056	Respirometry	Mixed	This work
0.30	0.083	Batch experiments fitting	Mixed	Gee et al. (1990)
0.14	0.11	Experimental data fitting	Mixed	Sheintuch et al. (1995)
0.203*	0.08*	Respirometry and literature	Mixed	Chandran and Smets (2000a)
-	0.015	Experimental data fitting	Mixed	Copp and Murphy (1995)
0.15	0.042	From stoichiom. and literature	Pure	Wiesmann (1994)
0.12	0.042	From stoichiom. and literature	Pure	Hunik et al. (1994a)
0.05	0.02	Taken from literature	Pure	Knowles et al. (1965)
0.04-0.13	0.02-0.07	Taken from literature	Pure	EPA (1993)

* Original parameters were in terms of nitrogenous oxygen demand.

If the TAN assimilated by AOB and NOB was not considered, the calculated Y_A would be 0.27 g COD g^{-1} N (50 % error) and if only the TAN assimilated by AOB was taken into account the Y_A would be 0.20 g COD g^{-1} N (11 % error). These results show that, if the ammonium assimilation by both AOB and NOB is disregarded, Y_A is wrongly estimated. It also demonstrates the sensitivity of this calculation. These reasons may explain the wide range of values found in the literature (Table 3.4). Other reasons may be the variety of methods used for

its estimation, the fact that not all the pure or mixed population are identical and the definition of this parameter, which can be referred to oxidized nitrogen (as in this study) or to consumed nitrogen. The ratio Y_A/Y_N is 2.3 in this work and it ranges from 1.3 to 3.6 in the other reported references.

4.4 AFFINITY CONSTANTS FOR OXYGEN OF AOB AND NOB ($K_{O,A}$, $K_{O,N}$)

$K_{O,A}$ and $K_{O,N}$ were calculated in the respirometer with LSS respirometry using method A (see section 3.3.1). The followed procedure consisted of monitoring the DO drop when the aeration was turned off and the biomass was consuming without substrate limitations. This procedure was already used by Wiesmann (1994) to calculate the affinity constant for *Nitrobacter* although a different mathematical approach was considered. Moreover, three other modifications were included: the oxygen transfer from the atmosphere was taken into account, the DO measurements were modified with the response time of the DO probe and sodium azide was used for the estimation of $K_{O,A}$.

If the oxygen transfer from the atmosphere is considered, the final DO balance for the respirometer is the following expression (equation 3.19):

$$\frac{dS_O}{dt} = k_L a^{sup} \cdot \left(S_O{}^* - S_O(t)\right) - \left(OUR_{end} + OUR_{max}\right) \cdot \frac{S_O}{K_O + S_O} \qquad (3.19)$$

where k_La^{sup} is the global oxygen transfer constant through the liquid-gas surface, $S_O{}^*$ is the DO saturation concentration (8.49 at 25ºC, Tchobanoglous and Burton (1991)) and K_O is the affinity constant for oxygen.

With respect to k_La^{sup}, it was previously calculated with a set of experiments conducted in an erlenmeyer (1 L) under the same operational conditions than in the K_O estimation experiments and a value of 4.08 d^{-1} was found (Guisasola 2005).

On the other hand, the DO probe time constant (τ) was calculated to be 5.8 s (Guisasola 2005) and the measured DO values were corrected according to Stephanopoulos (1984):

$$S_O^{corr}(t) = \frac{S_O^{meas}(t) - \left(1 - \frac{\Delta t}{\Delta t + \tau}\right) \cdot S_O^{meas}(t-1)}{\frac{\Delta t}{\Delta t + \tau}} \qquad (3.20)$$

where $S_O{}^{corr}$ was the corrected value of DO concentration, $S_O{}^{meas}$ was the measured DO concentration and Δt was the data collection interval.

In order to calculate $K_{O,A}$, a pulse of 25 mg N-TAN L^{-1} was injected together with a pulse of sodium azide (1.56 mg L^{-1}) at 25 ºC and a pH of 7.5. When the maximum OUR was attained,

the aeration was stopped and the DO drop was monitored. This was performed twice. Figure 3.9.A shows the DO profile of one of the repetitions.

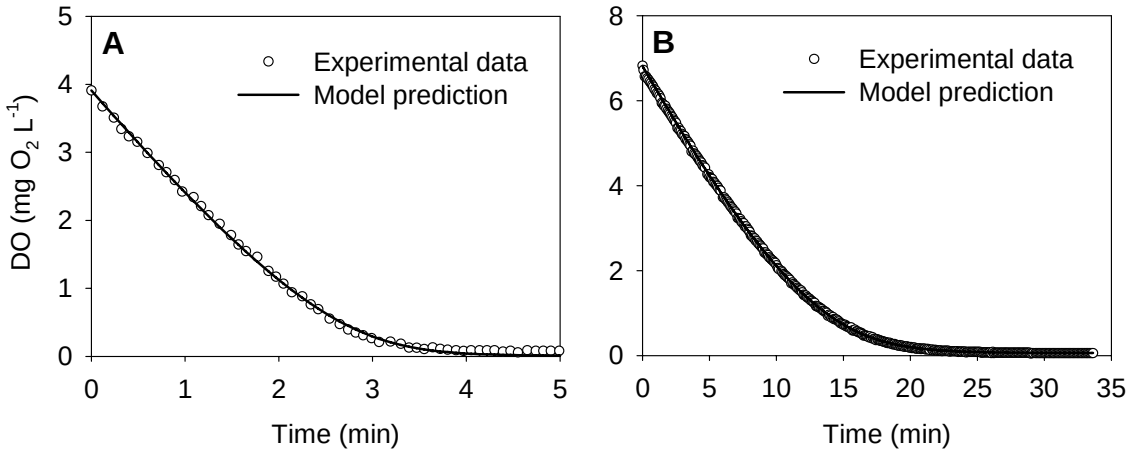

Figure 3.9 K_O determination: DO drop vs time and model prediction with fitted parameters **A.** $K_{O,A}$ determination with 25 mg N-TAN L^{-1} and 1.56 mg L^{-1} sodium azide. **B.** $K_{O,N}$ determination with 60 mg N-TNN L^{-1}.

The same procedure was performed twice with 60 mg N-TNN L^{-1} to calculate $K_{O,N}$. In this case, no specific inhibitor was needed. Figure 3.9.B shows one of the obtained DO profiles.

$K_{O,A}$ and $K_{O,N}$ were estimated by fitting these experimental DO profiles to equation 3.19 after DO values were corrected with equation 3.20. The averaged results for the two repetitions and the estimation errors predicted using the FIM methodology were: $K_{O,A} = 0.74 \pm 0.02$ mg O_2 L^{-1} and $K_{O,N} = 1.75 \pm 0.01$ mg O_2 L^{-1}. It can be observed that the error predicted for $K_{O,A}$ was twice the one predicted for $K_{O,N}$. This is understandable since the experiments with nitrite as substrate were slower and then, the data collection frequency and the amount of information increased. However, in both cases, the parameter estimation errors are very small, so the estimated vales can be considered quite reliable.

These values are, in general, higher than those found in the literature (Table 3.5). The differences can be due to the different used methodologies and also to the biomass composition and the floc size and morphology. On the one hand, it seems that working under low DO conditions puts a selective pressure upon the system for organisms coping well with limited oxygen availability (Wyffels et al. 2004) whose K_O is smaller. The biomass used in this study was working in the pilot plant at high DO concentration ($\approx$ 3 mg O_2 L^{-1}) and thus, organisms with low affinity for oxygen were favored. On the other hand, the floc size directly influences the substrates diffusion not only in the biofilm processes but also in the activated sludge systems. This effect is effectively reflected in the affinity constants which are usually one order of magnitude higher than those reported for single suspended cells (Pérez et al. 2005). Moussa et al. (2005) found different $K_{O,A}$ (see Table 3.5) for the same system working at a sludge retention time (SRT) of 30 or 100 days because of the raise in the floc size (from 70 to 90 μm).

Table 3.5 Affinity constants for DO of AOB and NOB calculated in this work and values from the literature.

$K_{O,A}$ (mg O_2 L^{-1})	$K_{O,N}$ (mg O_2 L^{-1})	Temp. (ºC)	Methodology	Reference
0.74	1.75	25	DO drop fitting	This work
0.3	1.1	25	DO drop fitting and from literature	Wiesmann (1994)
0.3	0.6	28	Respirometric experiment	Nowak et al. (1995)
0.16	0.54	30	From literature and DO drop fitting	Hunik et al. (1994a)
1.66*	3*	30	Maximum rates vs DO concentration	Sánchez et al. (2001)
0.24	1.5	30	Respirometic experiment	Wyffels et al. (2004)
1 / 3 **	1	30	Calibrated with exp. data of an SBR cycle	Moussa et al.(2005)

* Obtained at 24 g NaCl L^{-1}. ** For SRT of 30 and 100 days respectively.

Considering the estimated affinity constants, the DO effect on the maximum nitritation and nitratation rates can not be neglected even at high DO concentration. For example, at 3 mg O_2 L^{-1}, the Monod term for oxygen (see equation 3.19) is 0.8 for nitritation and 0.62 for nitratation, and at 6 mg O_2 L^{-1} it is 0.9 for nitritation and 0.77 for nitratation. Hence, the DO limitation is considered in the following parameter estimation.

4.5 KINETIC PARAMETERS OF NOB

Kinetic parameters of NOB were firstly determined because nitratation process can be easily studied without the influence of nitritation and without the need for the use of specific inhibitors if only TNN is used as a substrate.

4.5.1 OPTIMAL EXPERIMENT DESIGN FOR KINETIC PARAMETERS DETERMINATION

In this section, the determination of the following kinetic parameters of NOB using only OUR measurements is detailed: $\mu_{max,N}$, b_N, $K_{S,TNN,N}$ and $K_{I,TNN,N}$.

The main goal here was to define and perform an experiment to determine $\mu_{max,N}$ and $K_{S,TNN,N}$. The typical short batch respirometric experiment was not convenient since the NOB fraction was unknown and only the combination $\mu_{max,N} \cdot X_N$ could be estimated given that Y_N was known (Spanjers and Vanrolleghem 1995). Therefore, a long batch respirometric test (high TNN concentration pulse) was designed with the idea to be able to estimate also the initial biomass fraction ($f_N(0)$), see equation 3.21). Then, with this kind of experiment, the decay process and the substrate inhibition term had to be considered and their parameters had to be also estimated.

$$X_N(0) = X(0) * f_N(0) \tag{3.21}$$

Nomenclature for equation 3.21 is: $f_N(0)$ is the initial NOB fraction, $X_N(0)$ is the initial X_N value, and X(0) is the initial total biomass concentration.

In conclusion, two processes were needed to describe this experiment: processes number 2 (growth of NOB) and 5 (decay of NOB) in Table 3.2. Since only S_{TNN}, S_{NO3}, S_O and X_N were considered, the process rates and stoichiometry could be described as shown in Table 3.6. Previously determined Y_N was used here.

Table 3.6 Process stoichiometry and kinetics for NOB-related parameters determination.

Component	S_{TNN}	S_{NO3}	S_O	X_N	Process rate
Process	mg N L^{-1}		mg COD L^{-1}		
Growth	$-\frac{1}{Y_N}$	$\frac{1}{Y_N}$	$-\frac{1.14 - Y_N}{Y_N}$	1	$\mu^*_{max,N} \cdot \frac{S_{TNN}}{K_{S,TNN,N} + S_{TNN} + \frac{S_{TNN}^2}{K_{I,TNN,N}}} \cdot X_N \cdot \left(1 - e^{-t/k_t}\right)$
Decay	0	0	1	-1	$b_N \cdot X_N$

The term $\mu^*_{max,N}$ in the growth rate refers to the maximum specific growth rate of NOB under the specific experimental conditions of pH, T and DO (see equation 3.22). This parameter was estimated and then equation 3.22 was used to calculate $\mu_{max,N}(T,pH)$ with the previously calibrated $K_{O,N}$.

$$\mu^*_{max,N} = \mu_{max,N}(T,pH) \cdot \frac{S_O}{K_{O,N} + S_O} \tag{3.22}$$

An empirical factor was added to the growth rate expression to describe the fast transient period in reaching the maximum OUR observed after the substrate was added. This phenomenon, named "start-up" was also detected in Vanrolleghem et al. (1998) where they studied the possible reasons for this behavior. They concluded that it could be only partially described by the dynamics of the DO probe response and that the transport and sequence of metabolic reactions inside the cell could be the main cause. It was mathematically described as the response of a first order model to a step input as in Guisasola et al. (2003). The "start-up" time coefficient (k_t) represents the time required for the system to reach the 63 % of the final value. Guisasola (2005) demonstrated that if this phenomenon was not included, the estimated parameters would be wrongly determined. This "start-up" time coefficient was also optimized here.

The objective function to be minimized in the parameters estimation was:

$$J(\theta) = \left(\sum_{i=1}^{n} \left(OUR_{exp,i} - OUR(\theta)_i \right)^2 \right)^{1/2} \tag{3.23}$$

where OUR_{exp} and $OUR(\theta)$ were vectors of n measured values and model predictions at times t_i (i = 1 to n) and θ was the vector of the parameters of the model.

First experimental design: one nitrite pulse

A respirometric test consisting of one pulse of 500 mg N-TNN L^{-1} was performed in the reactor using LSS respirometry (method B described in section 3.3.2). Experimental conditions were: T = 22.2 ± 0.3 ºC, pH = 7.10 ± 0.02, DO = 3.0 ± 0.1 mg O_2 L^{-1} and VSS = 1900 ± 100 mg L^{-1}. Experimental OUR data are shown in Figure 3.10.

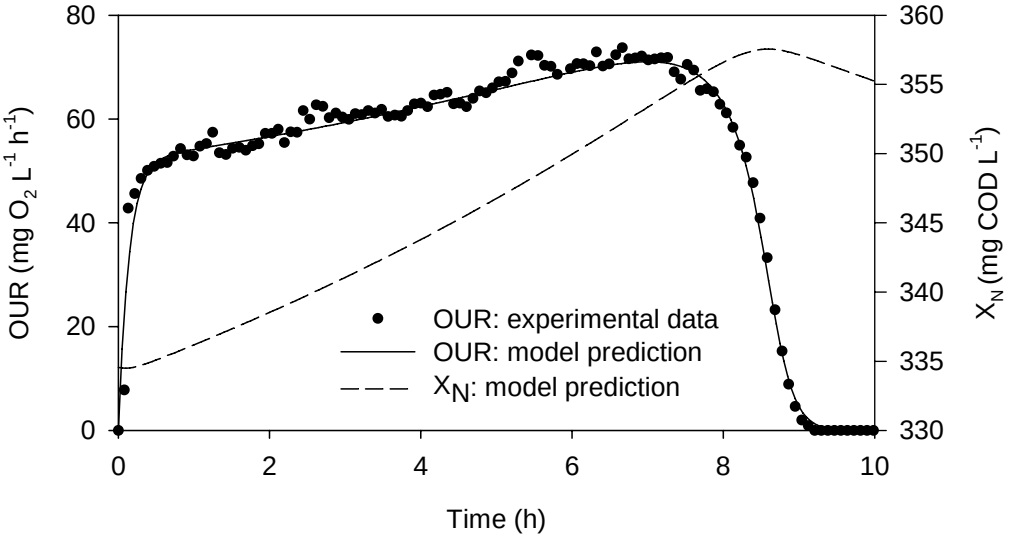

Figure 3.10 Experimental OUR data used in the nitratation model calibration with one nitrite pulse and model prediction for OUR and X_N.

Table 3.7 Parameters obtained in the nitratation model calibration with one nitrite pulse and objective function value (J_{min})

Fitting code	$f_N(0)$ (g COD_{XN} g^{-1} COD_X)	$\mu^*_{max,N}$ (d^{-1})	b_N (d^{-1})	$K_{S,TNN,N}$ (mg N L^{-1})	$K_{I,TNN,N}$ (mg N L^{-1})	k_t (d)	J_{min} (mg O_2 L^{-1} h^{-1})
1	0.12	0.456	0.132	13.1	869	$5.8 \cdot 10^{-3}$	25.7
2	0.07	0.720	0.007	12.4	1315	$5.8 \cdot 10^{-3}$	25.3
3	0.02	1.608	0.264	11.4	5156	$5.4 \cdot 10^{-3}$	25.0
Mod 1	0.02	1.608	0.079	11.0	-	$5.4 \cdot 10^{-3}$	24.5
Mod 2	0.18	-	-	13.7	714	$5.8 \cdot 10^{-3}$	25.0

These data were used to calibrate the model parameters. Different sets of parameters were obtained depending on the initial values of the parameters in the optimization process (see Table 3.7, rows 1-3). As the model predictions for these sets of parameters were very similar, only one curve is shown in Figure 3.10. This figure also shows the model prediction for NOB concentration. The parameters values obtained in each optimization differed largely except for the $K_{S,TNN,N}$ and k_t. It was observed that $f_N(0)$, $\mu^*_{max,N}$ and $K_{I,TNN,N}$ were correlated i.e. $K_{I,TNN,N}$ and $\mu^*_{max,N}$ increased when $f_N(0)$ decreased. No tendency was detected for b_N as the estimated values were very different in each optimization. This was because the experiment was not long

enough to show the effect of this parameter in the biomass decay. The analysis of these sets of parameters indicated that the parameters related to growth/decay and inhibition were not identifiable with this experimental design.

The practical identifiability was analyzed using contour plots of the objective function with respect to different pairs of parameters. Each parameter was modified around the optimum value of the first set of parameters in Table 3.7. Figure 3.11 shows the contour plots and the optimised parameters values. The valley in each contour plot corroborated the correlation between parameters.

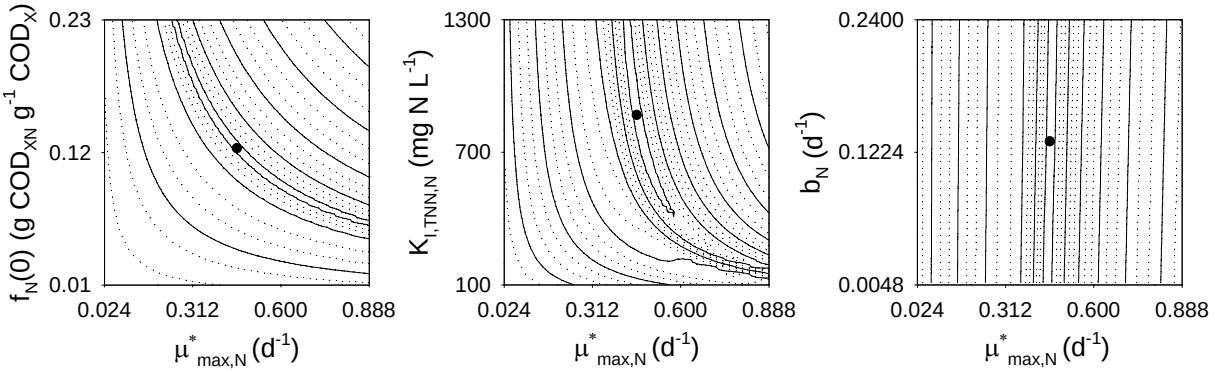

Figure 3.11 Contour plots of the objective function for pairs of parameters: $\mu^*_{max,N}$-$f_N(0)$, $\mu^*_{max,N}$ - $K_{I,TNN,N}$ and $\mu^*_{max,N}$ -b_N. Experimental design of one nitrite pulse.

In fact, the no identifiability of these parameters made it impossible to assess if the increase in the OUR values between 1h and 7h (Figure 3.10) was due to inhibition or to biomass growth. Two model modifications were proposed to evaluate each process. The first one (Mod 1) considered no inhibition by changing the Haldane-type kinetics for a Monod-type kinetics in the growth rate. The second one (Mod 2) considered no growth, which meant constant biomass concentration. The OUR predictions after fitting these models are shown in Figure 3.12 (first pulse). Both model modifications fitted well the experimental OUR profile. The obtained parameters and the objective function values are shown in Table 3.7, rows 4 and 5.

A second TNN pulse (500 mg N L^{-1}) added just after the first pulse depletion (time = 10 h) was simulated for each model modification (Figure 3.12). Although the first nitrite pulse predictions were similar, the second ones were very different. Mod 1 predicted a shorter and higher second peak because of the biomass growth, while Mod 2 predicted two equal peaks because the biomass concentration was the same. In practice, the OUR profile of a second pulse of nitrite would probably have a shape in between these two predictions indicating the simultaneous occurrence of both phenomena.

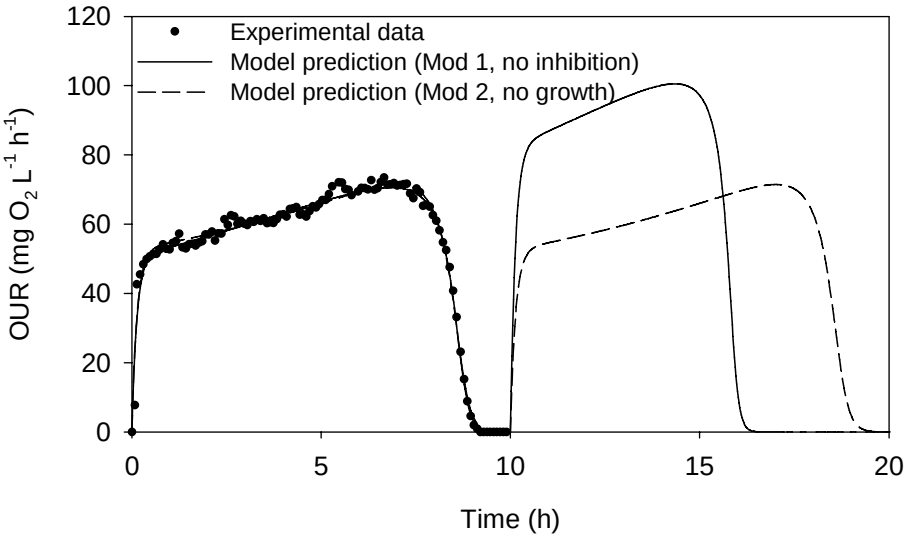

Figure 3.12 Experimental OUR data used in the nitratation model calibration with one nitrite pulse and model fits and prediction for OUR using two model modifications.

Second experimental design: three nitrite pulses

Taking into account the observations made in the previous sections, a new experimental design was proposed and performed to assess the model parameters. It consisted of three successive TNN pulses of 500 mg N L^{-1}. The first nitrite pulse was added to biomass under starvation conditions. After the first pulse depletion, a second pulse was immediately added to allow the detection of biomass growth. Finally, a third pulse was added after a long time delay to assess the decay kinetics.

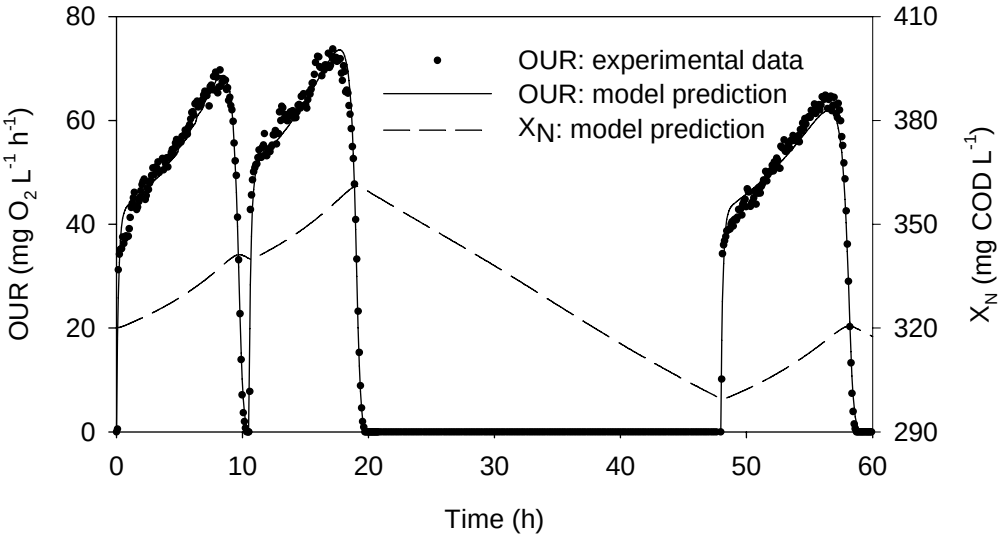

Figure 3.13 Experimental OUR data used in the nitratation model calibration with three nitrite pulses and model prediction for OUR and X_N.

This methodology was performed with the following experimental conditions: T = 22.2 ± 0.3 ºC, pH = 7.10 ± 0.02, DO = 3.0 ± 0.1 mg O_2 L^{-1} and VSS = 1900 ± 100 mg L^{-1}. Obtained experimental OUR data are shown in Figure 3.13. The second OUR peak was higher than the first one, indicating the occurrence of biomass growth. Furthermore, the OUR data of the second pulse, after the "start-up" period, were lower than the maximum OUR data of the first pulse, indicating that inhibition was also occurring. Finally, a third amount of nitrite was added 27 hours after the second pulse was totally consumed. The maximum OUR value reached in this third pulse was lower than that obtained in the second one because of the effect of the decay process.

Parameter estimation results, their confidence intervals and the objective function minimum (J_{min}) are shown in Table 3.8. Model prediction fitted properly the experimental data (Figure 3.13), i.e. the set of estimated parameters described accurately the nitrite consumption by NOB. Figure 3.13 also shows the model prediction for NOB concentration during the experiment. The strength of the proposed approach is that the whole set of parameters can be simultaneously estimated with the same biomass and operational conditions and with a simple experimental procedure.

Table 3.8 Parameters obtained in the nitratation model calibration with three nitrite pulses, confidence intervals (α = 0.01) and objective function value (J_{min}). Experimental conditions: T = 22.2 ± 0.3 ºC, pH = 7.10 ± 0.02, DO = 3.0 ± 0.1 mg O_2 L^{-1} and VSS = 1900 ± 100 mg L^{-1}

Parameter	Units	Value
$f_N(0)$	g COD_{XN} g^{-1} COD_X	0.119 ± 0.002
$\mu^*_{max,N}$	d^{-1}	0.456 ± 0.009
b_N	d^{-1}	0.142 ± 0.002
$K_{S,TNN,N}$	mg N-TNN L^{-1}	12.6 ± 0.5
$K_{S,FNA,N}$ †	mg FNA L^{-1}	$8.1 \cdot 10^{-3} \pm 3 \cdot 10^{-4}$
$K_{I,TNN,N}$	mg N-TNN L^{-1}	690 ± 20
$K_{I,FNA,N}$ †	mg FNA L^{-1}	0.45 ± 0.01
k_t	d	$6.8 \cdot 10^{-3} \pm 3 \cdot 10^{-4}$
J_{min}	mg O_2 L^{-1} h^{-1}	51.3

† Calculated with TNN-FNA equilibrium.

As in the first experimental design (one nitrite pulse), the objective function was re-calculated with different parameter values around the optimum values. Figure 3.14 shows the optimal parameters values and the contour plots for the same pairs of parameters. In this case, there was a clear minimum in the first and in the third plots. In comparison with Figure 3.11, these contour plots show that the identifiability of $f_N(0)$, $\mu^*_{max,N}$ and b_N improved.

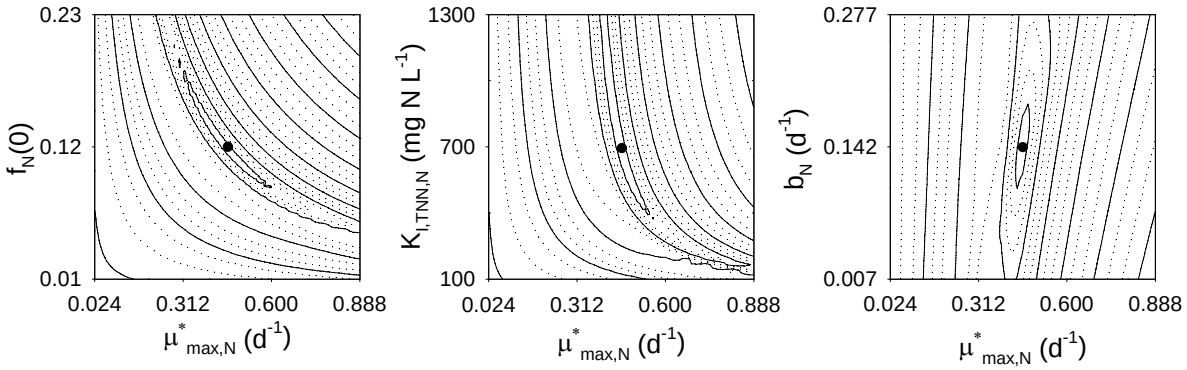

Figure 3.14 Contour plots of the objective function for pairs of parameters: $\mu^*_{max,N}$-$f_N(0)$, $\mu^*_{max,N}$ - $K_{I,TNN,N}$ and $\mu^*_{max,N}$ -b_N. Experimental design of three nitrite pulses.

The FIM for both experimental designs was calculated. Using equation 3.9 and data obtained during endogenous respiration, a Q value of 0.257 was calculated. The values obtained for each experimental design and for each criterion are summarized in Table 3.9. Another experiment design was evaluated (one pulse x 3) in order to test whether the difference on these values was due to the larger amount of experimental data in the three pulses experimental design or it was due to the different experimental design. No extra experiments were required as data from the experimental design with one pulse was used three times as if three independent pulses would have been performed. The experimental design with three pulses was the best one considering any of the criteria.

Table 3.9 Comparison of the different experimental designs using OED/PE criteria.

Criterion →	A	Modified A	D	E	Modified E
	tr(FIM^{-1})	tr(FIM)	det(FIM)	λ_{min}(FIM)	[λ_{max}(FIM) /λ_{min}(FIM)]
Optimal →	minimum	maximum	maximum	maximum	minimum
One pulse	$1.66 \cdot 10^{7}$	$2.30 \cdot 10^{9}$	$1.09 \cdot 10^{13}$	$6.04 \cdot 10^{-8}$	$3.81 \cdot 10^{16}$
One pulse x 3	$5.52 \cdot 10^{6}$	$6.90 \cdot 10^{9}$	$7.93 \cdot 10^{15}$	$1.81 \cdot 10^{-7}$	$3.81 \cdot 10^{16}$
Three pulses	$3.95 \cdot 10^{2}$	$7.21 \cdot 10^{9}$	$7.17 \cdot 10^{26}$	$2.53 \cdot 10^{-3}$	$2.60 \cdot 10^{12}$

It was clearly demonstrated that the new experimental design consisting of three nitrite pulses (two consecutive pulses and a delayed third one) was useful to estimate the kinetic parameters related to NOB growth and decay processes. This method improved the parameter identifiability with respect to a sole nitrite pulse.

4.5.2 pH AND TEMPERATURE INFLUENCE ON $\mu_{max,N}$ AND b_N

The previously estimated $\mu^*_{max,N}$ and b_N were only valid for the specific experimental conditions used in the estimation experiment, i.e. T = 22.2 ºC, pH = 7.10 and DO = 3.0 mg O_2 L^{-1}. Using equation 3.22 with $K_{O,N}$ = 1.75 mg O_2 L^{-1}, a value of $\mu_{max,N}$ (T,pH) = 0.722 d^{-1} was calculated which was not dependent on the DO concentration.

Temperature and pH influence on $\mu_{max,N}$

The influence of temperature on biological activity is most often modeled by and Arrhenius-type of equation. Hunik et al. (1994b) and Shammas (1986) used this equation for AOB and NOB populations. Equation 3.24 shows the Arrhenius-type function applied to $\mu_{max,N}$. This equation is valid only for temperature below 40 ºC because higher temperatures provoke the decrease of the specific growth rate.

$$\mu_{max,N}(T) = A_{\mu maxN} \cdot \exp\left(\frac{-Ea_N}{R \cdot (273+T)}\right) \tag{3.24}$$

In equation 3.24, $A_{\mu maxN}$ is the Arrhenius pre-exponential factor for $\mu_{max,N}$, Ea_N is the activation energy of NOB, R is the universal gas constant (8.31 J mol^{-1} K^{-1}) and T is the temperature in ºC. Hunik et al. (1994b) determined the activation energies of *Nitrosomonas europaea* and *Nitrobacter agilis* and found 65 and 45 kJ mol^{-1} respectively. In this work, activation energies of 68 and 44 kJ mol^{-1} for AOB and NOB were assumed because they were successfully used in Hao et al. (2002a) and Wyffels et al. (2004) for modeling purposes using mixed populations.

The specific growth rate of both nitritation and nitratation processes are maxima around a pH of 7.5-8 and decrease for pH above and below this range in a bell-type shape. This behavior was experimentally tested for the nitrification as a sole process (Antoniou et al. 1990; Galí et al. 2006; Shammas 1986) and for AOB and NOB separately (Bae et al. 2002; Grunditz and Dalhammar 2001). Since the pH effect on AOB and NOB was found to be very similar, the same expression was considered in this study for both populations. Equation 3.25 shows the used expression which can also be found in Antoniou et al. (1990) and Dochain and Vanrolleghem (2001) to account for the pH effect on nitrification:

$$\mu_{max,N}(pH) = \frac{\mu_{max,N}(pH_{optim})}{1 + \frac{10^{-pK1}}{10^{-pH}} + \frac{10^{-pH}}{10^{-pK2}}} \tag{3.25}$$

where pK1 and pK2 are the high and low pH vales at which the $\mu_{max,N}$ is half the $\mu_{max,N}$ at the optimum pH ($\mu_{max,N}(pH_{optim})$). Antoniou et al. (1990) determined these coefficients with data from real plants but considering the nitrification as a one-step process. They found pK1 = 8.69 and pK2 = 6.78 and 7.8 as the optimal pH, which was in agreement with observations made in pilot plant. Therefore, these parameters were used in this work for both $\mu_{max,N}$ and $\mu_{max,A}$ dependence on pH.

Equations 3.24 and 3.25 were combined, the coefficient values were included, and as a result, an expression to describe the temperature and pH influence on $\mu_{max,N}$ was obtained (equation 3.26).

$$\mu_{max,N}(pH,T) = \frac{A_{\mu maxN} \cdot \exp\left(\frac{-44 \cdot 10^3}{8.31 \cdot (273+T)}\right)}{1 + \frac{10^{-8.69}}{10^{-pH}} + \frac{10^{-pH}}{10^{-6.78}}} \tag{3.26}$$

The previously estimated $\mu_{max,N}(T,pH)$ (0.722 d^{-1}) and the corresponding experimental conditions (T = 22.2 ºC and pH = 7.10) were used to calculate $A_{\mu maxN}$ which resulted to be $6.69 \cdot 10^7$ d^{-1}. Finally, equation 3.26 turned to 3.27, which defines the influence of temperature and pH on the maximum specific growth rate of NOB.

$$\mu_{max,N}(pH,T) = \frac{6.69 \cdot 10^7 \cdot \exp\left(\frac{-5295}{273+T}\right)}{1 + \frac{2.05 \cdot 10^{-9}}{10^{-pH}} + \frac{10^{-pH}}{1.66 \cdot 10^{-7}}} \qquad [d^{-1}] \tag{3.27}$$

The estimated $\mu_{max,N}$ was compared to values found in the literature. For a more reliable comparison, equation 3.27 was used to calculate the estimated $\mu_{max,N}$ (this work) under the same conditions than those reported in the literature (see Table 3.10). It can be observed that the value estimated in this work is in the range of values found in the literature although they are quite scattered.

Table 3.10 Specific maximum rates of NOB found in the literature compared with the value determined in this work under the same conditions.

$\mu_{max,N}$ (d^{-1}) this work**	$\mu_{max,N}$ (d^{-1})	T (ºC)	pH	Methodology	Reference
0.75	1.08	20	8.0	From literature	Wiesmann (1994)
0.80	0.48	22	7.3	Respirometric determination	Vadivelu et al. (2006d)
1.06	0.67	30	7 - 7.5	Respirometric determination	Pambrun et al. (2006)
0.68	0.13	18	? / 7.8*	Model fit to system behavior	Sheintuch et al. (1995)
0.77	0.33	20	? / 7.8*	Respirometric determination	Copp and Murphy (1995)
0.77	0.79	20	? / 7.8*	From literature	Hao et al. (2002a)
1.25	2.50	28	? / 7.8*	Model fit to system behavior	Nowak et al. (1995)
1.41	0.86	30	? / 7.8*	From literature	Hunik et al. (1994a)

* pH not specified in the reference (used 7.8 because is the optimum one in our system).
** Calculated with the equation found in this work (equation 3.27) under the same conditions as those reported in the reference.

Temperature influence on b_N

With respect to the decay rate, it is generally considered dependant only on temperature. Some authors considered that the temperature influences the expression μ_{max}-b (Antoniou et al. 1990) whereas other considered the μ_{max} and b dependences on temperature separately. In this study, an independent expression for b was used although the same Arrhenius-type of function and the same activated energy as in the μ_{max} case were considered (Hao et al. 2002a; Head and Oleszkiewicz 2004; Wyffels et al. 2004). Temperature dependency for b_N is shown in equation 3.28:

$$b_N(T) = A_{bN} \cdot \exp\left(\frac{-Ea_N}{R \cdot (273 + T)}\right) \tag{3.28}$$

where A_{bN} is the Arrhenius pre-exponential factor for b_N. Using $b_N = 0.142$ d^{-1}, T = 22.2 ºC and $Ea_N = 44$ kJ mol^{-1}, A_{bN} was be estimated as $8.626 \cdot 10^6$ d^{-1} and the temperature dependency was described as shown in equation 3.29.

$$b_N(T) = 8.626 \cdot 10^6 \cdot \exp\left(\frac{-5295}{273 + T}\right) \quad [d^{-1}] \tag{3.29}$$

This equation was used to calculate b_N under different temperatures to be able to compare the estimated value in this work with other values found in the literature. Table 3.11 shows this comparison. It can be observed that the value estimated in this work is in the same range of values found in the literature. However, reported values are quite scattered probably because the methods used for their determination are also very different.

Table 3.11 Decay rates of NOB found in the literature compared with those determined in this work at the same temperature.

b_N (d^{-1}) this work*	b_N (d^{-1})	T (ºC)	Methodology	Reference
0.12	0.05	20	From literature	Wiesmann (1994)
0.12	0.14	20	Respirometric determination	Copp and Murphy (1995)
0.12	0.03	20	From literature	Hao et al. (2002a)
0.12	0.20	20	Model fit to full-scale experiments	Wett and Rauch (2003)
0.14	0.07	22	Respirometric determination	Vadivelu et al. (2006d)
0.15	0.10	23	Assumed the same as that of AOB	Gee et al. (1990)
0.20	0.50	28	Model fit to system behavior	Nowak et al. (1995)
0.22	0.20	30	Respirometric determination	Moussa et al. (2005)

* Calculated with the equation found in this work (equation 3.29) under the same conditions as those reported in the reference.

Temperature and pH influence on $\mu_{max,N}$-b_N

The temperature and pH dependency on the nitratation model was checked by the calculation of $\mu_{max,N}$-b_N at different pH and temperature values. Figure 3.15 shows that the temperature increases the effective nitratation rate while the optimum pH is around 7.5-8.

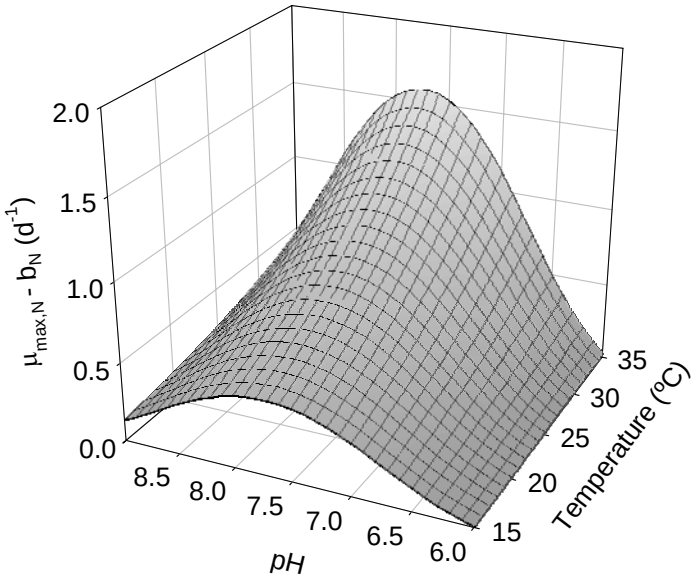

Figure 3.15 pH and temperature influence on the effective NOB growth rate.

4.5.3 MODEL VALIDATION AND COMMENTS ON $K_{S,TNN,N}$ AND $K_{I,TNN,N}$

Three respirometric experiments (LSS respirometry in the reactor using method D) were performed with similar biomass than in the calibration experiment but at different temperatures, pH, biomass concentration and initial TNN to validate the calibrated parameters. All the experiments were performed at 3.0 mg O_2 L^{-1}. Table 3.12 shows the used experimental conditions. Parameters estimated in section 4.5.1 (Table 3.8) were used to simulate these experiments and pH and temperature dependence of $\mu_{max,N}$, b_N, $K_{S,TNN,N}$ and $K_{I,TNN,N}$ were included in the model. The only parameters fitted here were $f_N(0)$ and k_t since they are not constant and they depend on the history of the biomass in the pilot plant. All these values are reported in Table 3.12 under the denomination of "Model prediction 1". To confirm that the substrate and the inhibition compound is FNA instead of TNN, another model prediction was obtained considering that $K_{S,TNN,N}$ and $K_{I,TNN,N}$ are constants (instead of considering that $K_{S,FNA,N}$ and $K_{I,FNA,N}$ are constants). The estimated values for $f_N(0)$ and k_t in this "Model prediction 2" are also reported in Table 3.12.

Figure 3.16 shows the experimental results of the three respirometric pulses and the different model predictions. The first model prediction (considering K_S and K_I constant parameters in terms of FNA) fitted very well experimental data whereas the second model prediction (considering K_S and K_I constant parameters in terms of TNN) did not agree with experimental

data, especially at high pH. These results confirm that the real substrate, and at the same time the inhibitory compound, is FNA and hence K_S and K_I are constant parameters in terms of FNA. The same result was obtained by Van Hulle et al. (2004) and Vadivelu et al. (2006c). Conversely, Pambrun et al. (2006) considered NO_2^- as the substrate based on the results of their respirometric experiments.

Table 3.12 Experimental conditions for model validation and estimated $f_N(0)$ and k_t using two model predictions (considering either FNA or TNN as substrate and inhibitory compounds).

Exp	T (ºC)	pH	VSS (mg VSS L^{-1})	TNN (mg N L^{-1})	Model prediction	$f_N(0)$ (g COD_{XN} g^{-1} COD_X)	k_t (d)
A	26.6	7.1	1150	500	1	0.072	$1.2 \cdot 10^{-2}$
					2	0.075	$1.2 \cdot 10^{-2}$
B	24.5	7.5	2750	1500	1	0.084	$7.1 \cdot 10^{-4}$
					2	0.127	$2.0 \cdot 10^{-5}$
C	26.5	7.9	2100	1500	1	0.147	$4.7 \cdot 10^{-3}$
					2	0.25	$1.4 \cdot 10^{-5}$

All these experiments were performed with biomass from the pilot plant that was operating as a complete nitrification system with some TAN and TNN in the first reactor. Therefore, the estimated parameters were considered appropriate for the simulation of acclimated biomass, i.e. biomass rich in nitrifiers able to treat high nitrogen loading rate (NLR).

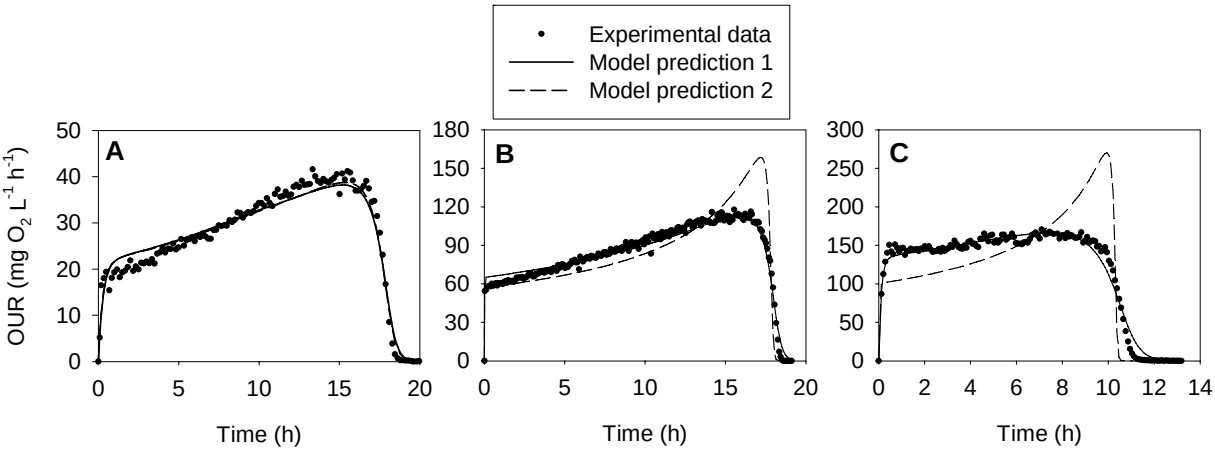

Figure 3.16 Nitrite pulses under different experimental conditions (**A, B, C** see Table 3.12) and model predictions considering either FNA (Model prediction 1) or TNN (Model prediction 2) as substrate and inhibitory compounds.

4.5.4 $K_{S,FNA,N}$ AND $K_{I,FNA,N}$ DETERMINATION WITH NON ACCLIMATED BIOMASS

$K_{S,FNA,N}$ and $K_{I,FNA,N}$ were determined again with a very different biomass. In this case, the biomass was not very rich in nitrifying microorganisms because the pilot plant had been inoculated one month ago and the NLR and TAN and TNN concentrations were low.

The used method was LSS respirometry in the reactor (method C described in section 3.5.1) and the environmental conditions were: pH = 7.5 ± 0.1, T = 23.0 ± 0.5 ºC and DO = 2.0 - 3.0 mg O_2 L^{-1}. Increasing amounts of TNN were progressively added to the reactor. TNN and OUR measurements were determined twice for every substrate concentration, considering as statistical error two times the standard deviation. Nitrite uptake rates (NUR) were calculated from OUR measurements using the stoichiometric coefficients shown in Table 3.3 as depicted in equation 3.30.

$$NUR = \frac{OUR}{1.14 - Y_N} \tag{3.30}$$

Experimental data were fitted to a Haldane-type equation (see equation 3.31) and parameters NUR_{max}, $K_{S,FNA,N}$ and $K_{I,FNA,N}$ were estimated using SigmaPlot® 8.0 software (2002). Figure 3.17 shows experimental data and model prediction with the fitted parameters and Table 3.13 summarizes the obtained values for the fitted parameters.

$$NUR = NUR_{max} \cdot \frac{S_{FNA}}{K_{S,FNA,N} + S_{FNA} + \frac{S_{FNA}^{\ 2}}{K_{I,FNA,N}}} \tag{3.31}$$

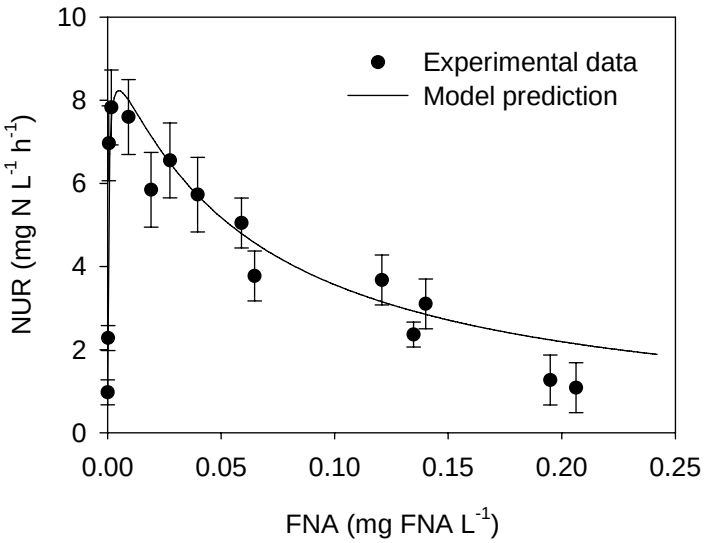

Figure 3.17 Experimental data and model fitting for $K_{S,FNA,N}$ and $K_{I,FNA,N}$ determination with LSS respirometry in the reactor.

Table 3.13 Obtained parameters with LSS respirometric experiments in the reactor.

Parameter	Units	Value
NUR_{max}	mg N L^{-1} h^{-1}	9.6 ± 0.6
$K_{S,FNA,N}$	mg FNA L^{-1}	$4 \cdot 10^{-4} \pm 1 \cdot 10^{-4}$
$K_{I,FNA,N}$	mg FNA L^{-1}	0.06 ± 0.01

Although the methodology used in this section is different from that used in section 4.5.1, the obtained parameters are very different: the parameters here are an order of magnitude lower. This can be explained with the different biomass used in the experiments. Several authors have also considered the possibility that substrate affinity coefficients and inhibition coefficients can vary depending on the biomass acclimation to substrate and inhibitory compounds and/or to the biomass composition (Antileo et al. 2002; Pambrun et al. 2006). Table 3.14 shows some of the values found in the literature. Since it was demonstrated that FNA was the real substrate and also the inhibitory compound, only the values which could be transformed into FNA were considered. It can easily be observed that there exist many different values for these parameters. This is probably due to differences in the used biomass, however, the possible floc diffusion problems and the fact that different methodologies could lead to different values should also be taken into account.

Table 3.14 Affinity coefficient for substrate and Haldane inhibition coefficient of NOB found in the literature and estimated in this work.

$K_{S,FNA,N}$ (mg FNA L^{-1})	$K_{I,FNA,N}$ (mg FNA L^{-1})	Methodology	Reference
$4.0 \cdot 10^{-4}$	0.06	Respirometric det. Non acclimated biomass	This work
$8.1 \cdot 10^{-3}$	0.45	Respirometric det. Acclimated biomass	This work
$8.0 \cdot 10^{-5}$	-	Model fit to batch experiments	Gee et al. (1990)
$1.1 \cdot 10^{-4}$	0.87	From literature	Wiesmann (1994)
$4.9 \cdot 10^{-5}$	0.006	Biomass activity det. under different conditions	Sheintuch et al. (1995)
$1.3 \cdot 10^{-3}$	-	Biomass activity det. under different conditions	López-Fiuza et al. (2002)
$1.0 \cdot 10^{-3}$	0.35	Respirometric det., immobilized biomass	Carvallo et al. (2002)
$4.2 \cdot 10^{-4}$	-	Model fit to the system behavior	Moussa et al. (2005)
$6.1 \cdot 10^{-4}$	-	Respirometric det. Enriched NOB population	Vadivelu et al. (2006d)

Therefore, the parameters estimated in this section were used in the simulations with non acclimated biomass (see Chapter 6) and the parameters fitted in section 4.5.1 were used in the simulations with acclimated biomass (see Chapter 7).

The methodology used in this section was very useful when only $K_{S,FNA,N}$ and $K_{I,FNA,N}$ where required since the experiment length was shorter and the parameters identifiability was very good (see Figure 3.18). However, it was not as automatic as the experiment shown in section 4.5.1 because it required sample withdrawals and TNN analysis.

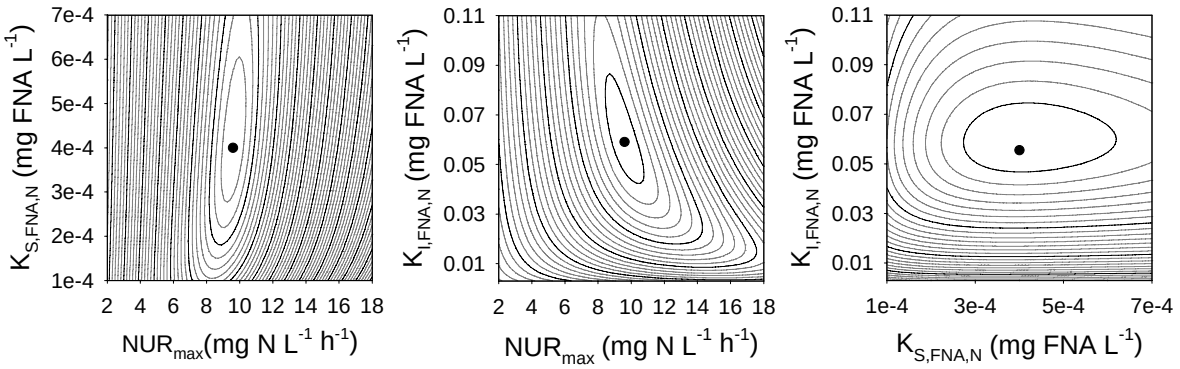

Figure 3.18 Contour plots of the objective function for pairs of parameters: NUR_{max}-$K_{S,FNA,N}$, NUR_{max}-$K_{I,FNA,N}$ and $K_{S,FNA,N}$ –$K_{I,FNA,N}$. LSS respirometry in the reactor with method C.

4.5.5 $K_{I,FA,N}$ DETERMINATION WITH ACCLIMATED BIOMASS

The only parameter left for the complete characterization of NOB-related processes is $K_{I,FA,N}$. It was considered constant in terms of FA for a specific biomass although its value could probably change either due to biomass acclimation to FA or NOB population changes.

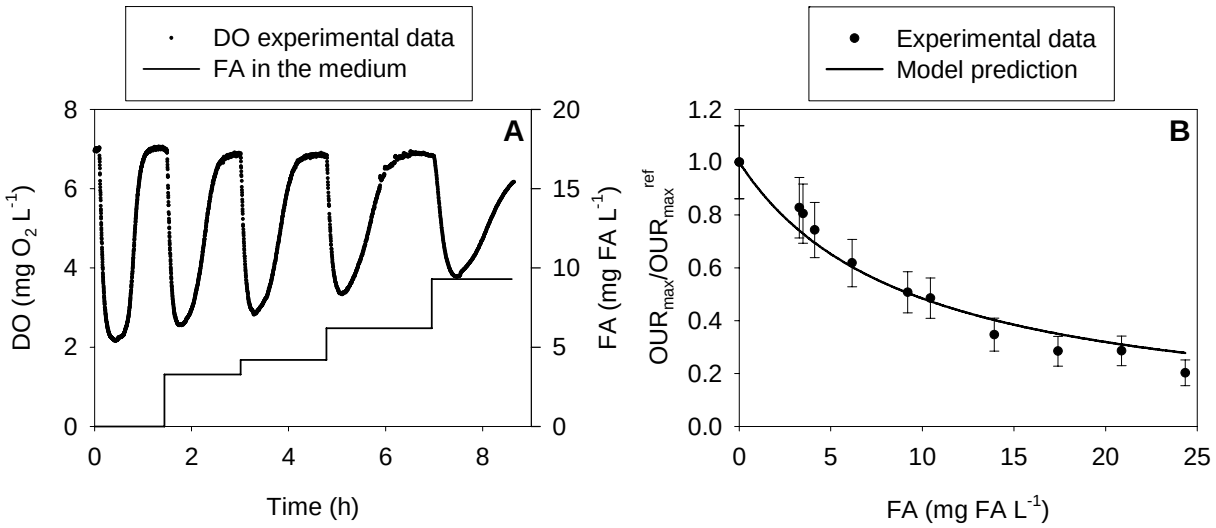

Figure 3.19 $K_{I,FA,N}$ determination with LFS respirometry in the respirometer. **A.** DO profile and FA concentration in the medium along TNN pulses. B. OUR/OUR_{max} vs FA concentration, experimental data and model prediction with fitted parameter.

This parameter was determined using LFS respirometry in the respirometer with biomass withdrawn from the pilot plant. The pilot plant was operating as a complete nitrification system with high concentration of TAN and TNN in the first reactor and producing an effluent free of TAN and TNN. The experimental conditions in the respirometric experiment were: pH = 8.4 ± 0.1 and T = 28.0 ± 0.5 ºC. These high pH and T were used to favor the presence of the inhibitory compound (FA) and also to avoid FNA inhibition to NOB. ATU (10 mg L^{-1}) was used as specific inhibitor for AOB. The experiment consisted of successive equal TNN pulses (30 mg N L^{-1}) with different FA concentration in the medium that was assured by the injection

of TAN into the liquid after the depletion of each TNN pulse. The first TNN pulse was carried out with the medium free of FA. Figure 3.19.A shows the DO profile of some TNN pulses and the liquid FA concentration as an example of the used methodology.

For increasing concentration of FA, the minimum DO level (S_O^{min}) was increasing, indicating that the nitratation rate was decreasing. The maximum nitratation rate in each pulse was proportional to the maximum OUR (OUR_{max}^*) which could be calculated with a DO balance in the respirometer. In this experiment, it was important that the injected TNN concentration was higher enough to reach the maximum nitratation rate (without substrate limitations). Considering the DO balance in the respirometer (equation 3.6) and the fact that $dS_O/dt = 0$ when OUR was maximum, OUR_{max}^* for each pulse could be calculated as:

$$OUR_{max}^{*} = k_L a \cdot (S_{OE} - S_O^{min}) \tag{3.32}$$

where OUR_{max}^* is the maximum OUR reached in a TNN pulse at the DO concentration of S_O^{min}.

The DO influence on the OUR_{max}^* had to be considered because the reached S_O^{min} values were very different among them and therefore OUR_{max}^* values were influenced by the specific S_O^{min} values. On the other hand, the OUR_{max} of each pulse was referred to the OUR_{max}^{ref} (the maximum OUR reached in the pulse without FA) to avoid the need for the k_La value calculation. The final obtained equation was:

$$\frac{OUR_{max}}{OUR_{max}^{ref}} = \frac{\left(S_{OE} - S_O^{min}\right)\cdot\left(\frac{S_O^{min}}{K_{O,N} + S_O^{min}}\right)_{ref}}{\left(S_{OE} - S_O^{min}\right)_{ref}\cdot\left(\frac{S_O^{min}}{K_{O,N} + S_O^{min}}\right)} \tag{3.33}$$

where OUR_{max} is the maximum OUR reached in a TNN pulse without the DO limitation, $K_{O,N}$ is the affinity constant for DO (1.75 mg O_2L^{-1}) and "ref" refers to the reference pulse (pulse without FA in the medium).

Using equation 3.33, a pair of values (FA, $OUR_{max}/OUR_{max}^{ref}$) was obtained for each pulse (Figure 3.19.B). Errors were calculated with the errors propagation equation derived from equation 3.33 and considering an error of 0.1 mg O_2 L^{-1} in the S_{OE} measurement and an error of 0.01 mg O_2 L^{-1} in the $K_{O,N}$ estimation. Experimental data was fitted to equation 3.34 using SigmaPlot® 8.0 software (2002) and a value of 9.5 ± 0.7 mg FA L^{-1} was estimated for $K_{I,FA,N}$. Figure 3.19.B also shows the model prediction using this value.

$$\frac{OUR_{max}}{OUR_{max}^{ref}} = \frac{K_{I,FA,N}}{S_{FA} + K_{I,FA,N}} \tag{3.34}$$

Few references are found in which this parameter was estimated. In Wett and Rauch (2003) a value of 1.9 mg FA L^{-1} achieved the best fit during calibration. However, when the process (SBR with 1400-2000 mg N-TAN L^{-1} in the influent) was operated under stable conditions the inhibition constant increased to 24.3 mg FA L^{-1} due to sludge adaptation. In Chandran and Smets (2000b), a value of 1.33 mg FA L^{-1} was obtained from batch respirometric experiments. In that case the biomass had previously been enriched in nitrifying bacteria in a SBR with a 500 mg N-TAN L^{-1} feed. It is clear that this inhibition coefficient depends on the population and its acclimation to FA.

4.6 KINETIC PARAMETERS OF AOB

In order to calibrate $\mu_{max,A}$ and b_A, an experiment with three ammonium pulses, similar to the experiment used to calibrate $\mu_{max,N}$ and b_N, would have been required. Several attempts were performed with pulses of 500-1000 mg N-TAN L^{-1} at high pH (>8) but none of them succeed. Sometimes, external disturbances such as changes in the air flow rate negatively influenced the OUR profile; but usually, the problem was the unexpected behavior in the OUR profile, which showed tendency changes that could not be modeled with the existing model. The main problems were the length of the experiment (more than 5 days) which made it impossible to maintain the environmental conditions steady and the high initial amount of TAN required to produce inhibition and biomass growth. Furthermore, in this case, two different processes were active: nitritation and nitratation. In view of the difficulties to apply this method for the calibration of the kinetic parameters of AOB, a different approach was used.

4.6.1 $\mu_{max,A}$ AND b_A ESTIMATION FROM $\mu_{max,N}$ AND b_N

It is known that the influence of the temperature on the growth rate of AOB and NOB is similar: as higher the temperature is, higher the growth rates are. However, at low temperature, $\mu_{max,N}$ is higher than $\mu_{max,A}$ and the opposite is true at high temperatures. The temperature at which they intersect seems to be around 13-20 ºC: Hunik (1993) calculated it to be 13 ºC, Van Hulle (2005) and Hao et al. (2002a) considered 20 ºC. In this work it was considered that $\mu_{max,A}$ and $\mu_{max,N}$ intersect at 20 ºC.

Temperature and pH influence on $\mu_{max,A}$

The temperature influence on $\mu_{max,A}$ was modeled with the same type of equation than that used for $\mu_{max,N}$, but using the corresponding activation energy (68 kJ mol^{-1}). The dependence on pH was modeled with the same equation and the same parameters. Using these equations and considering $\mu_{max,A}$ (20 ºC) = $\mu_{max,N}$ (20ºC), equation 3.35 was obtained.

$$\mu_{max,A}(pH,T) = \frac{1.28\cdot10^{12}\cdot\exp\left(\frac{-8183}{273+T}\right)}{1+\frac{2.05\cdot10^{-9}}{10^{-pH}}+\frac{10^{-pH}}{1.66\cdot10^{-7}}} \qquad [d^{-1}] \qquad (3.35)$$

Equation 3.35 was used to compare $\mu_{max,A}$ with values found in the literature. Table 3.15 shows the values found in the literature and the pH and T conditions in which they were determined or used. Using these conditions and equation 3.35, $\mu_{max,A}$ was calculated for this work in each case and compared to the reported value. It can be observed that in most of the cases the calculated value is similar to the value found in the literature. This makes the used approach more reliable.

Table 3.15 Specific maximum rates of AOB found in the literature compared with the value determined in this work under the same conditions.

$\mu_{max,A}$ (d^{-1}) this work**	μ_{maxA} (d^{-1})	T (ºC)	pH	Methodology	Reference
0.75	0.77	20	8.0	From literature	Wiesmann (1994)
0.86	1.03	22	7.3	Respirometric determination	Vadivelu et al. (2006b)
1.90	1.96	30	7 - 7.5	Respirometric determination	Pambrun et al. (2006)
1.93	2.02	30	7.9	Respirometric determination	Wyffels et al. (2004)
0.64	0.11	18	? / 7.8*	Model fit to system behavior	Sheintuch et al. (1995)
0.77	0.80	20	? / 7.8*	From literature	Hao et al. (2002a)
1.64	2.2	28	? / 7.8*	Model fit to system behavior	Nowak et al. (1995)
1.95	1.37	30	? / 7.8*	From literature	Hunik et al. (1994a)

* pH not specified in the reference (used 7.8 because is the optimum one in our system).
** Calculated with the equation found in this work (equation 3.35) under the same conditions as those reported in the reference.

Temperature influence on b_A

b_A was considered equal to b_N at 20 ºC. Other authors also considered or calculated similar values at 20 ºC for both nitrifying populations (Gee et al. 1990; Moussa et al. 2005; Wett and Rauch 2003; Wiesmann 1994). b_A dependence on temperature was also modeled with an Arrhenius-type of equation using 68 kJ mol^{-1} as activation energy. Equation 3.36 describes the temperature influence on the decay rate of AOB.

$$b_A(T) = 1.651\cdot10^{11}\cdot\exp\left(\frac{-8183}{273+T}\right) \qquad [d^{-1}] \qquad (3.36)$$

Table 3.16 shows b_A values found in the literature with their respective temperature compared with the values obtained with equation 3.36. Again, a wide range of values were found. Some

of them are similar to the value found in this work and others differ in a large extent. This shows the difficulties in choosing a value from previously reported studies and supports the proposal of estimating it for each specific biomass.

Table 3.16 Decay rates of AOB found in the literature compared with those determined in this work at the same temperature.

b_A (d^{-1}) this work*	b_A (d^{-1})	T (ºC)	Methodology	Reference
0.12	0.05	20	From literature	Wiesmann (1994)
0.12	0.05	20	From literature	Hao et al. (2002a)
0.12	0.23	20	Model fit to full-scale experiments	Wett and Rauch (2003)
0.15	0.26	22	Respirometric determination	Vadivelu et al. (2006b)
0.16	0.10	23	Model fit to a batch experiment	Gee et al. (1990)
0.26	0.22	28	Model fit to system behavior	Nowak et al. (1995)
0.31	0.30	30	Respirometric determination	Moussa et al. (2005)

* Calculated with the equation found in this work (equation 3.36) under the same conditions as those reported in the reference.

Temperature and pH influence on $\mu_{max,A}$-b_A

Similarly than in section 4.5.2, the temperature and pH dependency of the nitritation model was checked by the calculation of $\mu_{max,A}$-b_A at different pH and temperature values. Figure 3.20 shows that the temperature increases the effective nitritation rate while the optimum pH is around 7.5-8.

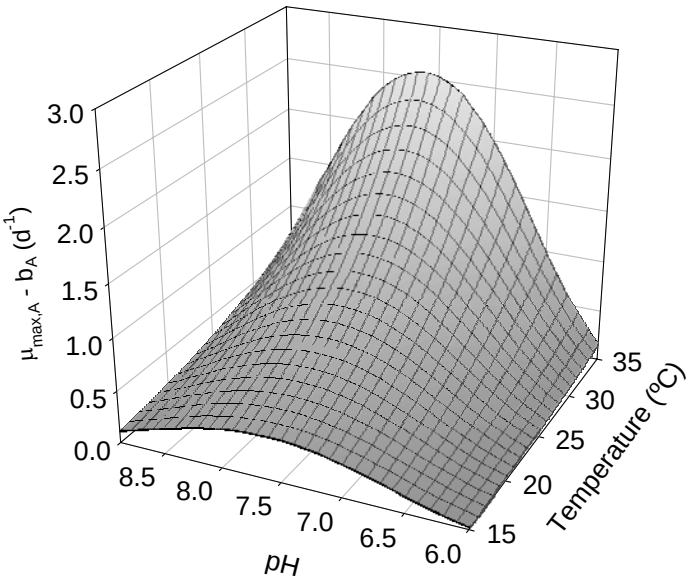

Figure 3.20 pH and temperature influence on the effective AOB growth rate.

Figure 3.21 shows the temperature effect on $\mu_{max,A}$, $\mu_{max,N}$, b_A and b_N. Maximum specific growth rates were calculated at a pH of 7.5.

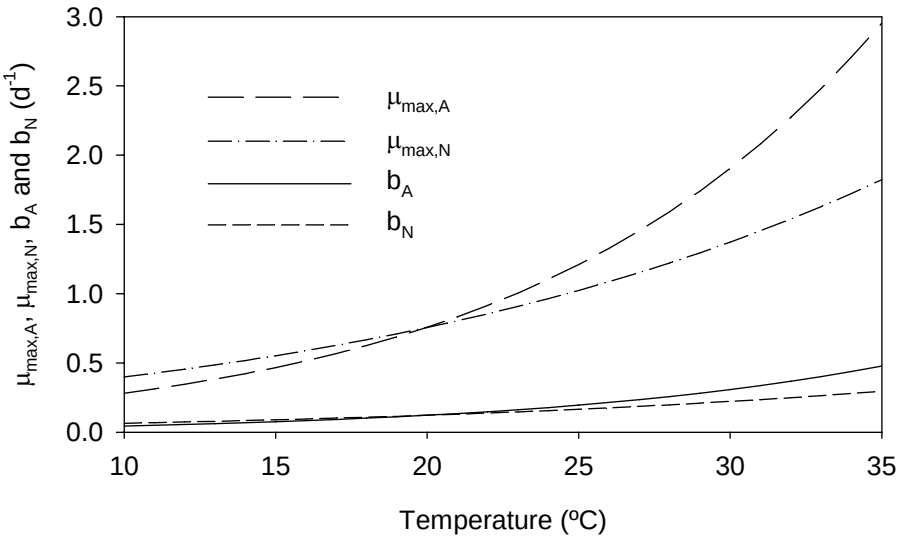

Figure 3.21 Temperature influence on the maximum specific growth rate of AOB and NOB at a pH of 7.5 and temperature influence on the decay rate of AOB and NOB.

4.6.2 $K_{S,FA,A}$ AND $K_{I,FA,A}$ DETERMINATION WITH NON ACCLIMATED BIOMASS

Simultaneously to the $K_{S,FNA,N}$ and $K_{I,FNA,N}$ determination with non acclimated biomass (see section 4.5.4), a similar experiment was performed to estimate $K_{S,FA,A}$ and $K_{I,FA,A}$. Therefore, the biomass was not very rich in nitrifying microorganisms because the pilot plant had been inoculated one month ago.

LSS respirometry in the reactor with method C was used under constant environmental conditions: pH = 7.5 ± 0.1, T = 23.0 ± 0.5 ºC and DO = 3.0 mg O_2 L^{-1}. Increasing amounts of TAN were progressively added to the reactor. TAN, TNN and OUR measurements were determined twice for every substrate concentration, considering as statistical error two times the standard deviation. Specific inhibitors were not used to avoid wasting 26 L of biomass.

Each OUR measurement was the sum of the oxygen simultaneously consumed in the nitritation and nitratation processes. Considering the stoichiometry of these processes, if TAN was completely oxidized to nitrate, 75 % of the OC would be due to the nitritation process and the rest to nitratation process. Consequently, nitritation rate could have been calculated as 75 % of the total OUR. However, nitratation could be inhibited by the high FA concentration. This was previously tested with a batch experiment in the same reactor under the same environmental conditions. A pulse of 1000 mg N-TAN L^{-1} was added and TAN and TNN were monitored. It was shown that while TAN was higher than 50 mg N L^{-1}, only 30 % of the produced TNN was oxidized to nitrate. For TAN below 50 mg N L^{-1}, all produced TNN was oxidized to nitrate.

Considering these results, it was possible to calculate the percentage of the OUR corresponding to the nitritation process (OUR_{AOB}) and consequently to calculate the ammonium uptake rate (AUR) using equation 3.37.

$$AUR = \frac{OUR_{AOB}}{3.43 - Y_A} \tag{3.37}$$

Experimental data were fitted to a Haldane-type equation (equation 3.38) and parameters AUR_{max}, $K_{S,FA,A}$ and $K_{I,FA,A}$ were estimated using SigmaPlot® 8.0 software (2002). Figure 3.22 shows experimental data and model prediction with the fitted parameters and Table 3.17 summarizes the obtained results. It was demonstrated in section 4.5.4 that the parameters identifiability is very good using this methodology. Both $K_{S,FA,A}$ and $K_{I,FA,A}$ were considered constants in terms of FA since it is quite accepted that this is the true substrate and inhibitor (Pambrun et al. 2006; Vadivelu et al. 2006a; Van Hulle et al. 2004).

$$AUR = AUR_{max} \cdot \frac{S_{FA}}{K_{S,FA,A} + S_{FA} + \frac{S_{FA}^2}{K_{I,FA,A}}} \tag{3.38}$$

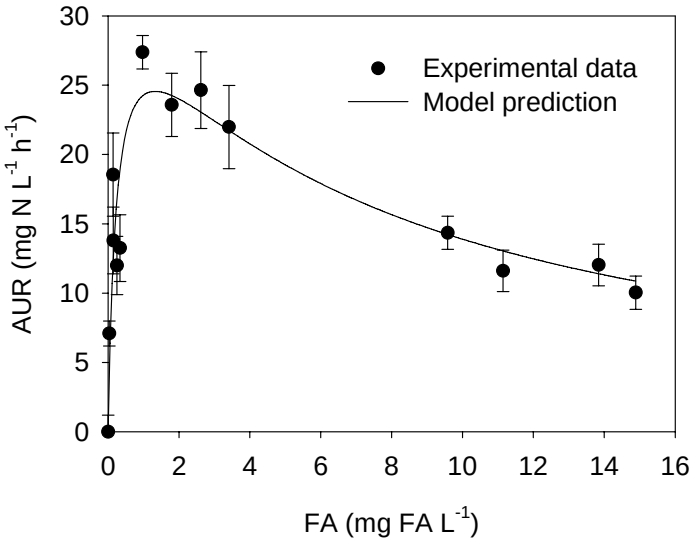

Figure 3.22 Experimental data and model fitting for $K_{S,FA,A}$ and $K_{I,FA,A}$ determination with LSS respirometry in the reactor.

Table 3.17 Obtained parameters with LSS respirometric experiments in the reactor.

Parameter	Units	Value
AUR_{max}	mg N L^{-1} h^{-1}	34 ± 5
$K_{S,FA,A}$	mg FA L^{-1}	0.24 ± 0.09
$K_{I,FA,A}$	mg FA L^{-1}	7 ± 3

4.6.3 $K_{S,FA,A}$ AND $K_{I,FA,A}$ DETERMINATION WITH ACCLIMATED BIOMASS

The same parameters were estimated again with an improved method and using biomass acclimated to high ammonium concentration. The pilot plant was operating as a partial nitrification system when the biomass was withdrawn. Even though only AOB were present in the system, sodium azide (1.56 mg L^{-1}) was used to make sure that the nitratation process was completely suppressed.

The experiment was carried out in the respirometer using LSS respirometry (method B) as described in section 3.3.2. Experimental conditions were controlled at a temperature of 24 ± 0.5 ºC and a pH of 8.4 ± 0.1. This pH was chosen to achieve high FA concentration using relative low amount of TAN. OUR values were calculated with respect to the biomass concentration to be able to use data from different days. Figure 3.23 shows the obtained OUR data at different FA concentrations which were calculated from the analyzed TAN concentrations using the TAN-FA equilibrium. Error bars indicate two times the standard deviation of the measurement.

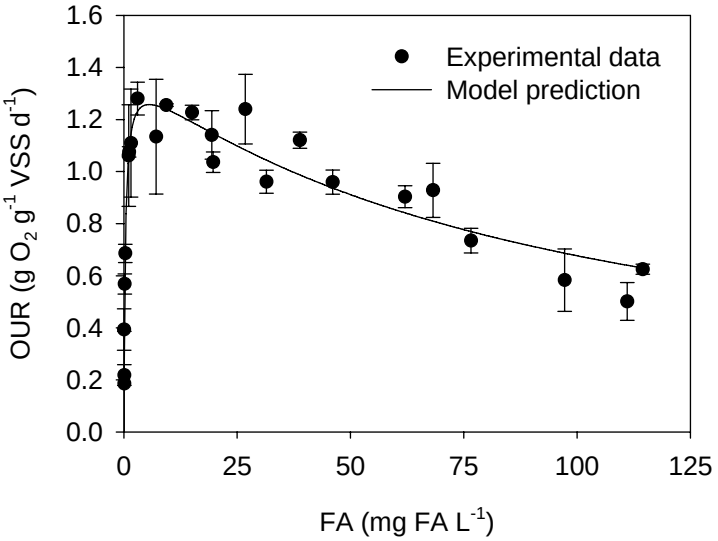

Figure 3.23 Experimental data and model fitting for $K_{S,FA,A}$ and $K_{I,FA,A}$ determination with LSS respirometry in the respirometer.

Experimental data were fitted to equation 3.39 and OUR_{max}, $K_{S,FA,A}$ and $K_{I,FA,A}$ were estimated (see Table 3.18). Figure 3.23 also shows the model prediction with the fitted parameters.

$$. \ OUR = OUR_{max} \cdot \frac{S_{FA}}{K_{S,FA,A} + S_{FA} + \frac{S_{FA}^{\ 2}}{K_{I,FA,A}}} \tag{3.39}$$

$K_{S,FA,A}$ obtained in this experiment and this biomass was a little bit higher than that determined in the previous section, however, $K_{I,FA,A}$ was more than one order of magnitude higher than that

previously estimated value. This clearly indicated that either AOB acclimated to FA or the different AOB population reacted differently in front of high FA concentrations.

Table 3.18 Obtained parameters with LSS respirometric experiments in the respirometer.

Parameter	Units	Value
OUR_{max}	g O_2 g^{-1} VSS d^{-1}	1.41 ± 0.06
$K_{S,FA,A}$	mg FA L^{-1}	0.34 ± 0.06
$K_{I,FA,A}$	mg FA L^{-1}	93 ± 14

Table 3.19 shows values for these parameters found in the literature which were obtained with different biomasses and different methods. Only when the reported values were in FA units or the pH and T were specified the references were considered. In this way, these parameters can be compared in terms of FA. It can be seen that the range of values for $K_{S,FA,A}$ is quite high. With respect to $K_{I,FA,A}$, also a great variety of values are found, ranging from 3 to 656 mg FA L^{-1}. It must be pointed out that Antileo et al. (2002) also determined different parameters when using acclimated or non acclimated biomass, however, their values are very different from the values found in this work. The highly scattered values found in the literature indicate that the biomass acclimation and composition must be considered in order to choose appropriate values for these parameters.

Table 3.19 Affinity coefficient and Haldane inhibition coefficient of AOB found in literature and estimated in this work.

$K_{S,FA,A}$	$K_{I,FA,A}$	Methodology	Reference
(mg FA L^{-1})			
0.24	7	Respirometric det. Non acclimated biomass	This work
0.34	93	Respirometric det. Acclimated biomass	This work
0.04	529	Model fit to batch experiments	Gee et al. (1990)
0.03	656	From literature	Wiesmann (1994)
0.25	-	Biomass activity det. under different conditions	Sheintuch et al. (1995)
0.04	3	Biomass activity det. under different conditions	López-Fiuza (2002)
0.20	61	Respirometric det., immobilized biomass	Carvallo et al. (2002)
3.64	27	Batch experiment. Non acclimated biomass	Antileo et al. (2002)
5.83	43	Batch experiment. Acclimated biomass	Antileo et al. (2002)
0.85	-	Respirometric determination	Wyffels et al. (2004)
0.91	-	Respirometric det. Enriched AOB population	Van Hulle et al. (2004)
0.15	-	Model fit to the system behavior	Moussa et al. (2005)
0.64	293	Respirometric determination	Pambrun et al. (2006)
0.44	-	Respirometric det. Enriched AOB population	Vadivelu et al. (2006a)

As it happened in NOB kinetic parameters determination, two different pairs of parameters for the Haldane equation were found: one pair to be used when non acclimated biomass was modeled, and another pair to be used when acclimated biomass was simulated.

4.6.4 $K_{I,FNA,A}$ DETERMINATION WITH ACCLIMATED BIOMASS

Just after the $K_{S,FA,A}$ and $K_{I,FA,A}$ determination with acclimated biomass, $K_{I,FNA,A}$ was also estimated with the same methodology. Experimental conditions were maintained at 25 ºC and pH of 7.0 to favor the existence of FNA. Sodium azide was also used (1.56 mg L^{-1}) although no nitratation activity was detected in the pilot plant. A TAN pulse of 100 mg N L^{-1} was injected to the respirometer and OUR was calculated in quadruplicate at increasing TNN concentration until TAN was depleted. TAN was periodically measured in order to assure no limiting concentrations. Data from four different experiments (each one with fresh biomass from the pilot plant) were used and hence, OUR values had to be calculated with respect to the biomass concentration. Figure 3.24 shows the obtained experimental data. Each OUR value was the averaged value of the four repetitions and the error bars were calculated as two times the standard deviation of the measurements.

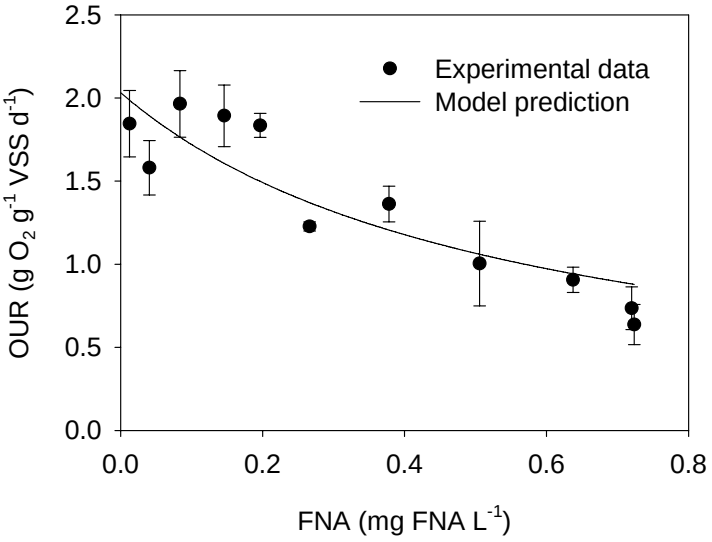

Figure 3.24 Experimental data and model prediction for $K_{I,FNA,A}$ determination with LSS respirometry in the respirometer.

In order to estimate the inhibition coefficient, these data were fitted to equation 3.40 using SigmaPlot® 8.0 software (2002). Table 3.20 shows the obtained results.

$$. \ OUR = OUR_{max} \cdot \frac{K_{I,FNA,A}}{K_{I,FNA,A} + S_{FNA}} \qquad (3.40)$$

Table 3.20 Obtained parameters with LSS respirometric experiments in the respirometer.

Parameter	Units	Value
OUR_{max}	g O_2 g^{-1} VSS d^{-1}	2.0 ± 0.02
$K_{I,FNA,A}$	mg FNA L^{-1}	0.55 ± 0.14

Table 3.21 shows values for $K_{I,FNA,A}$ found in the literature compared together with the value found in this work. They are expressed in terms of FNA as this is the inhibitory compound (Van Hulle et al. 2004). The value found in this work is in accordance with that used in Hellinga et al. (1998), however, the other reported values were either quite higher or quite lower than our estimated value. In these cases, the different biomass acclimation to FNA would be the reason for these scattered values.

Table 3.21 FNA inhibition coefficient values of AOB found in literature and estimated in this work.

$K_{I,FNA,A}$ (mg FNA L^{-1})	Methodology	Reference
0.55	Respirometic determination	This work
0.67	From literature	Hellinga et al. (1998)
2.80	Model fit to full-scale experiments	Wett and Rauch (2003)
6.85	Respirometic determination	Van Hulle et al. (2004)
0.18	Respirometic determination	Pambrun et al. (2006)

4.7 CONSIDERATIONS ABOUT INHIBITION COEFFICIENTS DETERMINATION

In the previous sections, affinity constants for substrate and inhibition coefficients (substrate inhibition and non-competitive inhibition) were determined using different methods, basically LSS and LFS respirometry. Although all these methods were correctly applied and the obtained results were compared, a unique method should be used in further determinations. If LFS and LSS respirometry are compared, the best technique is the LSS respirometry because data are easily obtained and the length of the experiment is shorter. With respect to the use of the respirometer or the reactor for these experiments, the main difference is that in the reactor, the OUR determination is automatic and the volume is higher. However, the fact that the pilot plant must be stopped to use the reactor as a respirometer makes the respirometer the suitable vessel for parameter estimation. On the other hand, if the respirometer was bigger and the OUR determination was automated; the pilot plant reactor would no longer be a choice for parameter estimation. Therefore, the best methodology would be LSS respirometry in the respirometer with method B (see section 3.3.2).

4.8 KINETIC AND STOICHIOMETRIC PARAMETERS FOR HETEROTROPHIC BACTERIA AND OTHER PARAMETERS

In the previous sections all the model parameters related to AOB and NOB were calibrated or estimated. The only parameters left from the complete kinetic and stoichiometric model were the parameters related to heterotrophic biomass (Y_H, $\mu_{max,H}$, b_H, $K_{O,H}$, $K_{S,H}$) and the parameters related to biomass decay and hydrolysis processes (i_{XP}, f_P, k_a, k_h, K_x). Since the main goal was to study the nitrification processes, these parameters were not calibrated in this work: they were obtained from the literature. Actually, they were taken from ASM1 and ASM2d at 20 ºC (Henze et al. 2000). All of them were considered as constants except for $\mu_{max,H}$ and b_H. The temperature dependency of these parameters was taken into account as shown in equations 3.41 and 3.42 (Henze et al. 2000), where the temperature is in ºC

$$\mu_{max,H} = 6 \cdot (1.07)^{(T-20)} \qquad [d^{-1}] \tag{3.41}$$

$$b_H = 0.4 \cdot (1.07)^{(T-20)} \qquad [d^{-1}] \tag{3.42}$$

4.9 SUMMARY OF MODEL PARAMETERS

Table 3.22 summarizes all the model parameters required to describe the nitrification as a two-step process considering also heterotrophic bacteria. Parameters dependent on pH and temperature (maximum specific growth rates and decay rates) were calculated at 25 ºC and a pH of 7.5. The expressions to calculate them under other conditions are firstly summarized.

Equations to calculate maximum specific growth rates and decay rates (indicated in Table 3.22) are:

(a) $$\mu_{max,A}(pH,T) = \frac{1.28 \cdot 10^{12} \cdot \exp\left(\frac{-8183}{273+T}\right)}{1 + \frac{2.05 \cdot 10^{-9}}{10^{-pH}} + \frac{10^{-pH}}{1.66 \cdot 10^{-7}}}$$

(b) $$b_A(T) = 1.651 \cdot 10^{11} \cdot \exp\left(\frac{-8183}{273+T}\right)$$

(c) $$\mu_{max,N}(pH,T) = \frac{6.69 \cdot 10^{7} \cdot \exp\left(\frac{-5295}{273+T}\right)}{1 + \frac{2.05 \cdot 10^{-9}}{10^{-pH}} + \frac{10^{-pH}}{1.66 \cdot 10^{-7}}}$$

(d) $$b_N(T) = 8.626 \cdot 10^{6} \cdot \exp\left(\frac{-5295}{273+T}\right)$$

(e) $$\mu_{max,H} = 6 \cdot (1.07)^{(T-20)}$$

(f) $$b_H = 0.4 \cdot (1.07)^{(T-20)}$$

All of these equations are expressed in terms of d^{-1}. Temperature is required in ºC.

Table 3.22 Stoichiometric and kinetic parameters for the two-step nitrification model including heterotrophic bacteria at T = 25 ºC and pH = 7.5.

Name	Units	Symbol	Value
Parameters related to AOB			
Growth yield	g COD g^{-1} N	Y_A	0.18
Maximum specific growth rate	d^{-1}	$\mu_{max,A}$	1.21 (a)
Decay rate	d^{-1}	b_A	0.20 (b)
Affinity constant for DO	mg O_2 L^{-1}	$K_{O,A}$	0.74
Affinity constant for FA	mg FA L^{-1}	$K_{S,FA,A}$	0.24† / 0.34††
Inhibition coefficient for FA	mg FA L^{-1}	$K_{I,FA,A}$	7.0† / 93††
Inhibition coefficient for FNA	mg FNA L^{-1}	$K_{I,FNA,A}$	0.55††
Parameters related to NOB			
Growth yield	g COD g^{-1} N	Y_N	0.08
Maximum specific growth rate	d^{-1}	$\mu_{max,N}$	1.02 (c)
Decay rate	d^{-1}	b_N	0.17 (d)
Affinity constant for DO	mg O_2 L^{-1}	$K_{O,N}$	1.75
Affinity constant for FNA	mg FNA L^{-1}	$K_{S,FNA,N}$	$4 \cdot 10^{-4}$† / $8 \cdot 10^{-3}$††
Inhibition coefficient for FNA	mg FNA L^{-1}	$K_{I,FNA,N}$	0.06† / 0.45††
Inhibition coefficient for FA	mg FA L^{-1}	$K_{I,FA,N}$	9.5††
Parameters related to heterotrophs			
Growth yield	g COD g^{-1} COD	Y_H	0.67 *
Maximum specific growth rate	d^{-1}	$\mu_{max,H}$	8.42 (e) *
Decay rate	d^{-1}	b_H	0.56 (f) *
Affinity constant for S_{O2}	mg O_2 L^{-1}	$K_{O,H}$	0.2 *
Affinity constant for S_S	mg COD L^{-1}	K_S	4 *
Other parameters			
Nitrogen content of X_A, X_N, X_H	g N g^{-1} COD	i_{XB}	0.08 **
Nitrogen content of X_P	g N g^{-1} COD	i_{XP}	0.06 *
Fraction of biomass leading X_P	g COD g^{-1} COD	f_P	0.08 *
Ammonification rate	L mg^{-1} COD d^{-1}	k_a	0.08 *
Maximum specific hydrolysis rate	g COD g^{-1} COD d^{-1}	k_h	3.0 *
Affinity constant for X_S	g COD g^{-1} COD	K_X	0.03 *

* From Henze et al. (2000) ** From Guisasola (2005) (i) Calculated with equation i (see above).
† Determined with non acclimated biomass †† Determined with acclimated biomass

5. CONCLUSIONS

- A model to describe the reactions involved in a mainly nitrifying activated sludge system required 9 processes and 11 compounds because it included the dynamics of AOB, NOB and heterotrophs. TAN and TNN were state variables in this model although FA and FNA were considered the substrate and the inhibitory compounds. Equilibrium equations were also included in the model.

- ATU selectively inhibited the nitritation process at a concentration of 10 mg L^{-1} in a mixed population and sodium azide selectively inhibited the nitratation process at a concentration of 1.56 mg L^{-1} in the same mixed population.

- Several respirometric experiments were needed for the reliable determination of Y_A and Y_N. It was demonstrated that if the TAN assimilated by AOB and NOB was not considered, Y_A calculation would lead to erroneous results (up to 50 %).

- LSS respirometry was useful for the determination of $K_{O,A}$ and $K_{O,N}$ provided that oxygen transfer from the atmosphere was taken into account, DO measurements were modified with the time response of the DO probe and sodium azide was used as specific inhibitor.

- An experimental design (LSS respirometry in the reactor) consisting of two consecutive pulses of nitrite and a delayed third one was needed for the determination of $\mu_{max,N}$, $K_{S,FNA,N}$, $K_{I,TNN,N}$ and b_N because the parameters identifiability was much better than in the experimental design with a sole nitrite pulse.

- $\mu_{max,A}$ and b_A were estimated from $\mu_{max,N}$ and b_N respectively considering that these parameters are equal at 20 ºC.

- Temperature and pH influences on $\mu_{max,A}$ and $\mu_{max,N}$ were modeled with an Arrhenius-type of equation and a bell-type of equation and temperature effect on b_A and b_N were modeled with an Arrehius-type of equation.

- Several different respirometric techniques were used to estimate the affinity constants for substrate and the inhibition coefficients for both AOB and NOB. The best methodology resulted to be LSS respirometry in the respirometer because of its simplicity and the speed of the method.

- Affinity constants for substrate and the Haldane inhibition coefficients for both AOB and NOB were assessed with two different sludges and different results were obtained. This indicates that these parameters change with biomass acclimation to the substrate.

6. REFERENCES

Anthonisen AC, Loehr RC, Prakasam TBS, Srinath EG. 1976. Inhibition of nitrification by ammonia and nitrous acid. *Journal of the Water Pollution Control Federation* 48(5):835-852.

Antileo C, Aspe E, Urrutia H, Zaror C, Roeckel M. 2002. Nitrifying biomass acclimation to high ammonia concentration. *Journal of Environmental Engineering* 128(4):367-375.

Antoniou P, Hamilton J, Koopman B, Jain R, Holloway B, Lyberatos G, Svoronos SA. 1990. Effect of temperature and pH on the effective maximum specific growth rate of nitrifying bacteria. *Water Research* 24(1):97-101.

APHA. 1995. Standard methods for the examination of water and wastewater. 19th Ed. Washington DC, USA: American Publishers Health Association.

Bae W, Baeck S, Chung J, Lee Y-W. 2002. Optimal operational factors for nitrite accumulation in batch reactors. *Biodegradation* 12:359-366.

Baeza JA, Gabriel D, Lafuente J. 1999. An expert supervisory system for a pilot WWTP. *Environmental Modelling and Software* 14(5):383-390.

Baeza JA, Gabriel D, Lafuente J. 2002. In-line fast OUR measurements for monitoring and control of WWTP. *Water Science and Technology* 45(4-5):19-28.

Belser LW, Mays EL. 1980. Specific inhibition of nitrite oxidation by chlorate and its use in assessing nitrification in soils and sediments. *Applied and Environmental Microbiology* 39(3):505-510.

Bernet N, Sanchez O, Cesbron D, Steyer JP, Delgenès JP. 2005. Modeling and control of nitrite accumulation in a nitrifying biofilm reactor. *Biochemical Engineering Journal* 24(2):173-183.

Brouwer H, Klapwijk A, Keesman KJ. 1998. Identification of activated sludge and wastewater characteristics using respirometric batch-experiments. *Water Research* 32(4):1240-1254.

Carrera J. 2001. Biological ammonium removal from high-strength ammonium wastewater. Process parameters study and design of a full-scale industrial WWTP (in Spanish). PhD Thesis. Bellaterra: Universitat Autònoma de Barcelona.

Carrera J, Baeza JA, Vicent T, Lafuente J. 2003. Biological nitrogen removal of high-strength ammonium industrial wastewater with two-sludge system. *Water Research* 37(17):4211-4221.

Carvallo L, Carrera J, Chamy R. 2002. Nitrifying activity monitoring and kinetic parameters determination in a biofilm airlift reactor by respirometry. *Biotechnology Letters* 24(24):2063-2066.

Coelho MAZ, Russo C, Araújo OQF. 2000. Optimization of a sequencing batch reactor for biological nitrogen removal. *Water Research* 34(10):2809-2817.

Copp JB, Murphy KL. 1995. Estimation of the active nitrifying biomass in activated sludge. *Water Research* 29(8):1855-1862.

Chandran K, Smets BF. 2000a. Applicability of two-step models in estimating nitrification kinetics from batch respirograms under different relative dynamics of ammonia nitrite oxidation. *Biotechnology and Bioengineering* 70(1):54-64.

Chandran K, Smets BF. 2000b. Single-step nitrification models erroneously describe batch ammonia oxidation profiles when nitrite oxidation becomes rate limiting. *Biotechnology and Bioengineering* 68(4):396-406.

Chandran K, Smets BF. 2005. Optimizing experimental design to estimate ammonia and nitrite oxidation biokinetic parameters from batch respirograms. *Water Research* 39(20):4969-4978.

Chung J, Bae W, Lee Y-W, Rittmann BE. 2007. Shortcut biological nitrogen removal in hybrid biofilm/suspended growth reactors. *Process Biochemistry* 42(3):320-328.

Dochain D, Vanrolleghem P. 2001. Dynamical modelling and estimation in wastewater treatment processes. London, UK: IWA Publishing.

Dochain D, Vanrolleghem PA, Van Daele M. 1995. Structural identifiability of biokinetic models of activated sludge respiration. *Water Research* 29(11):2571-2578.

Dold PL, Jones RM, Bye CM. 2005. Importance and measurement of decay rate when assessing nitrification kinetics. *Water Science and Technology* 52(10-11):469-477.

Egli K, Langer C, Siegrist HR, Zehnder AJB, Wagner M, Van der Meer JR. 2003. Community analysis of ammonia and nitrite oxidizers during start-up of nitritation reactors. *Applied and Environmental Microbiology* 69(6):3213-3222.

EPA. 1993. Manual of Nitrogen Control. Washington, DC, USA: US Environmental Protection Agency.

Galí A, Dosta J, Mace S, Mata-Alvarez J. 2006. Start-up of a biological sequencing batch reactor to treat supernatant from anaerobic sludge digester. *Environmental Technology* 27(8):891-899.

Gee CS, Suidan MT, Pfeffer JT. 1990. Modeling of Nitrification under Substrate-Inhibiting Conditions. *Journal of Environmental Engineering-ASCE* 116(1):18-31.

Gernaey AK, Petersen B, Ottoy JP, Vanrolleghem P. 2001. Activated sludge monitoring with combined respirometric-titrimetric measurements. *Water Research* 35(5):1280-1294.

Gernaey K, Vanrolleghem P, Verstraete W. 1998. On-line estimation of Nitrosomonas kinetic parameters in activated sludge samples using titration in-sensor-experiments. *Water Research* 32(1):71-80.

Ginestet P, Audic J-M, Urbain V, Block J-C. 1998. Estimation of Nitrifying Bacterial Activities by Measuring Oxygen Uptake in the Presence of the Metabolic Inhibitors Allylthiourea and Azide. *Appl. Environ. Microbiol.* 64(6):2266-2268.

Grunditz C, Dalhammar G. 2001. Development of nitrification inhibition assays using pure cultures of Nitrosomonas and Nitrobacter. *Water Research* 35(2):433-440.

Guisasola A. 2005. Modelling biological organic matter and nutrient removal processes from wastewater using respirometric and titrimetric techniques. PhD Thesis. Bellaterra: Universitat Autònoma de Barcelona.

Guisasola A, Baeza JA, Carrera J, Casas C, Lafuente J. 2003. An off-line respirometric procedure to determine inhibition and toxicity of biodegradable compounds in biomass from an industrial WWTP. *Water Science and Technology* 48(11-12):267-275.

Guisasola A, Baeza JA, Carrera J, Sin G, Vanrolleghem PA, Lafuente J. 2006. The influence of experimental data quality and quantity on parameter estimation accuracy. Andrews inhibition model as a case study. *Education for Chemical Engineers* 1:139-145.

Hao X, Heijnen JJ, Van Loosdrecht MCM. 2002a. Model-based evaluation of temperature and inflow variations on a partial nitrification-ANAMMOX biofilm process. *Water Research* 36(19):4839-4849.

Hao X, Heijnen JJ, Van Loosdrecht MCM. 2002b. Sensitivity analysis of a biofilm model describing a one-stage completely autotrophic nitrogen removal (CANON) process. *Biotechnology and Bioengineering* 77(3):266-277.

Head MA, Oleszkiewicz JA. 2004. Bioaugmentation for nitrification at cold temperatures. *Water Research* 38(3):523-530.

Hellinga C, Schellen AAJC, Mulder JW, Van Loosdrecht MCM, Heijnen JJ. 1998. The SHARON process: An innovative method for nitrogen removal from ammonium-rich waste water. *Water Science and Technology* 37(9):135-142.

Henze M, Gujer W, Mino T, Van Loosdrecht M. 2000. Activated sludge models ASM1, ASM2, ASM2D and ASM3. Scientific and technical report no. 9. London: IWA Publishing.

Hunik JH. 1993. Engineering aspects of nitrification with immobilized cells. PhD Thesis. Wageningen: Agricultural University.

Hunik JH, Bos CG, Van den Hoogen MP, De Gooijer CD, Tramper J. 1994a. Co-immobilized Nitrosomonas europaea and Nitrobacter agilis cells: Validation of a dynamic model for simultaneous substrate conversion and growth in k-carrageenan gel beads. *Biotechnology and Bioengineering* 43(11):1153-1163.

Hunik JH, Tramper J, Wijffels RH. 1994b. A strategy to scale up nitrification processes with immobilized cells of Nitrosomonas europaea and Nitrobacter agilis. *Bioprocess Engineering* 11(2):73-82.

Hynes RK, Knowles R. 1983. Inhibition of chemoautrophic nitrification by sodium chlorate and sodium chlorite: A reexamination. *Applied and Environmental Microbiology* 45(4):1178-1182.

Kim DJ, Seo D. 2006. Selective enrichment and granulation of ammonia oxidizers in a sequencing batch airlift reactor. *Process Biochemistry* 41(5):1055-1062.

Knowles G, Downing AL, Barrett MJ. 1965. Determination of kinetic constants for nitrifying bacteria in mixed culture, with the aid of an electronic computer. *Journal of General Microbiology* 38:263-278.

Liebig T, Wagner M, Bjerrum L, Denecke M. 2001. Nitrification performance and nitrifier community composition of a chemostat and a membrane-assisted bioreactor for the nitrification of sludge reject water. *Bioprocess and Biosystems Engineering* 24(4):203-210.

López-Fiuza J, Buys B, Mosquera-Corral A, Omil F, Méndez R. 2002. Toxic effects exerted on methanogenic, nitrifying and denitrifying bacteria by chemicals used in a milk analysis laboratory. *Enzyme and Microbial Technology* 31(7):976-985.

Marsili-Libelli S, Tabani F. 2002. Accuracy analysis of a respirometer for activated sludge dynamic modelling. *Water Research* 36(5):1181-1192.

MATLAB. 2002. User's guide. Version 6.5 (Release 13). Mathworks T, editor. Natick, USA.

Moussa MS, Hooijmans CM, Lubberding HJ, Gijzen HJ, Van Loosdrecht MCM. 2005. Modelling nitrification, heterotrophic growth and predation in activated sludge. *Water Research* 39(20):5080-5098.

Novák L, Larrea L, Wanner J. 1994. Estimation of maximum specific growth rate of heterotrophic and autotrophic biomass: A combined technique of mathematical modelling and batch cultivations. *Water Science and Technology* 30(11):171-180.

Nowak O, Schweighofer P, Svardal K. 1994. Nitrification inhibition - A method for the estimation of actual maximum autotrophic growth rates in activated sludge systems. *Water Science and Technology* 30(6):9-19.

Nowak O, Svardal K, Schweighofer P. 1995. The dynamic behaviour of nitrifying activated sludge systems influenced by inhibiting wastewater compounds. *Water Science and Technology* 31(2):115-124.

Pambrun V, Paul E, Spérandio M. 2006. Modeling the partial nitrification in sequencing batch reactor for biomass adapted to high ammonia concentrations. *Biotechnology and Bioengineering* 95(1):120-131.

Pérez J, Picioreanu C, Van Loosdrecht M. 2005. Modeling biofilm and floc diffusion processes based on analytical solution of reaction-diffusion equations. *Water Research* 39(7):1311-1323.

Petersen B, Gernaey K, Devisscher M, Dochain D, Vanrolleghem PA. 2003. A simplified method to assess structurally identifiable parameters in Monod-based activated sludge models. *Water Research* 37(12):2893-2904.

Picioreanu C, Van Loosdrecht MCM, Heijnen JJ. 1997. Modelling the effect of oxygen concentration on nitrite accumulation in a biofilm airlift suspension reactor. *Water Science and Technology* 36(1):147-156.

Sánchez O, Martí MC, Aspé E, Roeckel M. 2001. Nitrification rates in a saline medium at different dissolved oxygen concentrations. *Biotechnology Letters* 23(19):1597-1602.

Shammas NK. 1986. Interactions of temperature, pH, and biomass on the nitrification process. *Journal of the Water Pollution Control Federation* 58(1):52-59.

Sheintuch M, Tartakovsky B, Narkis N, Rebhun M. 1995. Substrate inhibition and multiple states in a continuous nitrification process. *Water Research* 29(3):953-963.

SigmaPlot‒8.0. 2002. Programming Guide. SPSS Science Marketing Department. SPSS, editor. Chicago, IL 60606-6307, USA.

Sözen S, Orhon D, San HA. 1996. A new approach for the evaluation of the maximum specific growth rate in nitrification. *Water Research* 30(7):1661-1669.

Spanjers H, Vanrolleghem P. 1995. Respirometry as a tool for rapid characterization of wastewater and activated sludge. *Water Science and Technology* 31(2):105-114.

Spanjers H, Vanrolleghem P, Olsson G, Dold PL. 1997. Respirometry in control of the activated sludge process: principles. Scientific and technical report no. 7. London: IWA Publishing.

Stephanopoulos G. 1984. Chemical Process Control. An introduction to theory and practice: Prentice/Hall International, Inc. New Jersey.

Surmacz-Gorska J, Gernaey K, Demuynck C, Vanrolleghem P, Verstraete W. 1996. Nitrification monitoring in activated sludge by oxygen uptake rate (OUR) measurements. *Water Research* 30(5):1228-1236.

Tchobanoglous G, Burton F. 1991. Wastewater engineering: treatment, disposal and reuse. Metcalf, Eddy, editors. New York: McGraw-Hill.

Vadivelu VM, Keller J, Yuan Z. 2006a. Effect of free ammonia and free nitrous acid concentration on the anabolic and catabolic processes of an enriched Nitrosomonas culture. *Biotechnology and Bioengineering* 95(5):830-839.

Vadivelu VM, Keller J, Yuan Z. 2006b. Stoichiometric and kinetic characterisation of Nitrosomonas sp. in mixed culture by decoupling the growth and energy generation processes. *Journal of Biotechnology* 126(3):342-356.

Vadivelu VM, Yuan Z, Fux C, Keller J. 2006c. The inhibitory effects of free nitrous acid on the energy generation and growth processes of an enriched Nitrobacter culture. *Environmental Science and Technology* 40(14):4442-4448.

Vadivelu VM, Yuan Z, Fux C, Keller J. 2006d. Stoichiometric and kinetic characterisation of Nitrobacter in mixed culture by decoupling the growth and energy generation processes. *Biotechnology and Bioengineering* 94(6):1176-1188.

Van Hulle SWH. 2005. Modelling, simulation and optimization of autotrophic nitrogen removal processes. PhD Thesis. Gent: Gent University.

Van Hulle SWH, Volcke EIP, López Teruel J, Donckels BMR, Van Loosdrecht MCM, Vanrolleghem P. Influence of temperature and pH on the kinetics of the SHARON nitritation process. *In: Proceedings of 4th IWA World Water Congress and Exhibition* 2004; Marrakech, Morocco. IWA Publishing.

Vanrolleghem P, Gernaey K, Petersen B, De Clercq B, Coen F, Ottoy JP. Limitations of short-term experiments designed for identification of activated sludge biodegradation models by fast dynamic phenomena. *In: Proceedings of 7th IFAC Conference on Computer Applications in Biotechnology* 1998; Osaka, Japan.

Vanrolleghem PA, Van Daele M, Dochain D. 1995. Practical identifiability of a biokinetic model of activated sludge respiration. *Water Research* 29(11):2561-2570.

Wett B, Rauch W. 2003. The role of inorganic carbon limitation in biological nitrogen removal of extremely ammonia concentrated wastewater. *Water Research* 37(5):1100-1110.

Wiesmann U. 1994. Biological nitrogen removal from wastewater. *Advances in biochemical engineering/biotechnology* 51:113-154.

Wyffels S, Van Hulle SWH, Boeckx P, Volcke EIP, Van Cleemput O, Vanrolleghem PA, Verstraete W. 2004. Modeling and simulation of oxygen-limited partial nitritation in a membrane-assisted bioreactor (MBR). *Biotechnology and Bioengineering* 86(5):531-542.

Yuan Z, Bogaert H, Devisscher M, Vanrolleghem P, Verstraete W. 1999. On-line estimation of the maximum specific growth rate of nitrifiers in activated sludge systems. *Biotechnology and Bioengineering* 65(3):265-273.

PART II - Chapter 4

PILOT PLANT DESCRIPTION AND MODELING

The pilot plant used in this work consisted of three mixed reactors and a settler. Each reactor was equipped with dissolved oxygen (DO), pH and temperature probes which were connected to a programmable logic controller (PLC) and a process computer (PC) for control and monitoring purposes. Automatic in-line oxygen uptake rate (OUR) estimation was available in each reactor and supervisory control was implemented. Water evaporation was detected during normal operation. It was calculated to be 2.5 ± 0.8 L d^{-1}. Ammonia stripping rate was measured and compared to the biological nitrogen removal rate. Results showed that the percentage of stripped ammonia was less than 1 %. The hydraulic model for the reactors and the settler was built. Reactors were modeled as ideal continuous stirred tank reactors (CSTR) and the settler was modeled as a one-dimensional settler with ten layers and without biological reactions. The settling velocity was calculated with a double-exponential velocity model as suggested in Takács et al. (1991).

1. INTRODUCTION

Research on wastewater treatment is usually performed at laboratory scale because of its advantages: the wastewater flow is low; the required space is small; the system can easily be handled; the amount of biomass required for the inoculation is low; and the environmental conditions are easily controlled.

However, before the implementation of the new technologies and processes to full scale, a transitional step is required: the pilot scale. In pilot scale systems, the working volume is higher than in the laboratory scale, the space required is bigger, and the wastewater container must also be bigger. On the other hand, the advantages of the pilot scale are that the used instruments, valves and pumps are more similar to the ones used in full scale and thus the system behavior is also closer to full scale. Therefore, most of the research in this thesis was performed in a pilot plant.

When modeling a wastewater treatment system, the correct modeling of the physical processes and the hydraulic configuration is as much important as the accurate modeling of the biological processes. This means that if problems like incorrect reactor mixing in continuous stirred tank reactors (CSTR), dispersion in plug flow reactors (PFR), water evaporation, ammonia or carbon dioxide stripping, biomass wall growth, biological reactions in the settler, bad settling properties of the sludge, etc, were occurring but not considered, the final model would be inappropriate for the system description. In other words, if a very good model for the description of the biological reactions is available but the system is poorly described, the final result will not be truthful. On the other hand, too complex models involve the calibration of a lot of parameters and require high computer capacity and speed. Thus, there must be a compromise between accurate description and model simplicity.

Regarding CSTR modeling, they are usually modeled as ideal reactors and accurate results are obtained. However, with respect to secondary settlers, their complex behavior has made the settling process a major issue for researchers working within the field of mathematical modeling and several models are available in the literature. They vary from simple ideal separators, with no retention time, to the one-dimensional layered settler of Takács et al. (1991). For a very comprehensive overview on modeling approaches see Jeppsson (1996). In most of the studies, the assumption of no reactions taking place is used although it may not be valid if considerable amount of sludge is stored in the bottom of the settler. In these cases reactive settler models are also available (Gernaey et al. 2006).

2. OBJECTIVES

The main objective of this chapter is to build a model for the description of the physical behavior of the experimental system (pilot plant): the reactors and the settler. It implies the examination of the ammonia stripping and water evaporation phenomena to decide whether they must be included in the model or not.

3. MATERIALS AND METHODS

This section shows the description of the pilot plant used in most of the chapters of this thesis. This description includes the available instrumentation and control loops, the automatic oxygen uptake rate estimation (OUR) and the implemented supervisory control. The evaporation flow assessment and the ammonia stripping assessment are also detailed in this section.

3.1 PILOT PLANT DESCRIPTION

The experimental system used in this thesis was a pilot-scale activated sludge system. It was built and provided with in-line sensors and controllers by Juan Baeza as part of his PhD thesis (Baeza 1999). It was previously operated as an A^2/O system for biological removal of organic matter and nutrients from municipal wastewater (Baeza et al. 1999; Baeza et al. 2002a; Baeza et al. 2002b; Baeza et al. 2004). In addition, the research group has experience with a similar pilot plant operating as a nitrification/denitrification system for the treatment of a high-strength ammonium wastewater (Carrera 2001; Carrera et al. 2003; Carrera et al. 2004). Figures 4.1 and 4.2 show a schematic diagram and a picture, respectively, of the whole pilot plant set-up.

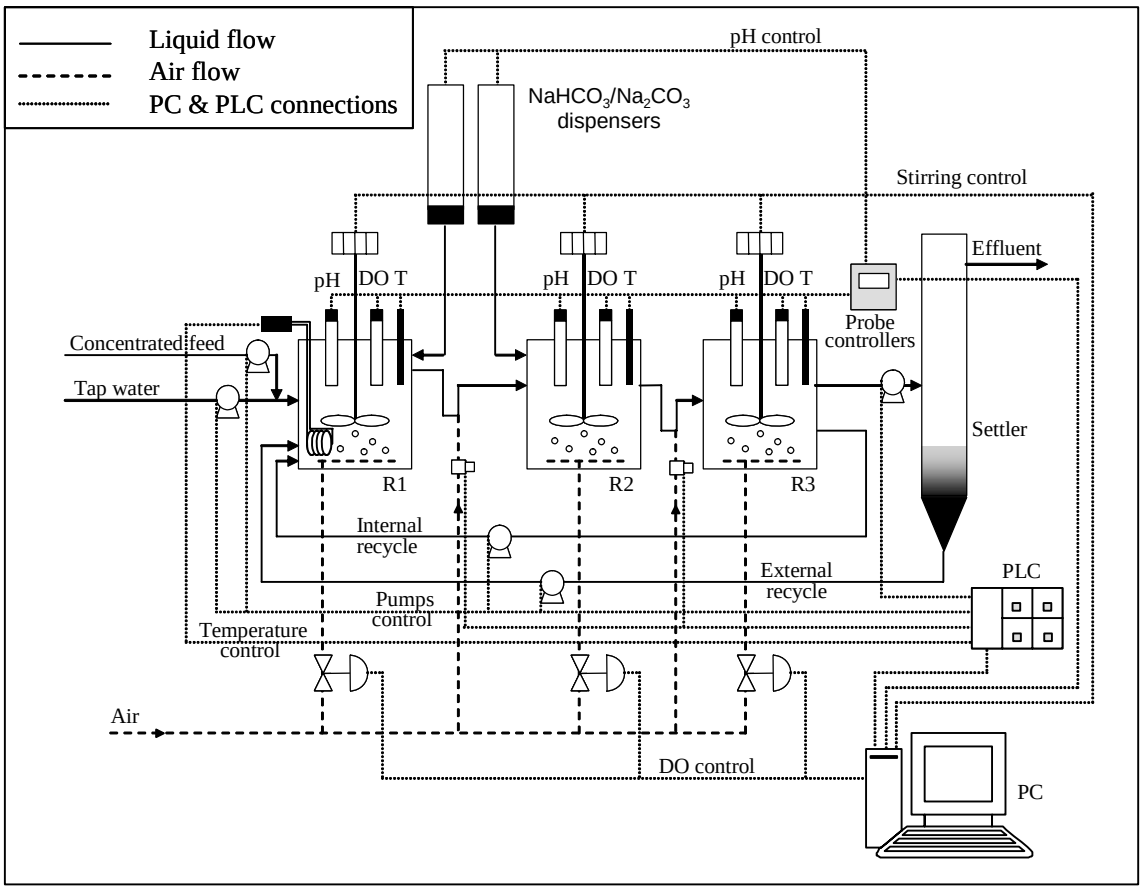

Figure 4.1 Schematic representation of the pilot plant.

Figure 4.2 Pilot plant picture.

The experimental system consisted of three aerobic reactors (named R1, R2 and R3) with a working volume of 26 L followed by a 25 L settler. The reactors were connected in series and they worked under completely mixed conditions. The mixed liquor was flowing from R1 to R2 and from R2 to R3 with the help of two pneumatic pumps. However, these pumps were substituted for intermittent air injections into the connection pipe because they proved better performance. The liquid flow between R3 and the settler was driven by a peristaltic pump and the concentrated sludge, underflow of the settler, was recycled to R1 (external recycle) with the help of a membrane dosing pump. A fraction of R3 effluent was also recycled to R1 (internal recycle) with a peristaltic pump to increase the dynamics of the system and to improve the mixing between reactors. Each reactor was provided with mechanical stirring and aeration. The air was supplied through three air diffusers placed at the bottom of the reactors. Mixed liquor was withdrawn daily from the three reactors in order to keep a desired sludge retention time (SRT).

The influent consisted of synthetic wastewater with high ammonium concentration and low COD concentration. A concentrated solution (x10) was prepared fortnightly and stored at 8 ºC. This solution was in-situ diluted with tap water before entering R1. Two membrane dosing pumps were used to supply both concentrated feed and tap water to R1. The final composition of the wastewater entering the system (after dilution) is shown in Table 4.1.

Table 4.1 Feed composition

Component	Concentration (mg L^{-1})
NH_4Cl	11500 (3000 mg N L^{-1})
CH_3COONa	145 (100 mg COD L^{-1})
$CaCl_2 \cdot 2H_2O$	8
KH_2PO_4	40
NaCl	16
$MgCl_2 \cdot 7H_2O$	18
$FeSO_4 \cdot 7H_2O$	0.4
$MnSO_4 \cdot H_2O$	0.3
$ZnSO_4 \cdot 7H_2O$	0.4
$CuSO_4 \cdot 5H_2O$	0.2
H_3BO_3	0.02

3.1.1 INSTRUMENTATION AND CONTROL

Each reactor was equipped with a dissolved oxygen (DO) probe (initially Crison Oxi-92 and then replaced for WTW Oxi 340i CellOx 325), a pH probe (Crison pH 52-03) and a temperature probe (Pt-100). All of them were connected to a probe controller equipment (Crison pHrocon18) which actuated as a pH on-off controller in R1 and R2 by the addition of

solid $NaHCO_3$ (or Na_2CO_3 for pH > 8) through solid dispensers. The probe controller equipment was connected to a process computer (PC). The software for this PC, developed in C language, included monitoring, data backup, programmable logic controller (PLC) supervision and control of the key process parameters (DO, temperature, flow-rates and stirring rates). This computer allowed the pilot plant to be controlled via a set of predetermined set points.

The DO control was based on a digital proportional-integral-derivative (PID) algorithm programmed in the computer, which modified the airflow through the manipulation of the pneumatic control valves of every reactor (via 4-20 mA loop). The flow rates of the recycle pumps and the stirring rates of each reactor could also be modified through the PC. The temperature control, based on an on-off control, was implemented in R1. The PC (through the PLC) was in charge of switching on an electric heating device (10 seconds per minute) when the temperature was below the set point.

The hardware architecture of the pilot plant comprised also the PLC which was connected to the PC and controlled some on-off devices (inflow pumps, flows between reactors, recycle pumps and level detectors). The PLC was programmed as a distributed direct digital controller (DDDC). This means that it was in charge of the process control while the PC actuated as a supervisor by changing the operation mode and the set points. Moreover, if case of PC failure, the system continued running with the same operation mode because of the PLC.

R1, R2 and the settler were equipped with level detectors in order to avoid mixed liquor overflow which could cause lost of biomass and laboratory flooding. Moreover, two dampness detectors were placed on the floor under the pilot plant to detect liquid spillage. When either level detectors or dampness detectors were activated, the inflow pumps were automatically deactivated. However, DO control and pH control were still working to keep the biomass under the optimal conditions.

R3 was also equipped with a level detector. In this case, it was used by the PLC to start the liquid flow from R3 to the settler through by activating the corresponding peristaltic pump. Furthermore, the liquid flows from R1 to R2 and from R2 to R3 were also controlled by the PLC. In this case, it actuated over the air electrovalves. The external and internal recycle pumps were also connected to the PLC.

3.1.2 IN-LINE OUR ESTIMATION

Automatic in-line OUR estimation was implemented in each reactor. Baeza et al. (2002b) used these measurements in the same pilot plant for monitoring and control of the system. Although it was previously described in Chapter 3, were it was used for model parameters calibration, an extended description is shown here.

The OUR measurement was performed every 5 or 10 minutes and it was based on the DO decrease in the liquid phase with no air inlet: LSS respirometry (Spanjers et al. 1997). Each OUR measurement began with the deactivation of the PID controller over aeration. Then, the aeration valve was shut down and the stirring speed reduced from normal operation (200 rpm) to 100 rpm to minimize surface oxygen transfer. Next, DO measurements were acquired every 4 seconds until the DO decreased by 1.5 mg O_2 L^{-1} or during a maximum period of 4 minutes. At this point, the stirring speed was increased to normal operation. Finally, the acquired measurements were fitted to a linear regression to calculate the OUR value. In this calculation, the first three DO measurements were not used in order to avoid the effect of the sensor dynamics. Baeza et al. (2002b) calculated that, for a first order dynamics, the 95 % of the correct response was obtained after three times the time constant of the sensor (experimentally assessed as 4.6 ± 0.6 s).

The high salt content of the mixed liquor (due to the high ammonia concentration and the pH control) influenced the saturation oxygen concentration in the liquid since it decreases when the salt content increases. This phenomenon was taken into account in the DO probe calibration. Otherwise, DO and OUR measurements would have been overestimated.

3.1.3 SUPERVISORY CONTROL

The PC was linked via Ethernet to a data server executed in a Sun Sparcstation running the Solaris operating system. This allowed a database to be maintained in real time with the produced information. The Knowledge-Based Expert System (KBES) was on the top of the system architecture. It was developed using G2® (Gensym 1995) as a tool to develop real-time expert systems and it was implemented in the Sun Sparcstation and used in a previous work to improve the nitrogen removal efficiency of the A^2/O pilot plant (Baeza et al. 2000; Baeza et al. 2002a). In the work presented in this thesis, only little of the KBES potential was used for the implementation of expert rules for the improvement of a partial nitrification system (see Chapter 7).

Moreover, the data server was also connected to Internet and real-time data could be checked from any computer with Internet connection. Therefore, the state of the system could always be known at any time from anywhere.

3.2 EVAPORATION FLOW ASSESSMENT

In order to quantify the evaporation flow, the effluent from the system was collected during a 24-hour period. The collected liquid volume was then compared to the volume of feed that entered the system during the same period. The difference between both liquid volumes was considered to be the evaporated water. This experiment was performed 16 times under different conditions of temperature and aeration flow.

3.3 AMMONIA STRIPPING ASSESSMENT

Ammonia stripping rate was evaluated with a batch experiment in one of the pilot plant reactors using tap water to avoid biological removal. The temperature and pH set points were fixed to 29 ºC and 8.5 respectively to favor the occurrence of this phenomenon. The aeration valve was fixed to 70 % opened (control signal of 15 mA). An ammonium pulse was added to the reactor giving a final concentration of 180 mg N L^{-1} in terms of total ammonium nitrogen (TAN) and 42 mg L^{-1} in terms of free ammonia (FA). Samples were periodically withdrawn to monitor FA concentration. TAN was analyzed by means of a continuous flow analyzer (CFA) based on potentiometric determination of ammonia (Baeza et al. 1999) and FA concentration was calculated with the equilibrium equation (see Chapter 3). Evaporated water was replaced with tap water and thus, the liquid volume was kept constant throughout the whole experiment.

The ammonia stripping rate can be calculated using equation 4.1, in which it is considered that the highest resistance to the mass transfer is in the liquid phase:

$$\frac{dS_{FA}}{dt} = k_L a_{FA} \cdot \left(S_{FA}^{*} - S_{FA}\right) \qquad (4.1)$$

where k_La_{FA} is the global FA transfer constant, S_{FA} is the FA concentration in the liquid phase and S_{FA}^{*} is the FA saturation concentration in equilibrium with the gas phase. Musvoto et al. (2000) already described the transfer rate independent of the ammonia in the gas phase since the concentration of ammonia in the gas phase is usually zero ($S_{FA}^{*} = 0$) and hence:

$$\frac{dS_{FA}}{dt} = -k_L a_{FA} \cdot S_{FA} \qquad (4.2)$$

If this differential equation is solved, equation 4.3 is obtained:

$$S_{FA}(t) = S_{FA}(0) \cdot \exp\left(-k_L a_{FA} \cdot t\right) \qquad (4.3)$$

where, $S_{FA}(t)$ is the FA concentration at a specific time (t) and $S_{FA}(0)$ is the initial FA concentration. Experimental data (FA vs t) were fitted to equation 4.3 using Matlab 6.5® (2002) and k_La_{FA} was estimated.

4. RESULTS AND DISCUSSION

After the examination of some practical considerations, the hydraulic model for the description of the reactors and the settler are shown in this section. The mass balances and the settling velocity equations are also depicted.

4.1 PRACTICAL CONSIDERATIONS

Previously to the pilot plant model construction, some practical considerations as water evaporation, ammonia stripping and wall growth were examined in order to be able to accurately describe the processes occurring in the reactors.

With respect to the wall growth, the existence of this attached biomass could result in higher SRT than the calculated one and could also favor anoxic conditions. Although the occurrence of these phenomena would not have had a significant effect on the overall performance of the system, biomass was manually scrapped of the reactors walls every day. Evaporation and ammonia stripping are considered in the next sections.

4.1.1 EVAPORATION

Dry air was used for reactor aeration and therefore water evaporation occurred. Evaporation was also detected in Fux et al. (2002) when they observed that the sum of the dissolved nitrogen compounds in the effluent of a partial nitrification system was 3% higher than the inlet ammonium concentration. Another example can be found in Van Hulle et al. (2005), where they calculated that about 14 to 37 % of the inflow of a SHARON reactor evaporated.

In this work, evaporation was also detected because higher total nitrogen concentration in the effluent than in the influent was observed. The obtained average evaporation flow was 2.5 ± 0.8 L d^{-1}, which was about 10 to 25 % of the system inflow. Since the evaporation rate is proportional to the system temperature and air flow rate, experimental data were plotted against these variables. However, the air flow rate was not available and the control signal (4-20 mA) for the aeration valve of R1 was used as an alternative (as much higher the control signal was, higher the aeration flow was). Figure 4.3.A shows evaporation flow data vs temperature and Figure 4.3.B shows the same experimental data vs the control signal for the aeration valve.

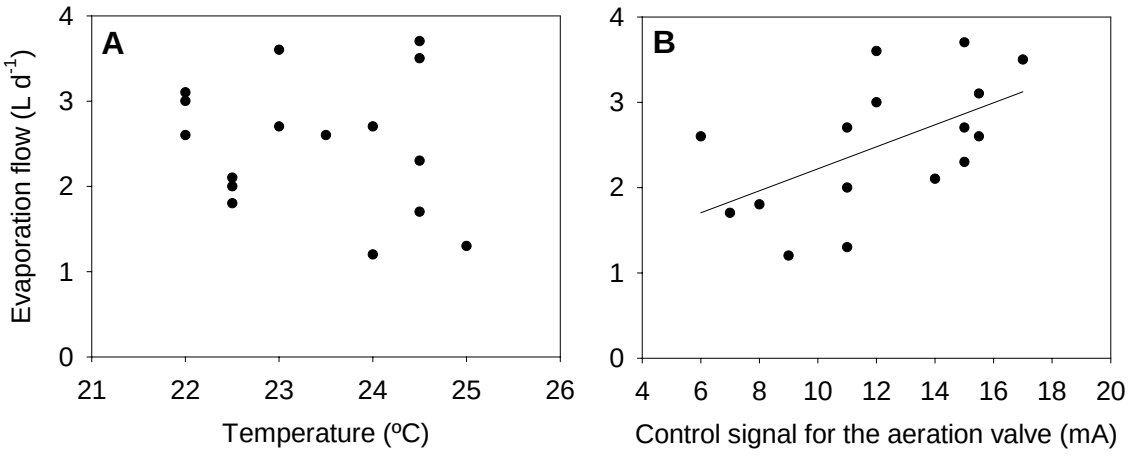

Figure 4.3 Effect of temperature (**A**) and aeration (**B**) on the water evaporation in the pilot plant.

It can be concluded that the temperature effect on the evaporation was not significant because experimental data showed to be quite scattered and without a clear tendency. Probably, the tested temperature range was too narrow and furthermore, other factors were also affecting the system. On the contrary, an increasing trend was observed when the aeration was considered. In this case, higher aeration led to higher evaporation flow, as expected.

The evaporation flow was daily compensated with the addition of tap water. The volume of added water ranged from 1.7 to 3.3 L d^{-1} depending on the aeration flow in R1. Therefore, the evaporation was not considered in the pilot plant modeling.

4.1.2 AMMONIA STRIPPING

Figure 4.4 shows the time course of FA concentration that was used for k_La_{FA} calculation. It was estimated to be 0.32 d^{-1} under the used experimental conditions: T = 29 ºC, pH = 8.5, airflow corresponding to 70 % opened aeration valve and tap water. Figure 4.4 also shows the long-term model prediction.

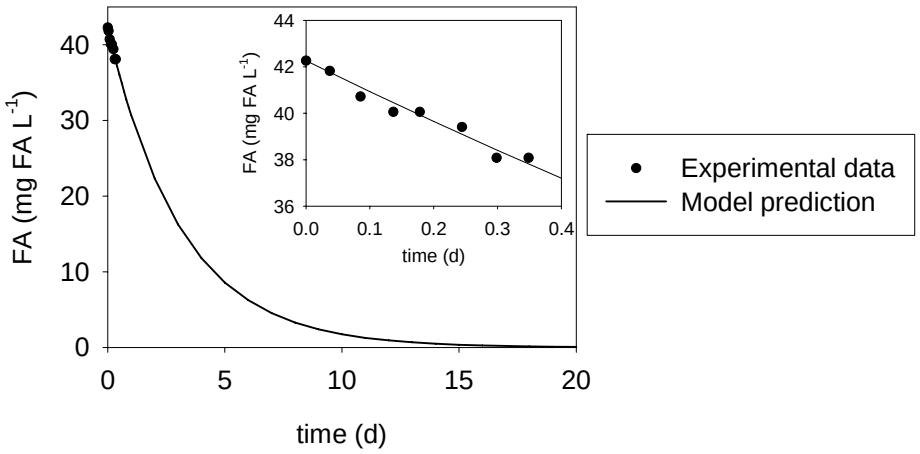

Figure 4.4 Experimental data and long-term model prediction for the ammonia stripping assessment.

With this coefficient and equation 4.2, the maximum ammonia stripping rate occurring in the pilot plant could be roughly estimated. If TAN concentration in R1, R2 and R3 were 150, 25 and 2 mg N L^{-1} respectively, and the conditions were pH = 8.5 and T = 25 ºC, FA concentration would be 28, 5 and 0.4 mg FA L^{-1} in R1, R2 and R3, respectively. These concentrations would lead to the following ammonia stripping rates: 8.96, 1.6 and 0.13 mg FA L^{-1} d^{-1}. Considering the reactors volume and transforming the result into g N-FA L^{-1}, the total daily amount of stripped ammonia was 0.23 g N-FA d^{-1}.

A typical nitrogen removal rate in the pilot plant was considered (400 mg N-TAN L^{-1} d^{-1}) to determine the significance of the stripping process into the biological nitrogen removal. Taking into account the system volume, the total daily amount of removed nitrogen was calculated as 31.2 g N-TAN d^{-1}, which compared to the daily amount of stripped ammonia

showed that the stripping accounted for less than 1 % of the total removed nitrogen. In view of these results, ammonia stripping was not considered in the pilot plant modeling.

4.2 HYDRAULIC MODEL

The hydraulic model used to describe the pilot plant is presented in this section. Figure 4.5 shows a simplified diagram of the pilot plant which includes the used nomenclature.

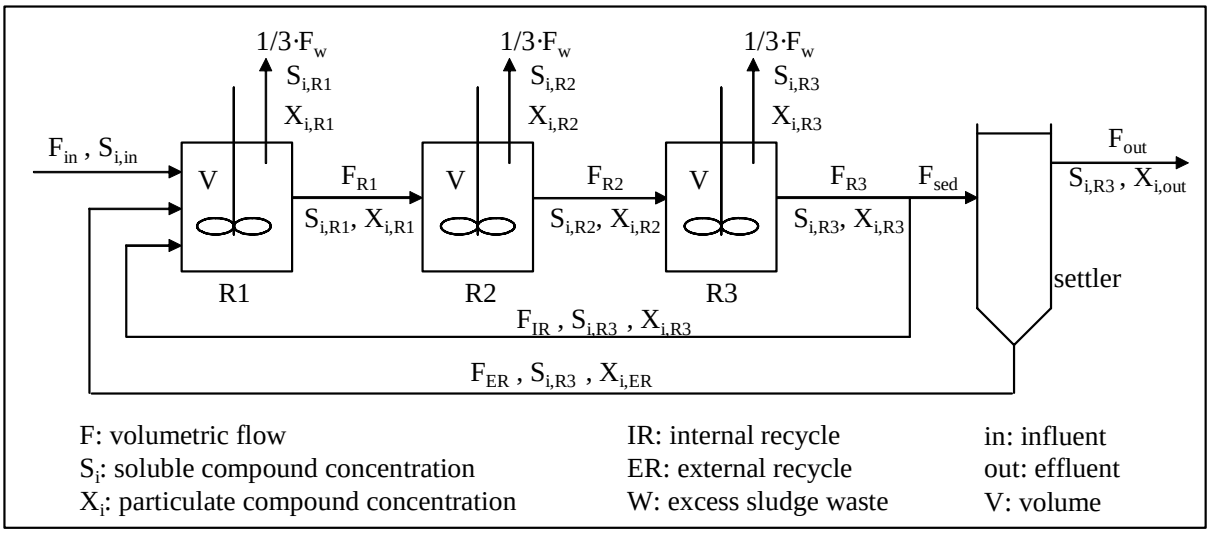

Figure 4.5 Simplified diagram of the pilot plant with used nomenclature.

4.2.1 REACTORS

Gabriel (1996) studied the performance of the pilot plant reactors and showed that their behavior were quite close to the ideal behavior of CSTR, therefore, they were modeled as ideal CSTR, i.e. homogenous composition in the entire volume and equal to the effluent composition. The volume was considered invariable.

Equations 4.4 to 4.8 describe the total mass balances in the system.

$$F_{out} = F_{in} - F_W \tag{4.4}$$

$$F_{R1} = F_{in} + F_{IR} + F_{ER} - \frac{1}{3}F_W \tag{4.5}$$

$$F_{R2} = F_{R1} - \frac{1}{3}F_W \tag{4.6}$$

$$F_{R3} = F_{R2} - \frac{1}{3}F_W \tag{4.7}$$

$$F_{sed} = F_{R3} - F_{IR} \tag{4.8}$$

Equations 4.9 to 4.11 show the mass balances for a soluble compound (S_i) for R1, R2 and R3, respectively. The biological reaction rates (described in Chapter 3) are indicated as r_{Si}. Note that the evaporation and ammonia stripping are not considered as already explained.

$$\frac{dS_{i,R1}}{dt} = \frac{F_{in}}{V}\cdot S_{i,in} + \frac{F_{IR}}{V}\cdot S_{i,R3} + \frac{F_{ER}}{V}\cdot S_{i,R3} - \frac{F_{R1}}{V}\cdot S_{i,R1} - \frac{F_W}{3\cdot V}\cdot S_{i,R1} + r_{Si,R1} \tag{4.9}$$

$$\frac{dS_{i,R2}}{dt} = \frac{F_{R1}}{V}\cdot S_{i,R1} - \frac{F_{R2}}{V}\cdot S_{i,R2} - \frac{F_W}{3\cdot V}\cdot S_{i,R2} + r_{Si,R2} \tag{4.10}$$

$$\frac{dS_{i,R3}}{dt} = \frac{F_{R2}}{V}\cdot S_{i,R2} - \frac{F_{R3}}{V}\cdot S_{i,R3} - \frac{F_W}{3\cdot V}\cdot S_{i,R3} + r_{Si,R3} \tag{4.11}$$

Equations 4.12 to 4.14 show the mass balances for a particulate compound (X_i) for each reactor. The biological reaction rates (described in Chapter 3) are indicated as r_{Xi}.

$$\frac{dX_{i,R1}}{dt} = \frac{F_{IR}}{V}\cdot X_{i,R3} + \frac{F_{ER}}{V}\cdot X_{i,ER} - \frac{F_{R1}}{V}\cdot X_{i,R1} - \frac{F_W}{3\cdot V}\cdot X_{i,R1} + r_{Xi,R1} \tag{4.12}$$

$$\frac{dX_{i,R2}}{dt} = \frac{F_{R1}}{V}\cdot X_{i,R1} - \frac{F_{R2}}{V}\cdot X_{i,R2} - \frac{F_W}{3\cdot V}\cdot X_{i,R2} + r_{Xi,R2} \tag{4.13}$$

$$\frac{dX_{i,R3}}{dt} = \frac{F_{R2}}{V}\cdot X_{i,R2} - \frac{F_{R3}}{V}\cdot X_{i,R3} - \frac{F_W}{3\cdot V}\cdot X_{i,R3} + r_{Xi,R3} \tag{4.14}$$

4.2.2 SETTLER

The settler was modeled as an one-dimensional settler with ten layers (Vitasovic 1985) and it was based on the solids flux concept which states that the solid flux of particles due to gravity sedimentation J_S, depends on the sludge concentration (X_{TSS}) and its settling velocity (Kynch 1952).

The main assumptions, based on conditions known to exist in a continuous thickener and initial and boundary conditions, were (Jeppsson 1996): (1) the continuous thickener did not exhibit vertical dispersion; (2) the concentration of total suspended solids (TSS) was completely uniform within any horizontal plane within the settler; (3) there was no significant biological reaction affecting the solids mass concentration within the separator, i.e. it was considered as a non reactive settler; (4) the mass flux into a differential volume could not exceed the mass flux that the volume was capable of passing, nor could it exceed the mass flux which the volume

immediately below it was capable of passing; (5) the gravitational settling velocity was a function only of the TSS concentration except when the fourth assumption was violated.

Considering these assumptions, TSS mass balance around each of the ten layers was written as shown in Figure 4.6, using the following nomenclature: $X_{TSS,i}$ is the TSS concentration in the layer i, $J_{S,i}$ is the TSS flux from layer i, h_L is the layer height, A is the cross-sectional area of the settler and F_{out}, F_{sed} and F_{RE} are the effluent, influent and underflow respectively. The layers were numbered from the bottom to the top and the feed level was placed in layer 5. Figure 4.6 also shows a schematic overview of the one-dimensional model.

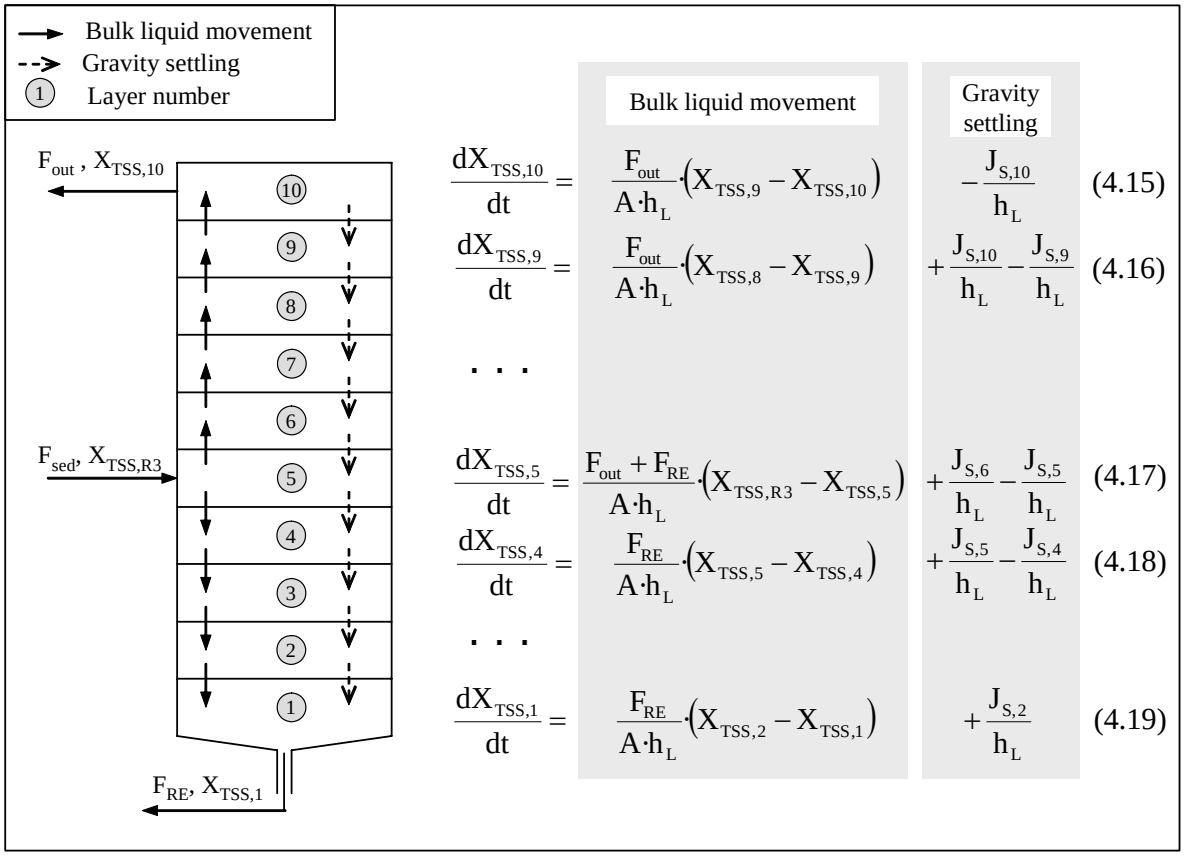

Figure 4.6 Schematic overview and TSS mass balances for the one-dimensional settler model with 10 equidistant layers and constant cross-sectional area.

Each TSS flux was calculated using equation 4.20, where $v_{S,i}$ is the settling velocity of TSS in layer i.

$$J_{S,i} = \min\left(v_{S,i} \cdot X_{TSS,i}, v_{S,i-1} \cdot X_{TSS,i-1}\right) \tag{4.20}$$

Settling velocity was calculated with the double-exponential velocity model suggested by Takács et al. (1991) shown in equation 4.21. This equation reflects the settling velocity of both the large, well flocculating particles, and the smaller, slowly settling particles:

$$v_{S,i} = \max\left(0, \min\left(v'_0, v_0 \cdot e^{-r_h \cdot (X_{TSS,i} - X_{TSS,min})} - v_0 \cdot e^{-r_p \cdot (X_{TSS,i} - X_{TSS,min})}\right)\right) \quad (4.21)$$

where v'_0 is the maximum practical settling velocity and v_0 is the maximum theoretical settling velocity, r_h is a settling parameter characteristic of the hindered settling zone and r_p is a parameter associated with the settling behavior at low solids concentration. X_{min} is the minimum attainable concentration of TSS in the effluent and is in turn a function of the settler influent concentration of solids (equation 4.22):

$$X_{TSS,min} = f_{ns} \cdot X_{TSS,R3} \quad (4.22)$$

where f_{ns} is the non-settleable fraction of $X_{TSS,R3}$. The inclusion of this equation directly influenced the behavior of the settler, especially within the clarification zone (upper part of the settler). In practice, f_{ns} was calculated as the ratio between the experimental TSS concentration in the clarified effluent ($X_{TSS,out}$) and the experimental TSS entering the settler ($X_{TSS,R3}$).

Values for all the model parameters required in this settler model are detailed in Table 4.2.

Table 4.2 Settling and settler parameters required in the settler model.

Parameter	Value	Reference
v'_0	100 m d^{-1}	Jeppsson (1996)
v_0	145 m d^{-1}	Jeppsson (1996)
r_h	0.000576 m^3 g^{-1} TSS	Copp et al. (2002)
r_p	0.00286 m^3 g^{-1} TSS	Copp et al. (2002)
f_{ns}	$X_{TSS,out}/X_{TSS,R3}$	Experimental data
A	0.0314 m^2	Experimental data
h_L	0.0925 m	Experimental data

It is important to note that within the settler, the sludge is considered to be present in the form of flocs that contain all the particulate compound of the model because the settling velocity function depends only on the TSS concentration. This implies that for a certain concentration there is only one unique settling velocity, which is a rough approximation valid only if all flocs are completely uniform in size, composition, structure, etc (Jeppsson and Diehl 1996). In order to couple this settler model to the reactors model in an accurate way, a proper method for transforming the different COD fractions into a TSS equivalent was required (Diehl and Jeppsson 1998). In this case, all particulate compounds were transformed using the coefficient: 0.704 g TSS g^{-1} COD (Henze et al. 2000). The only parameter which was not included in this calculation was X_{ND} because it is a subset of the other particulate components and is already included in their concentration. The same coefficient was used in the transformation of the underflow TSS concentration to the concentration of the specific particulate compounds which

were recycled to R1. It was considered that the fraction of each particulate compound in the underflow was the same as in the settler inflow.

With respect to the soluble compounds, since it was considered that there were no biological reactions in the settler, their concentration remained unchanged. This approach was considered appropriate for various reasons: (1) the oxygen concentration was very low and no nitrification or heterotrophic aerobic growth could take place; (2) biodegradable COD was too low for significant anoxic growth; (3) the height of the sludge blanket was always very low indicating that the SRT of the settler was very low and that the decay process could not significantly affect the system.

As a summary, the developed model consisted of 5 total mass balances and 43 differential equations: 11·3 mass balances for R1, R2 and R3 (one for each component: S_{TAN}, S_{TNN}, S_{NO3}, S_{ND}, S_S, X_A, X_N, X_H, S_P, X_S and X_{ND}) and 10 mass balances for the settler (one TSS mass balance for each layer). This model was implemented in Matlab 6.5® (2002) and the differential equations were solved using the ode15s function, a variable order solver based on the numerical differentiation formulas.

5. CONCLUSIONS

- The evaporation flow was calculated to be 2.5 ± 0.8 L d^{-1} (about 10-25 % of the inflow), however it was compensated by the addition of the same amount of tap water, and consequently, there was no need for the inclusion of this phenomenon into the system modeling.

- Ammonia stripping accounted for less than 1 % of the total removed nitrogen and thus it was not considered in the modeling.

- Reactors were modeled as ideal CSTRs.

- The settler was modeled as a one-dimensional settler with ten layers and without biological reactions. It was considered that the solid flux particles due to gravity depended only on the sludge concentration and its settling velocity. The settling velocity was calculated with a double-exponential velocity model (Takács et al. 1991).

- The final model consisted of 48 equations, 43 of them differential equations. It was implemented in Matlab 6.5® (2002) for further system simulation.

6. REFERENCES

Baeza JA. 1999. Development and implementation of a supervisory system for the management and control of WWTPs (in Spanish). PhD Thesis. Bellaterra: Universitat Autònoma de Barcelona.

Baeza JA, Ferreira EC, Lafuente J. 2000. Knowledge-based supervision and control of wastewater treatment plant: A real-time implementation. *Water Science and Technology* 41(12):129-137.

Baeza JA, Gabriel D, Lafuente J. 1999. An expert supervisory system for a pilot WWTP. *Environmental Modelling and Software* 14(5):383-390.

Baeza JA, Gabriel D, Lafuente J. 2002a. Improving the nitrogen removal efficiency of an A2/O based WWTP by using an on-line Knowledge Based Expert System. *Water Research* 36(8):2109-2123.

Baeza JA, Gabriel D, Lafuente J. 2002b. In-line fast OUR measurements for monitoring and control of WWTP. *Water Science and Technology* 45(4-5):19-28.

Baeza JA, Gabriel D, Lafuente J. 2004. Effect of internal recycle on the nitrogen removal efficiency of an anaerobic/anoxic/oxic (A2/O) wastewater treatment plant (WWTP). *Process Biochemistry* 39(11):1615-1624.

Carrera J. 2001. Biological ammonium removal from high-strength ammonium wastewater. Process parameters study and design of a full-scale industrial WWTP (in Spanish). PhD Thesis. Bellaterra: Universitat Autònoma de Barcelona.

Carrera J, Baeza JA, Vicent T, Lafuente J. 2003. Biological nitrogen removal of high-strength ammonium industrial wastewater with two-sludge system. *Water Research* 37(17):4211-4221.

Carrera J, Vicent T, Lafuente J. 2004. Effect of influent COD/N ratio on biological nitrogen removal (BNR) from high-strength ammonium industrial wastewater. *Process Biochemistry* 39(12):2035-2041.

Copp JB, Spanjers H, Vanrolleghem P. 2002. Respirometry in control of the activated sludge process: benchmarking control strategies. Scientific and technical report no. 11. London: IWA Publishing.

Diehl S, Jeppsson U. 1998. A model of the settler coupled to the biological reactor. *Water Research* 32(2):331-342.

Fux C, Boehler M, Huber P, Brunner I, Siegrist H. 2002. Biological treatment of ammonium-rich wastewater by partial nitritation and subsequent anaerobic ammonium oxidation (anammox) in a pilot plant. *Journal of Biotechnology* 99(3):295-306.

Gabriel D. 1996. Design and automation of a monitoring system for nitrate, nitrite and ammonium through flow analysis: application to a pilot WWTP with nitrification and denitrification (in Catalan). MSc Thesis. Bellaterra: Universitat Autònoma de Barcelona.

Gensym. 1995. G2 Reference manual. Version 4.0. Cambridge, MA, USA: Gensym Corporation.

Gernaey KV, Jeppsson U, Batstone DJ, Ingildsen P. 2006. Impact of reactive settler models on simulated WWTP performance. *Water Science and Technology* 53(1):159-167.

Henze M, Gujer W, Mino T, Van Loosdrecht M. 2000. Activated sludge models ASM1, ASM2, ASM2D and ASM3. Scientific and technical report no. 9. London: IWA Publishing.

Jeppsson U. 1996. Modelling aspects of wastewater treatment processes. PhD Thesis. Lund: Lund Institute of Technology (LTH).

Jeppsson U, Diehl S. 1996. On the modelling of the dynamic propagation of biological components in the secondary clarifier. *Water Science and Technology* 34(5-6):85-92.

Kynch GJ. 1952. A theory of sedimentation. *Trans. Faraday Soc.* 48:166-176.

MATLAB. 2002. User's guide. Version 6.5 (Release 13). Mathworks T, editor. Natick, USA.

Musvoto EV, Wentzel MC, Ekama GA. 2000. Integrated chemical-physical processes modelling - II. Simulating aeration treatment of anaerobic sludge digester supernatants. *Water Research* 34(6):1868-1880.

Spanjers H, Vanrolleghem P, Olsson G, Dold PL. 1997. Respirometry in control of the activated sludge process: principles. Scientific and technical report no. 7. London: IWA Publishing.

Takács I, Patry GG, Nolasco D. 1991. A dynamic model of the clarification-thickening process. *Water Research* 25(10):1263-1271.

Van Hulle SWH, Van Den Broeck S, Maertens J, Villez K, Donckels BMR, Schelstraete G, Volcke EIP, Vanrolleghem PA. 2005. Construction, start-up and operation of a continuously aerated laboratory-scale SHARON reactor in view of coupling with an Anammox reactor. *Water SA* 31(3):327-334.

Vitasovic ZZ. 1985. An integrated control system for the activated sludge process. PhD Thesis. Houston, Texas: Rice University.

PART III - Chapter 5

BIOMASS FRACTIONS DETERMINATION

Part of this chapter was presented as oral presentation:

Jubany I, Baeza JA, Carrera J, Casas C, Sternberg C, Smets BF. Flow cytometric determination of biomass fractions in activated sludge: nitrification case study. International Symposium on Environmental Biotechnology. Leipzig, Germany. July 2006.

Part of this chapter is in preparation for publication as:

Jubany I, Baeza JA, Carrera J, Lafuente, J. Automatic method for biomass fraction determination with FISH and confocal microscopy. Biotechnology letters.

The fluorescence in situ hybridization (FISH) is a powerful technique for biomass fractions determination. This can be coupled with epifluorescence microscopy and flow cytometry if single cells are available or with confocal microscopy if the whole aggregates are to be studied. This chapter shows the quantification of the nitrifying fractions of a nitrifying activated sludge system using all these equipments. It also shows the fractions calculation with simulation tools. Previous to the quantifications, several procedures and steps were optimized as the area-based quantification method, the sonication step, the in-solution FISH protocol and the flow cytometric analysis. The obtained results were compared and the advantages and disadvantages of the tested methodologies were discussed considering the accuracy of the results, the speed of the analysis and the availability of the equipment.

1. INTRODUCTION

Traditionally culture-dependent most probable number (MPN) and plate count methods have been used for enumeration of nitrifying bacteria. However, their culturing time is too long and the obtained counts are usually underestimated due to cluster formation and/or difference of culturability among the species. In the case of AOB quantification, Konuma et al. (2001) and Li et al. (2006) showed that MPN leads to counts underestimation compared to other methods like dot blot hybridization, antibody method and fluorescence in situ hybridization (FISH). FISH has been successfully used for nitrifying bacteria quantification (Coskuner et al. 2005; Gieseke et al. 2001; Hallin et al. 2005; Konuma et al. 2001).

FISH of whole cells using 16S rRNA-targeted oligonucleotides probes is a powerful technique with which to evaluate the phylogenetic identity, morphology, number, and spatial arrangements of microorganisms in environmental settings (Amann et al. 1995). rRNA molecules are ideal targets for nucleic acid probes for several reasons (Stahl and Amann 1991): (1) they are functionally conserved molecules present in all organisms; (2) the primary structures of 16S and 23S rRNA molecules are composed of sequence regions of higher and lower evolutionary conservation; (3) 16S rRNA sequences have already been determined for a large fraction of the validly described bacterial species and (4) their natural amplification with high copy numbers per cell (usually more than 10^4) greatly increases the sensitivity of rRNA-targeted probing. Due to the variable evolutionary conservation within the 16S rRNA, molecule probes can be designed to specifically target narrow to broad phylogenetic groups (from species to domain). Therefore, the main step in probe design is the identification of short regions (usually 15-25 nucleotides in length) in a sequence alignment unique to the target group of interest, centralizing mismatches to non-target organisms.

As stated in Hugenholtz et al. (2001), FISH method involves application of oligonucleotides probes to permeabilized whole microbial cells. The probes enter the cells and specifically

hybridize to their complementary target sequence in the ribosomes. If no target sequence is present in the cells ribosomes, probes are unable to hybridize and unbound probe is removed by a subsequent wash step. Hence, only specifically targeted cells retain the probes under appropriate stringency conditions in the hybridization and wash steps. Probes are typically 5' end-labeled with fluorochrome reporters, and cells containing hybridized probes can be directly observed under epifluorescence microscopy due to the natural amplification of the fluorescent signal by large numbers of ribosomes in any given target cell. An advantage is that multiple probes with varying target specificity can be used in the same preparation providing they are labeled with clearly distinguishable fluorochromes (i.e., well separated emission wavelengths).

One of the problems of the FISH technique is the quantification of cells; manual counting is not only time-consuming but in biofilms or aggregates often not accurate, possibly due to the formation of dense microcolonies (Schramm 2003). In these cases, conventional fluorescence microscopy fails to detect stained cells, since fluorescence is collected from the total depth of the sample. Confocal laser scanning microscopes (CLSM) can solve this problem. The technique of optical sectioning removes out-of-focus fluorescence because the collected signal is restricted to a thin section and leads to sharp and clear images devoid of noise. CLSM is an ideal tool for the analysis of spatial distribution of immobilized microbial communities like those forming the activated sludge flocs (Amann et al. 1995).

Several groups have therefore developed more or less automated image analysis methods for the quantification of FISH-positive cells in biofilms, aggregates, flocs, and other heterogeneous samples. Most of these procedures quantify the probe-specific area or volume expressed as fraction of the area or volume occupied by all bacteria (Kim and Kim 2006; Manser et al. 2005; Persson et al. 2002; Satoh et al. 2003). Others use calibrations for translation into cell numbers (Coskuner et al. 2005; Daims et al. 2001c; Hallin et al. 2005; Schramm et al. 1999).

There exist several probes specifically designed for nitrifying bacteria detection but none of them targeting the whole AOB or NOB population. The reason is that nitrifying bacteria have been described from six different phylogenetic lines: AOB of the beta and gamma subclasses of *Proteobacteria*, and NOB of the genera *Nitrobacter*, *Nitrococcus*, *Nitrospira* and *Nitrospina* (Schramm 2003). Therefore, the detection of all known nitrifiers by FISH would require a large set of probes.

Another useful technique for cell quantification is flow cytometry. Although it was initially developed to study mammalian cells, it has effectively been used, together with fluorescent probes (FISH), for specific bacterial group identification and quantification (Wallner et al. 1995). It has also been used for non-specific bacterial discrimination on the basis of nucleic acid staining, specific identification based on immunological characteristics, and characterization of basic cell functions in biomedical biotechnology and environmental microbiology research (Gruden et al. 2004).

Flow cytometry is the measurement of physicochemical characteristics of cells as they flow through an observation channel. Figure 5.1.A shows a conceptual illustration of this technique, performed in a flow cytometer (FCM). A single-file flow of microbes inside the observation channel is achieved by injection of the sample into a coaxial fluid stream where the mixture is focused using a sheath flow of aqueous solution. A laser beam is directed at the observation point and the resulting light scatter and emitted fluorescence is detected with a photosensor (photomultiplier tubes). Several parameters of detection are monitored: low angle or forward light scatter (FSC), right angle or side light scatter (SSC), and several fluorescence detection channels with wavelengths ranges defined by selected short and long pass filters. Figure 5.1.B schematically shows the interaction of light with a cell and indicates the scattered light and emitted fluorescence. While FSC information is related to particle size and SSC to cellular characteristics, the key to flow cytometry is that specific fluorescent probes can be added to the sample such that fluorescence only occurs when microbes are present. Fluorescence can be obtained with FISH, DNA staining or antibody-antigen-methods. The fluorescent emission from these cells is separated from the scattered light using a filer or dichroic mirror and is collected by a high-sensitivity, low-noise photosensor (photomultiplier tube)

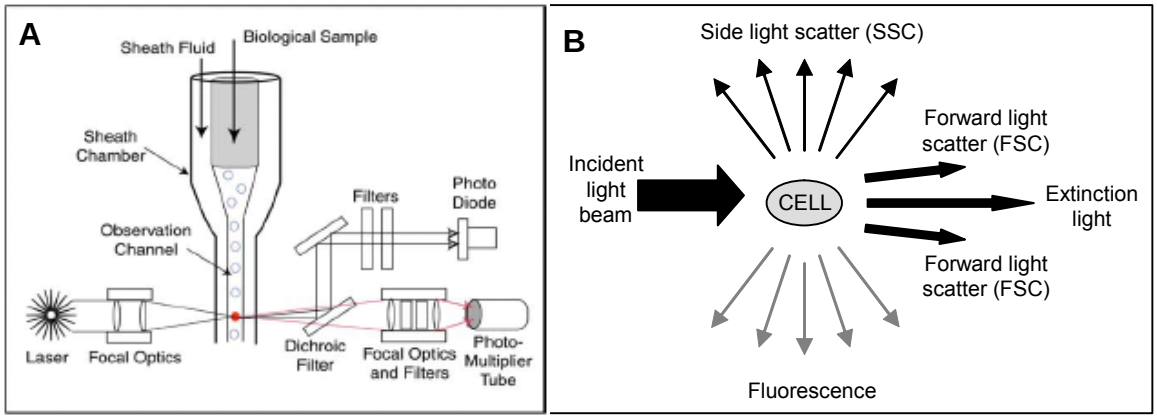

Figure 5.1 A. Conceptual illustration of flow cytometry (Gruden et al. 2004). **B.** Illustration of light interaction with a cell (adapted from Shapiro 1995).

For environmental sample analysis with flow cytometry, the limitations on fluorescence-based assays may be dependent on the presence or absence of background fluorescence, on the heterogeneity of the sample, on the fluorescence distribution, on the signal-to-noise ratio, on adequate cell recovery and on efficient hybridization between the probe and the target microorganism (Gruden et al. 2004). Therefore, environmental sample preparation for FCM analysis can involve repeated cell pelleting and ressuspension to minimize matrix effect.

The main advantages of flow cytometry are (Vives-Rego et al. 2000): (1) the high-speed analysis (typically at a rate of around 10^3 cells s^{-1}), (2) the multiparametric data acquisition and multivariate data analysis and (3) the sorting capacity of some FCMs that allows the transfer of specific populations or even single cells to a determined location, thus allowing further physical, chemical, biological or molecular analysis. Moreover, many FCMs allow the

operator to set electronic thresholds at the acquisition step to minimize the recording of background noise. In addition, electronic gates may be set around an area defining a subpopulation of interest in one histogram, thus resulting in the data histograms for the other measured parameter (which are said to be gated on the first parameter) displaying data reflecting only the subpopulation of interest (Davey and Kell 1996).

In general terms, there are two main disadvantages of flow cytometry, the substantial cost of the equipment and the requirement of skilled operators to obtain the optimum performance (Davey and Kell 1996). However, when using flow cytometry with activated sludge samples or biofilm samples, the main drawback is that single-cell suspensions (or small aggregates) are required and therefore, previous cell aggregates disruption is needed. This can be achieved in a number of ways: sonication (Forster et al. 2002), mechanical blending (Ziglio et al. 2002) and forced flow though needles (Völsch et al. 1990). However, this last method can lead to problems with clogging and is very tedious to perform. Although Nebe-von-Caron et al. (2000) stated that ultrasonic treatment is the most convenient disaggregation method, Buesing and Gessner (2002) found different optimal treatments depending on the sample. In fact, these methods have already been used in sample preparation for individual cell counting with epifluorescence microscopy (Eschenhagen et al. 2003; Hibiya et al. 2003; Li et al. 2006; Wagner et al. 1995). In this study, sonication was used as the method for aggregates dispersions.

Flow cytometry in the wastewater treatment field was firstly tested with pure cultures and mixtures of pure strains in which the bacterial aggregation did not exist (Amann et al. 1990; Wallner et al. 1993). Afterwards, it was applied to real environmental samples from activated sludge systems (Röske et al. 1998; Wallner et al. 1995). However, in these studies the concern was mainly the quantification of the main bacterial groups instead of specific bacterial populations. Only some studies can be found in the literature where the goal is the quantification of the nitrifiers (Coskuner et al. 2005; Völsch et al. 1990).

These quantification techniques have been used for several purposes in the wastewater treatment research. A great number of studies aimed to determine the substrate oxidation rate per cell (Coskuner et al. 2005; Kim and Kim 2006). Other studies compared the experimentally assessed fraction with those obtained by simulation (Mota et al. 2005; Persson et al. 2002) or used them to calibrate model parameters (Vadivelu et al. 2006; Ziglio et al. 2002). Quantification was also used to study the evolution of bacterial fractions in dynamic systems (Egli et al. 2003).

2. OBJECTIVES

The main objective of this chapter is the assessment of the AOB and NOB fractions of a nitrifying sludge by using different methodologies (single cell counting with epifluorescence microscopy and flow cytometry, area-based quantification with confocal microscopy and mathematical simulation) in order to discuss their advantages and disadvantages. Other secondary goals are the automation and optimization of the area-based quantification method and the development and optimization of a protocol for flow cytometric analysis of nitrifying activated sludge samples.

3. MATERIALS AND METHODS

This section presents the bacterial populations used for biomass quantification and the experimental system modeling. Moreover, the FISH technique is extensively described, from the chemicals preparation and available probes to the required equipment for fluorescence observation and quantification. The procedure used for the determination of the size distribution of sludge aggregates is also illustrated.

3.1 NITRIFYING REACTOR

The activated sludge system used in the experiments of this chapter was located in the Environment and Resources Department at the Technical University of Denmark (DTU).

3.1.1 EXPERIMENTAL SET-UP

The nitrifying reactor consisted of a 10 L reactor and a 2.6 L settler (see Figure 5.2). Oxygen needed for nitrification was supplied by an air pump through an air diffuser. Aeration was also used for liquid mixing. pH was controlled at 7.2-7.6 with the automatic addition of a sodium carbonate solution (0.5 N) and dissolved oxygen (DO) and temperature were continuously measured. The reactor was fed with synthetic media which contained 300 mg N L^{-1} and the required micronutrients for bacterial growth. The hydraulic retention time (HRT) was maintained at 1 d and the sludge retention time (SRT) was fixed at around 17 d by controlling the solids waste. Mixed liquor entered the settling zone by its bottom and the effluent was collected from the top of the settler. The system was inoculated with enriched nitrifying biomass from the pilot plant at UAB. After 70 days of operation under constant conditions, the biomass concentration in the reactor was 550 ± 50 mg VSS L^{-1} and 600 ± 50 mg TSS L^{-1}, and the solids concentration in the effluent was 13 ± 10 mg TSS L^{-1}. These values were determined according to Standard Methods (APHA 1995). Total ammonium nitrogen (TAN), total nitrite nitrogen (TNN) and nitrate concentration were 0.3 ± 0.2, 0.1 ± 0.2 and 290

± 30 mg N L^{-1}, respectively. Nitrogenous species were measured with Spectroquant kits from Merk (Darmstadt, Germany).

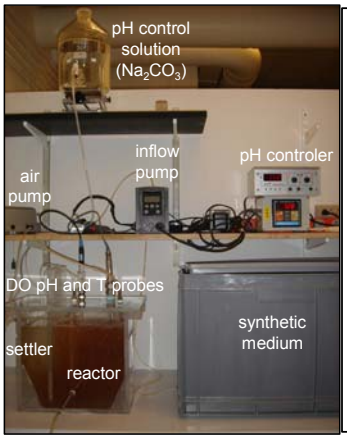

Figure 5.2 Picture of the experimental set-up at DTU.

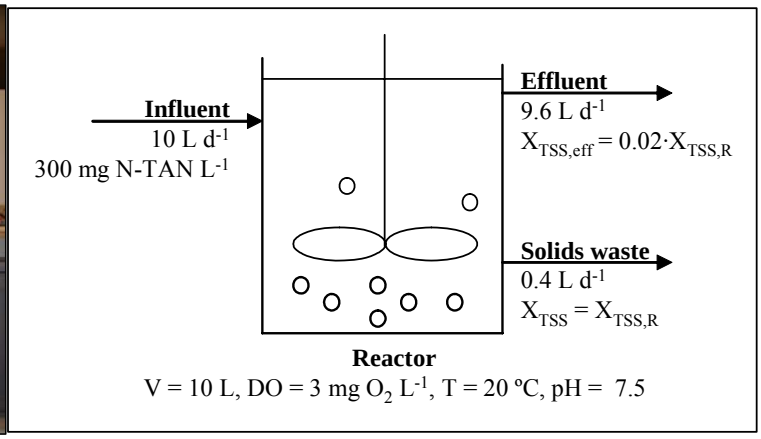

Figure 5.3 Schematic representation of the nitrifying reactor with the main inputs for modeling.

3.1.2 REACTOR MODELING

This experimental set-up was modeled as a continuous stirred tank reactor (CSTR) without settler but considering some special restrictions to account for the biomass retention. The effluent composition of soluble compounds was considered the same as the composition in the reactor. However, the composition of particulate compound in the effluent was calculated using the experimental ratio between the solids concentration in the reactor and the effluent ($X_{TSS,eff}/X_{TSS,R}$ = 13/600 = 0.02). Eleven compounds were modeled to describe the biological reactions: TAN (S_{TAN}), TNN (S_{TNN}), nitrate (S_{NO3}), soluble COD (S_S), soluble organic nitrogen (S_{ND}), AOB (X_A), NOB (X_N), heterotrophs (X_H), particulate biodegradable organic nitrogen (X_{ND}), particulate inert COD (X_P) and slowly biodegradable COD (X_S). The process stoichiometry and kinetics described and calibrated in Chapter 3 were used here. The only difference was that the inhibition processes were not considered since TAN and TNN concentrations were always below 1 mg N L^{-1}. Figure 5.3 shows a schematic representation of the modeled system with the main inputs for modeling.

Simulations were performed with Matlab 6.5® (2002). The ode15s function, a variable order solver based on the numerical differentiation formulas, was used to solve the differential equations of the system balances.

3.2 BACTERIAL STRAIN AND CULTURE CONDITIONS

A culture of *Pseudomonas putida* KT2440 (Nelson et al. 2002) was grown in shaken liquid LB medium at 30 ºC by Dr. Arnaud Dechesne. It was used as a reference (positive control) for flow cytometry optimization.

3.3 FISH

This section extensively describes the FISH technique: available FISH probes targeting nitrifying bacteria, reagents preparation and the whole protocol for on-slide FISH (OS-FISH).

3.3.1 AVAILABLE FISH PROBES

Several probes have been developed for the detection of AOB and NOB with different specificity. Tables 5.1 and 5.2 summarize the available probes for AOB and NOB detection, respectively. They are always used in combination with domain-specific probes which hybridize to all eubacteria. Table 5.3 shows the three probes that are usually used together to cover the entire eubacteria group. A very useful resource for an up-to-date research on available FISH probes is the web page of the Department of Microbial Ecology at the University of Wien: http://www.microbial-ecology.net/probebase/ (Loy et al. 2003).

Table 5.1 FISH probes for AOB, target group and required formamide concentration for hybridization.

Probe	Target	Formamide (%)	Reference
Cluster 6a192 (1)	*Nitrosomonas oligothropha*-lineage	35	Adamczyk et al. (2003)
NEU (1)	Most halophilic and halotolerant *Nitrsomonas spp*.	40	Wagner et al. (1995)
Nmo218	*Nitrosomonas oligothropha*-lineage	35	Gieseke et al. (2001)
NmV (Ncmob)	*Nitrosococcus mobilis* ("*Nitrosomonas*") lineage	35	Juretschko et al. (1998)
Nscoc1248	*Nitrosococcus oceani*, *Nitrosococcus halophilus*	(2)	Juretschko (2000)
Nscoc65	*Nitrosococcus oceani*, *Nitrosococcus halophilus*	(2)	Juretschko (2000)
Nscry1004	N*itrosomonas cryotolerans*	(2)	Juretschko (2000)
Nse1472	*Nitrosomonas europaea*, *N. halophila*, *N. eutropha*, Kraftisried-Isolat Nm103	50	Juretschko et al. (1998)
Nsm156	*Nitrosomonas spp*., *Nitrosococcus mobilis*	5	Mobarry et al. (1996)
NSMR34	*Nitrosospira tenius*-like AOB	20	Burrell et al. (2001)
NSMR76	*Nitrosomonas marina*-like AOB	20	Burrell et al. (2001)
Nso1225	Betaproteobacterial AOB	35	Mobarry et al. (1996; 1997)
Nso190	Betaproteobacterial AOB	55(3)	Mobarry et al. (1996)
Nsv443	*Nitrosospira spp*.	30	Mobarry et al. (1996)
NmII	*Nitrosomonas communis*-lineage	25	Pommerening-Röser et al. (1996)
NmIV	*Nitrosomonas cryotolerans*-lineage	-	Pommerening-Röser et al. (1996)
NOLI191	Some *Nitrosomonas oligotropha*-lineage	30	Rath (1996)

(1) Use together with a competitive probe. (2) Not published yet. (3) Re-optimized as 35 % (section 4.1.1)

Table 5.2 FISH probes for NOB, target group and required formamide concentration for hybridization.

Probe	Target	Formamide (%)	Reference
NIT3 [2]	*Nitrobacter spp*.	40	Wagner et al. (1996)
NSR1156	*Nitrospira moscoviensis*, freshwater *Nitrospira spp*.	30	Schramm et al. (1998)
NSR447	*Nitrospira spp*.	30	Schramm et al. (1998)
NSR826	*Nitrospira moscoviensis*, freshwater *Nitrospira spp*.	20	Schramm et al. (1998)
Ntcoc84	*Nitrococcus mobilis*	[1]	Juretschko (2000)
Ntspa1026	*Nitrospira moscoviensis*, activated sludge clones A4 and A11	20	Juretschko et al. (1998)
Ntspa662 [2]	genus *Nitrospira*	35	Daims et al. (2001a)
Ntspa685	*Nitrospira moscoviensis*, *Nitrospira marina* and 710-9 clone	20	Hovanec et al. (1998)
Ntspa712 [2]	Most members of the phylum *Nitrospirae*	50	Daims et al. (2001a)
Ntspn693	*Nitrospina gracilis*	[1]	Juretschko (2000)
Ntspa454	*Nitrospira moscoviensis*, aquarium clone 710-9	[1]	Hovanec et al. (1998)

[1] Not published yet. [2] Use together with the competitive probe.

Table 5.3 FISH probes for eubacteria, target group and required formamide for hybridization.

Probe	Target	Formamide (%)	Reference
EUB338	Domain *bacteria*	0-50	Amann et al. (1990)
EUB338 II	*Planctomycetales*	0-50	Daims et al. (1999)
EUB338 III	*Verrucomicrobiales*	0-50	Daims et al. (1999)
nonEUB	Non-binding control	Not determined	Wallner et al. (1993)

3.3.2 SOLUTIONS PREPARATION

Stock phosphate buffered saline (30xPBS): 0.3 M P-PO_4^{3-}. For pH = 7.2, the ratios of disodium:sodium phosphates must be 7.2:2.8. For 1 L solution, use 77.37 g of $Na_2HPO_4 \cdot 12H_2O$ (final concentration 0.216 M), 13.1 g of $NaH_2PO_4 \cdot 2H_2O$ (final concentration 0.084 M) and 226.2 g NaCl (final concentration 3.9 M).

Phosphate buffered saline (3xPBS): 0.03 M P-PO_4^{3-}. Dilute 50 mL of 30xPBS in 500 mL of MilliQ water. Autoclave and store at room temperature.

Phosphate buffered saline (PBS) working solution: 0.01 M P-PO_4^{3-}. Dilute 16.7 mL of 30xPBS in 500 mL of MilliQ water. Autoclave and store at room temperature.

Paraformaldehyde (4% PFA). Heat 65 mL of MilliQ water (to ≈ 60ºC) in a fume hood. Add 4 g paraformaldehyde. Add 2M NaOH (drop by drop) and stir rapidly until the solution has nearly clarified (1-2 min). Remove from the heat source and add 33 mL of 3xPBS. Adjust pH to 7.2 with HCl. Remove any remaining crystals by sterile friltration (0.2 µm). Quickly cool to 4 ºC and store at this temperature for no longer than 2 days or store in 1.5 mL aliquots (in 2 mL centrifuge tubs at -20ºC).

1 M Tris-HCl, pH 7.2. Dissolve 121.1 g Tris in 800 mL distilled water and add 42 mL HCl conc., let cool, adjust pH and fill to 1 L with distilled water. Autoclave and store at room temperature. Alternatively: Dissolve 157.6 g TrisHCl ($C_4H_{11}NO_3 \cdot HCl$) in 800 mL distilled water adjust pH and fill to 1 L with distilled water. Autoclave and store at room temperature.

5 M NaCl. Dissolve 292.2 g NaCl in 800 mL H_2O_{dest}. Fill to 1 L with distilled water. Autoclave and store at room temperature.

Formamide. Prepare it from deionized formamide. Store at 4 °C and use it quickly after fresh bottle was opened. Alternative: store in 2 mL aliquots at –20 °C. Caution: formamide is very toxic. Work with gloves in the fume hood and collect waste.

Sterile H_2O_{dest}. Autoclave distilled water or MilliQ water and store at room temperature.

10% SDS. Heat 50 g of SDS (sodium dodecyl sulfate, electrophoresis-quality) in 450 mL milliQ water to 68 °C. Adjust pH with HCl conc. to 7.2. Fill to 500 mL. No sterilization required. Caution: wear mask when weighing SDS.

0.5 M EDTA. Dissolve 18.6 g EDTA in 80 mL distilled water by adjusting the pH to 8.0 (ca. 2 g NaOH pellets required) and fill to 100 mL. Autoclave and store at room temperature.

Ethanol. Store 100 mL of ethanol 96% at -20 ºC to be used in the sample fixation. Prepare 50 mL of ethanol at 50, 80 and 96 % in falcon tubes for the dehydration step.

DAPI (4',6-diamidino-2-phenylindoldihydrochlorid). It is a nucleic acid stain. Stock solution: 1 mg mL^{-1}; working solution: 1 µg mL^{-1}. Store in 2 mL aliquots at –20°C (wrap tube in aluminum foil). Caution: DAPI binds to DNA and is therefore mutagenic/carcinogenic. Wear gloves, be careful and collect all waste (including used pipette tips).

TE buffer: nuclease free water. It contains 10 mM Tris HCl (pH = 7.5 – 8) and 1 mM EDTA. Add 0.5 mL Tris-HCl 1M and 0.1 mL EDTA 0.5 M to 50 mL of MilliQ water. Autoclave and store at room temperature.

3.3.3 FISH PROBES PREPARATION

FISH probes are usually supplied as dried powder. The protocol for preparing the working solution is described below:

I. Dilute the dried probe in TE buffer to a stock concentration of 500 ng/μL. The supplied amount of probe can be read in the quality certificate and used to calculate the volume of TE required for probe dilution.

II. Aliquot 5 μL of stock solution into sterile microcentrifuge tubes of 1.5 mL. This is diluted to 50 μL of total volume (i.e. add 45 μL TE) to give working concentration (50 ng/μL). For the EUBmix probe (EUBI + EUB II + EUB III): use 5 μL of each probe and 35 μL of TE to get to 50 μL.

III. Label the top of each tube with the name of the probe and the fluorochrome. It can be store at -20 or -80 ºC for a few years.

3.3.4 OS-FISH PROTOCOL

The following protocol was adapted from Manz et al. (1992), Amann (1995) and Hugenholtz (2001). It was used for the hybridization of samples which were then observed and/or quantified with a conventional epifluorescence microscope (EFM) or a CLSM.

3.3.4.1 Sample fixation

For Gram-negative microorganisms add 3 volumes of 4 % PFA (1.5 mL) to 1 volume of sample (0.5 mL). The sample can be concentrated by centrifugation if higher biomass concentration is required. Hold at 4 ºC for 1-3 h. Pellet the cells by centrifugation (5000g) and remove fixative. Wash the cells with PBS and resuspend in one volume (0.5 mL) of PBS per one volume (0.5 mL) of ice cold ethanol and mix. Fixed cells can be spotted onto glass slides or stored at -20ºC for several months.

3.3.4.2 Sonication (if required)

Only if the sample is finally observed with the EFM, sonicate the fixed sample. Add 0.5 mL of the fixed sample to 20 mL of MilliQ water in a 25 mL sterile glass bottle. Sonicate it continuously in an ice cold bath to prevent sample heating. The sonication time depends on the equipment. For a Branson Sonifier Model 250, with a probe diameter of 3 mm, sonicate for 10 minutes with the Output Control = 1 (sonication time optimized in this chapter). Make sure that the control settings, the liquid volume and the probe immersion (1 cm) are always equal because the power supplied to the sample depends on these parameters.

3.3.4.3 Application of samples to slides

Apply 5-20 μL (depending on sample concentration) of fixed sample (or sonicated sample) to each well in the glass slide. Let air dry (max. 60ºC). Dehydrate in ethanol series (3 min each): 50 %, 80 % and 96 (or 98 %) and let air dry. Slides can be stored at room temperature for one month (or at -20 ºC for several months).

3.3.4.4 Probe hybridization

The hybridization buffer is prepared in 2 mL microcentrifuge tubes at the time of use. Table 5.4 shows the receipt for its preparation. Formamide concentration is not specified since it depends on the probe (see Tables 5.1 to 5.3).

Table 5.4 Receipt for the preparation of 2 mL of hybridization buffer.

Reagent	Volume to prepare 2 mL (microcentrifuge tube)	Final concentration
5M NaCl (autoclaved)	360 µL	900 mM
1M Tris/HCl (autoclaved)	40 µL	20 mM
10 % SDS (not autoclaved) (1)	2 µL	0.01 %
Formamide	0- 1600 µL (2)	0-80 % (2)
MilliQ water	up to 2 mL	-

(1) Place it on the lid of the tube to avoid salt precipitation.
(2) Formamide concentration depends on the probe (see Tables 5.1 to 5.3 and Table 5.5).

Table 5.5 Required formamide, NaCl and EDTA for hybridization and washing buffers preparation with respect to the reported formamide percentage.

	Hybridization buffer	Washing buffer	
Reported formamide (%)	Formamide (µL)(1)	5M NaCl (µL)(2)	0.5M EDTA (µL)(2)
0	0	9000	-
5	100	6300	-
10	200	4500	-
15	300	3180	-
20	400	2150	500
25	500	1490	500
30	600	1020	500
35	700	700	500
40	800	460	500
45	900	300	500
50	1000	180	500
55	1100	100	500
60	1200	40	500
65	1300	- (3)	500
70	1400	- (3)	350
75	1500	- (3)	250
80	1600	- (3)	175

(1) To prepare 2 mL of hybridization buffer.
(2) To prepare 50 mL of washing buffer. (3) Enough Na^+ in EDTA.

Use Table 5.5 to transform the hybridization concentration to the volume needed in the hybridization buffer preparation. Use gloves (powder free because the powder is highly autofluorescent) to handle formamide. The addition of detergent (SDS) is essential for access of probe molecules to their intracellular targets (Wallner et al. 1993). Add 8 µL of this hybridization buffer to each well on the slide. Pour the remainder in the hybridization tube (50 mL polypropylene screw-top tube) that contains cellulose tissue (or simply a piece of toilet paper) to keep the chamber in the tub moist. Add 0.5 µL (or 1 µL) of each probe solution (50 ng/µL) and mix carefully. Usually two probes, labeled with different fluorochromes, are used in the same well, one specific probe that targets the population which is to be quantified, and one domain-specific probe set (EUBmix) that detects all bacteria. Keep at least one of the wells without probe or add only the nonEUB probe. This well is required for the intensity threshold determination in the quantification step. Place the slide into the 50 mL tube containing the moistened tissue. Close and put in the hybridization oven at 46 ºC for 1-2 h (preferably 2h). Make sure the oven has been preheated for several hours and the temperature is steady.

3.3.4.5 Washing

Prepare 50 mL of washing buffer solution in a 50 mL polypropylene crew-top tube and warm it at 48ºC in a water bath during the hybridization. Table 5.6 shows the receipt for its preparation. NaCl and EDTA concentration depend on the formamide used in the hybridization buffer (see Table 5.5).

Table 5.6 Receipt for the preparation of 50 mL of washing buffer.

Reagent	Volume to prepare 50 mL (screw-top tube)	Final concentration
5M NaCl (autoclaved)	0-9 mL (1)	0-900 mM (1)
0.5M EDTA (autoclaved)	0-500 µL (2)	0-5 mM(2)
1M Tris/HCl (autoclaved)	1 mL	20 mM
MilliQ water	up to 50 mL	-
10% SDS (not autoclaved)	50 µL	0.01%

(1) NaCl concentration and (2) EDTA depend on the formamide used in the hybridization (see Table 5.5).

After hybridization, the slides are carefully removed from the tube and splashed with warm wash buffer into a beaker. Slide is then placed into the washing buffer tube and into the water bath at 48ºC for 10-15 min. Rapid transfer of slides prevents cooling which leads to non specific probe binding. After the washing time, the slide is gently rinsed (to avoid biomass detachment from the slide) in cold MilliQ water. Water is directed above wells and allowed to flood over them. Both sides of the slide are washed to remove any salt which is highly autofluorescent. After the washing step, all droplets of water have to be removed from the wells. Apply compressed air direct at the side of the slide to ensure that all water droplets are removed or let them air dry.

3.3.4.6 DAPI staining (if required)

Apply 10 µL DAPI (working solution 1 µg mL^{-1}), stain for 10 min on ice, rinse with lots of distilled water and let air dry.

3.3.4.7 Embedding

Apply small drops of anti-bleaching reagent (e.g. Citifluor, which is toxic: avoid inhalation and contact with skin) to the wells on slides. Cover slides with a large coverslip and make sure the anti-bleaching reagent covers all the wells. Press the coverslip down gently to remove excess reagent. Slides at this point can be kept at -20ºC for some weeks without fluorescent loss.

3.3.4.8 Microscope observation and quantification

Observe slides using an EFM or a CLSM with the filters set corresponding to the used probes. Quantify by counting cells (EFM) or quantify the area covered by the specific probe with respect to the area covered by the general probe (CLSM).

3.4 EQUIPMENT FOR FLUORESCENCE DETECTION

The three fluorescence microscopes and the flow cytometer used in this chapter are described in this section. Table 5.7 summarizes the main fluorescent organic dyes used in the FISH technique and the nucleic acid staining.

Table 5.7 Fluorescent organic dyes: properties and required laser.

Short name	Compound	Excitation maximum (nm)	Emission maximum (nm)	Emission color	Laser emission (nm)
DAPI*	4',6-diamidino-2-phenylindoldihydrochlorid	365	418	Blue	364
SYTO 9*	Cyanine compound	483	503	Green	488
FLUOS	5(6)-carboxyfluorescein-N-hydroxysuccinamide ester	488	518	Green	488
FITC	Fluorescein isothiocyanate	490	520	Green	488
Fluo	Fluorescein	495	520	Green	488
Cy3	Indocarbocyanine	550	570	Yellow	530/543
TRITC	Tetramethylrhodamine isothiocyanate	557	576	Yellow	543
Texas Red	sulforhodamine	583	603	Red	543
SYTO 64*	Cyanine compound	598	620	Red	568
Cy5	Indodicarbocyanine	649	670	Red	633/647

* Nucleic acid stains.

3.4.1 FLUORESCENCE STEREO MICROSCOPE (FSM)

A Leica MZ16 FA fluorescence stereo microscope with 71.2 magnifications was used for aggregates detection when size distribution of samples was analyzed. It was equipped with a digital camera. An appropriate filter for DAPI detection was used.

3.4.2 EPIFLUORESCENCE MICROSCOPE (EFM)

A ZEISS epifluorescence microscope with x100 neofluar objective provided of a digital camera was used for individual cells detection. Three filters were available which allowed the use of three different dyes at the same time. The detectable emission colors were blue, green and red.

3.4.3 CONFOCAL LASER SCANNING MICROSCOPE (CLSM)

A Leica TCS SP2 AOBS confocal laser scanning microscope at a magnification of x63 (objective HCX PL APO ibd.B1 63x1.4 oil) was used for biomass fraction quantification. Two HeNe lasers were used with light emission at 561 and 633 nm. It was located in the Microscopy Service at UAB and it was used under the supervision of the technical staff.

3.4.4 FLOW CYTOMETER (FCM)

The flow cytometer was a FACS Vantage SE Becton Dickinson. It was handled by Claus Sternberg from the Biocentrum at the Technical University of Denmark (DTU).

The FCM nozzle had a diameter of 70 μm. It was equipped with three lasers: an UV laser (364 nm), a blue light laser (488 nm) and a red light laser with multiple light wavelengths (530, 568, 647 nm). Several filters for the emission light were available: 485 ± 22 nm, 530 ± 30 nm, 575 ± 26 nm, 610 ± 20 nm, 630 ± 22 nm and 675 ± 20 nm. Data acquisition was triggered by FSC to reduce interference of non-fluorescent particles. Usually, $3 \cdot 10^4$ events were analyzed. The used software was BD FACSDiva Software.

3.5 STRINGENCY CONDITIONS OPTIMIZATION OF FISH PROBES

The stringency conditions (formamide concentration in the hybridization buffer) were optimized for two AOB probes: Nso190 and Nso1225.

A sample of reactor mixed liquor was fixed and sonicated. Several slides were prepared with parts of the sonicated sample and were hybridized with these probes at different formamide concentration ranging from 20 to 50 %. Probe Nso190 was fluorescently labeled with Cy3 and probe Nso1225 was fluorescently labeled with Fluo. Figure 5.4 shows the probes distribution through the wells of one of the slides.

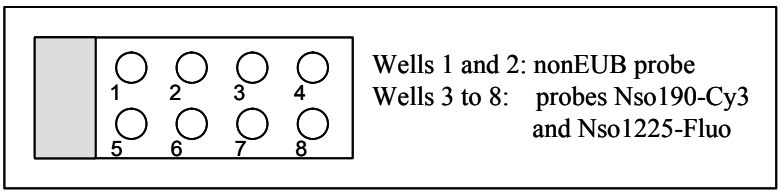

Figure 5.4 Probes distribution through the wells of one slide.

The EFM was used for image acquisition. One microscopic field with mainly individual cells was chosen for each well and two pictures were taken, one to detect probe Nso190 and the other to detect probe Nso1225. Therefore, two pictures of negative control and six pictures of the sample with probe were taken for each formamide concentration and each probe. Only individual cells were considered because the intensity of the objects was to be analyzed and it depends on the aggregate size.

Image analysis was performed with Image Pro Plus software (Media Cybernetics). Each cell was detected as an object and its area (A) and sum of pixels intensity (I) was listed. The surface-averaged intensity (SAI) of the objects of an image was calculated using equation 5.1:

$$SAI = \frac{\sum_{i=1}^{n} I_i}{\sum_{i=1}^{n} A_i} \qquad (5.1)$$

where i refers to object and n is the total number of objects in the image. The SAI of all control images for one probe was calculated and subtracted to the SAI of each image with probe. Then, the media and standard deviation were calculated for each formamide concentration and were plotted.

3.6 BIOMASS SIZE DISTRIBUTION DETERMINATION

The study of the biomass size distribution was used for the optimization of the sonication time and for the study of the effect of the in-solution FISH (IS-FISH) protocol to the biomass.

Biomass size distribution determination was based on the fluorescence detection of cells and aggregates after nucleic acid staining with DAPI. Size quantification was performed with the help of image analysis software.

A sample of mixed liquor was collected from the reactor and concentrated to avoid using high amount of fixative. 3 volumes of 4 % PFA were added to 1 volume of concentrated sample. After 2 h at 4 ºC, the sample was washed twice with PBS (centrifugation at 5000g). At the end, the cells were resuspended in one volume of PBS per one volume of ice cold ethanol. Fixed cells could be stored at -20 ºC for several months.

When needed, the sample was sonicated to disperse the aggregates. A volume of 0.2 mL of fixed sample was added to 20 mL of MilliQ water in a 25 mL sterile glass bottle and mixed. It was sonicated continuously with a Branson Sonifier Model 250 (with a probe diameter of 3 mm and the output control set to 1) in an ice cold bath to prevent heating. It was important that the control settings, liquid volume and probe immersion (1 cm) were always equal because the power supplied to the sample depends on these parameters. Under the used conditions the supplied power was 53 W.

Then, DAPI staining was performed. 0.75 μL DAPI stock solution (1 mg mL^{-1}) was added to the sonicated sample. The solution was mixed and stained for 5 minutes. Then, 10 mL were filtered. If the sample was too concentrated, a dilution step was included and 10 mL of the diluted solution was filtered. The filtration unit was connected to a vacuum pump. The filter was a black polycarbonate filter (OSMONICS INC., 0.22 μm of pore size, 25 mm 100/Pk) supported by a backing filter (Whatman glass microfibre filter). After suspension filtration, MilliQ water was added to wash the excess of DAPI and the filter was dried with the same vacuum system.

For microscope observation, the filter was mounted on a sterile glass slide (on a non-fluorescent immersion oil drop) and another drop was added on the filter before covering it with a cover slide. At this point, the preparation could be stored at -20 ºC for some weeks.

Two microscopes at different magnification were used to cover all the particle size range: the FSM and the EFM. 10 and 20 pictures were randomly taken for each slide with the FSM and EFM, respectively. Images were saved in grey scale for easy further treatment.

The detectable size range for each microscope was calculated considering 1 pixel as the diameter size of the smallest measurable object and the picture width as the diameter of the biggest measurable object. Since the size range of both microscopes overlapped a threshold of 10 μm of object equivalent diameter (d_{eq}) was defined. Therefore, objects with d_{eq} in between $7 \cdot 10^{-2}$ μm and $1.4 \cdot 10^{3}$ μm could be detected without double counting. Figure 5.5 shows the size ranges covered by both microscopes and the size ranges considered for each one.

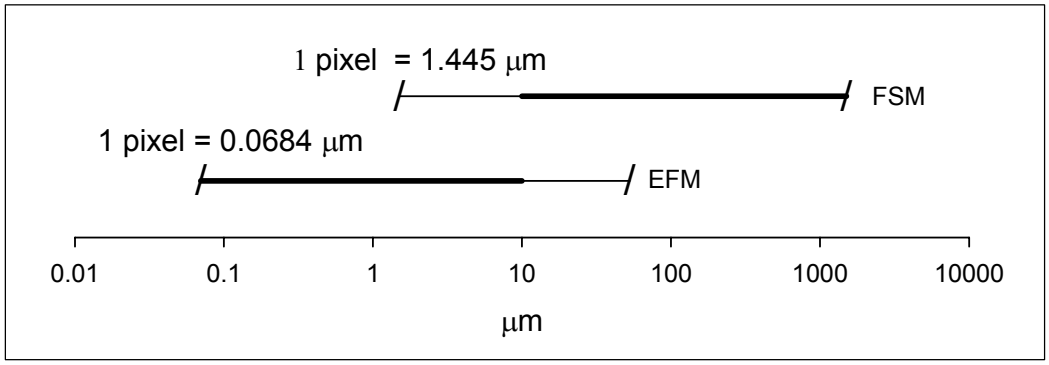

Figure 5.5 Total size range covered by the FSM and the EFM and, in bold, size range considered for each microscope. Threshold: 10 μm.

The area of the filter containing the sample was 176.6 mm^2. From this area, 17 % was analyzed with the FSC (10 pictures) but only 0.043 % was analyzed with the EFM. Therefore, the sample homogeneity was crucial to obtain representative images.

Image Pro Plus (Media Cybernetics) was used for image analysis and object counting. An intensity threshold was set to avoid counting debris particles. An Excel report with the list of objects and their area was generated for each sample. These reports were used in a developed Matlab (2002) program to calculate the d_{eq} for each object, to classify them into categories depending on the calculated d_{eq} and to estimate the objects concentration for each category in the reactor sample. Figure 5.6 shows images as example of object counting with each microscope. Counted objects are shown enclosed with red lines and some data of calculated d_{eq} are also depicted.

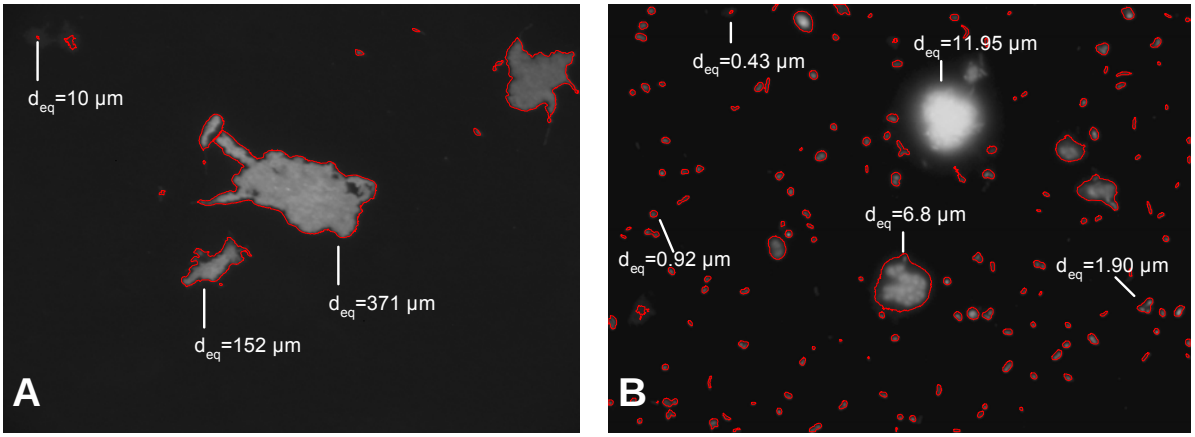

Figure 5.6 Images of DAPI stained samples indicating counted objects (red line) and including some d_{eq} data. **A.** FSM image of a non sonicated sample. **B.** EFM image of a 5 min sonicated sample.

4. RESULTS AND DISCUSSION

Firstly, some modifications and improvements were performed to the FISH protocol: stringency conditions optimization for two AOB probes, automation of the quantification of the relative abundance of specific microorganisms using CLSM images and study of the number of microscopic views required for reliable fraction estimation. Secondly, the FISH protocol was modified for the preparation of samples for flow cytometric analysis. This included sonication time optimization and the study of the size distribution of the sample at different steps of the protocol. Thirdly, the quantification using FCM was explored by using a pure culture of *Pseudomonas putida* and samples from the nitrifying activated sludge system. Finally, nitrifying biomass fractions were estimated with EFM, CLSM and FCM and were compared to modeling results.

4.1 IMPROVEMENTS IN THE OS-FISH PROTOCOL AND QUANTIFICATION METHOD

The stringency conditions for the hybridization of probes Nso190 and Nso1225 were optimized and the quantification method was designed and implemented.

4.1.1 STRINGENCY CONDITIONS OPTIMIZATION OF Nso190 AND Nso1225

Both probes Nso190 and Nso1225 target most AOB and are widely used to detect AOB in nitrifying systems. In this section, the optimal formamide concentration was determined for each one. With respect to Nso190, this study was required because some authors (Chandran et al. 2002; Konuma et al. 2001; Persson et al. 2002) pointed out that the originally reported formamide concentration was not optimal. With respect to Nso1225, this study was done to rigorously test it because it gave no hybridization when used at the target formamide concentration.

Figure 5.7.A shows the SAI of individual cells detected with Nso190-Cy3 after correcting it with the corresponding control images. An estimated tendency of the experimental data was also depicted. The optimal stringency is usually taken as the highest formamide concentration before specific hybridization signal is lost because this usually guarantees that the probe specifically hybridizes to the target organisms but not to the nontarget organisms (Hugenholtz et al. 2001). In this optimization it was considered that the optimal formamide concentration was that resulting in half the maximum intensity because nontarget organisms were not used in this study and the specificity with respect to other organisms could not be determined. From Figure 5.7.A, the maximum SAI was estimated as 17 and therefore, the optimal formamide concentration was 35 %. This result was in accordance with that obtained in Konuma et al. (2001). They used a pure culture of *Nitrosomonas europaea* and a 2-mismatch non-nitrifying culture of *Variovorax paradoxus* (IAM12373) and found that if formamide concentration was decreased around 25-30, high intensity was observed for *Nitrosomonas europaea* and low intensity for *Variovorax paradoxus*. Also in Chandran et al. (2002) 30 % formamide was used after an optimization procedure. Another study (Persson et al. 2002), showed that a clearer signal was obtained by lowering the concentration of formamide from 55 % to 50 %. They postulated that this indicated a sequence mismatch between the probe sequence and the target sequence of AOB of one or few bases.

With respect to the probe Nso1225, Figure 5.7.B shows that the SAI was very low, actually, it was around zero, meaning that no positive signal was obtained with this probe at any of the tested formamide concentrations. Since this probe was successfully used in other works (Gieseke et al. 2001; Hallin et al. 2005; Schramm et al. 1999), this result indicates that there were no target organisms in the investigated sludge.

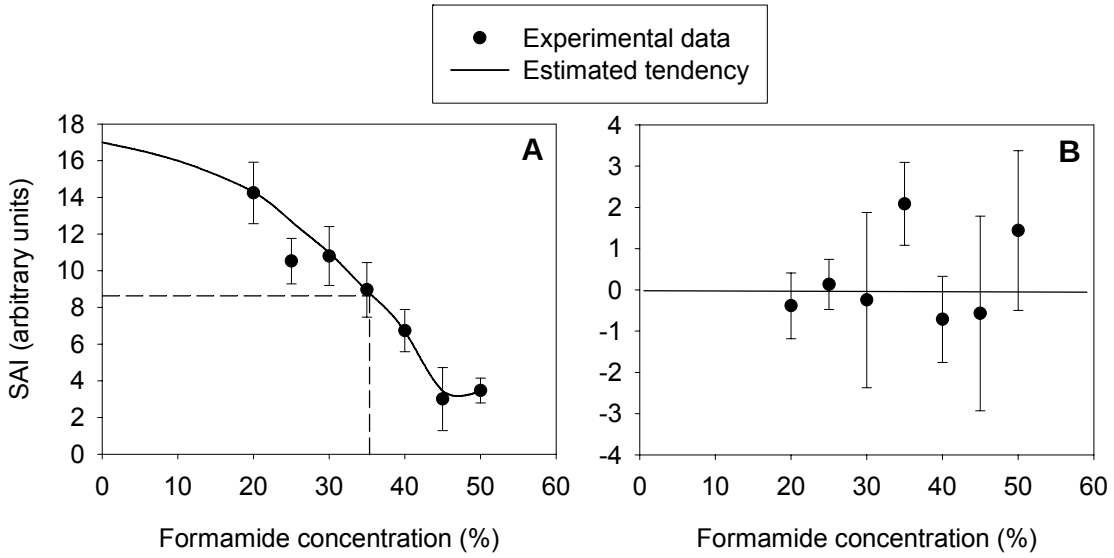

Figure 5.7 Formamide concentration optimization for (**A**) probe Nso190 and (**B**) probe Nso1225.

4.1.2 QUANTIFICATION METHOD FOR CLSM IMAGES

A quantification procedure was developed in Matlab 6.5® (2002) using the Image Processing Toolbox. It allowed automated quantification of the relative abundance (fraction) of specific nitrifying microorganisms based on the fluorescent area detected with a CLSM.

Each sample was hybridized with two different probes: a probe to detect the target organism (specific probe) and a probe to detect all bacteria (general probe). 5 randomly microscopic fields were acquired for the negative control sample (hybridized with nonEUB probe) and 50 for the hybridized sample (with specific and general probes). Two images were generated from each field: one using the appropriate laser to detect the specific probe (SP image) and the other one, using the appropriate laser for the general probe (GP image). Each image contained 1024x1024 pixels of different color intensity ranging from 0 to 255 (I = 0-255).

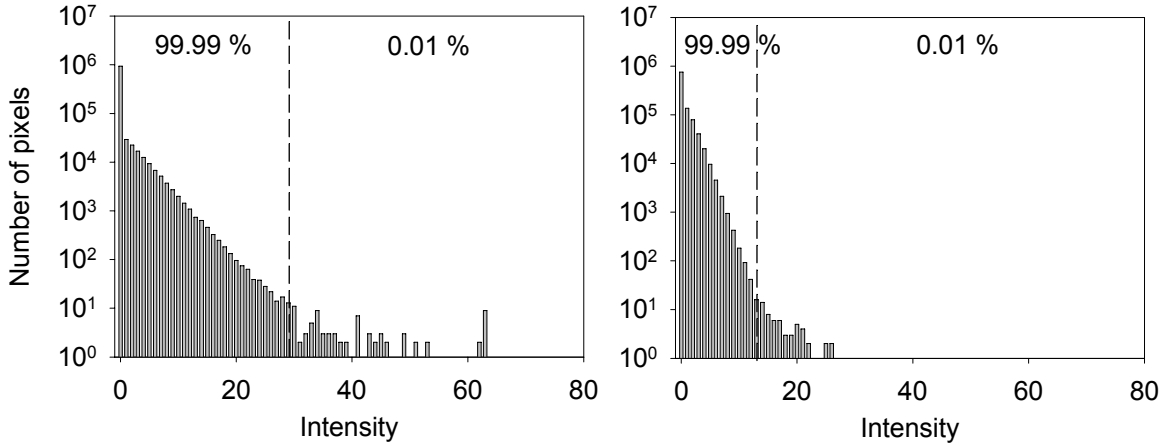

Figure 5.8 Histograms of the pixel intensity of two negative control images. Dashed line indicates the threshold (I_{thr}) since the amount of pixels on the left account for 99.99 % of the total pixels.

All images from a sample were grabbed after the photomultiplier settings for the CLSM were optimized, so the full range of intensity levels was used. The negative control images were used to set the threshold. The threshold (I_{thr}) was defined as the minimum intensity value that satisfies the following condition: the proportion of pixels with $I \leq I_{thr}$ is greater than 99.99 % in the negative control images. This was required to exclude the autofluorescence of the sample in the quantification of the positive signal of the hybridized sample. Figure 5.8 shows the intensity analysis of two negative control images. The histogram of the pixels intensity is shown and the threshold level is indicated.

A different I_{thr} was determined for each kind of images (SP and GP). These I_{thr}^{SP} and I_{thr}^{GP} were used in the analysis of the hybridized sample images. This automated algorithm for thresholding was useful to avoid systematic errors due to the subjectivity of the operator in the image analysis. It is a step forward in the FISH quantification since most published works either do not explain the quantification method or use more subjective methods of thresholding.

The sum of pixels with $I > I_{thr}^{SP}$ of each SP image (Z_i^{SP}) and the sum of pixels with $I > I_{thr}^{GP}$ of each GP image (Z_i^{GP}) were determined. Figure 5.9 shows a SP image and a GP image corresponding to the same microscopic field and the obtained images after correcting with the thresholds. From the analysis of the 50 fields, 50 Z_i^{SP} values and 50 Z_i^{GP} values were obtained. They were used to calculate the fraction of the target organism (f_{SP}) in the whole detected bacteria. Equation 5.2 was used for its calculation: sum of pixels detected in all SP images with respect to the sum of pixels detected in all the GP images.

$$f_{SP} = \frac{\sum_{i=1}^{n} Z_i^{SP}}{\sum_{i=1}^{n} Z_i^{GP}} \qquad n = 50 \text{ images} \tag{5.2}$$

This quantification method was preferred to the method in which the f_{SP} is obtained as the averaged value of the fractions calculated for each picture (see equation 5.3) to avoid giving the same weight to images with low biomass content and images with high biomass content.

$$f_{SP} = \frac{\sum_{i=1}^{n} \frac{Z_i^{SP}}{Z_i^{GP}}}{n} \qquad n = 50 \text{ images} \tag{5.3}$$

The error associated to each f_{SP} was calculated by changing I_{thr}^{SP} and I_{thr}^{GP} and quantifying again. The lower bound of the error was calculated with (I_{thr}^{SP}-5) and (I_{thr}^{GP}+5); and the upper bound was calculated with (I_{thr}^{SP}+5) and (I_{thr}^{GP}-5). The error was considered to be the average of the results of these two new quantifications.

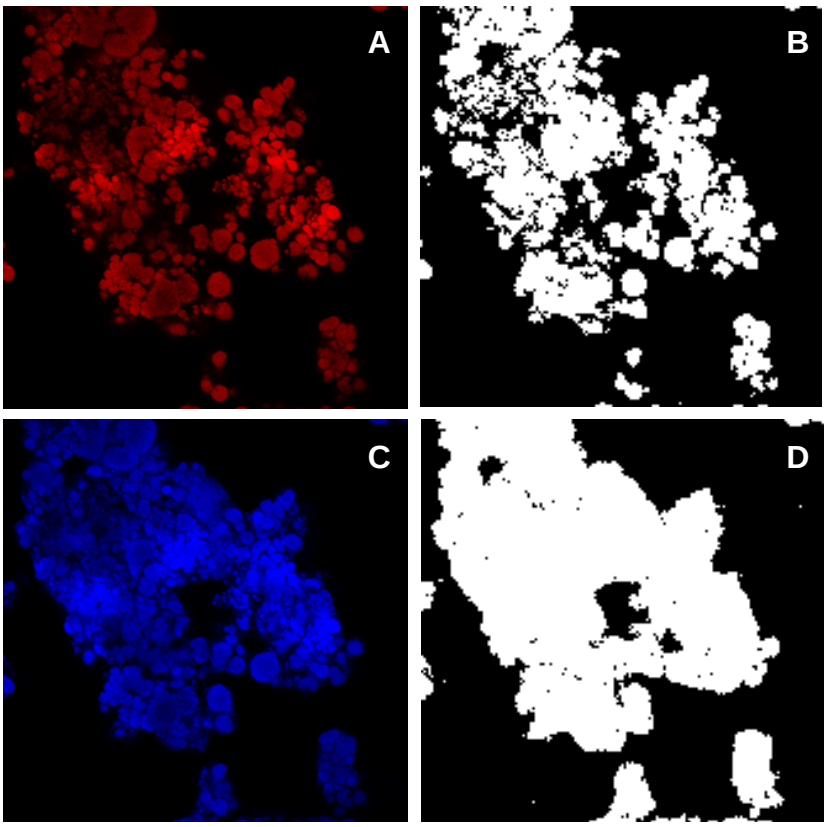

Figure 5.9 Example of the quantification method for CLSM images. All images correspond to the same microscopic field. **A.** SP image. **B.** SP image indicating (in white) the pixels with intensity above the threshold **C.** GP image. **D.** GP image indicating (in white) the pixels with intensity above the threshold.

4.1.3 OPTIMAL NUMBER OF MICROSCOPIC FIELDS FOR QUANTIFICATION WITH CLSM IMAGES

All the FISH quantifications shown in this thesis were performed using images from 40-50 microscopic fields; however, this number had not been previously optimized. Since the acquisition of this amount of images is very time consuming (around 2 h) the possibility to decrease this number was explored. Several samples which were quantified with FISH and CLSM were used. The specific bacteria fraction calculated with 50 images (from 50 microscopic fields) was taken as the reference number. The percentage of difference (error absolute) between this reference number and the fraction obtained with fewer images was calculated for 1 to 49 images. The results were plotted against the number of images. Figures 5.10.A and 5.10.B show the results obtained with probes Nso190 (AOB) and NIT3 (NOB), respectively. In both cases, the use of 30-35 images instead of 50 would result in an inaccuracy of less than 10 %; and the use of 20 images would produce around 20 % of error. There is only one sample in the NOB fraction determination for which these statements are not true (pointed out with an arrow in Figure 5.10.B). This sample contained less than 3 % of NOB while the others had around 10% of NOB. The lack of homogeneity of the images from this sample provoked that more images were required for good accuracy.

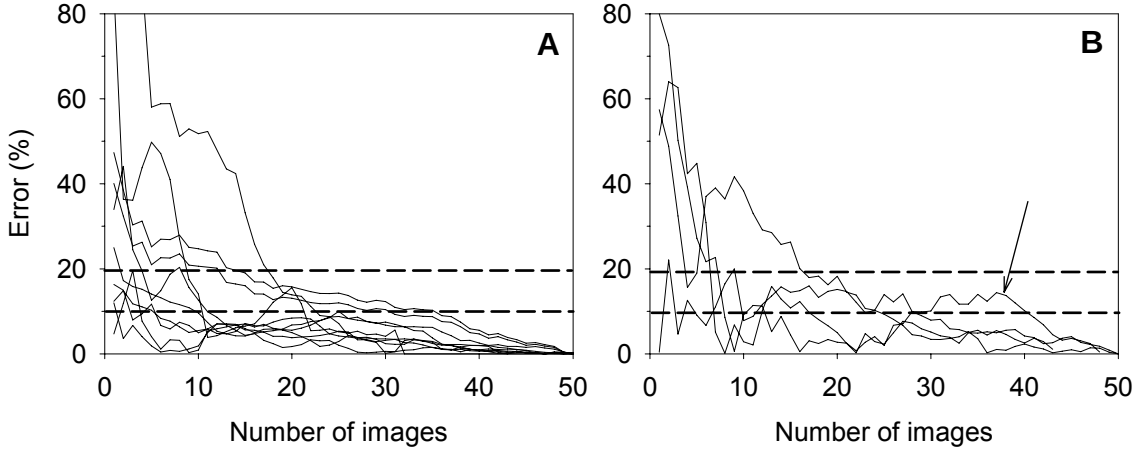

Figure 5.10 Percentage of difference (error absolute) between the biomass quantification with 50 images and less obtained from several different samples. Dashed lines indicate 10 and 20 % error. **A.** AOB fraction determination. **B.** NOB fraction determination.

These results showed that, depending on the purpose of the quantification and the homogeneity of the sample, the number of required images could range from 20 to 50 or even more. The final choice must be a compromise between desired accuracy and analysis time.

These results are in good agreement with those found in Manser et al. (2005) were a rapid method to quantify nitrifying bacteria in activated sludge was developed. For the examined activated sludge, they concluded that 10-15 microscopic fields for AOB and 6-8 microscopic fields for NOB were optimal regarding effort and accuracy. In their study the goal was to track population dynamics in activated sludge plants and therefore low analysis time was more important than accuracy.

4.2 DEVELOPMENT OF A PROTOCOL FOR FLOW CYTOMETRIC ANALYSIS OF FISH SAMPLES

One of the most significant differences when using a FCM instead of a CLSM for FISH sample quantification is the need of individual cells instead of aggregates. Another significant difference is that the samples are not fixed on a solid support (on-slide FISH, OS-FISH) but are prepared in solution (IS-FISH). This section shows the optimization of the cell dispersion and the in-solution FISH protocol.

4.2.1 SONICATION TIME OPTIMIZATION

The study of the sonication time effect to the biomass size distribution was performed at 0, 0.5, 1, 2, 5, 15 and 20 minutes in triplicate.

Fist of all, the object homogeneity on the filter was checked using all the analyzed samples. Counts obtained from all pictures of the same sample should be similar if cells were homogeneously spread on the filter, therefore the relative standard deviation (RSD) should be low. RSD was calculated for each sample and plotted against sonication time. Figure 5.11

shows the results. It can be observed that RSD was lower for the FSM than for the EFM because the big aggregates were more homogeneously spread than individual cells or small aggregates. The RSD could be lowered if more images were taken. However, RSD did never surpass 60 %.

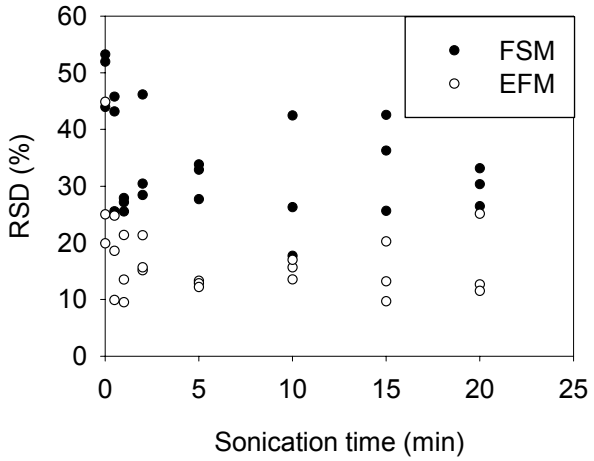

Figure 5.11 RSD of number of objects counted with each microscope for each sample.

For each sonication time, objects were classified into 25 classes with respect to their d_{eq}. From 0 to 10 μm, objects were classified into 10 classes (classes 1 to 10) of 1 μm wide, and from 10 to 385 μm, they were classified into 15 classes (classes 11 to 25) of 25 μm wide. Figure 5.12 shows the obtained bar graph. Each bar was calculated as the average of the tree repetitions. Error bar is the standard deviation of the repetitions.

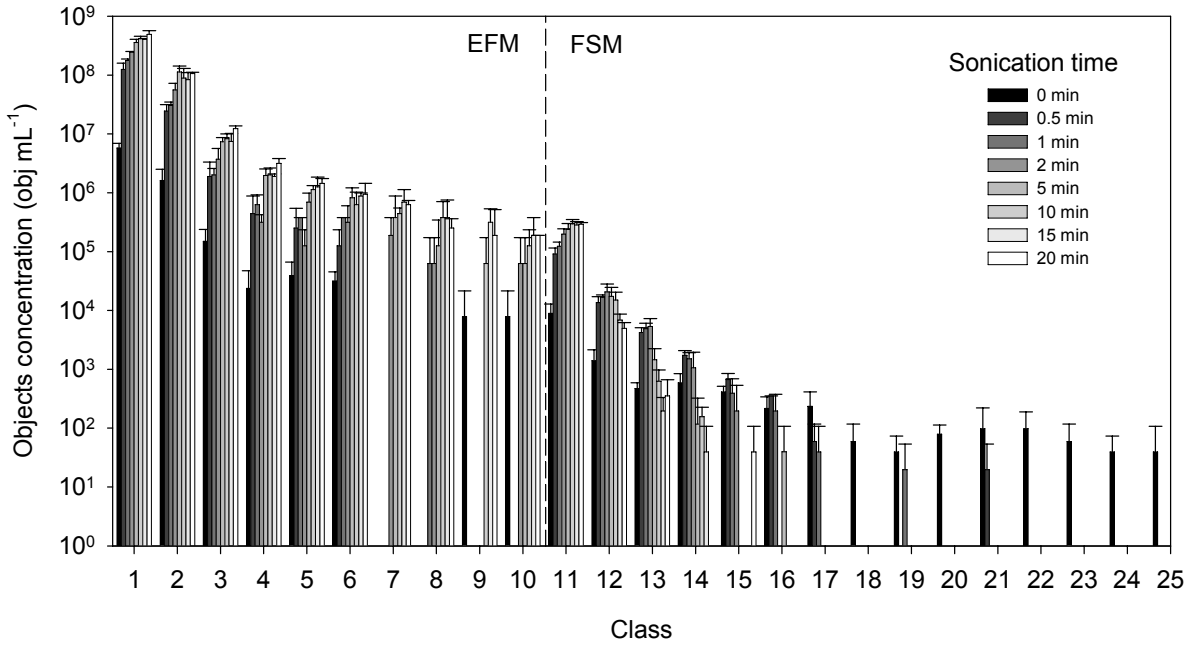

Figure 5.12 Size classification of objects detected from reactor samples after different sonication times. Error bars is the standard deviation of three samples.

Biggest aggregates ($d_{eq} \leq 385$ μm) were abundant in the reactor samples before sonication but they were immediately disrupted when sonication was applied. As the sonication time was increased, the aggregate size decreased. The number of individual cells (class 1 and 2) was also increasing with the sonication time. At 5 min of treatment, almost all aggregates had a d_{eq} below 100 μm. It can be observed that the concentration of objects with $d_{eq} < 35$ μm (class < 11) increased with sonication time and that the concentration of bigger objects decreased with sonication time.

The total objects concentration was plotted against the sonication time in Figure 5.13. The objects concentration increased with the sonication time during the first 5 minutes; however, longer sonication time did not lead to the same rate of objects concentration increase. 10 minutes was set as the optimal sonication time and the percentage of object with d_{eq} below 2, 5 and 10 μm was calculated as 97, 99.6 and 99.9 %, respectively. If the area of the objects was considered, 45, 60 and 71 % of the total area corresponded to objects with d_{eq} below 2, 5 and 10 μm, respectively. These results showed that although most of the objects were individual cells or small aggregates, the remaining big objects contained a high number of cells. The individual cells and small aggregates obtained with the sonicated sample could not be fully representative of the whole sample. This should be kept in mind when quantifying biomass fractions.

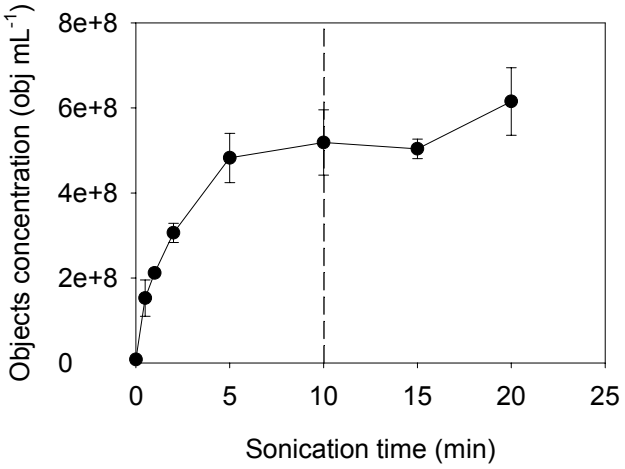

Figure 5.13 Total objects concentration vs sonication time. Dashed line is the optimal sonication time.

4.2.2 IS-FISH PROTOCOL

OS-FISH protocol (section 3.3.4) was modified in order to develop a new protocol in which the cells are in suspension instead of being fixed on a slide. The protocol described in Wallner et al. (1993) was used as a reference.

Optimization experiments were performed with a reactor sample and probes EUBmix and Nso190. The protocol was repeated several times with some modifications and the final fluorescence was observed with the EFM. The steps that were checked and optimized were:

- Dehydratation step. The dehydratation step using ethanol was not required in the IS-FISH protocol.

- Hybridization step. The optimal amount of probe in the hybridization step was 5 μL which gave a probe concentration in the hybridization buffer of 4.2 ng μL^{-1} when two probes were used. The optimal hybridization time was set to 4 h.

- Washing step. In Wallner et al (1993), the washing step was performed with the hybridization buffer instead of a buffer without formamide. It was observed that more fluorescence was obtained when a solution with the same composition as the washing buffer of the OS-FISH protocol was used.

- Last washing step. Using PBS instead of MilliQ water in the last washing step increased the fluorescence of the hybridized cells.

After the optimization experiments the protocol was as described below. Although most of the steps in the new protocol are equal or similar to steps in the OS-FISH protocol, they are again detailed in order to accurately describe the whole procedure.

4.2.2.1 Sample fixation

For Gram-negative microorganisms add 3 volumes of 4 % PFA (1.5 mL) to 1 volume of sample (0.5 mL). The sample can be concentrated by centrifugation if higher biomass concentration is required. Hold at 4 ºC for 1-3 h. Pellet the cells by centrifugation (5000g) and remove fixative. Wash the cells with PBS and resuspend in one volume (0.5 mL) of PBS per one volume (0.5 mL) of ice cold ethanol and mix. Fixed cells can be spotted onto glass slides or stored at -20ºC for several months.

Note that after each centrifugation step, the supernatant should be removed very carefully to avoid cell loss. This is the most difficult part of this protocol.

4.2.2.2 Sonication

Add 0.5 mL of the fixed sample to 20 mL of MilliQ water in a 25 mL sterile glass beaker. Sonicate it continuously in an ice cold bath to prevent sample heating. The sonication time depends on the equipment. For a Branson Sonifier Model 250, with a probe diameter of 3 mm, sonicate for 10 minutes with the Output Control = 1. Make sure that the control settings, the liquid volume and the probe immersion (1 cm) are always equal because the power supplied to the sample depends on these parameters.

4.2.2.3 Probe hybridization

For each sample and repetition, pellet 1.5 mL of sonicated sample by centrifugation (max 8000 g ≈ 10^4 rpm, 5 min) in a microcentrigue tube of 1.5 mL and remove all the liquid. At this point,

the total amount of cells should be around 10^5 – 10^6. Add 50 µL of previously warmed hybridization buffer to the cells. Then, add 5 µL of each probe at 50 ng μL^{-1} (working concentration), mix well and keep the tube at 46 ºC in a dry incubator for 4 h.

Table 5.8 Receipt for the preparation of 1.5 mL of hybridization buffer for IS-FISH.

Reagent	Volume to prepare 1.5 mL (microcentrifuge tube)	Final concentration
5M NaCl (autoclaved)	270 µL	900 mM
1M Tris/HCl (autoclaved)	30 µL	20 mM
10 % SDS (not autoclaved) (1)	1.5 µL	0.01 %
Formamide	0- 1200 µL (2)	0-80 % (2)
MilliQ water	up to 1.5 mL	-

(1) Place it on the lid of the tube to avoid salt precipitation.

(2) Formamide concentration depends on the probe (see Tables 5.1 to 5.3 and Table 5.9).

Table 5.9 Required formamide, NaCl and EDTA for hybridization and washing buffers preparation with respect to the reported formamide percentage. To be used in IS-FISH.

	Hybridization buffer	Washing buffer	
Reported formamide (%)	Formamide (µL)(1)	5M NaCl (µL)(2)	0.5M EDTA (µL)(2)
0	0	270	-
5	75	189	-
10	150	135	-
15	250	95	-
20	300	65	15
25	375	45	15
30	450	31	15
35	525	21	15
40	600	14	15
45	675	9	15
50	750	5	15
55	850	3	15
60	900	1.2	15
65	975	- (3)	15
70	1050	- (3)	10.5
75	1125	- (3)	7.5
80	1200	- (3)	5.3

(1) To prepare 1.2 mL of hybridization buffer.

(2) To prepare 1.5 mL of washing buffer. (3) Enough Na^+ in EDTA.

The hybridization buffer is prepared in 1.5 mL microcentrifuge tubes and previously warmed at 46 ºC. Table 5.8 shows the receipt for its preparation. Formamide concentration is not specified since it depends on the probe (see Tables 5.1 to 5.3). Use Table 5.9 to transform the hybridization concentration to the volume needed in the hybridization buffer preparation. Use gloves (powder free because the powder is highly autofluorescent) to handle formamide.

4.2.2.4 Washing

Pellet de cells by centrifugation (max 8000 g ≈ 10^4 rpm, 5 min) and remove the hybridization buffer. Add 500 µL of the washing buffer, mix well and transfer the tube to a 48 ºC dry incubator for 20 min. This washing step is to minimize non-specific probe binding. Table 5.10 shows the receipt for the washing buffer preparation. NaCl and EDTA concentration depend on the formamide used in the hybridization buffer (see Table 5.9). Then, pellet the cells by centrifugation (max 8000 g ≈ 10^4 rpm, 5 min) and add 500 µL of cold PBS to wash. Perform this step twice.

Table 5.10 Receipt for the preparation of 1.5 mL of washing buffer for IS-FISH.

Reagent	Volume to prepare 1.5 mL (microcentrifuge tube)	Final concentration
5M NaCl (autoclaved)	0-270 µL (2)	0-900 mM (2)
0.5M EDTA (autoclaved)	0-15 µL (3)	0-5 mM(3)
1M Tris/HCl (autoclaved)	30 µL	20 mM
10% SDS (not autoclaved)(1)	1.5 µL	0.01%
MilliQ water	up to 1.5 mL	-

(1) Place it on the lid of the tube to avoid salt precipitation. (2) NaCl concentration and (3) EDTA concentration depend on the formamide used in the hybridization (see Table 5.9).

4.2.2.5 Nucleic acid staining (if required)

Add the amount of required stain, mix and wait the required staining time. Table 5.11 shows some DNA stains, its fluorescent characteristics and the staining conditions.

Table 5.11 Nucleic acid stains and staining conditions.

Dye name	Fluorescence emission color	Working concentration	Staining time
DAPI	Blue	1 µg mL^{-1}	10 min
SYTO 9	Green	1 µM	15 min
SYTO 64	Red	20 µM	15 min

4.2.2.6 Filtration

Add 1 mL of PBS and filter with a 10 μm pore size filter. This step is required to remove big particles which could clog the FCM. Store it in the fridge until analysis with FCM.

4.2.3 BIOMASS SIZE DISTRIBUTION THROUGHOUT THE IS-FISH PROTOCOL

The biomass size distribution at the different stages of the sample preparation for flow cytometric analysis was determined. Specifically, it was determined after fixation (FIX), after sonication (SON), after hybridization (HYB) and after filtration (FIL) that was just before flow cytometric analysis. The used methodology was described in section 3.6.

Detected objects were classified into 29 classes with respect to their d_{eq}. From 0 to 10 μm, objects were classified into 10 classes (classes 1 to 10) of 1 μm wide, and from 10 to 385 μm, they were classified into 19 classes (classes 11 to 25) of 25 μm wide. Figure 5.14 shows the obtained bar graph. Each bar was calculated as the average of three repetitions. Error bars in FIX, SON and HYB is the standard deviation of the repetitions.

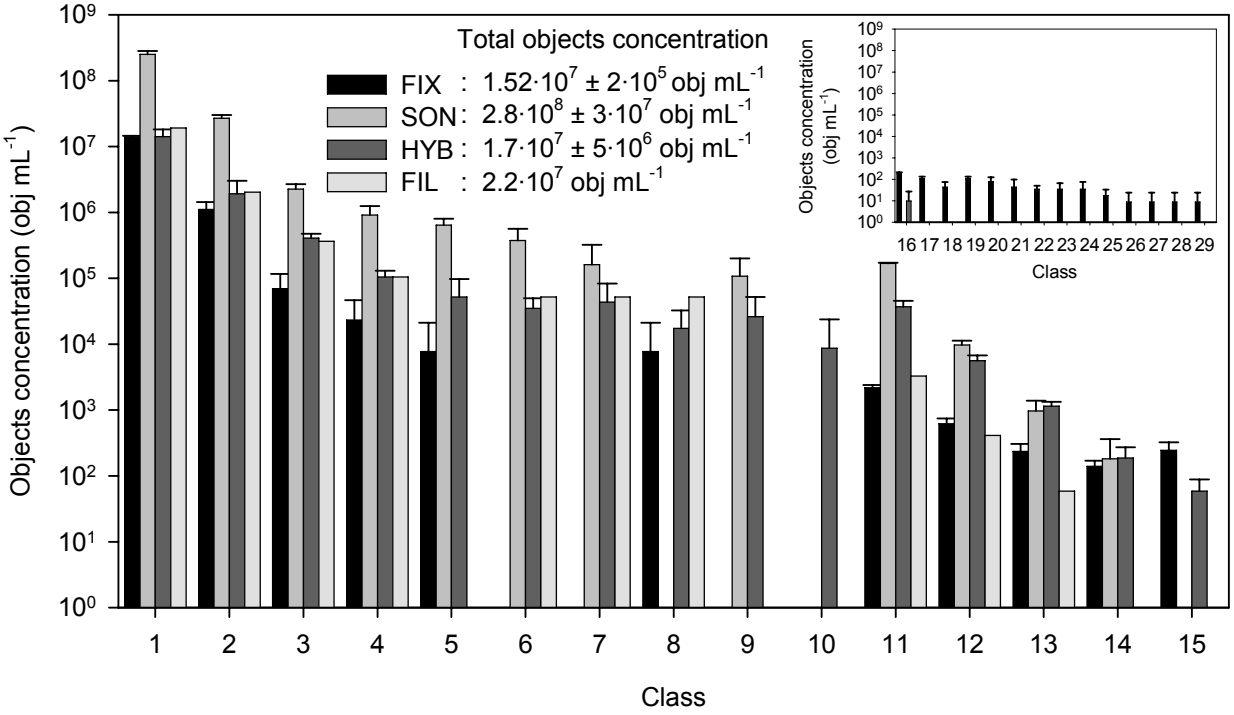

Figure 5.14 Size classification of objects detected at different stages of the IS-FISH protocol. Error bars indicate the standard deviation of three measures.

The size distribution of the aggregates before sonication (FIX) and after sonication (SON) is very different. As already demonstrated, the sonication process produces the dispersion of the biggest aggregates into smaller aggregates and individual cells. The biggest detected object in the reactors sample had a d_{eq} around 473 μm, and after sonication, the biggest object had a d_{eq}

around 98 μm. The big aggregates dispersion released a huge amount of individual cells and small aggregates. The total amount of cells after sonication increased one order of magnitude. This can be seen in figure 5.14, where is also depicted that the hybridization process provoked a considerable loss of cells. This was probably due to the several centrifugation steps in which the removal of the liquid took away a lot of cells. Figure 5.14 shows that most of the removed objects were individual cells and small aggregates. In fact, in the SON sample, 98.4 % of the objects had a d_{eq} below 2 μm, 1.6 between 2 and 10 μm and only 0.06 % above 10 μm; whereas in the HYB sample, these percentages were 95.6, 4.1 and 0.3 %, respectively. These differences may indicate either the individual cells (and smaller aggregates) were mostly eliminated during the hybridization protocol or this procedure favored cells aggregation. With respect to the second option, it must be noted that in HYB sample the biggest object had a d_{eq} of 148 μm while in the SON sample the biggest object had a d_{eq} of 98 μm. This result is in disagreement with Wallner et al. (1995) because they observed that IS-FISH of activated sludge samples resulted in considerable flocs dispersion. The last step, filtration, effectively reduced the concentration of objects with d_{eq} above 10 μm, while the total concentration of cells remained almost unchanged.

4.2.4 FLOW CYTOMETRY OPTIMIZATION FOR NITRIFYING BIOMASS QUANTIFICATION

The flow cytometry technique for the detection and quantification of nitrifiers from an activated sludge system was optimized. The main purposes of the optimization were: (1) to set the FCM parameters to distinguish bacteria from debris particles; (2) to choose the appropriate dye combination for fraction determination. For these purposes, dual staining of cells with a nucleic acid stain and fluorescent probes was performed. Nucleic acid staining was needed to detect the cells in case FISH signal was not bright enough or the hybridization was not working.

Table 5.12 Nucleic acid stains and fluorochomes used for labeling FISH probes. Excitation and emission wavelengths in brackets (in nm)

Combination	Nucleic acid stain	Label for FISH probe
1	DAPI (365/418)	Fluo (495/520)
2	SYTO 64 (598/620)	Fluo (495/520)
3	SYTO 9 (483/503)	Cy3 (550/570)
4	SYTO 9 (483/503)	Cy5 (649/670)

Table 5.12 shows the dye combinations that were tested, which, considering the maximum excitation and emission wavelengths of the dyes, were theoretically suitable with the available lasers. However two of these combinations (number 2 and 3) were not really appropriate due to the emission light filters: the red laser light (for the excitation of SYTO 64 or Cy3) was

detected with the filter used for the detection of the green light (emitted by Fluo or SYTO 9). Therefore, only two combinations were finally appropriate (numbers 1 and 4).

4.2.4.1 Pure culture samples

First of all, several tests were performed by using an overnight pure culture of *Pseudomonas putida* KT2440 as a positive control. This cell suspension was homogenous and contained only individual cells which were bigger than the individual cells from the nitrifying reactor. Nucleic acid staining was performed as described in section 4.2.2.5 and IS-FISH was performed using the above described protocol (section 4.2.2) without the sonication step.

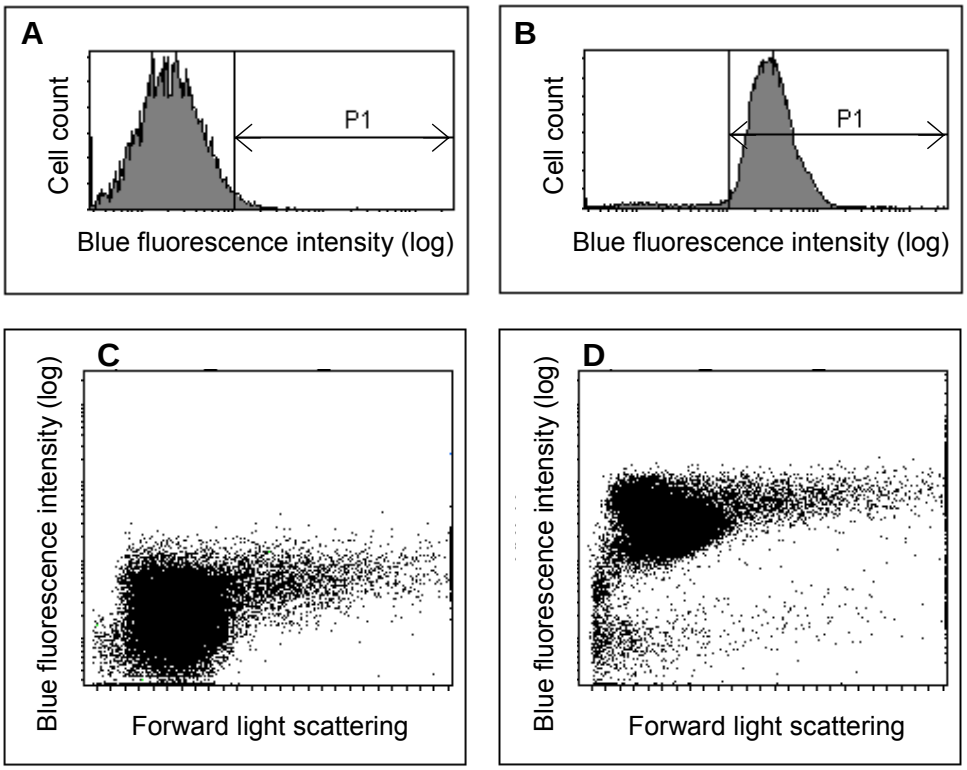

Figure 5.15 Cytograms of *P. putida*. **A.** Cell count vs blue FI of a non-stained sample. **B.** Cell count vs blue FI of a DAPI stained sample. **C.** Blue FI vs FSC of a non-stained sample. **D.** Blue FI vs FSC of a DAPI stained sample.

The first dye combination was number 1: DAPI as the nucleic acid stain and EUBmix-Fluo as the FISH probe. Figure 5.15 shows the results obtained with this dye combination. Figure 5.15.A shows the cell count vs the blue fluorescence intensity (FI) of a sample without any staining and Figure 5.15.B shows the same cytogram of a sample after DAPI staining. It can be observed that FI increased considerably in the stained sample and that a threshold value could be defined to distinguish between stained and non-stained cells. The gate named P1 enclosed 95 % of the total counted events. This gate was defined to include the maximum amount of cells for the stained sample and around 1% of the events for the non-stained sample. Figure 5.15.C shows blue FI vs FSC for the non-stained sample. If this cytogram is compared with the

one in Figure 5.15.D (stained sample) it can be observed that the stained cells can clearly be differentiated from the debris particles.

In Figure 5.16, the same kinds of cytograms are shown for the same samples but considering the green FI (light emitted by the EUBmix-Fluo). Figures showing the results obtained with the sample hybridized with the EUBmix-Fluo probe are clearly different from those showing the results obtained with the nonEUBmix-Fluo probe. The P1 gate enclosed 96 % of the total counted events in Figure 5.16.B. Since the results obtained with the DAPI staining and the FISH with Fluo were satisfactory, it was concluded that this dye combination was suitable and could be useful for quantification.

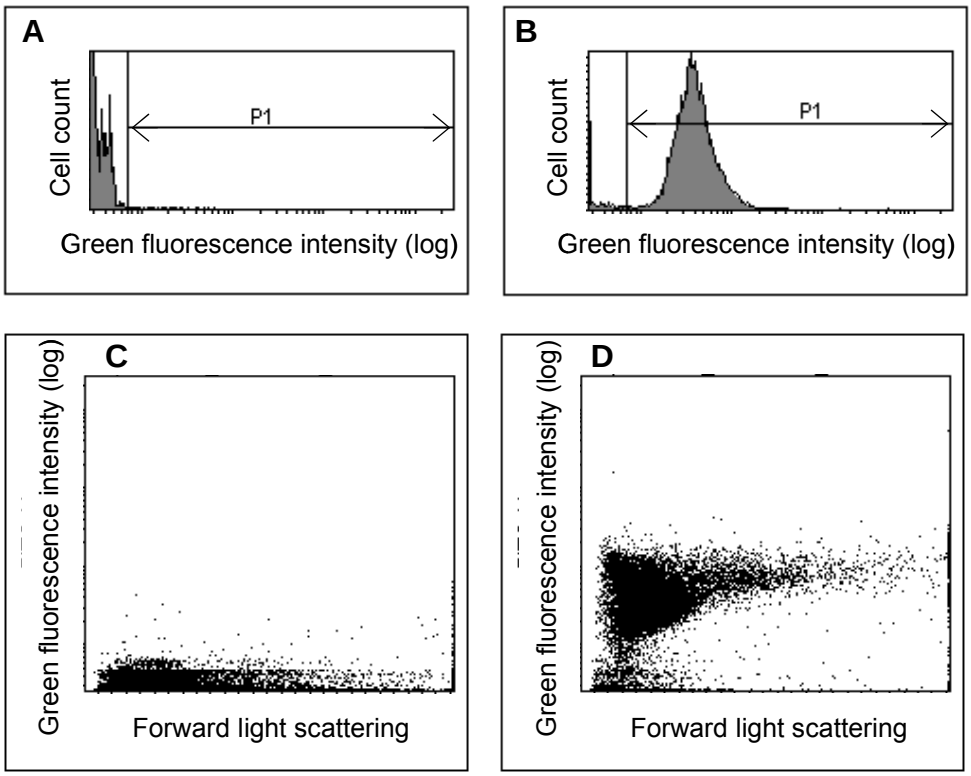

Figure 5.16 Cytograms of *P. putida*. **A.** Cell count vs green FI of a sample hybridized with nonEUB-Fluo. **B.** Cell count vs green FI of a sample hybridized with EUBmix-Fluo. **C.** Green FI vs FSC of a sample hybridized with nonEUB-Fluo. **D.** Green FI vs FSC of a sample hybridized with EUBmix-Fluo.

The dye combination number 4 was also tested with the same pure culture. In this case, SYTO 9 was the nucleic acid stain and EUBmix-Cy5 the FISH probe. Cytograms where cell count vs FI are depicted are only shown: Figure 5.17.A and 5.17.B show the results obtained with a non-stained sample and a SYTO 9 stained sample, respectively. In view of these results, a gate named P1 was drawn to enclose the stained cells without including the negative events. 99.7 % of the events were detected with this gate in the stained sample. FISH results with nonEUB-Cy5 and EUBmix-Cy5 probes (Figure 5.17.C and 5.17.D, respectively) also showed a clearly different peak for negative and positive events. In this case, the gate, named P2, included 88 % of the total detected cells in the EUBmix hybridized sample. Therefore, this dye combination was also suitable for quantification.

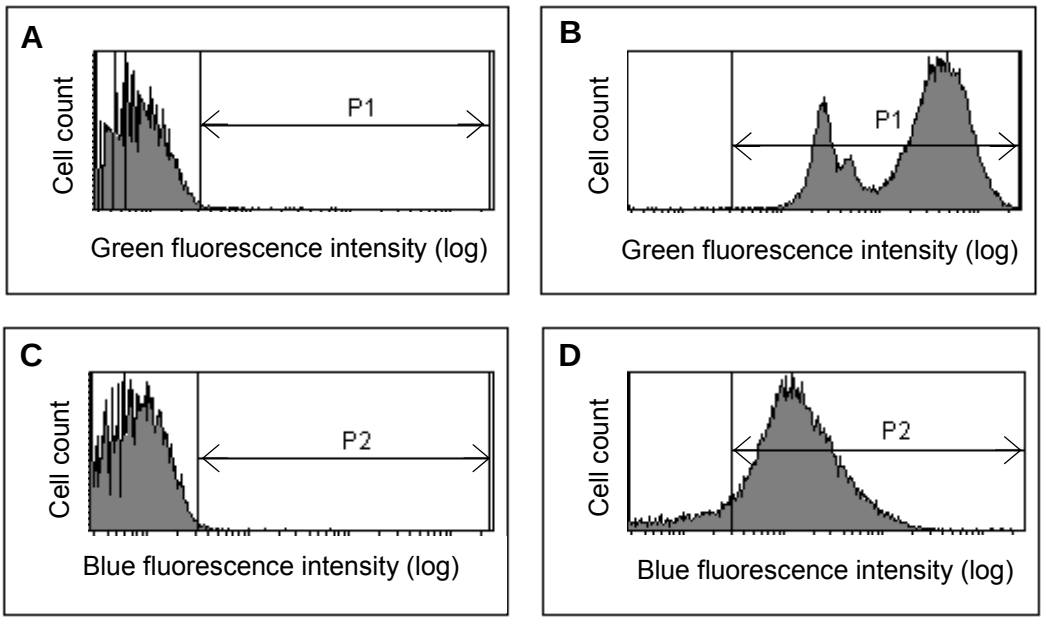

Figure 5.17 Cytograms of *P. putida.* **A.** Cell count vs green FI of a non-stained sample. **A.** Cell count vs green FI of a SYTO 9 stained sample. **C**. Blue FI of a sample hybridized with nonEUB-Cy5. **D.** Cell count vs blue FI of a sample hybridized with EUBmix-Cy5 (**D**).

4.2.4.2 Nitrifying reactor samples

The same tests were performed using samples from the nitrifying reactor. IS-FISH and nucleic acid stain were performed as described in the IS-FISH protocol (section 4.2.2).

Firstly, the dye combination number 1 was tested (DAPI and Fluo). With respect to the DAPI staining, the FI of the stained sample was not different enough to the FI of the non-stained sample to differentiate between stained cells and debris particles. Figures 5.18.A and 5.18.B show the cell count vs blue FI for the non-stained and stained samples, respectively. In this case, the gate, named P1, was drawn using the results of the non-stained sample to avoid counting negative events. The same gate in Figure 5.18.B only enclosed 13 % of the total cells. Figures 5.18.C and 5.18.D show that although the FI vs FSC was considered, there was not enough difference between the location of the non-stained and the stained cells.

Using the same samples, when the green FI was considered a similar result was obtained. The sample hybridized with EUBmix-Fluo (see Figures 5.19.B) showed only slightly higher FI than the sample hybridized with nonEUB-Fluo (see Figures 5.19.A). The gate drawn in Figures 5.19.A and 5.19.B, named P1, only enclosed 29 % of the total events of the EUBmix hybridized sample. When the green FI vs FSC was analyzed, another gatewas drawn. In this case, it included less that 1 % of the events in Figure 5.19.C and 32 % of the events in Figure 5.19.D. Although this last quantification was slightly better, the result was not satisfactory because there were still a lot of cells that had probably hybridized with the FISH probe but their intensities were not higher than the autofluorescence of the debris particles.

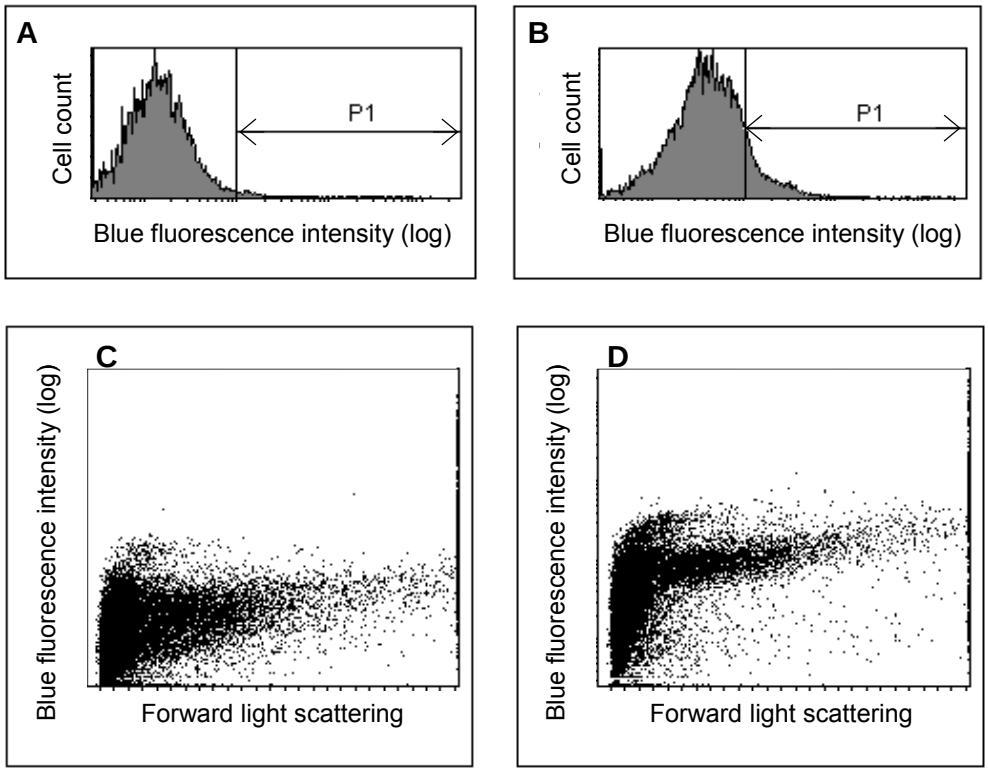

Figure 5.18 Cytograms of nitrifying reactor samples. **A.** Cell count vs blue FI of a non-stained sample. **B.** Cell count vs blue FI of a DAPI stained sample. **C.** Blue FI vs FSC of a non-stained sample. **D.** Blue FI vs FSC of a DAPI stained sample.

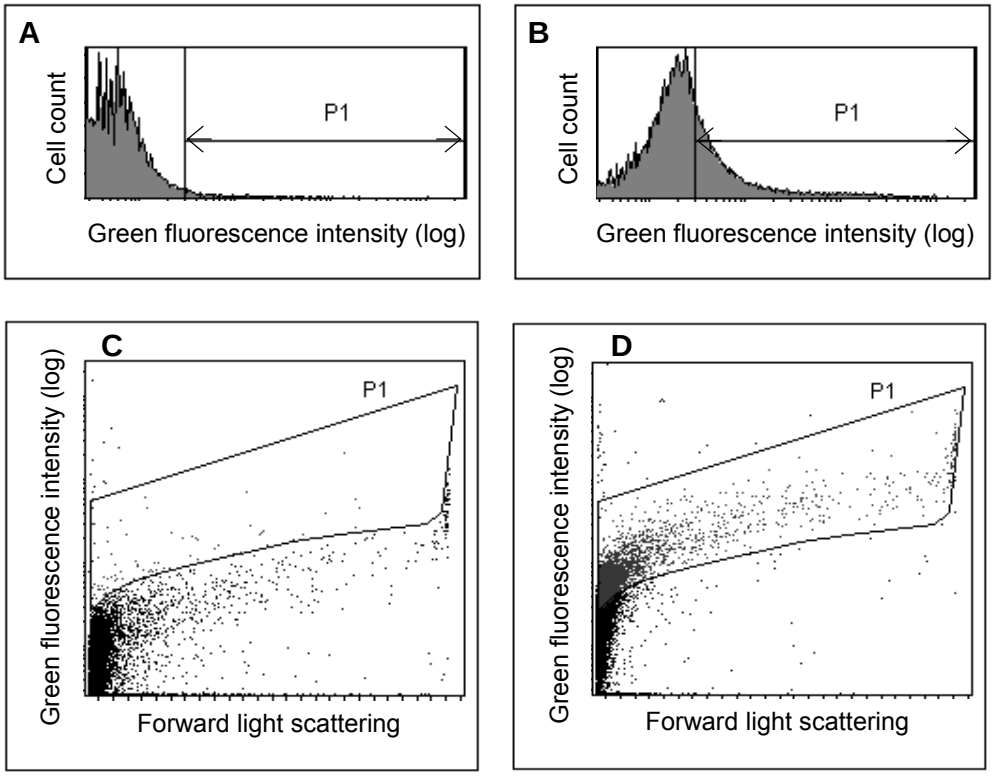

Figure 5.19 Cytograms of nitrifying reactor samples. **A.** Cell count vs green FI of a sample hybridized with nonEUB-Fluo. **B.** Cell count vs green FI of a sample hybridized with EUBmix-Fluo. **C.** Green FI vs FSC of a sample hybridized with nonEUB-Fluo. **D.** Green FI vs FSC of a sample hybridized with EUBmix-Fluo.

Secondly, the dye combination number 4 was tested (SYTO 9 and Cy5). The obtained results were very similar to those obtained with the dye combination number 1. Figure 5.20 show the results. In this case, only cytograms of cell count vs FI are shown. Figures 5.20.A and 5.20.B show that the use of SYTO 9 as nucleic acid stain, instead of DAPI, gave better results since the gate P1 included up to 85 % of the total counted objects for the stained sample. However, Figures 5.20.C and 5.20.D showed that the FISH result was similar than the previously tested FISH probe. In this case, the gate P2 enclosed 25 % of the total cell count.

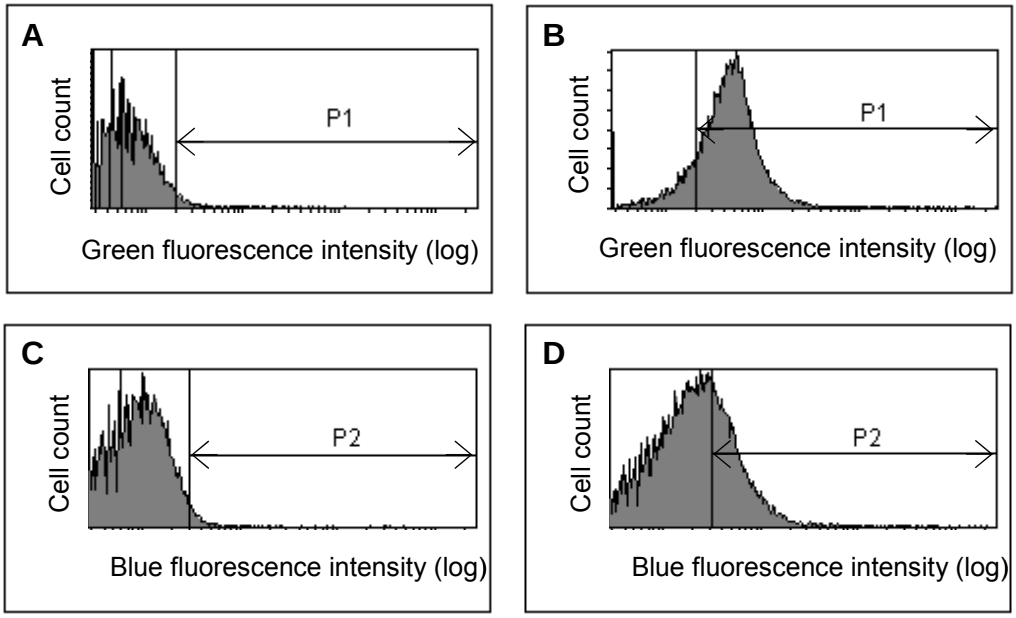

Figure 5.20 Cytograms of nitrifying reactor samples. **A.** Cell count vs green FI of a non-stained sample. **B.** Cell count vs green FI of a SYTO 9 stained sample. **C**. Cell count vs blue FI of a sample hybridized with nonEUB-Cy5. **D.** Cell count vs blue FI of a sample hybridized with EUBmix-Cy5 (**D**).

4.2.4.3 Discussion

Although these dye combinations led to satisfactory results with the pure culture, the use of a reactor sample led to completely different results. Some modifications were performed in order to improve the results but any of them was successful. These changes were: the modification of the sample collection method (including bacteria extraction with Nycodenz, Nycomed Pharma A/S), the use of more amount of FISH probe and the addition of multiple general and specific FISH probes (multiple labeling).

The reasons for the negative results could be: (1) the wide bacterial size distribution; (2) the high concentration of inorganic particles of the sample and (3) the small size of individual cells (around 1 μm). Probably, the use of a pure culture of nitrifiers (e.g. *Nitrosomonas europaea*) would help determining the reasons for these results.

However, Dr Susann Müller from the Department of Environmental Microbiology at UFZ-Center for Environmental Research (Leipzig, Germany) suggested (in a personal communication) that a preliminary step in the analysis of the reactor sample with the FCM was

missing. She explained that, when dealing with so small cells, the FCM should be aligned considering the SSC instead of the FSC. As a result of this alignment, the cytograms showing cell count vs SSC should contain two peaks, one for debris particles (noise) and another for bacterial cells. This equipment alignment should be performed with a known cells culture with a diameter similar to the cells in the reactor sample (probably a pure culture of nitrifiers). It would allow the definition of a threshold value in the SSC axis for bacterial cell detection, which would then be used when considering the FI signal. This approach was used in Wallner et al. (1995) because they found that the SSC channel was less noisy than the FSC. This could not be tested in this work; however, it opened new ways for further research in this field.

In case these improvements were not satisfactory, there would be still other techniques to increase the sensitivity of hybridized cells. These techniques, usually used to detect cells with small numbers of ribosomes, are (Amann et al. 1995): (1) indirect labeling like the attachment of a reporter molecule to the nucleic acid probe, which, following hybridization, is detected in a second step by a labeled binding protein; and (2) the use of more sensitive labels like enzyme-labeled oligonucleotides with enzymes like horseradish peroxidase.

4.3 BIOMASS FRACTION DETERMINATION

The biomass fractions of AOB and NOB were determined with three different experimental methodologies and with a mathematical approach. All the experimental assessments were based on the FISH technique but the used equipment for the quantification was different: EFM, CLSM and FCM.

From the available specific FISH probes, Nso190 and Nso1225 were used for AOB detection and NIT3 and Ntspa662 were used for NOB detection. However, only Nso190 and NIT3 hybridized to the bacteria from the reactor sample and thus, the other probes were rejected.

4.3.1 QUANTIFICATION USING AN EFM

Three samples of biomass were collected from the nitrifying reactor and OS-FISH (with sonication) was performed to each one. AOB were quantified after hybridization with EUBmix-Fluo and Nso190-Cy3 and NOB were quantified after hybridization with EUBmix-Fluo and NIT3-Cy3. 40 different microscopic fields were randomly chosen with the condition that they should only contain individual cells. Two pictures were taken to each field changing the emission filter, one to detect the fluorescence of the EUBmix probe and another to detect the specific probe. Two microscopic fields were also chosen for the negative control sample (hybridization with nonEUB) in order to set the intensity value for the threshold. Image Pro Plus (Media Cybernetics) was used for image analysis and object counting.

Results obtained with this methodology are summarized in Table 5.13. It can be observed that the number of bacteria detected in each sample was around 3000 to 5000 and that the amount

of nitrifying bacteria was quite lower. The obtained fraction of AOB and NOB was 55 ± 6 % and 21 ± 2 %.

Table 5.13 Nitrifying biomass fractions determination using an EFM.

	Cell count for AOB fraction determination			Cell count for NOB fraction determination		
Sample	EUBmix	Nso190	Ratio	EUBmix	NIT3	Ratio
1	4939	2864	0.58	3190	759	0.24
2	3866	2259	0.58	3681	742	0.20
3	4133	1990	0.48	5216	1068	0.20
Average			0.55±0.06			0.21±0.02

4.3.2 QUANTIFICATION USING A CLSM

A sample from the nitrifying reactor was hybridized following the OS-FISH protocol described in section 3.3.4 and using the FISH probes: EUBmix labeled with Cy5 and one of the specific probes labeled with Cy3. Quantification was performed as explained in section 4.1.2. Figure 5.21 shows two representative CLSM images corresponding to AOB and NOB quantification. The obtained fractions were 40 ± 4 % of AOB and 16 ± 3 % of NOB.

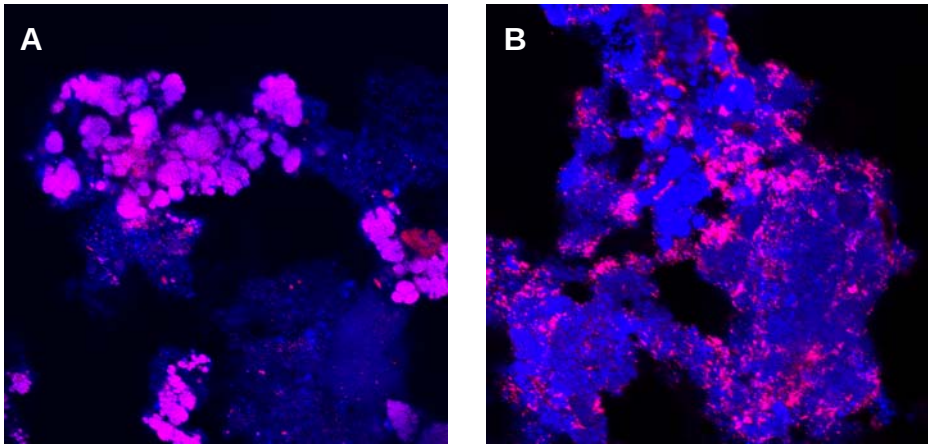

Figure 5.21 FISH/CLSM representative images for nitrifying biomass fractions determination. **A.** EUBmix (blue) and Nso190 (pink). **B.** EUBmix (blue) and NIT3 (pink).

4.3.3 QUANTIFICATION USING A FCM

Although unsatisfactory results were obtained in the optimization of the flow cytometry technique for nitrifying biomass quantification, a preliminary result was obtained by the hybridization with FISH probes labeled with Fluo. In this case, any nucleic acid stain was used. As shown in Figures 5.19.C and 5.19.D, the green FI vs FSC representation allowed drawing a gate to count the positive events. Even though it was clear that this gate was not enclosing the

entire targeted cells, the same gate was used for samples hybridized with the specific probe. Figure 5.22 shows the cytograms obtained from reactor samples hybridized with nonEUB-Fluo (Figure 5.22.A), EUBmix-Fluo (Figure 5.22.B), Nso190-Fluo (Figure 5.22.C) and NIT3-Fluo (Figure 5.22.D).

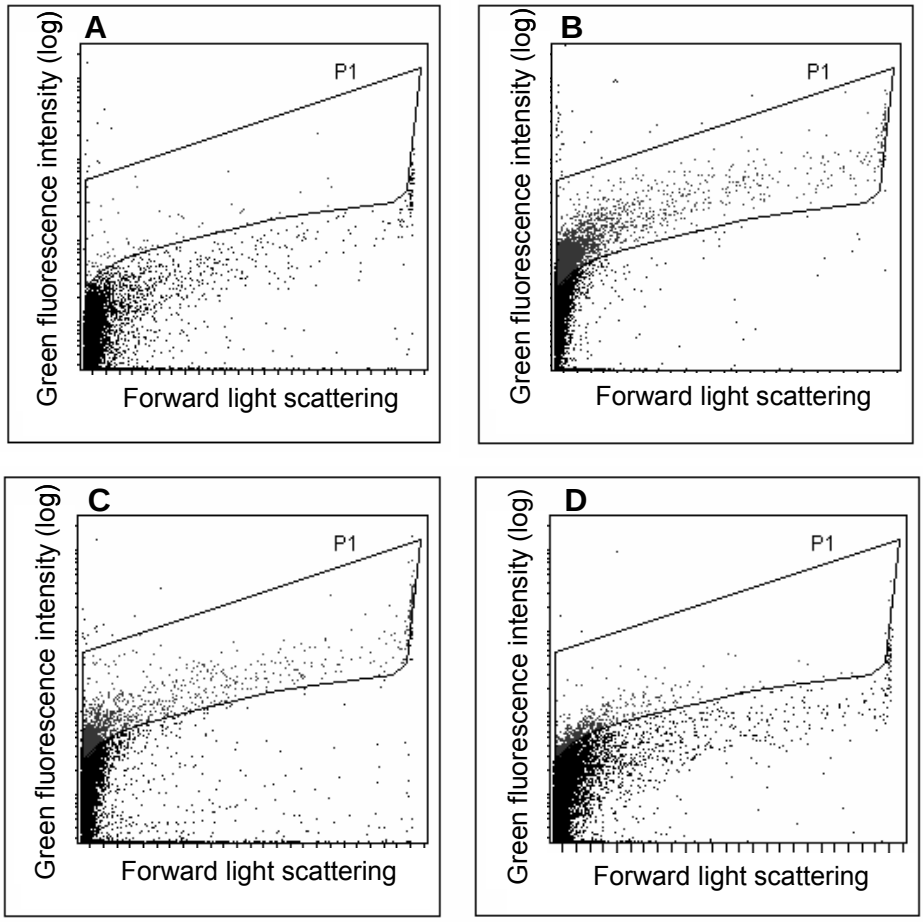

Figure 5.22 Cytograms of nitrifying reactor samples. **A.** nonEUB-Fluo. **B.** EUBmix-Fluo. **C.** Nso190-Fluo **D.** NIT3-Fluo.

Table 5.14 Results of FCM analyses of three reactor samples.

	Sample 1		Sample 2		Sample 3		Average		Std		CV
	Counts	%	Counts	%	Counts	%	Counts	%	Counts	%	%
nonEUB	754	0.6	703	0.6	552	0.5	670	0.6	105	0.1	16
EUBmix	38581	32.2	39706	33.1	36126	30.1	38138	31.8	1831	1.5	5
AOB	19907	16.6	15513	12.9	10403	8.7	15274	12.7	4756	4.0	31
NOB	1750	1.5	3319	2.8	2545	2.1	2538	2.1	785	0.7	31

Three samples from the nitrifying reactor were fixed and hybridized following the IS-FISH protocol described in section 4.2.2 but using only one probe. Each sample was divided into two sub-samples. Each sub-sample was hybridized with probes nonEUB, EUBmix, Nso190 and NIT3 separately. Each preparation was analyzed in duplicate with the FCM. Table 5.14 shows the obtained results. Note that each “counts” figure is the sum of 4 different analyses (2 sub-

samples x 2 repetitions) and that the percentages were calculated with the total number of recorded events (4 x $3 \cdot 10^4$). Considering these results, AOB and NOB fractions were calculated as 39 ± 12 % and 5 ± 2%, respectively (Table 5.15).

Table 5.15 Biomass fractions determination using the FCM (in %).

	Sample 1	Sample 2	Sample 3	Average	Std
AOB/EUBmix	50.6	38.0	27.7	39	12
NOB/EUBmix	2.6	6.7	5.6	5	2

4.3.4 MODEL PREDICTION

The ratio between AOB and NOB can be calculated with their growth yields (Y_A and Y_N) provided that their decay rates are equal and there is complete nitrification. Nevertheless, the calculation of the absolute value of the biomass fractions requires the system simulation.

The reactor behavior was simulated (section 3.1.2) until the steady state was reached. The obtained concentrations of the main particulate compounds are shown in Table 5.16. This table also shows the concentration of three additional particulate compounds, $X_{P,A}$, $X_{P,N}$, $X_{P,H}$, that correspond to the fraction of X_P coming from the decay of X_A, X_N and X_H, respectively.

Table 5.16 Steady state concentrations of the main particulate compounds.

Compound	X_A	X_N	X_H	X_P	$X_{P,A}$	$X_{P,N}$	$X_{P,H}$
Concentration (mg COD L^{-1})	297	132	148	149	48	21	80

The comparison of the FISH experimental data with the fractions calculated from simulation data is not straightforward. FISH probes target genetic material (rRNA), therefore, it is clear that the biomass defined in the model as X_A, X_N, and X_H should be experimentally detected. With respect to X_S and X_{ND}, they are particulate compounds but they are not whole cells and thus, they must not be detected with this hybridization technique. The problem arises when dealing with X_P. In the components description of ASM1 (Henze et al. 2000), it is stated that the incorporation of this component in the model is one way of accounting for the fact that not all biomass in an activated sludge system is active. If this non-active biomass had the same cell structure, DNA and rRNA content than an active cell, this component would also be detected with FISH probes. However, if this non-active biomass did not keep a typical cellular structure, it would never be hybridized to the probes.

Considering this problem, biomass fractions (f_i) were calculated using two different approaches. In the first one (equation 5.4), it was considered that X_P was not detected with FISH probes, while in the second approach (equation 5.5), X_P was included in the fractions

calculation. Table 5.17 shows the calculated fractions. It can be observed that the maximum difference between calculated values is in the heterotrophs fraction (5%). These differences depend on the X_P fraction with respect to the total particulate compounds, in this case 20 %. Since the consideration of X_P in the fractions calculations represents an increase in the model complexity and the obtained results were not very different, the first approach was considered appropriate for fractions calculation.

$$f_i = \frac{X_i}{X_A + X_N + X_H} \tag{5.4}$$

$$f_i = \frac{X_i + X_{P,i}}{X_A + X_N + X_H + X_P} \tag{5.5}$$

Table 5.17 Biomass fractions obtained by simulation (in %).

Calculation approach	AOB	NOB	Heterotrophs
1 (without X_P)	51	23	26
2 (with X_P)	48	21	31

4.3.5 COMPARISON AND DISCUSSION

Table 5.18 summarizes the obtained biomass fractions and the AOB/NOB ratio for each case. It can be observed that this ratio was similar in all the methods except for the flow cytometric count where fewer NOB cells were detected. These results were expected since the gating method in the flow cytometric analysis was not appropriate. This result showed that NOB were more underestimated that AOB, probably due to their smaller cell size. It confirms that more research is required to get a good estimation of the biomass fractions using a FCM.

Table 5.18 Summary of experimental and calculated biomass fractions.

%	EFM	CLSM	FCM	Model
AOB	55 ± 6	40 ± 4	39 ± 12	51
NOB	21 ± 2	16 ± 3	5 ± 2	23
Heterotrophs	24*	44*	56*	26
AOB/NOB ratio	2.6	2.5	7.8	2.2

* Calculated as the remaining biomass fraction.

With respect to the use of EFM and CLSM, although the AOB/NOB ratio was similar, the obtained fractions were quite different. The main difference between these techniques was the sonication step and the quantification methodology. In the sonication time optimization it was shown that not all aggregates could be disrupted into individual cells and furthermore, some of the initial individual cells could have been damaged. With respect to the quantification method,

with the EFM, individual cells were counted while with the CLSM, the area was considered. The comparison of these results among them and with the simulation output could not be appropriate unless all bacteria had the same size and density and all the aggregates had the same density of cells, which in fact was not true: Manser et al. (2005) determined that AOB and NOB diameters are 1-1.2 and 0.5-0.8 μm, respectively. An example of the effect of the quantification method on the fractions determination can be found in Daims et al. (2001b), where an AOB/NOB ratio of 6.9 was calculated with area-based quantification and a ratio of 1.3 when these data were transformed to single cell numbers (using the previously estimated average single cell area of each population). The system studied in that work was different from the system studied in this chapter, therefore their results can not be extrapolated. With respect to the biomass fractions obtained from the simulations, they are expressed in terms of weight of bacteria. Therefore, both EFM and CLSM could be used for biomass fractions determinations if the limitations of each methodology were taken into account. Moreover, if experimental results were to be compared with model prediction, some corrections should be considered (bacteria size, bacteria density and/or density of aggregates).

Table 5.19 Comparison of instruments for biomass fractions determination.

	EFM	CLSM	FCM
#cells/sample	$\approx 3 \cdot 10^3$ (40 pictures)	$\approx 3 \cdot 10^5$ (50 pictures)	$\geq 3 \cdot 10^4$
Time/sample	> 4 h	> 2 h	≈ 5 min
Equipment availability	High	Low	Very low

Apart from experimental results, other considerations should be taken into account in the comparison of these techniques. Table 5.19 shows some information about the number of counted cells per sample; the analysis time and the equipment availability. Undoubtedly, the best equipment in terms of experimental time is the FCM because a great number of samples can be analyzed in a short time while using microcopy several hours are required for the analysis of only one sample. However the equipment availability is very low and the technique is not yet totally optimized. With respect to EFM, only few thousands cells were counted although 40 microscopic fields were analyzed. The main problem was that high-magnification was required in order to have single-cell resolution and therefore, each image contained relatively few cells. In this thesis, CLSM was preferred to EFM because it was more automated, fast and allowed the study of spatial distribution of the bacterial populations.

5. CONCLUSIONS

- Hybridization conditions for probe Nso190 were optimized at 35 % of formamide instead of the 55 % reported in the literature.

- The most important step in the CLSM images quantification is the definition of the appropriate intensity threshold. Thresholding can be automated using control images (hybridized with nonEUB or without probe) and analyzing the pixel intensity. The threshold intensity was chosen to remove 99.9 % of the pixels of the control images.

- The optimal number of CLSM images for biomass quantification depends of the required accuracy and the homogeneity of the target organism. In general terms, a difference of 10 % in the final result will be obtained if 30-35 images, instead of 50, are used.

- Optimum sonication time for nitrifying activated sludge samples is 10 min (supplying 53 W) considering the total number of objects. With this sonication time, 99.9 % of the objects have a d_{eq} below 10 μm.

- IS-FISH protocol does not require a dehydration step; the optimal probe concentration is around 4.2 ng μL^{-1}; a washing step without formamide is required; and a final washing step with PBS instead of water is better.

- IS-FISH procedure favors cell aggregation and causes single cell loss.

- Quantification of *Pseudomonas putida* with flow cytometry can be easily performed either after nucleic acid staining or FISH with EUBmix because fluorescent-positive and fluorescent-negative cells could be clearly differentiated.

- Clear differentiation between fluorescent-positive and fluorescent-negative cells could not be obtained with activated sludge samples with any of the used nucleic acid stains or FISH probes. Probably, signal-to-noise ratio could have been improved if a previous alignment of the FCM had been done using SSC.

- The fraction of AOB and NOB was 40-55 % and 15-23 % depending on the method. With the exception of flow cytometry, all the used methods obtained a AOB/NOB ratio of 2.2-2.6.

- Single cell count with epifluorescence microscopy is time consuming and needs a sonication step in the sample preparation. However, the equipment is cheap and easily available.

- Quantification with CLSM images can lead to biased results due to the area-based quantification. However, it does not require a destructive step (sonication) in the sample preparation, it allows the study of the spatial distribution of the bacterial populations and it can be easily automated and performed.

- Flow cytometric count of activated sludge cells requires a sonication step in the sample preparation and is still under development. However, the fact that a great number of cells can be counted with a very short time provides a clear incentive to refine it.

6. REFERENCES

Adamczyk J, Hesselsoe M, Iversen N, Horn M, Lehner A, Nielsen PH, Schloter M, Roslev P, Wagner M. 2003. The isotope array, a new tool that employs substrate-mediated labeling of rRNA for determination of microbial community structure and function. *Applied and Environmental Microbiology* 69(11):6875-6887.

Amann R. 1995. In situ identification of microorganisms by whole cell hybridization with rRNA-targeted nucleic acid probes. Akkerman AD, Van Elsas LJD, de Bruijn FJ, editors. Dordrecht, The Netherlands: Kluwer Academic Publishers. 1-15 p.

Amann RI, Binder BJ, Olson RJ, Chisholm SW, Devereux R, Stahl DA. 1990. Combination of 16S rRNA-targeted oligonucleotide probes with flow cytometry for analyzing mixed microbial populations. *Applied and Environmental Microbiology* 56(6):1919-1925.

Amann RI, Ludwig W, Schleifer KH. 1995. Phylogenetic identification and in situ detection of individual microbial cells without cultivation. *Microbiological Reviews* 59(1):143-169.

APHA. 1995. Standard methods for the examination of water and wastewater. 19th Ed. Washington DC, USA: American Publishers Health Association.

Buesing N, Gessner MO. 2002. Comparison of detachment procedures for direct counts of bacteria associated with sediment particles, plant litter and epiphytic biofilms. *Aquatic Microbial Ecology* 27(1):29-36.

Burrell PC, Phalen CM, Hovanec TA. 2001. Identification of Bacteria Responsible for Ammonia Oxidation in Freshwater Aquaria. *Applied and Environmental Microbiology* 67(12):5791-5800.

Coskuner G, Ballinger SJ, Davenport RJ, Pickering RL, Solera R, Head IM, Curtis TP. 2005. Agreement between theory and measurement in quantification of ammonia-oxidizing bacteria. *Applied and Environmental Microbiology* 71(10):6325-6334.

Chandran K, Hu Z, Krach W, Smets BF. Dynamics of genotypics, biokinetics and performance in a continuously operated nitrifying bioreactor. *In: Proceedings of 3rd International Water Association World Congress* 2002; Melbourne, Australia. IWA Publishing.

Daims H, Brühl A, Amann R, Schleifer KH, Wagner M. 1999. The domain-specific probe EUB338 is insufficient for the detection of all bacteria: Development and evaluation of a more comprehensive probe set. *Systematic and Applied Microbiology* 22(3):434-444.

Daims H, Nielsen JL, Nielsen PH, Schleifer KH, Wagner M. 2001a. In Situ Characterization of Nitrospira-Like Nitrite-Oxidizing Bacteria Active in Wastewater Treatment Plants. *Applied and Environmental Microbiology* 67(3-12):5273-5284.

Daims H, Purkhold U, Bjerrum L, Arnold E, Wilderer PA, Wagner M. 2001b. Nitrification in sequencing biofilm batch reactors: Lessons from molecular approaches. *Water Science and Technology* 43(3):9-18.

Daims H, Ramsing NB, Schleifer KH, Wagner M. 2001c. Cultivation-independent, semiautomatic determination of absolute bacterial cell numbers in environmental

samples by fluorescence in situ hybridization. *Applied and Environmental Microbiology* 67(12):5810-5818.

Davey HM, Kell DB. 1996. Flow cytometry and cell sorting of heterogeneous microbial populations: The importance of single-cell analyses. *Microbiological Reviews* 60(4):641-696.

Egli K, Langer C, Siegrist HR, Zehnder AJB, Wagner M, Van der Meer JR. 2003. Community analysis of ammonia and nitrite oxidizers during start-up of nitritation reactors. *Applied and Environmental Microbiology* 69(6):3213-3222.

Eschenhagen M, Schuppler M, Röske I. 2003. Molecular characterization of the microbial community structure in two activated sludge systems for the advanced treatment of domestic effluents. *Water Research* 37(13):3224-3232.

Forster S, Snape JR, Lappin-Scott HM, Porter J. 2002. Simultaneous fluorescent gram staining and activity assessment of activated sludge bacteria. *Applied and Environmental Microbiology* 68(10):4772-4779.

Gieseke A, Purkhold U, Wagner M, Amann R, Schramm A. 2001. Community Structure and Activity Dynamics of Nitrifying Bacteria in a Phosphate-Removing Biofilm. *Applied and Environmental Microbiology* 67(3):1351-1362.

Gruden C, Skerlos S, Adriaens P. 2004. Flow cytometry for microbial sensing in environmental sustainability applications: Current status and future prospects. *FEMS Microbiology Ecology* 49(1):37-49.

Hallin S, Lydmark P, Kokalj S, Hermansson M, Sörensson F, Jarvis A, Lindgren PE. 2005. Community survey of ammonia-oxidizing bacteria in full-scale activated sludge processes with different solids retention time. *Journal of Applied Microbiology* 99(3):629-640.

Henze M, Gujer W, Mino T, Van Loosdrecht M. 2000. Activated sludge models ASM1, ASM2, ASM2D and ASM3. Scientific and technical report no. 9. London: IWA Publishing.

Hibiya K, Terada A, Tsuneda S, Hirata A. 2003. Simultaneous nitrification and denitrification by controlling vertical and horizontal microenvironment in a membrane-aerated biofilm reactor. *Journal of Biotechnology* 100(1):23-32.

Hovanec TA, Taylor LT, Blakis A, Delong EF. 1998. Nitrospira-like bacteria associated with nitrite oxidation in freshwater aquaria. *Applied and Environmental Microbiology* 64(1):258-264.

Hugenholtz P, Tyson G, Blackall LL. 2001. Design and evaluation of 16S rRNA-targeted oligonucleotide probes for fluorescence in situ hybridization. In: Aquino de Muro M, Rapley R, editors. *Methods is Molecular Biology, vol. 176: Gene probes: principles and protocols*. Totowa, NJ.: Humana Press Inc. p 29-42.

Juretschko S. 2000. Mikrobielle populationsstruktur und -dynamik in einer nitrifizierenden/denitrifizierenden belebtschlammanlage (in German). PhD Thesis. München: Technische Universität München.

Juretschko S, Timmermann G, Schmid M, Schleifer KH, Pommerening-Röser A, Koops HP, Wagner M. 1998. Combined molecular and conventional analyses of nitrifying bacterium diversity in activated sludge: Nitrosococcus mobilis and Nitrospira-like bacteria as dominant populations. *Applied and Environmental Microbiology* 64(8):3042-3051.

Kim DJ, Kim SH. 2006. Effect of nitrite concentration on the distribution and competition of nitrite-oxidizing bacteria in nitratation reactor systems and their kinetic characteristics. *Water Research* 40(5):887-894.

Konuma S, Satoh H, Mino T, Matsuo T. 2001. Comparison of enumeration methods for ammonia-oxidizing bacteria. *Water Science and Technology* 43(1):107-114.

Li H, Yang M, Zhang Y, Yu T, Kamagata Y. 2006. Nitrification performance and microbial community dynamics in a submerged membrane bioreactor with complete sludge retention. *Journal of Biotechnology* 123(1):60-70.

Loy A, Horn M, Wagner M. 2003. probeBase: an online resource for rRNA-targeted oligonucleotide probes. *Nucleic Acids Research* 31(1):514-516.

Manser R, Muche K, Gujer W, Siegrist H. 2005. A rapid method to quantify nitrifiers in activated sludge. *Water Research* 39:1585-1593.

Manz W, Amann R, Ludwig W, Wagner M, Schleifer KH. 1992. Phylogenetic oligodeoxynucleotide probes for the major subclasses of proteobacteria: Problems and solutions. *Systematic and Applied Microbiology* 15(4):593-600.

MATLAB. 2002. User's guide. Version 6.5 (Release 13). Mathworks T, editor. Natick, USA.

Mobarry BK, Wagner M, Urbain V, Rittmann BE, Stahl DA. 1996. Phylogenetic probes for analyzing abundance and spatial organization of nitrifying bacteria. *Applied and Environmental Microbiology* 62(6):2156-2162.

Mobarry BK, Wagner M, Urbain V, Rittmann BE, Stahl DA. 1997. Erratum: Phylogenetic probes for analyzing abundance and spatial organization of nitrifying bacteria (Applied and Environmental Microbiology 62:6 (2157)). *Applied and Environmental Microbiology* 63(2):815.

Mota C, Ridenoure J, Cheng J, De Los Reyes Iii FL. 2005. High levels of nitrifying bacteria in intermittently aerated reactors treating high ammonia wastewater. *FEMS Microbiology Ecology* 54(3):391-400.

Nebe-von-Caron G, Stephens PJ, Hewitt CJ, Powell JR, Badley RA. 2000. Analysis of bacterial function by multi-colour fluorescence flow cytometry and single cell sorting. *Journal of Microbiological Methods* 42(1):97-114.

Nelson KE, Weinel C, Paulsen IT, Dodson RJ, Hilbert H, dos Santos V, Fouts DE, Gill SR, Pop M, Holmes M and others. 2002. Complete genome sequence and comparative analysis of the metabolically versatile *Pseudomonas putida* KT2440. *Environmental Microbiology* 4(12):799-808.

Persson F, Wik T, Sörensson F, Hermansson M. 2002. Distribution and activity of ammonia oxidizing bacteria in a large full-scale trickling filter. *Water Research* 36(6):1439-1448.

Pommerening-Röser A, Rath G, Koops HP. 1996. Phylogenetic diversity within the genus Nitrosomonas. *Systematic and Applied Microbiology* 19(3):344-351.

Rath G. 1996. Entwicklung eines nachweissystems zur in situ-analyse nitrifizierender bakkterienpopulationen auf des basis spezifischer 16S rRNA-gensequenzen (in German). PhD Thesis. Hamburg: University of Hamburg.

Röske I, Röske K, Uhlmann D. 1998. Gradients in the taxonomic composition of different microbial systems: Comparison between biofilms for advanced waste treatment and lake sediments. *Water Science and Technology* 37(4-5):159-166.

Satoh H, Okabe S, Yamaguchi Y, Watanabe Y. 2003. Evaluation of the impact of bioaugmentation and biostimulation by in situ hybridization and microelectrode. *Water Research* 37(9):2206-2216.

Schramm A. 2003. In situ analysis of structure and activity of the nitrifying community in biofilms, aggregates, and sediments. *Geomicrobiology Journal* 20(4):313-333.

Schramm A, De Beer D, Van Den Heuvel JC, Ottengraf S, Amann R. 1999. Microscale distribution of populations and activities of Nitrosospira and Nitrospira spp. along a macroscale gradient in a nitrifying bioreactor: Quantification by in situ hybridization and the use of microsensors. *Applied and Environmental Microbiology* 65(8):3690-3696.

Schramm A, De Beer D, Wagner M, Amann R. 1998. Identification and activities in situ of Nitrosospira and Nitrospira spp. as dominant populations in a nitrifying fluidized bed reactor. *Applied and Environmental Microbiology* 64(9):3480-3485.

Shapiro HM. 1995. Practical flow cytometry. Third edition. Shapiro HM, editor. New York, USA: Wiley-Liss.

Stahl DA, Amann R. 1991. Development and application of nucleic acid probes. In: Stackebrandt E, Goodfellow M, editors. *Nucleic Acid Techniques in Bacterial Systematics*: John Wiley & Sons Ltd.

Vadivelu VM, Yuan Z, Fux C, Keller J. 2006. The inhibitory effects of free nitrous acid on the energy generation and growth processes of an enriched Nitrobacter culture. *Environmental Science and Technology* 40(14):4442-4448.

Vives-Rego J, Lebaron P, Nebe-von-Caron G. 2000. Current and future applications of flow cytometry in aquatic microbiology. *FEMS Microbiology Reviews* 24:429-448.

Völsch A, Nader WF, Geiss HK, Nebe G, Birr C. 1990. Detection and Analysis of 2 Serotypes of Ammonia-Oxidizing Bacteria in Sewage Plants by Flow-Cytometry. *Applied and Environmental Microbiology* 56(8):2430-2435.

Wagner M, Rath G, Amann R, Koops HP, Schleifer KH. 1995. In situ identification of ammonia-oxidizing bacteria. *Systematic and Applied Microbiology* 18(2):251-264.

Wagner M, Rath G, Koops HP, Flood J, Amann R. 1996. In situ analysis of nitrifying bacteria in sewage treatment plants. *Water Science and Technology* 34(1):237-244.

Wallner G, Amann R, Beisker W. 1993. Optimizing Fluorescent Insitu Hybridization with rRNA-Targeted Oligonucleotide Probes for Flow Cytometric Identification of Microorganisms. *Cytometry* 14(2):136-143.

Wallner G, Erhart R, Amann R. 1995. Flow cytometric analysis of activated sludge with rRNA-targeted probes. *Applied and Environmental Microbiology* 61(5):1859-1866.

Ziglio G, Andreottola G, Barbesti S, Boschetti G, Bruni L, Foladori P, Villa R. 2002. Assessment of activated sludge viability with flow cytometry. *Water Research* 36(2):460-468.

PART IV - Chapter 6

CONTROLLED START-UP OF A COMPLETE NITRIFICATION SYSTEM WITH HIGHLY CONCENTRATED AMMONIUM WASTEWATER

Part of this chapter was presented as oral presentation:

Jubany I, Carrera J, Baeza JA, Lafuente J. Design and control strategy for optimal start-up of a high-strength nitrification system. 2nd IWA Conference on instrumentation, control and automation for water and wastewater treatment and transport systems. Busan, Korea, may-june 2005.

Part of this chapter was published as:

Jubany I, Baeza JA, Carrera J, Lafuente J. (2007) Model-based design of a control strategy for optimal start-up of a high-strength nitrification system. Environmental Technology 28(2): 185-194.

Part of this chapter is being prepared for publishing as:

Jubany I, Baeza JA, Carrera J, Lafuente J. Optimal start-up of a nitrification system with automatic control to treat highly concentrated ammonium wastewater. Chemical Engineering Journal

The start-up of a nitrifying system to treat high-strength ammonium wastewater must be done carefully to avoid ammonium or nitrite build-up and subsequent system destabilization. This chapter shows the results of the optimization of the start-up of a complete nitrification system. Firstly, a manual start-up was performed with manual increases in the nitrogen loading rate (NLR). Secondly, a model-based design of a control strategy for optimal start-up was carried out and two strategies were optimized and compared. Thirdly, both strategies were successfully implemented in pilot plant and compared with simulated results. FISH technique was used to check the enrichment of the sludge in nitrifying microorganisms. Finally, simulation tools were used for long-term prediction of the pilot plant performance.

1. INTRODUCTION

The start-up of a biological process always requires special attention. If the start-up strategy is not appropriate, lost of biomass or destabilization of the process can easily occur (Van Hulle et al. 2005). Start-up usually consists of progressively enrichment of the bacterial population in a specific group of microorganisms (nitrifying, polyphosphate accumulating organisms (PAOs), heterotrophs, etc). Usually, the growing conditions of the inoculum are gradually changed until the desired conditions are reached. These conditions could be the temperature, contaminant load, shear stress, etc. Therefore, a faster start-up is accomplished when the inoculated population is already enriched in the target population or acclimated to the final conditions. For example, in Chen et al. (1996), an activated sludge reactor for biological denitrification reached the steady state 80-100 after the inoculation with fresh sludge from a wastewater treatment plant (WWTP), but only 25-30 days after inoculation when acclimated sludge was used as seeding.

Some particular processes need special care in the start-up process. This is the case for substratum colonization in biofilm formation (Villaverde et al. 2000), granulation process in upflow anaerobic sludge blanket (UASB) technology (Show et al. 2004) or anaerobic ammonia-oxidizing bacteria (anammox) growth in oxygen-limited autotrophic nitrification-denitrification process (OLAND) (Pynaert et al. 2004).

With respect to the biological nitrogen removal (BNR) with high-strength ammonium wastewaters, one of the most problematic steps is the start-up of the nitrifying process. In the nitrification process, accumulation of ammonium, due to disturbances as changes in temperature, inflow or dissolved oxygen concentration, can provoke its inhibition and consequently the BNR instability. Reported experiences for the start-up procedure for highly nitrogenous wastewaters show that it is quite delicate and time-consuming (3 to 4 months (Verstraete et al. 1977) or around 100 days (Vallés-Morales et al. 2004)). During this operation, if the nitrogen-loading rate (NLR) is higher than the maximum nitrification rate

(MNR) of the system, a large accumulation of ammonium can take place. Therefore, the start-up must be carried out with a gradual and controlled increase of the NLR, so that the nitrification rate is as close as possible to the MNR (Carrera et al. 2003).

The start-up of the nitrifying process is usually carried out with manual control based on total ammonia nitrogen (TAN), total nitrite nitrogen (TNN), nitrate or oxygen uptake rate (OUR) measurements (Galí et al. 2006; Ghyoot et al. 1999; Teichgräber and Stein 1994; Vallés-Morales et al. 2004). In these studies, nitrogenous compounds or OUR, in the effluent or in the aerobic reactor, were measured and the NLR was manually changed accordingly: increased if the percentage of nitrification was satisfactory or decreased if the undesirable compounds were building up. Each NLR was maintained for some days (2-10 days) before a new NLR was applied. The NLR was changed by either increasing inflow or concentration, depending on whether constant HRT was required. In some studies, a combination of both options were used (Campos et al. 1999).

In spite of the importance of a fast and stable start-up of the nitrifying system, there is a lack of studies to improve this process. However, several works proposed automatic control strategies for fast start-up of anaerobic digestion systems. Anaerobic digestion also includes several different microorganisms with possible inhibitions due to different substrates or products. Liu et al (2004) designed and implemented a cascade controller embedded into a rule-based supervisory system based on extremum-seeking control for an upflow fixed-bed reactor. Puñal et al (2001) applied two start-up strategies: fed batch and continuous operation using the biogas production as the only on-line variable. The same strategies were used afterwards to control the system in front of environmental changes.

Automatic control has been widely applied to improve nitrogen removal in WWTPs with either simple or sophisticated controllers. Control strategies based on on-line TAN analyzers were applied in Suescun et al. (2001): simple input simple output (SISO) controllers based on the results of a relative gain analysis (RGA); Sorensen et al. (1994): duration phases control in a plant operated according to Bio-denitro^{TM} method; Puznava et al. (2000): proportional-integral (PI) controller included in a cascade control loop; and Baeza et al. (2002a): knowledge based expert system to minimize nitrogen in the outlet of an anaerobic/anoxic/oxic system while using the minimum amount of energy. Other researchers preferred in-line measurements as pH, oxido-reduction potential (ORP) and dissolved oxygen (DO) because the complexity of measuring the chemical compounds in real-time is neither simple nor economical (Marsili-Libelli 2006). In Teichgräber (1993), on-line monitoring of the influent and effluent turbidity, closed loop control of DO and pH and also on-line monitoring of nitrogenous compounds was combined to a three level control pattern in a nitrification/denitrification process to treat reject water. In-line measurements have been widely used to decrease the length of the different phases in sequencing batch reactors (SBR) (Casellas et al. 2006; Kishida et al. 2004; Puig et al.

2005; Yu et al. 1998). OUR was also successfully used to control and optimize BNR operation. In Surmacz-Gorska et al. (1995), a method based on off-line OUR measurements combined with the application of selective nitrification inhibitors was presented to monitor and control a nitrifying system. Brouwer et al. (1998) developed a device called RESCUE, which performed on-line respirometric batch-experiments (OUR estimation), model calibration and state estimation in order to control the aerobic volume of WWTPs. In Baeza et al. (2002b), the aerobic volume of a WWTP was controlled by in-line OUR measurements using artificial neural networks. Although automatic control is still being studied and applied in pilot plant and full-scale systems to improve nutrients removal, there is a lack of studies to improve their start-up process with automatic control strategies.

Simulation tools play an important role in the control strategies design and testing because different strategies can be simulated in short time in order to choose the best one and also optimize them. Furthermore, various operational conditions and system disturbances can also be simulated and the system response can be studied. Simulation is much faster and cheaper than the implementation of all the strategies and conditions in pilot- or full-scale systems and usually, accurate results are obtained. Several studies simulated the proposed strategies before implementing them in pilot or full-scale systems (Corominas et al. 2006; Galluzzo et al. 2001; Guisasola et al. 2006; Katsogiannis et al. 1999; Marsili-Libelli 2006; Suescun et al. 2001). Other authors used simulation tools in order to test several control strategies, optimize them and choose the best one (Krause et al. 2002; Marsili-Libelli and Giunti 2002).

2. OBJECTIVES

The first objective of this chapter is to design, with the help of simulation tools, optimal control strategies for the start-up of a nitrifying system from a mainly heterotrophic sludge to treat high-strength ammonium wastewater. The second objective is to implement the optimized strategies in a pilot plant to reach a chosen high NLR, compare the results among them and also with a previous start-up without automatic control. The third objective is to check the validity of the used model to predict the experimental results for the start-ups with automatic control. Finally, the fourth objective is to calculate the steady-state of the system based on model predictions.

3. MATERIALS AND METHODS

This section includes the description of the experimental conditions and the inoculum characteristics for the three start-up experiments carried out in this chapter. The experimental inflow control loop is also shown and some details are pointed out with respect to modeling

and chemical analyses. In this section, some references are made to chapters 3, 4 and 5, where the pilot plant, the used model and the microbiological techniques are extensively described.

3.1 PILOT PLANT

3.1.1 EXPERIMENTAL CONDITIONS

The three start-up experiments (start-up I, II and III) shown in this chapter were performed in the pilot plant described in Chapter 4. The experimental conditions in these experiments were slightly different among them since the system performance was being improved as the experiments were being performed (Table 6.1). The main differences were the temperature control, implemented in the second reactor when start-up III was performed, and the in-line OUR estimation which was implemented in all reactors after start-up I.

LSS respirometry was performed off-line in the respirometer (see Chapter 3, section 3.1 for the respirometer description) to estimate the MNR in start-up I. A TAN pulse of 40 mg N L^{-1} (non-limiting concentration) was added to the respirometer and the DO drop was measured in triplicate. Temperature, pH and DO were kept equal than in the pilot plant. OUR estimated was corrected with the endogenous OUR and the MNR was calculated as shown in equation 6.1,

$$MNR = \frac{OUR}{[VSS]\cdot(4.57 - Y_A - Y_N)} \quad (6.1)$$

where [VSS] is the VSS concentration, 4.57 is the stoichiometric coefficient for oxygen in the global nitrification process and Y_A and Y_N are the growth yield coefficients for AOB and NOB, respectively.

Table 6.1 Controlled parameters and OUR estimation in each start-up experiment.

Experiment	pH	T	DO	OUR estimation
Start-up I	Controlled in R1 and R2 at 7.5	Not controlled	Controlled in each reactor at 3.5 mg O_2 L^{-1}	Manual off-line every week
Start-up II	Controlled in R1 and R2 at 7.5	Not controlled	Controlled in each reactor at 3.0 mg O_2 L^{-1}	Automatic in-line every 15 min
Start-up III	Controlled in R1 and R2 at 7.5	Controlled in R2	Controlled in each reactor at 3.0 mg O_2 L^{-1}	Automatic in-line every 5 min

Sludges from two municipal WWTPs from the area of Barcelona were used to inoculate the pilot plant for the different start-up experiments. These WWTPs were performing nitrification at the time of biomass collection but their nitrogen removal rates were very low since the

nitrogen load was low. This means that the fraction of nitrifying bacteria was also low in the seeded sludges. Characteristics of each WWTP are summarized in Table 6.2.

Table 6.2 WWTPs characteristics at the time of biomass collection for pilot plant inoculation.

	Start-up I and II	Start-up III
City and date	Centelles - March'02 Centelles - March'03	Manresa - September'04
Aerobic reactor type	Carousel reactor	Continuous stirred tank reactor (CSTR)
Volume of aerobic reactor (m^3)	5500	13500
Biomass concentration (mg VSS L^{-1})	3500	1650
Sludge residence time (d)	18 - 19	20
Inflow (m^3 d^{-1})	3500	28600
COD concentration in the inflow (mg COD L^{-1})	700 -800	270
TKN concentration in the inflow (mg N L^{-1})	60 - 70	40
NLR_s (g N g^{-1} VSS d^{-1})	0.013	0.05
OLR (g COD g^{-1} VSS d^{-1})	0.136	0.347

3.1.2 EXPERIMENTAL INFLOW CONTROL LOOP

In start-up II and III, an inflow control loop was implemented in a supervisory expert control system developed in G2© (version 4.0), running in a Sun workstation. This expert system had already been developed and applied in the same pilot plant (Baeza et al. 1999; Baeza et al. 2002a; Baeza et al. 2002b). The control loop consisted of a feedback controller where the measured variable was the OUR in R3. Every 10 minutes, the supervisory expert controller calculated an averaged OUR value with values from the last 30 minutes and compared it with the OUR set-point (OUR_{sp}). The difference among these two OUR values was used, together with the controller algorithm, to calculate a new inflow value. Finally, the control action was transmitted to the process computer that executed it by changing the pulse frequency of the inflow pumps. Figure 6.1 schematically shows the control loop implemented in the pilot plant. In this figure, only one pump is represented although in practice, there were two pumps: one for the concentrated medium and another for tap water (see Chapter 4). Pulse frequencies of both pumps were changed by the controller.

3.2 MODELING

Kinetic and stoichiometric model build in Chapter 3 and the pilot plant model described in Chapter 4 were used for modeling purposes in the present chapter. Parameters determined for non acclimated sludge were used.

All simulations were performed with Matlab 6.5® (2002). The ode15s function, a variable order solver based on the numerical differentiation formulas, was used to solve the differential equations of the system balances.

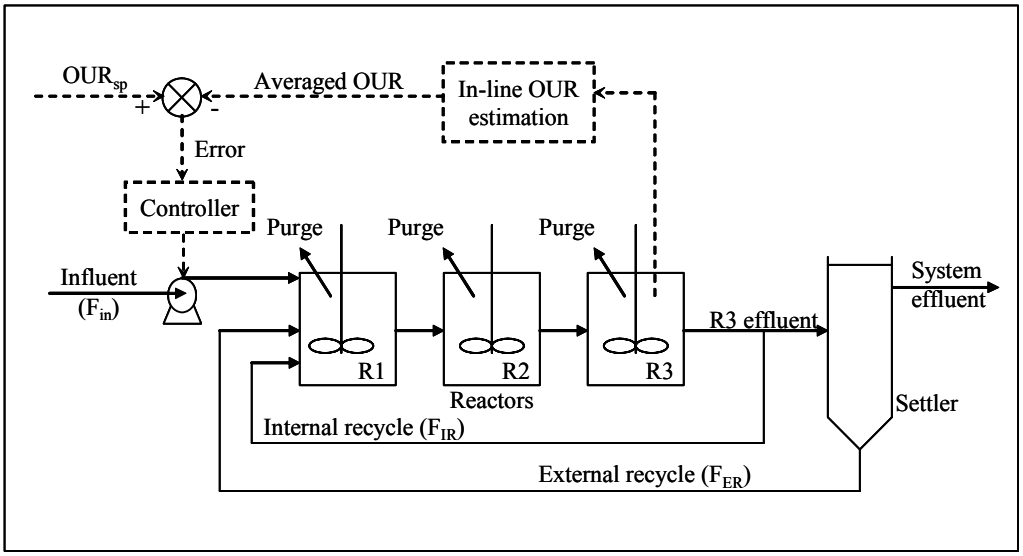

Figure 6.1 Diagram of the inflow control loop in the pilot plant with OUR as the measured variable.

3.3 ANALYSES AND FISH

TAN was analyzed by means of a continuous flow analyzer (CFA) based on potentiometric determination of ammonia (Baeza et al. 1999). TNN and nitrate were measured with capillary electrophoresis using a WATERS Quanta 4000E CE. The used electrolyte solution was a WATERS commercial solution and the conditions of the analyses were 20ºC, 15 kV from a negative source, indirect UV detection at 254 nm and 6 min of analysis (Carrera et al. 2003). Volatile suspended solids (VSS), total suspended solids (TSS) and sludge volumetric index (SVI) were determined according to Standard Methods (APHA 1995).

Fluorescence in situ hybridization (FISH) technique coupled with confocal microscopy was used to determine the predominant nitrifying species during start-up III. A Leica TCS SP2 AOBS confocal laser scanning microscope (CLSM) at a magnification of x63 (objective HCX PL APO ibd.B1 63x1.4 oil) equipped with two HeNe lasers with light emission at 561 and 633 nm was used for biomass quantification. The FISH technique and the quantification method were described in Chapter 5 (section 3.3.4 and 4.1.2, respectively). Hybridizations were carried out using, at the same time, a Cy3-labeled specific probe and Cy5-labeled EUBmix probes. Specific probes used for AOB detection were Nso190, Nso1225, Nmo218, Nsv443 and Nsm156; and for NOB detection were Ntspa662 and NIT3.

3.4 OPTICAL MICROSCOPY

The microscopical observations of the sludge were performed with an optical microscope Zeiss Axioskop equipped with a video camera (iAi Protec). A drop of mixed liquor was carefully deposited on a glass slide and covered with a cover slip before being observed through the microscope.

4. RESULTS

In this section, results for the three start-up experiments are presented. Simulations for control strategies optimization and for experimental data fitting are also shown. Discussion is performed in next section.

4.1 EXPERIMENTAL START-UP WITHOUT AUTOMATIC CONTROL (START-UP I)

The first start-up performed in the pilot plant was done with manual increases of the NLR. It was used as the reference start-up for the next experiments with automatic inflow control.

Biomass inoculated was withdrawn from the WWTP of Centelles (Barcelona). Operational conditions during the whole experiment are described in Table 6.3. SRT was very high at the beginning to keep the biomass in the system (specially the nitrifying bacteria) but it was progressively decreased until day 40, when it was set to 25 days to avoid excessive sludge mineralization (the averaged VSS/TSS ratio was 0.70 ± 0.4). Internal recycle (F_{IR}) and external recycle (F_{ER}) flows where fixed for the whole experiment.

Table 6.3 Operational conditions in start-up I.

pH	Temperature	DO	SRT	HRT	F_{IR}	F_{ER}
7.5	21 – 28 ºC	3.5 mg O_2 L^{-1}	25 d	2 - 5 d	300 L d^{-1}	88 L d^{-1}

At the beginning, the specific NLR (NLR_s) was fixed at the same value as it was in the full-scale plant (0.013 g N g^{-1} VSS d^{-1}). The aim of the start-up was to change the biomass composition from basically heterotrophic to mainly nitrifying. It was decided that, in all this period, TAN and TNN concentration in the effluent had to remain below 10 mg N L^{-1}. Therefore, the NLR_s had to be always below the MNR. The key point was to decide the best strategy to progressively increase the NLR_s and to avoid TAN or TNN accumulation in the effluent. The strategy was to measure periodically the MNR with off-line OUR measurements and change the NLR_s accordingly. NLR_s was increased by raising both inflow value (from 15 to 30 L d^{-1}) and the feed concentration (from 100 to 1000 mg N-TAN L^{-1} with N-TAN/COD ratio ≈ 3). Figure 6.2.A shows the evolution of both NLR_s and MNR. It also shows the

decrease in the ratio between MNR and NLR_s from a very conservative value (8) to a more optimal one (2) since the objective was to operate with NLR_s close to the MNR. TAN and TNN concentrations remained close to zero in all the experiment (data not shown).

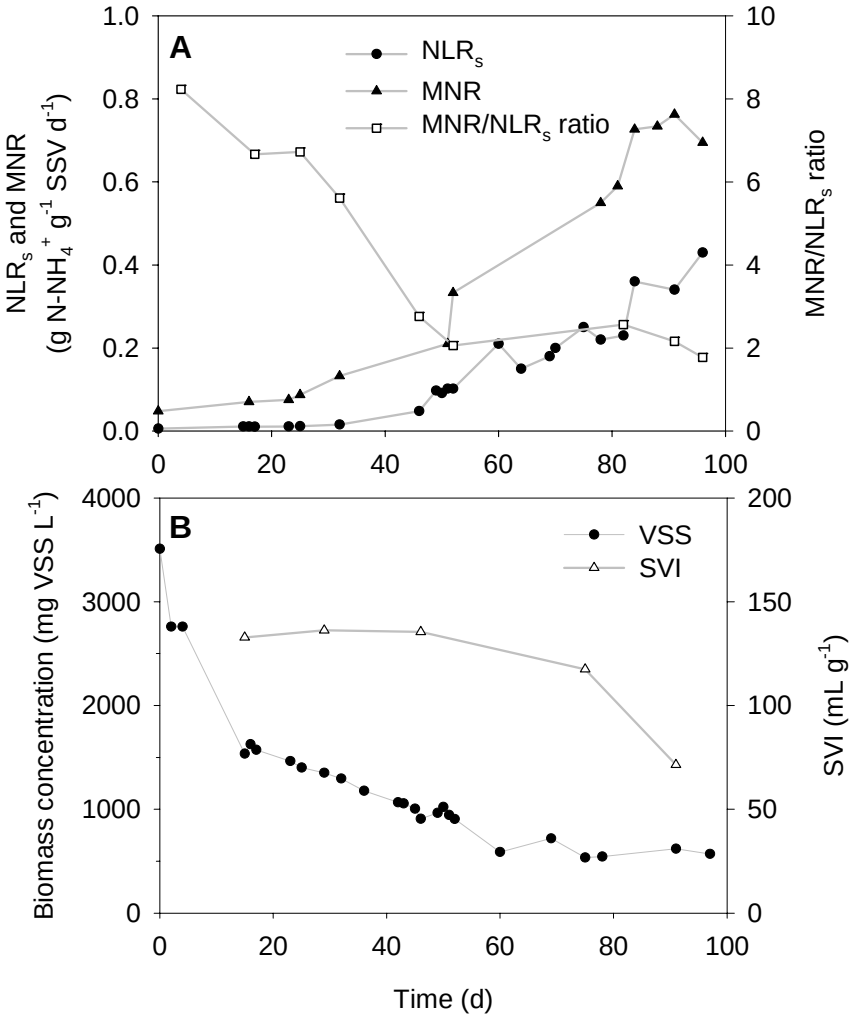

Figure 6.2 Start-up I. **A.** NLR_s, MNR and ratio between them. **B.** VSS and SVI.

Figure 6.2.B shows the evolution of the biomass concentration which decreased dramatically from 3500 to 600 mg VSS L^{-1}. This was due to the decay of heterotrophic bacteria because the organic loading rate (OLR) in the pilot plant through the experiment was approximately 10-100 times lower than in the municipal WWTP. This figure also shows that the SVI was lower than 150 mL g^{-1} which indicated, together with the fact that the TSS in the effluent were around 60±15 mg TSS L^{-1}, that the settling properties of the sludge were good.

At the end of this manual start-up (day 96) a nitrifying sludge capable of treating a NLR_s of 0.4 g N g^{-1} VSS d^{-1} was obtained even though the reached biomass concentration was quite low (600 mg VSS L^{-1}). The achieved NLR_s was used as the end point for the following start-ups with automatic control.

4.2 MODEL-BASED START-UP OPTIMIZATION

In this section, a reduced version of the model was used to speed-up the simulations and to simplify the complexity of the results. Only process related to AOB and NOB were considered: growth and decay of X_A and X_N. Heterotrophic bacteria were not taken into account since the main goal was to optimize the nitrification and it was considered that the effect of these bacteria in the nitrification process was negligible. Furthermore, simulated inflow did not included COD.

The operational conditions were fixed at pH = 7.5, T = 20 ºC and DO = 3 mg O_2 L^{-1}. The simulated inflow had a TAN concentration of 3000 mg N L^{-1}. The external and internal recycle flows were fixed at 14 and 290 L d^{-1} respectively. This high internal recycle was chosen to improve mixing between reactors and to accelerate the system dynamics. However, this recycle flow was not high enough to obtain a totally mixed system. Therefore, different concentrations of soluble compounds (and different rates) were expected in the reactors.

The settler in the pilot plant was modeled as an ideal zero-dimensional settler and the SRT was simulated constant (SRT = 25 d) by adding a biomass removal rate (excess sludge waste) in each reactor (equation 6.2),

$$\text{purge} = \frac{X_i}{SRT} \tag{6.2}$$

where X_i stands for each particulate compound concentration (X_A, X_N) in each reactor.

The initial conditions for the simulations were chosen to reproduce the sludge from a municipal WWTP in which the nitrifying biomass is a small fraction of the total biomass and it is not acclimated to high nitrogen loads. Thus, initial biomass concentration was fixed at 3500 mg VSS L^{-1} with only 3 % of nitrifying microorganisms. Initial AOB and NOB concentration was calculated as $X_A(0)$ = 103 mg COD L^{-1} and $X_N(0)$ = 46 mg COD L^{-1}, considering the active biomass fractions ratio (f_A/f_N) equal to the yields ratio (Y_A/Y_N) and the COD content of the biomass equal to 1.42 g COD g^{-1} VSS.

The simulated control configuration was based on the feedback control previously detailed (section 3.1.2) with the difference that TAN and TNN concentrations in the effluent of R3, instead of OUR, were the measured variables (Figure 6.3). The sum of TAN and TNN concentration (N_{sum}) was compared to the set point, the control action was calculated depending on the controller and finally, the inflow was changed accordingly. This control loop was programmed to actuate every 30 minutes as if on-line ammonium and nitrite analyzers with this sampling frequency were available. The maximum allowed ammonium and nitrite concentration in the effluent (N_{max}) was fixed at 10 mg N L^{-1} and the set point in the control loop ($N_{set\ point}$) was fixed at 6 mg N L^{-1} to avoid higher values than the limit required due to dynamics of the feedback control.

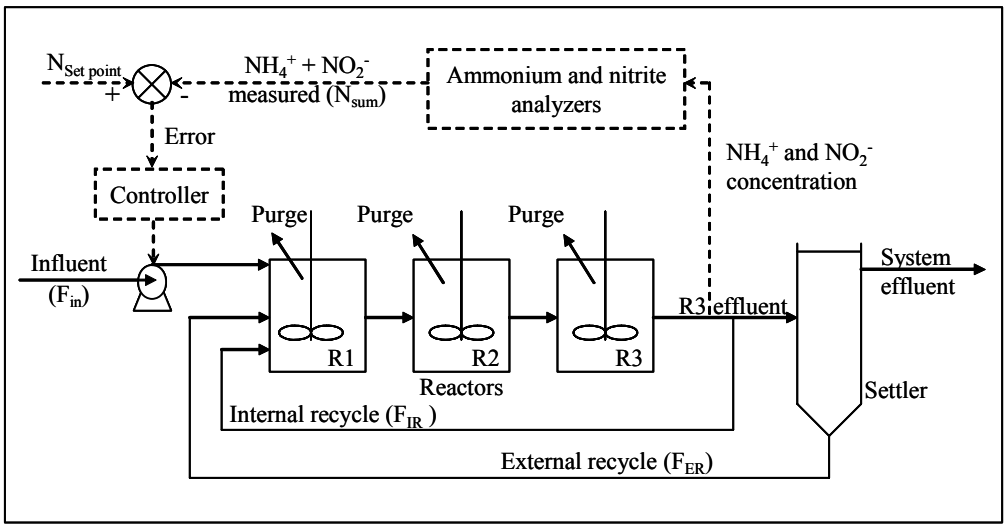

Figure 6.3 Diagram of the simulated inflow control loop with TAN and TNN as measured variables.

4.2.1 START-UP WITHOUT AUTOMATIC CONTROL

Before designing the best control strategy, several simulations were performed to show that different disturbances can severely affect the start-up of a high-loaded nitrifying system without automatic control.

Firstly, the maximum inflow that could be applied to the system without exceeding the N_{max} limitation in the effluent was evaluated with simulations and a value of F_{in} = 3.75 L d^{-1} was obtained. Figure 6.4.A shows TAN, TNN, AOB and NOB concentrations in R3 during the first 100 hours of the start-up using this inflow value. In this simulation, TNN accumulated up to 9 mg N L^{-1} and then decreased due to NOB growth, which increased nitrite removal capacity. TAN concentration in the first and second reactors reached a maximum of 26 and 8 mg N L^{-1} after 11 h (data not shown).

Secondly, a simulation with a 20 % increase in this maximum admissible flow (F_{in} = 4.5 L d^{-1}) was performed (see Figure 6.4.B). In this case, TNN concentration in the effluent immediately increased beyond the N_{max} value. This accumulation was due to NOB inhibition by FA in the first two reactors, where the TAN concentration was higher than in the third one (data not shown).

Finally, different disturbances affecting the operational conditions were tested. For example, when DO was decreased to 2 mg O_2 L^{-1}, TNN concentration increased up to 140 mg N L^{-1} after 100 h although no TAN accumulation was observed. Higher disturbances in this operational parameter and also in pH and temperature provoked also TAN build-up. In all cases, the system became unstable because nitritation and nitratation rates decreased considerably. These

simulations clearly demonstrate that nitrification process with high-strength ammonium wastewater is very sensitive to any disturbance that affects either nitrification rate or NLR.

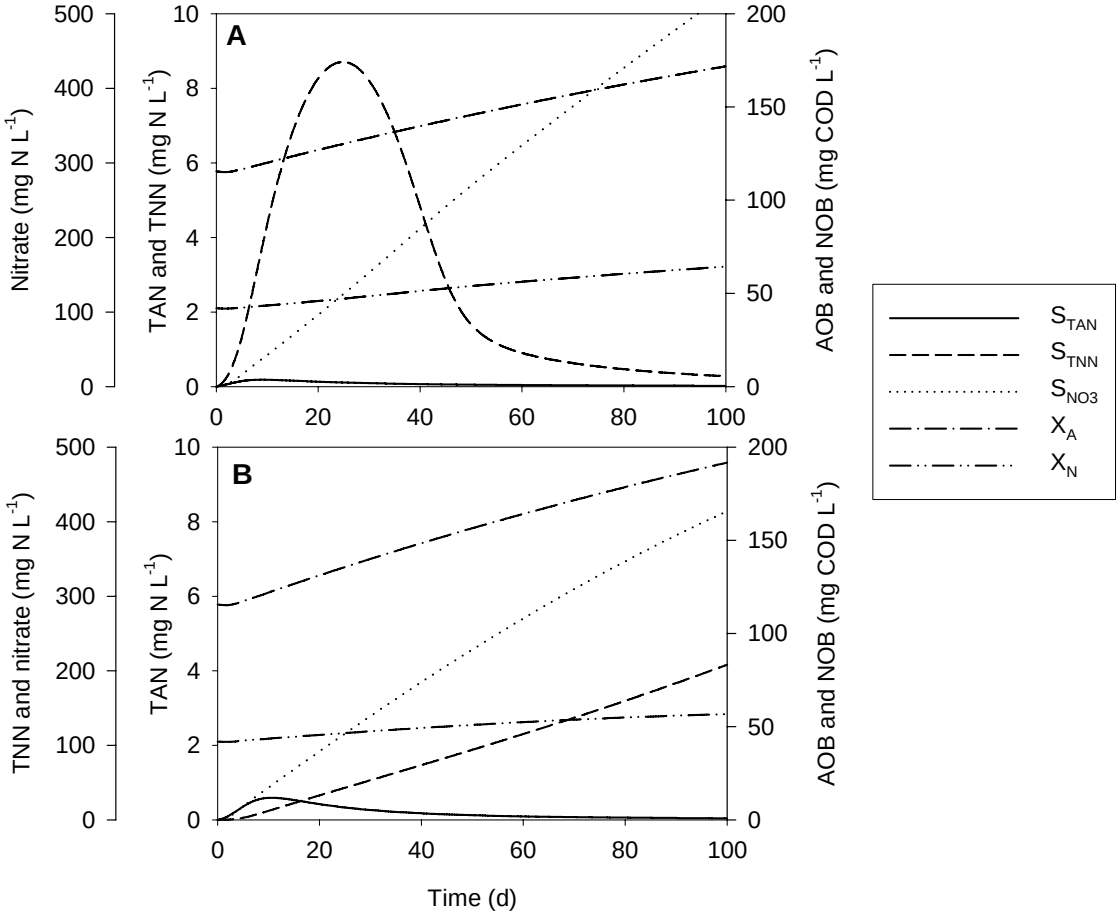

Figure 6.4 Simulation of 100 h start-up without control using different inflow values. Particulate (X) and soluble (S) components concentrations in the effluent of R3 **A.** Maximum inflow admitted without exciding 10 mg N L^{-1} of TAN+TNN in the effluent (F_{in} = 3.75 L d^{-1}). **B.** Inflow 20 % higher than in simulation A (F_{in} = 4.5 L d^{-1}).

As the start-up of the system implies an augmentation of the nitrifying capacity, the inflow must increase in accordance. In addition, the control of TAN and TNN concentration in the reactors is needed to avoid build-up or depletion. Therefore, two automatic control strategies were defined, optimized and compared to achieve a fast and controlled start-up.

4.2.2 FIRST CONTROL STRATEGY: ON-OFF CONTROLLER WITH SUCCESSIVE INFLOW INCREASES

The first control strategy consisted of an on-off controller. In this strategy, the feeding pump was stopped when the N_{sum} in the effluent of R3 was higher than the $N_{set\ point}$ (6 mg N L^{-1}), and the inflow was set to a fixed value (F_{in}^{step}) when the N_{sum} was lower than the $N_{set\ point}$. The inflow value for the on-control action was successively increased when the actual inflow value

did not cause ammonium and nitrite accumulation in the effluent of R3 for a period of 12 hours. This control strategy can be expressed as:

1. On-off controller:

$$\text{Off:} \quad \text{If } N_{sum} > N_{set\ point} \quad \text{then} \quad F_{in} = 0 \tag{6.3}$$

$$\text{On:} \quad \text{If } N_{sum} < N_{set\ point} \quad \text{then} \quad F_{in} = F_{in}^{step} \tag{6.4}$$

2. When the inflow remained steady for more than 12 h, increase F_{in}^{step} using:

$$F_{in}^{step}(i+1) = F_{in}^{step}(i)\cdot(1+r) \tag{6.5}$$

3. Repetition of steps 1 and 2.

This procedure required a value for the parameter *r* that defined the rate of F_{in}^{step} rise. This parameter was optimized with several start-up simulations (1000 hours) at different *r*-values between 0.05 and 1. Initial concentrations for the state variables were obtained from the steady state reached in the simulation with F_{in} = 3.75 L d^{-1}. Three factors were considered to compare the simulations at different *r*-values. The first factor was the percentage of the total time (t_{out}) in which the N_{sum} was above N_{max} (10 mg N L^{-1}). The second factor was the maximum N_{sum} reached in the effluent of R3, and the third factor was the amount of AOB and NOB in the effluent of R3 ($X_A + X_N$) at the end of the simulation. Figure 6.5 shows the results obtained with respect to the *r*-value. In the simulations with *r* below 0.3, the maximum N_{sum} accomplished always the restriction of $N_{sum} < N_{max}$ and above this value, the N_{sum} increased up to 30 mg N L^{-1}. Consequently, t_{out} was zero only below *r* = 0.3. On the other hand, biomass concentration profile reached a maximum at *r* = 0.3, indicating that the system was under-loaded at lower *r*-values. Therefore, the optimal *r*-value chosen was 0.3, which means a 30 % increase in F_{in}^{step} in each inflow increase.

Figure 6.6 shows the simulation results for the on-off controller with the optimal *r*-value. The inflow of the system was increased from 3.75 to 67.1 L d^{-1} in only 40 days and N_{sum} was always below the fixed N_{max}. In fact, only nitrite was present in the effluent as the ammonium was almost totally consumed (Figure 6.6.A). AOB and NOB grew significantly (Figure 6.6.A). This growth was parallel to the inflow increase (Figure 6.6.B); thus, NLR was being augmented as the nitrification rate of the system was increasing without observing any accumulation problem. Ammonium concentration in R1 increased up to 220 mg N L^{-1} during this simulation. In R2 it was always below 10 mg N L^{-1}. Nitrite accumulation at the end of the simulation in R1 and R2 reached 285 and 300 mg N L^{-1} respectively.

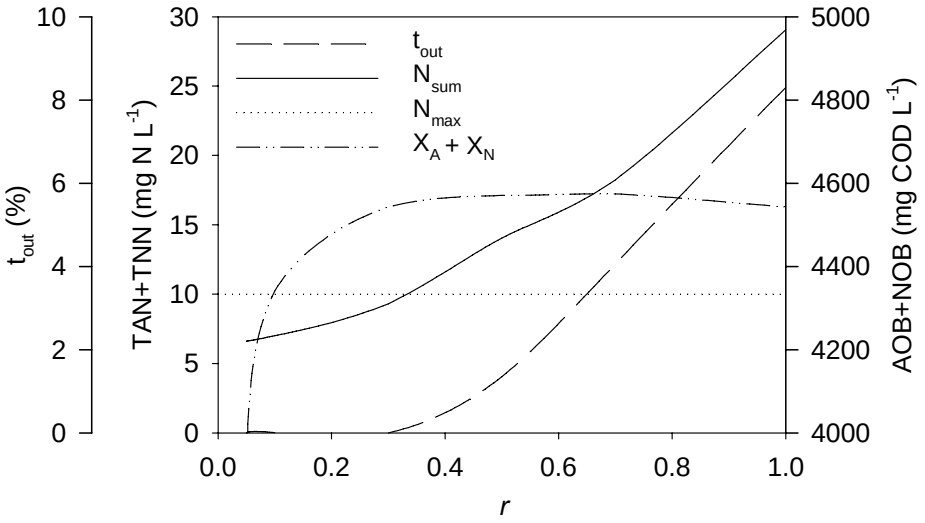

Figure 6.5 On-off control strategy results of several start-up simulations (1000 h) with different r-values: Biomass and TAN+TNN concentrations in R3 and percentage of time out of specifications.

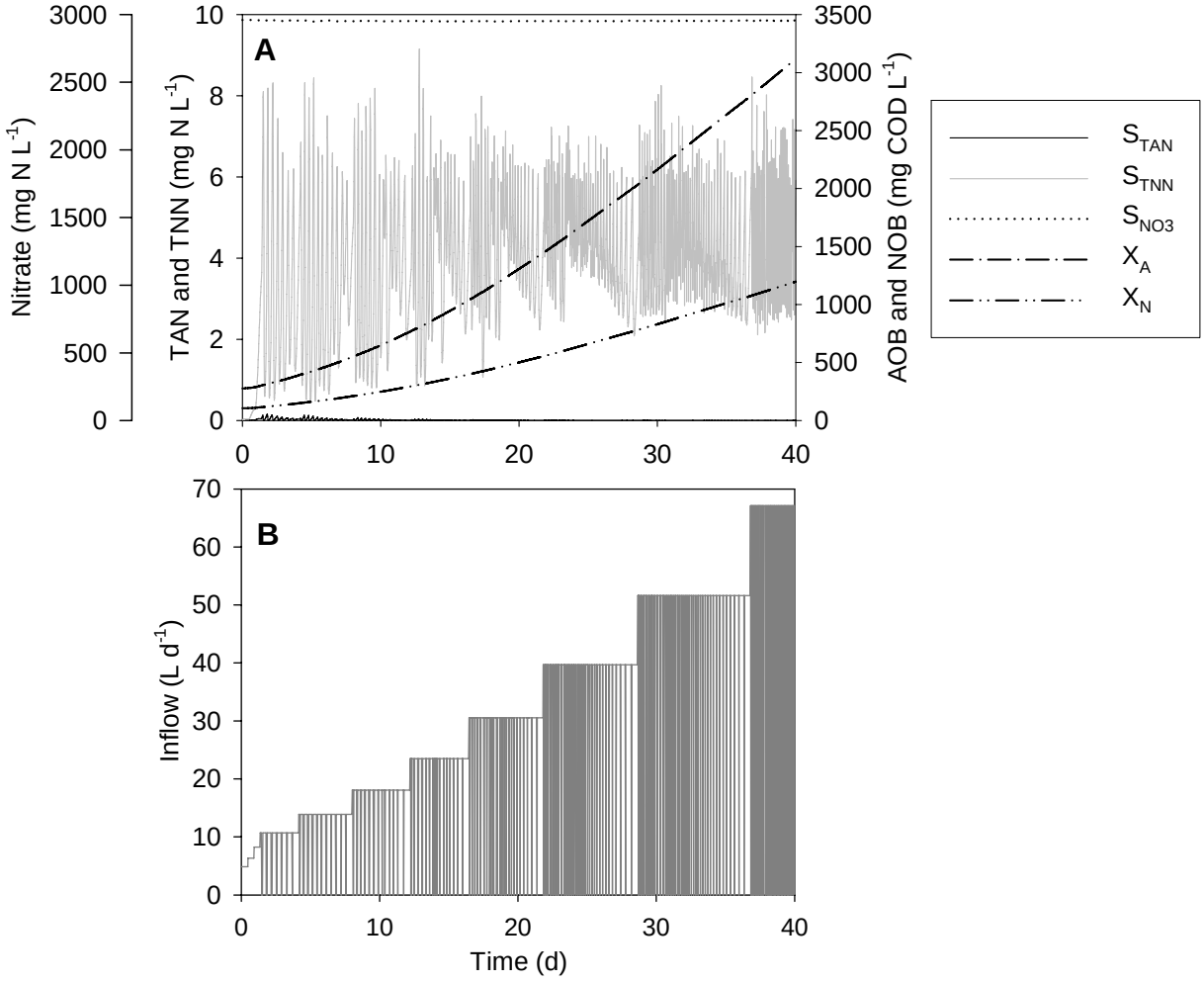

Figure 6.6 On-off control strategy results of 40 days start-up simulation. **A.** Particulate (X) and soluble (S) components in the effluent of R3. **B.** Inflow: each step represents a 30 % increase with respect to the former value.

4.2.3 SECOND CONTROL STRATEGY: PI CONTROLLER

The second control strategy was based on the classical PI controller. It was implemented in the simulator in the velocity form of the corresponding digital algorithm (equation 6.6):

$$C(t) = C_S + Kc\cdot\left[\varepsilon(t) + \frac{1}{\tau_I}\cdot\int_0^t \varepsilon(t)\cdot dt\right] \Rightarrow C_n = C_{n-1} + Kc\cdot\left[\left(\varepsilon_n - \varepsilon_{n-1}\right) + \frac{\Delta t}{\tau_I}\cdot\varepsilon_n\right] \qquad (6.6)$$

where C was the controller output variable (inflow value), C_s was the controller output signal when the error was zero, Kc was the proportional gain, τ_I was the integral time constant, Δt was the control interval time and ε was the deviation (error) of the measured variable (N_{sum}) from the desired set point ($N_{set\ point}$). Velocity form is generally a good algorithm because it does not need initialization (C_s), it is protected against integral "windup" and it preserves the process against computer failure (Stephanopoulos 1984).

The PI controller parameters (Kc and τ_I) were tuned with the ISE criterion (equation 6.7), which is based on the minimization of the integral of the square error (ISE) of the process entire response (Stephanopoulos 1984).

$$\text{ISE} = \int_0^\infty \varepsilon^2(t)\cdot d(t) \quad \text{or} \quad \text{ISE} = \sum_{i=1}^{n} \varepsilon_i^2 \qquad (6.7)$$

Controller parameter values that gave a minimum for this criterion (Kc = 0.5 L d^{-1} (mg N L^{-1})$^{-1}$ and τ_I = 0.25 d) were obtained from the optimization of 100 hours start-up with PI control and with the initial concentrations for the state variables from the steady state of F_{in} = 3.75 L d^{-1}.

Finally, a start-up of 40 days was simulated using this optimized controller. Results are shown in Figure 6.7. Inflow increased from 3.75 to 57.5 L d^{-1} (Figure 6.7.B) and N_{sum} was always below N_{max} and close to $N_{set\ point}$ (Figure 6.7.A). In this control strategy, TAN concentration in the effluent of R3 was also very low. Measured variable, which was almost equal to TNN concentration, swung around $N_{set\ point}$ during the first days but then, the error was lower and the actuation was less oscillatory, showing a typical PI controller response. At the end of the simulation, maximum TAN concentration was reached in R1 (185 mg N L^{-1}) whereas in R2 it never surpassed 4 mg L^{-1}. TNN concentrations at the end of the simulation in R1 and R2 were 288 and 320 mg N L^{-1} respectively.

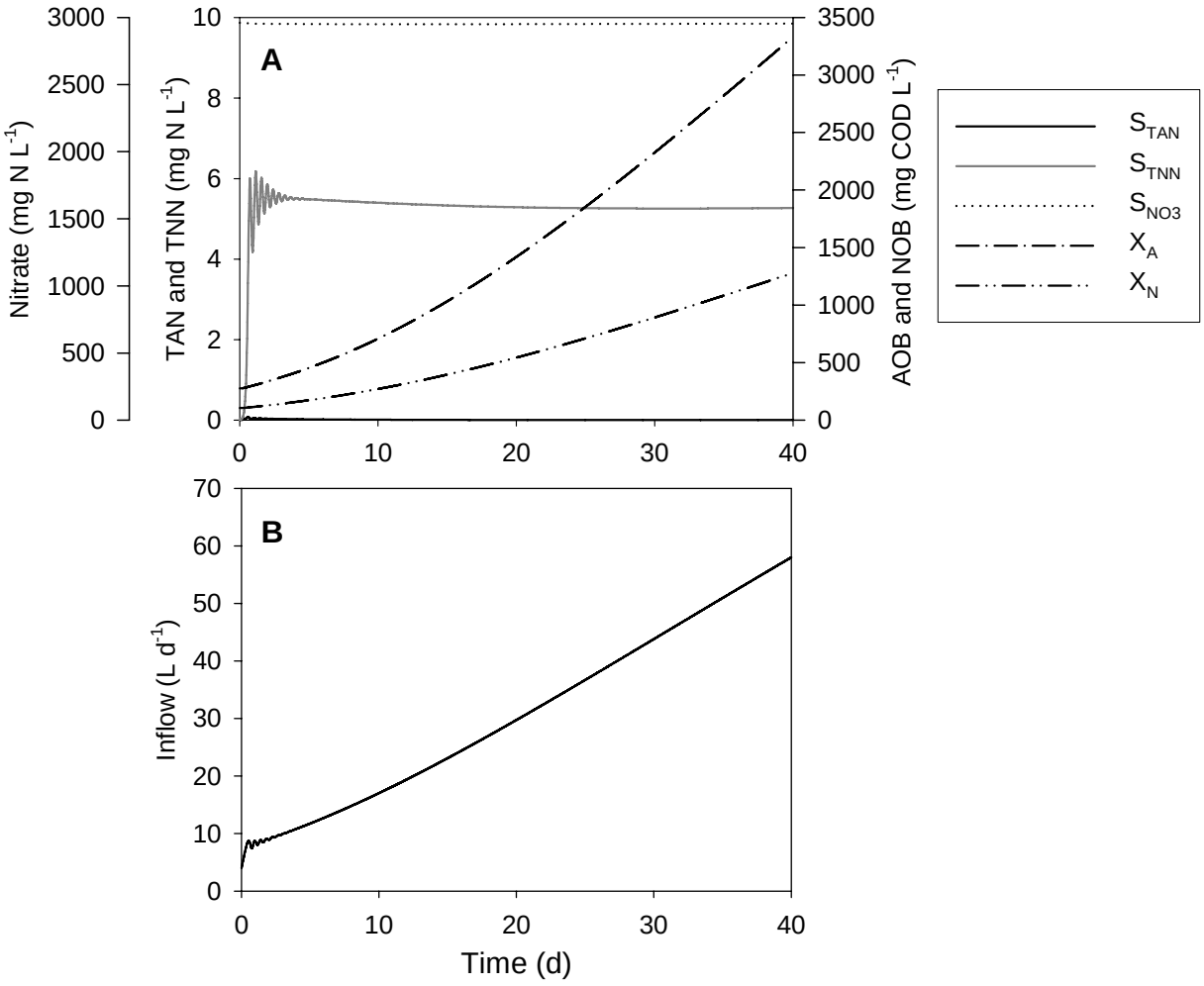

Figure 6.7 PI control strategy results of 40 days start-up simulation (Kc = 0.5 L d^{-1} (mg N L^{-1})$^{-1}$ and τ_I = 0.25 d). **A.** Particulate and soluble components in the effluent of R3. **B.** Inflow.

4.2.4 STRATEGIES COMPARISON

The main difference between both strategies was that the on-off controller caused higher oscillations in the system. However, general trend of nitrogenous compounds, biomass concentrations and inflow were similar. In fact, profiles in Figure 6.7 are similar to the averaged values of Figure 6.6. On the other hand, if final inflow value was considered, on-off controller appeared as the best option, but the inflow in the on-off controller was not steady on day 40th and thus, these values could not be compared. In addition, averaged specific growth rate with respect to the maximum specific growth rate (μ/μ_{max} ratio) was evaluated for each reactor and each control strategy for the whole start-up. These ratios were equal in both strategies for each reactor. $\mu_A/\mu_{max,A}$ (AOB) and $\mu_N/\mu_{max,N}$ (NOB) in R1 were 0.61 and 0.12 respectively. This low nitratation rate was due to NOB inhibition by FA, which reached high concentration. In R2, these averaged rates were $\mu_A/\mu_{max,A}$ = 0.37 and $\mu_N/\mu_{max,N}$ = 0.38 and, in R3 they were 0.006 and 0.50, respectively. In R3, $\mu_A/\mu_{max,A}$ was very low because TAN concentration was almost zero, whereas $\mu_N/\mu_{max,N}$ was the highest observed since no nitration inhibition by FA was present. On the other hand, the sum of X_A and X_N at the end of the

simulations for both control strategies was 4300 and 4600 mg COD l^{-1} respectively. Therefore, the best strategy seemed to be the PI controller since it was less oscillatory and the biomass growth was slightly faster. Nevertheless, both strategies were implemented and tested.

The specific results of this study (e.g. compounds concentrations) were obviously a function of the model, the used model parameters, the operational conditions and the initial conditions. In fact, the fast biomass growth predicted by the simulations could rarely be achieved in an experimental system because of operational and settling problems, which were not considered in the model. However, the proposed start-up strategies could be valid for any system with similar configuration because they were not dependent on these parameters and conditions. The only parameters that could be refit are PI controller parameters (K_C and τ_I), even though the optimized values were quite conservative and could be successfully used with different model parameters (data not shown). In addition, the proposed feedback control could be easily adapted to faster disturbances as for example a change in the wastewater concentration. The only requirement would be to tune again the PI controller, as for example increasing the gain to obtain a faster response.

4.2.5 PILOT PLANT IMPLEMENTATION USING IN-LINE OUR MEASUREMENTS

This theoretical study was based on on-line TAN and TNN analyzers. Although they could be implemented in this system (Baeza et al. 2002a), they usually need a lot of maintenance and can cause operational problems. A similar feedback control loop could be based on in-line OUR, an easier measurement which can be associated to substrate concentration. In order to design the controllers based on in-line OUR measurements, PI controller was optimized again using the ISE criterion (described previously).

OUR_{sp} was set to the OUR given by the biomass at the initial conditions and with 10 mg TNN L^{-1}. As the OUR due to nitritation is always higher than the OUR due to the nitratation step (see stoichiometry of these processes in Chapter 1), this set point assured a very low concentration of ammonium and nitrite. The optimal parameters for PI controller with OUR measurements were: Kc = 0.035 (L d^{-1})(mg O_2 L^{-1} d^{-1})$^{-1}$ and τ_I = 0.142 d. On the other hand, optimized *r*-value of the on-off controller was considered appropriate for using with in-line OUR measurements. The main problem of these strategies is that OUR_{sp} should be increased with time since it is directly related to the nitrifying biomass concentration. In case it is not increased (as in this theoretical study), the start-up is slower. Even though, this is an easy and cheap analysis which can have a high measurement frequency without increasing costs. The high measurement frequency helps to detect external perturbations (this was not considered in the theoretical study). OUR estimation was successfully used in the control of the same pilot plant in a previous work (Baeza et al. 2002b), although control purposes were different.

4.3 EXPERIMENTAL START-UP WITH AUTOMATIC ON-OFF CONTROL (START-UP II)

This section is divided into three parts. Firstly, the experimental results for the start-up with automatic on-off control are presented. Secondly, the model prediction is compared to the experimental data for TAN, TNN, nitrate, OUR and biomass concentration by using experimental initial conditions and experimental inflow profile as input variables in the model. A short-term experiment (one on-off cycle) is also simulated and compared to experimental data. Finally, the on-off controller is also simulated and used for long-term prediction.

4.3.1 EXPERIMENTAL RESULTS

Operational conditions for start-up II are described in Table 6.4. SRT was maintained very high during the first 22 days (with a low purge rate) in order to avoid biomass loss and was then decreased and maintained at 15 days.

Table 6.4 Operational conditions in start-up II.

pH	Temperature	DO	SRT	HRT	F_{IR}	F_{ER}
7.7 ± 0.3	23 ± 2 ºC	3.0 ± 0.8 mg O_2 L^{-1}	15 d	48 - 3 d	330 L d^{-1}	29 L d^{-1}

The pilot plant was inoculated with biomass from the municipal WWTP of Centelles (Barcelona) and immediately fed with similar NLR_s than the one in the full-scale plant but 80 times lower OLR. TAN and COD concentrations in the influent were 2800 mg N L^{-1} and 100 mg COD L^{-1}, respectively in the entire experiment, thus NLR_s was changed by changing only the inflow.

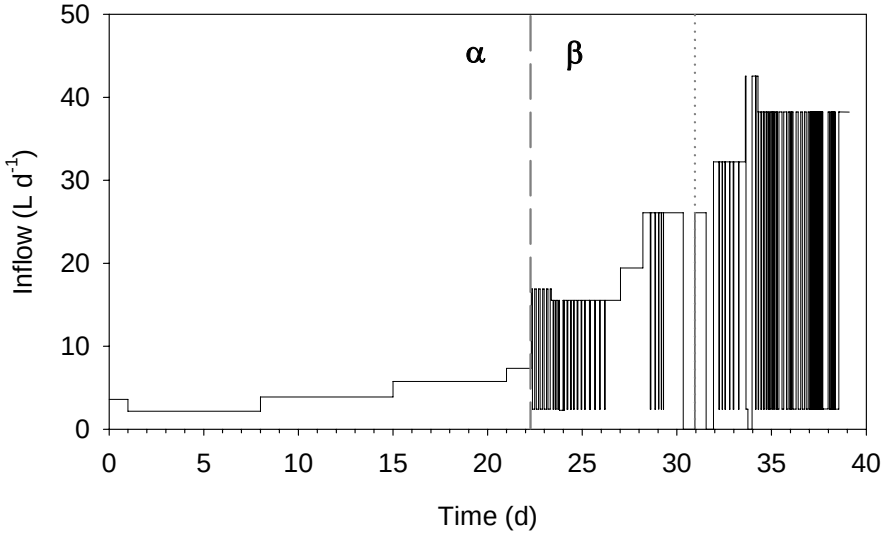

Figure 6.8 Inflow in start-up II. **Period α**: manual inflow increases. **Period β**: automatic inflow control. Dotted line indicates the beginning of automatic inflow increases.

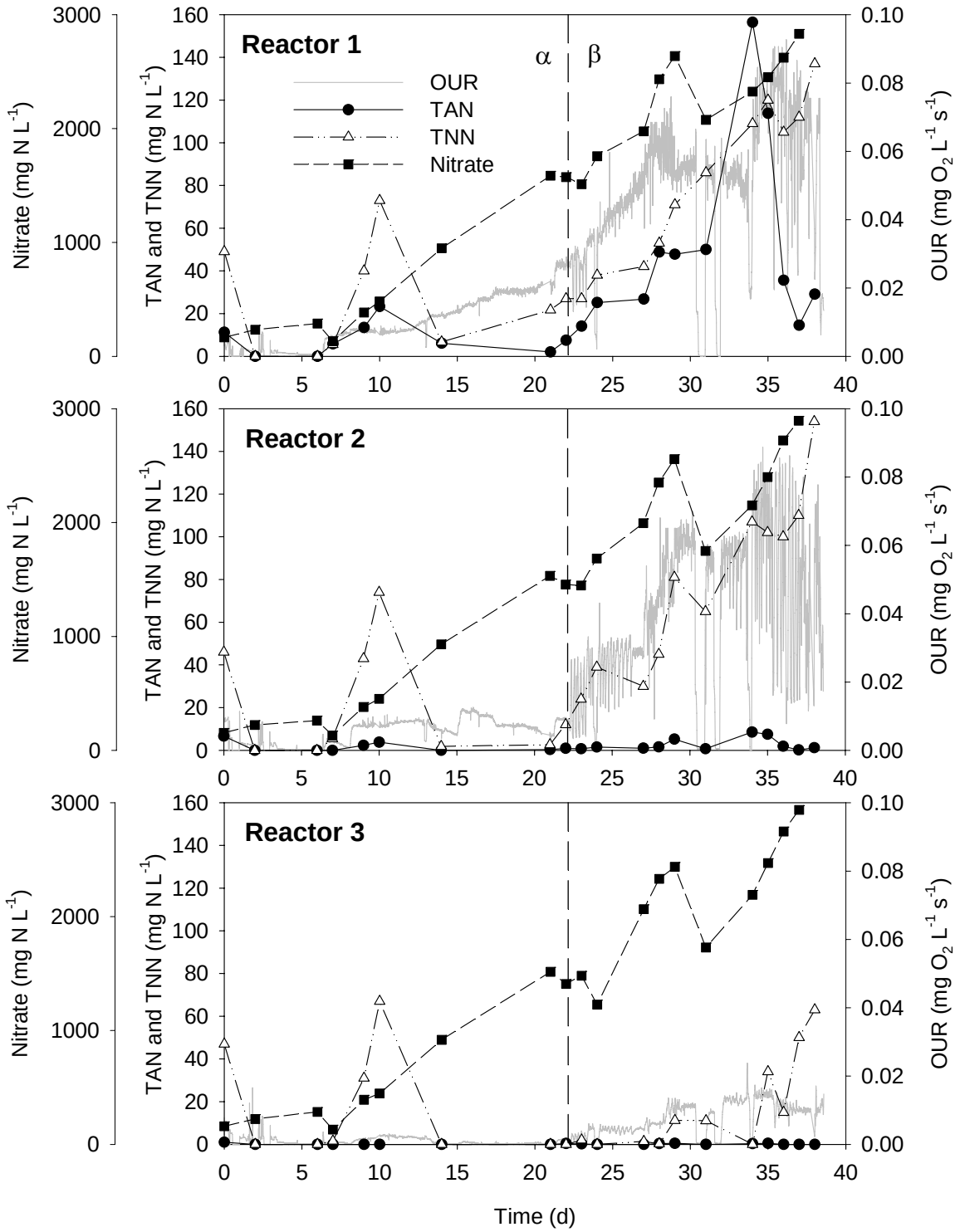

Figure 6.9 Nitrogenous compounds concentrations and OUR profile in each reactor during start-up II. **Period α**: manual inflow increases. **Period β**: automatic inflow control.

Figure 6.8 shows the inflow profile in this start-up experiment divided into two periods with different level of control strategy implementation. During the first 22 days (period α), the inflow control was done manually. At the beginning, the OUR in R3 was mainly due to endogenous decay of heterotrophs which were predominant. Moreover, this value was almost

equal to the maximum OUR due to nitrite consumption. This reason made it impossible to initialize the automatic control until the 22nd day (period β). Firstly, the automatic control was implemented without automatic inflow increases to test the behavior of the pure on-off controller. In practice, the *off position* was not zero but a minimum value (2.4 L d^{-1}) because of experimental restrictions. From day 22 to 31 the inflow was manually increased every time that the *on position* remained unchanged for several hours. On day 31 (indicated with a dotted line), complete on-off control strategy with automatic inflow increases was activated. Figure 6.8 also shows three long stops (inflow = 0 L d^{-1}) which occurred on days 30, 31 and 33 due to experimental problems. The effectiveness of the automatic controller was clearly seen since the inflow was quickly increased reaching values of 40 L d^{-1}. Inflow profile in period β was not so different to the results obtained in the on-off controller simulations (Figure 6.6) where the inflow was 40 L d^{-1} after 20 days of operation.

TNN sporadically accumulated during period α. Figure 6.9 shows the concentration of the nitrogenous compounds and the OUR profile in each reactor during the entire experiment. TAN was totally consumed in R2 unlike TNN which built up in R1 and R2. It was probably due to the slower growing rate of NOB than AOB and the presence of some FA in R1 (from day 22 onward). TNN in R3 (and thus in the effluent of the pilot plant) was higher than the nitrogen concentration allowed (10 mg N L^{-1}). It was a result of the OUR_{sp} tuning that was done during the experiment. In practice, OUR_{sp} value must be in between the endogenous OUR (OUR_{end}) and the maximum OUR due to nitratation (OUR_{NOB}^{max}). Figure 6.10 shows a simulated OUR profile of a TAN pulse in one reactor in batch mode. Under the existing operation conditions, ammonium is firstly depleted and then nitrite is totally consumed. This figure clearly shows that OUR_{sp} must be fixed at a value lower than OUR_{NOB}^{max}, and higher than OUR_{end} to guarantee no TAN and very low TNN in the effluent. In practice, OUR_{sp} was a really low value (≈ 10^{-3} mg O_2 L^{-1} s^{-1}), close to the minimum OUR experimentally determinable.

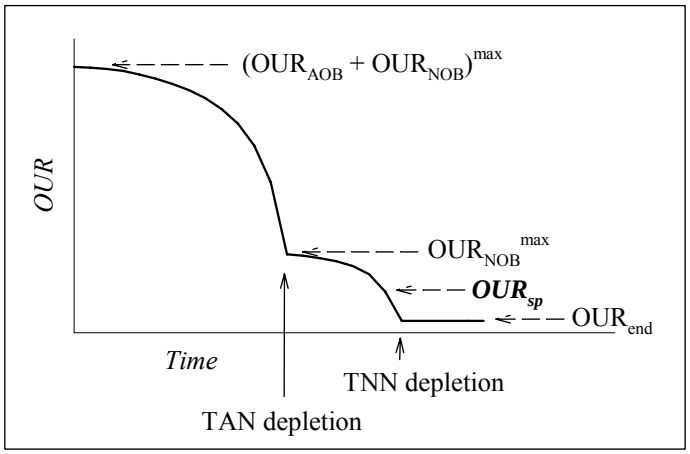

Figure 6.10 OUR profile of a batch ammonium pulse. Optimal OUR_{sp} compared to maximum OUR values when there is ammonium and/or nitrite in the bulk liquid.

OUR_{sp} in the controlled period of the experiment can be seen in Figure 6.11, together with the experimental OUR profile in R3. On day 22, the set point was fixed at a very low value. Later, it was increased because TAN+TNN in the effluent were very low indicating that higher NLR_s could be applied. This new set point was calculated with reference to OUR measurements in R1 and R2 (equation 6.8) which were the maximum values and were increasing at the same time as the NLR_s was being increased as a result of AOB and NOB growth. Since AOB and NOB were growing, also OUR_{sp} had to be increased accordingly to keep the system at the maximum NLR_s. Parameter *k* was being changed from 4, at the beginning, to 6 at the end since TNN in the effluent was accumulating. On day 29, automatic OUR_{sp} determination was activated to change this set point every 10 minutes using averaged OUR values in R1 and R2 from the last 30 minutes (only from day 34 to 36 it was disabled due to operational problems). This modification allowed automatic tuning of the OUR_{sp} but worsened the system performance (TNN buid-up in R3) since the chosen *k* value was too low.

$$\text{OUR set point} = \frac{\max(\text{averaged OUR}_{R1}; \text{averaged OUR}_{R2})}{k} \tag{6.8}$$

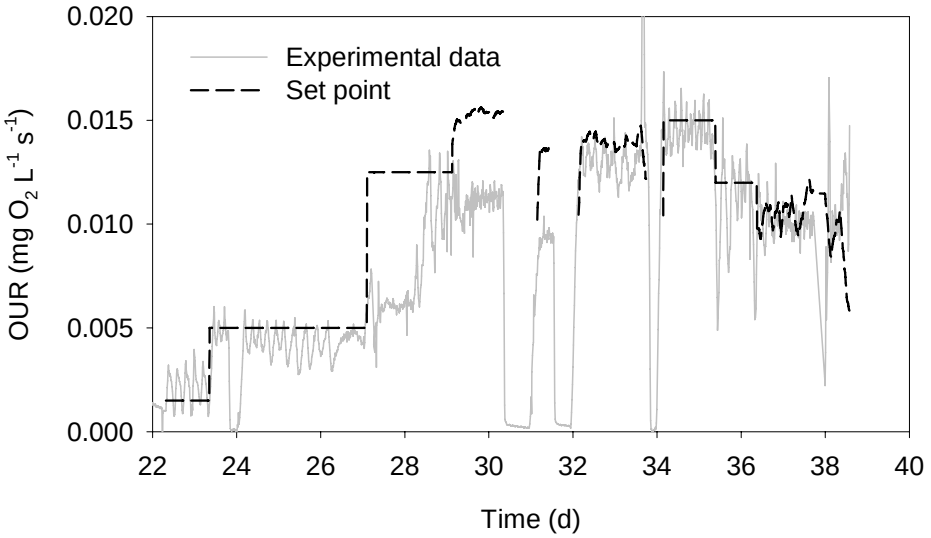

Figure 6.11 OUR profile and OUR_{sp} in R3 during period β (automatic inflow control) of start-up II.

Figure 6.12 shows the evolution of VSS concentration, SVI and NLR_s along the experiment. Biomass concentration decreased until the automatic inflow control was activated. At the end of the experiment the biomass concentration was around 1800 mg VSS L^{-1} and the VSS/TSS ratio was 0.62. SVI decreased indicating the improvement of the settling characteristics of the sludge but the TSS in the effluent increased from 50 to 150 (data not shown) probably due to the more disperse growth. NLR_s was calculated with averaged values (last 6 hours) of the inflow to soften the fluctuating behavior. It can clearly be observed that NLR_s was quickly increased when the automatic control was activated. It reached values of 0.8 g N g^{-1} VSS d^{-1}

when the OUR_{sp} was the highest and stabilized around 0.4 g N g^{-1} VSS d^{-1} at the end of the experiment.

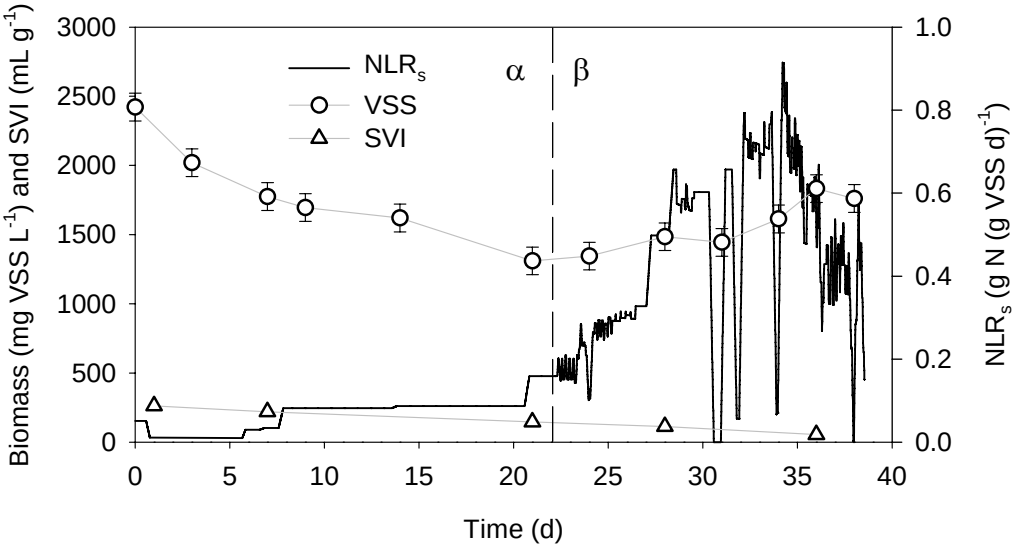

Figure 6.12 VSS, SVI and averaged NLR_s during start-up II (period α: manual inflow increases; period β: automatic inflow control).

4.3.2 DESCRIPTION OF THE START-UP EXPERIMENTAL RESULTS WITH SIMULATION TOOLS

The complete model, described in Chapters 3 and 4 was used to describe the start-up experimental results. This model included all processes related to AOB, NOB and heterotrophs to be able to simulate the total biomass concentration. Heterotrophs had to be considered because it has been shown that enriched nitrifying systems have a relatively high content of heterotrophic bacteria (Vadivelu et al. 2006; Wyffels et al. 2004) and furthermore, the influent of the real system contained some COD.

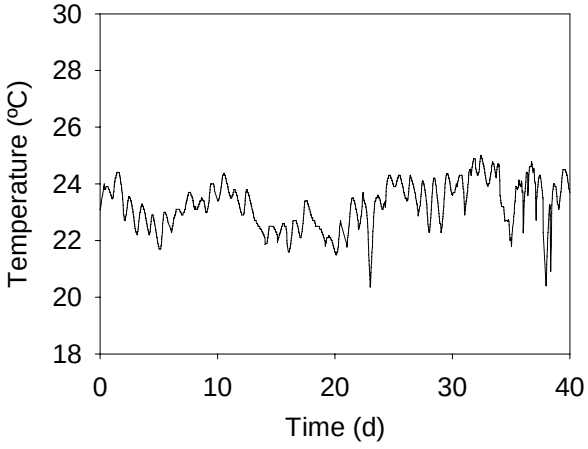

Figure 6.13 Temperature profile in start-up II.

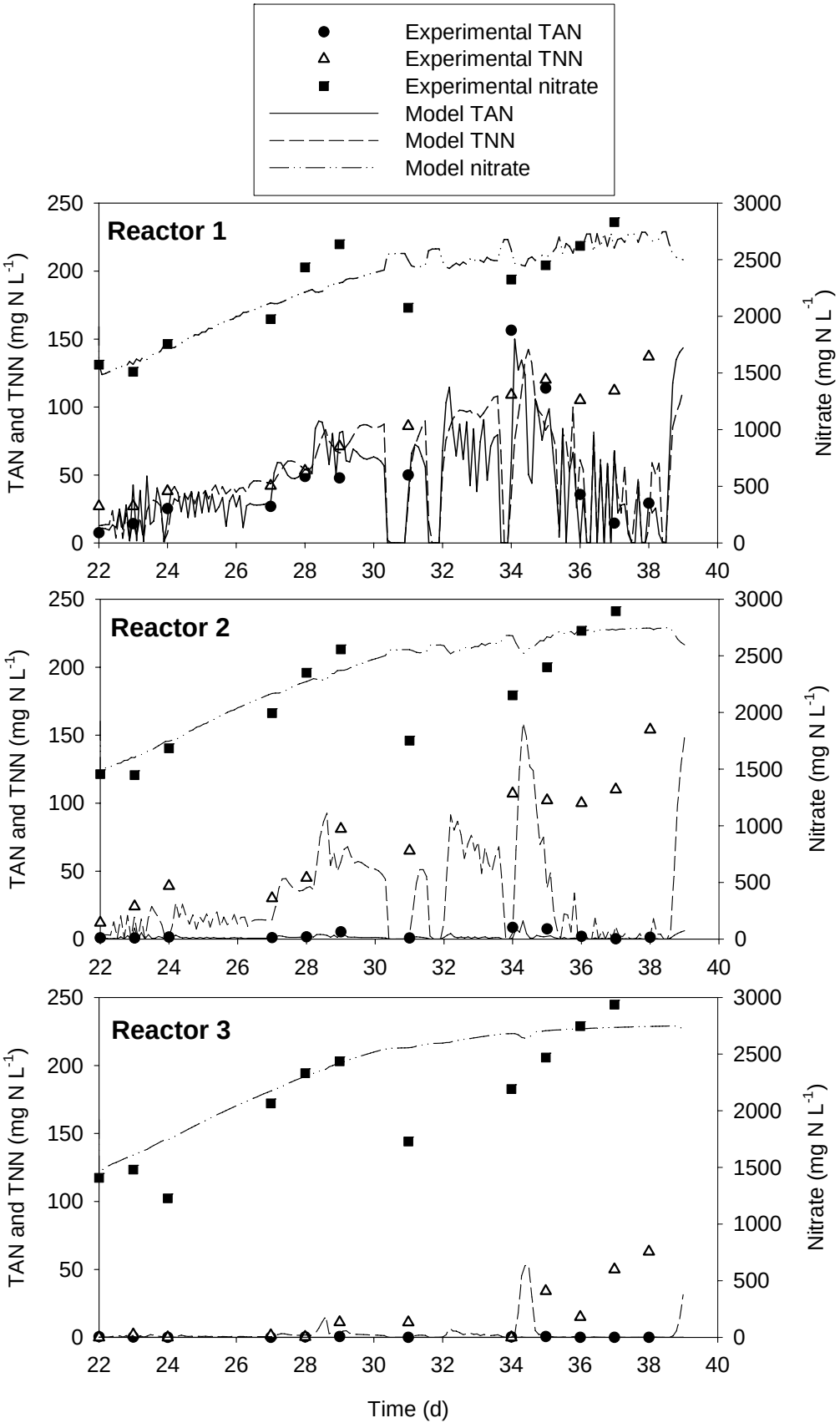

Figure 6.14 Nitrogenous compounds concentrations in each reactor during period β (automatic inflow control) of start-up II.

Temperature profile (Figure 6.13) was introduced in the simulations in order to calculate the temperature-dependent parameters every instant (like maximum specific growth rates, decay rates, inhibition coefficients, etc). Experimental pH and DO were controlled or were stable in each reactor and thus, considered constant and equal the experimental values.

Initial concentrations of particulate compounds were set to 1 % of AOB (X_A), 0.44 % of NOB (X_N) (estimated from X_A and the Y_N/Y_A ratio) and 10 % of particulate inert products (X_P). The rest of VSS were considered heterotrophs (X_H).

In this section, inflow profile was an input variable for the model and thus, the control loop was not simulated. The model prediction of TNN, TAN and nitrate for the same inflow pattern than in the experiment is studied here.

The 40-day start-up was simulated but only the controlled period was considered in order to be compare with experimental data because it is the period of interest. Two parameters had to be modified with the aim to get the best fit to the experimental data. Heterotrophic decay rate was decreased to half the default value to get a better estimation of biomass concentration. Moreover, NOB inhibition coefficient for FA was also modified. The best value for this parameter resulted to be 1.3 mg FA L^{-1}, a lower value than the one obtained with batch experiments with another non acclimated sludge ($K_{I,FA,N}$ = 9.5 mg FA L^{-1}, see Chapter 3). This modification was needed to predict the TNN accumulation in R1 which was shown in the experiment (see Figure 6.14). Model prediction for TAN and nitrate agreed better with experimental data than TNN did. The differences between the experimental data for TNN and model predictions could be due to some NOB inhibition that was not predicted by this model.

OUR calculated by simulation agreed well with OUR experimental data during the first 8 days of the controlled period and quite well the rest of the experiment (Figure 6.15). The main differences were found from day 29 onward, when simulations predicted higher OUR values in R1 than the experimental values.

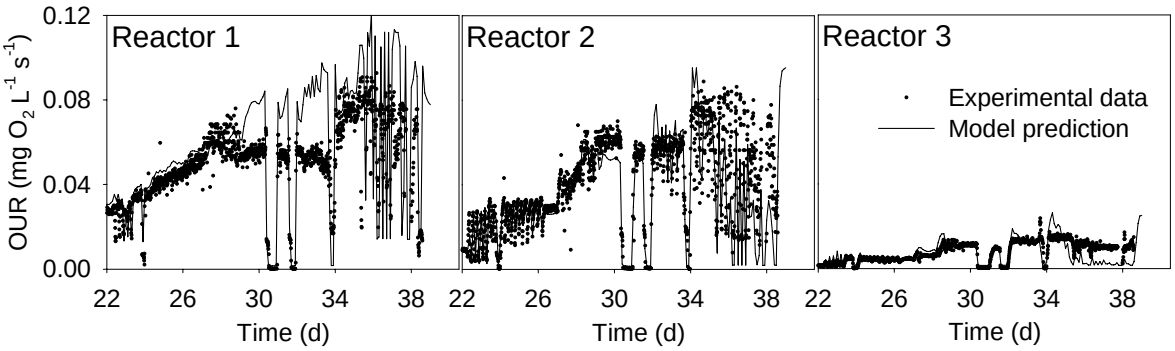

Figure 6.15 OUR experimental data and model prediction in each reactor during period β (automatic inflow control) of start-up II.

Figure 6.16 shows the experimental data and the model prediction for total biomass concentration in the same period. The simulations described correctly the general trend of the total biomass concentration. Figure 6.16 also shows AOB, NOB and heterotrophic biomass concentration profiles predicted by the simulation. While heterotrophic biomass concentration was decreasing, AOB and NOB were growing and thus, the sludge was being enriched in nitrifying bacteria.

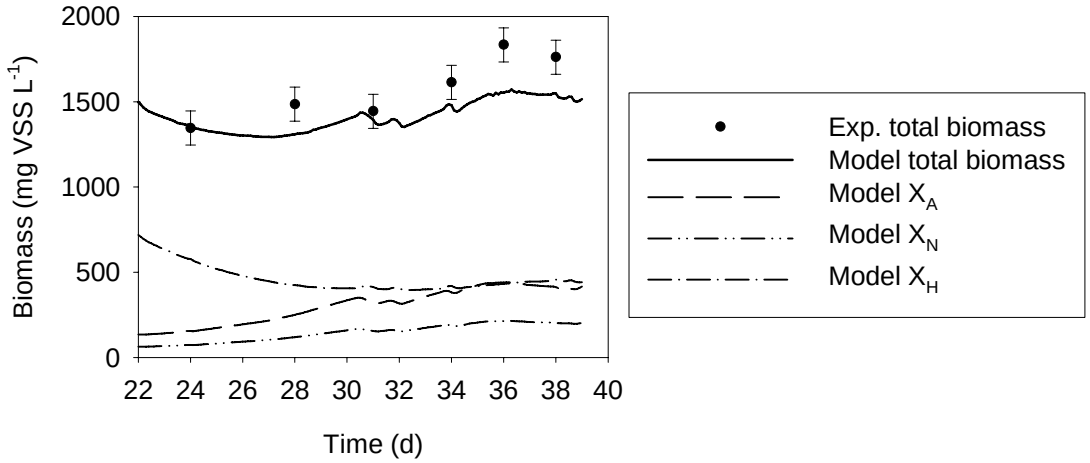

Figure 6.16 Total biomass, X_A, X_N and X_H during period β (automatic inflow control) of start-up II.

4.3.2.1 Simulation of one on-off cycle

On day 35, an on-off cycle was analyzed with the aim to study the TAN, TNN and OUR fluctuations in one cycle and to test the model suitability for short-term prediction. Samples from each reactor were taken regularly from the minute when the inflow was stopped since it was stopped again. This cycle was also simulated using the same model and model parameters as in the previous section. Initial values for particulate compounds and for COD soluble compounds were taken from day 35 in the simulation of the whole experiment. Initial values for TAN, TNN and nitrate were fixed at the measured values. Figure 6.17 shows these results and how the model predicted quite accurately the experimental data.

Results of the 40-day start-up simulation together with the results of the on-off cycle simulation indicate that this model can be successfully used both to describe long experiments (days) and to predict short-term behavior (hours).

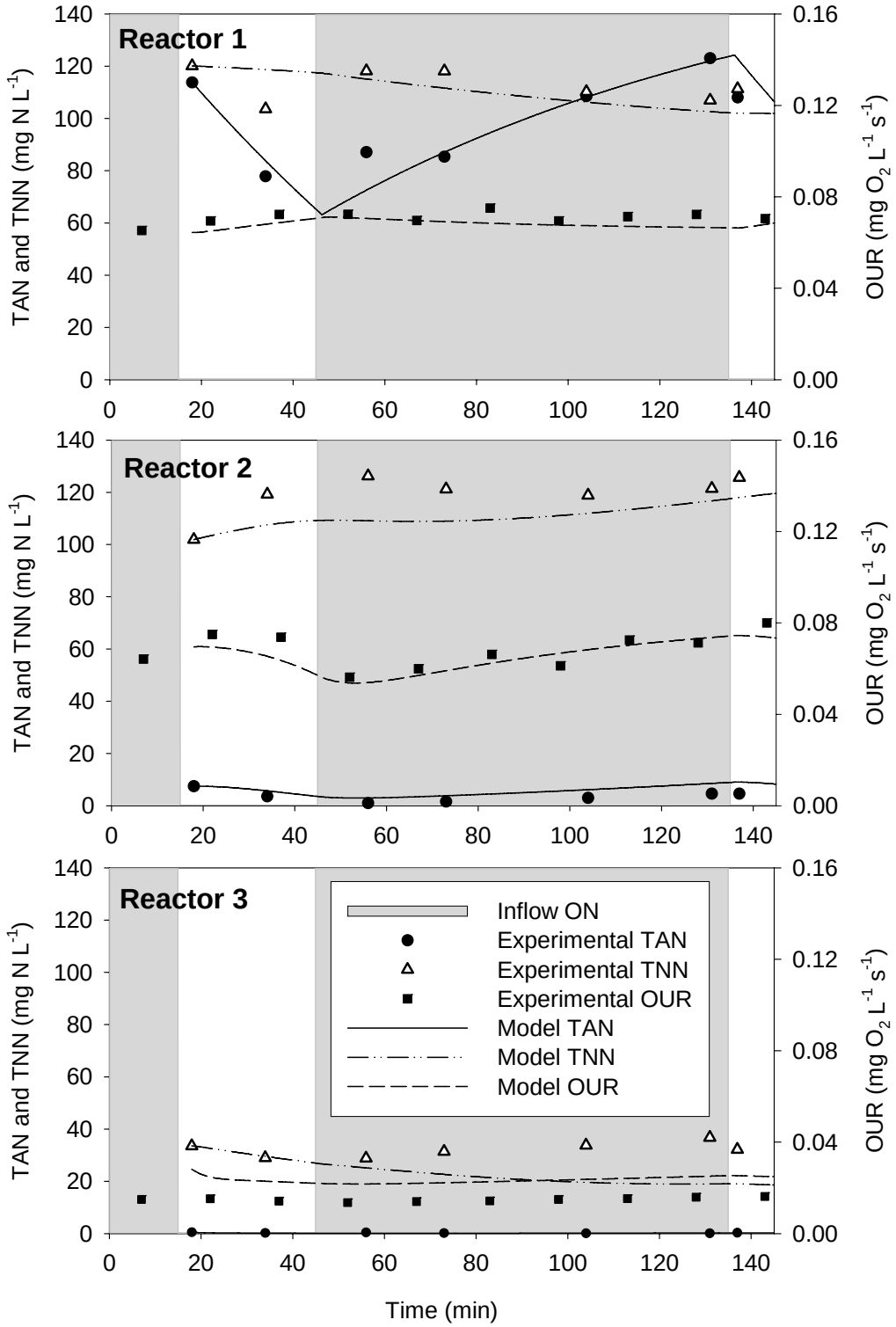

Figure 6.17 TAN, TNN and OUR in one on-off cycle (day 35) in start-up II: experimental data and model prediction.

4.3.3 CONTROL LOOP SIMULATION AND LONG-TERM PREDICTION

The experimental start-up was simulated again using the same model but simulating also the inflow control loop. In this case, the inflow was not introduced as an input variable in the controlled period (β) because it was calculated by the model. The simulated inflow control loop

was similar to the experimental one (see Figure 6.1). In the simulations, OUR was calculated every 15 minutes, then an averaged value, using the last 30 minutes OUR values, was calculated and finally, the new inflow value was determined. The control action was implemented every 30 minutes. The experimental OUR_{sp} profile was introduced in order to faithfully reproduce the experimental conditions.

This simulation was extended beyond the experimental time to predict the behavior of the system in the long term. During this extra time, the OUR_{sp} was determined with equation 6.8 and $k = 6$. Simulations were run until day 80 under these conditions.

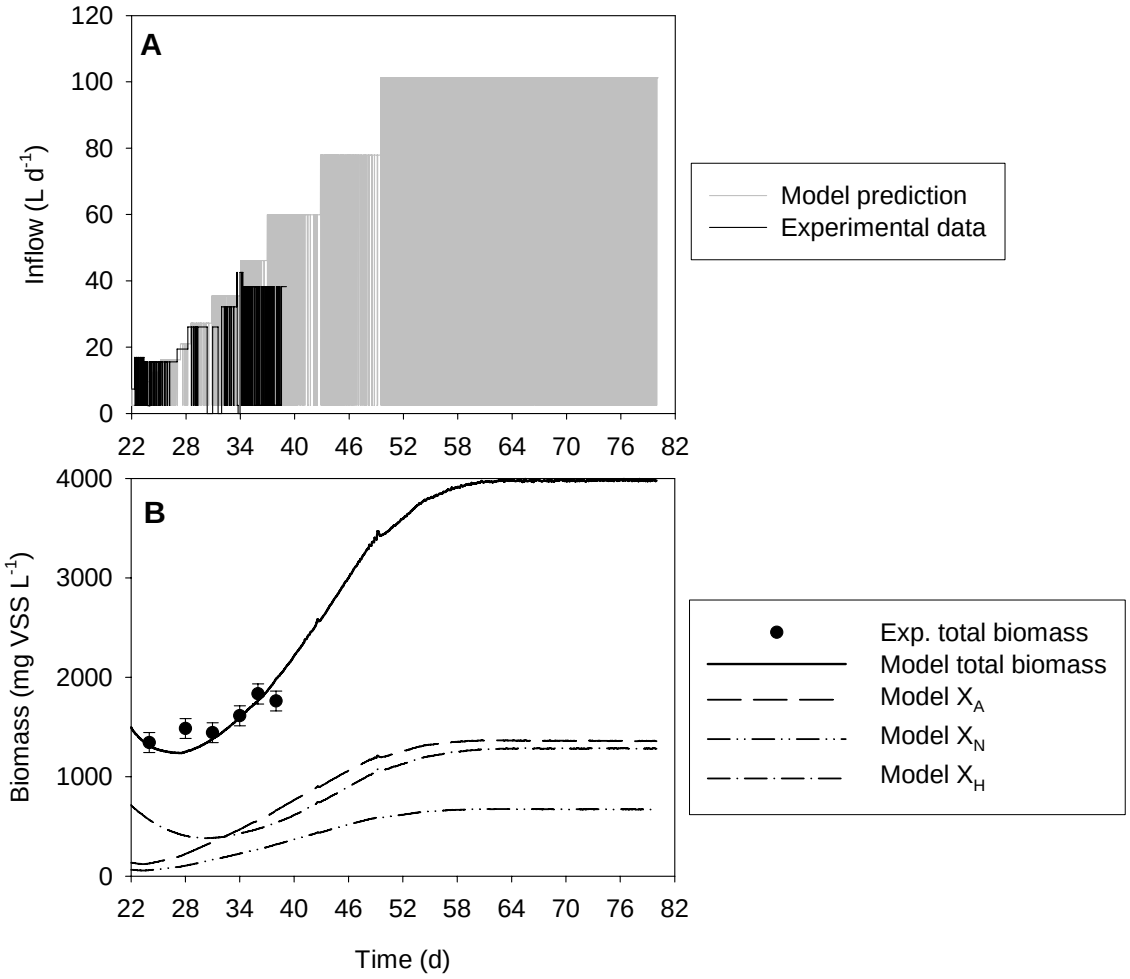

Figure 6.18 Model prediction and experimental data from day 22 to 80 in the start-up simulation with on-off control. **A.** Inflow. **B.** Total biomass, X_A, X_N and X_H.

Figure 6.18 shows the experimental data for the period β and the model prediction for the same period and extended to day 80, for the inflow and the biomass concentration. It is interesting to observe that model prediction agreed well with experimental data. In the long term, the simulation predicted a steady inflow increase until 100 L d^{-1} together with a biomass rise and

stabilization around 4000 mg VSS L^{-1}. Figure 6.18.B also shows AOB, NOB and heterotrophs concentrations predicted by the model. AOB and NOB showed a faster increase than in the previous section (Figure 6.16 in section 4.3.2) in which the experimental inflow was an input variable and thus, the occurred system stops were also simulated. On the contrary, in the present section, the inflow was the result of the simulated control loop and therefore, the stops were not simulated and the inflow increases were more regular. This explains the differences in the AOB, NOB and heterotrophic biomass concentration behaviors. The inflow was not stable on day 80 even though the system was on steady state. With this kind of controller the inflow would always be oscillatory. NLR_s on day 80 can be calculated as 0.823 g N g^{-1} VSS d^{-1} if an averaged inflow (85.6 L d^{-1}) is considered. This steady state indicates the maximum NLR_s which could be reached with this configuration and these operational conditions (T, pH, DO, SRT) if no operational problems occurred.

TAN, TNN, nitrate and OUR in each reactor are shown in Figure 6.19. Model predicted that TAN was totally consumed in R2 while TNN needed three reactors to be depleted. OUR was maximum in R1 but lower in R2 and R3 due to lower TAN and TNN concentrations.

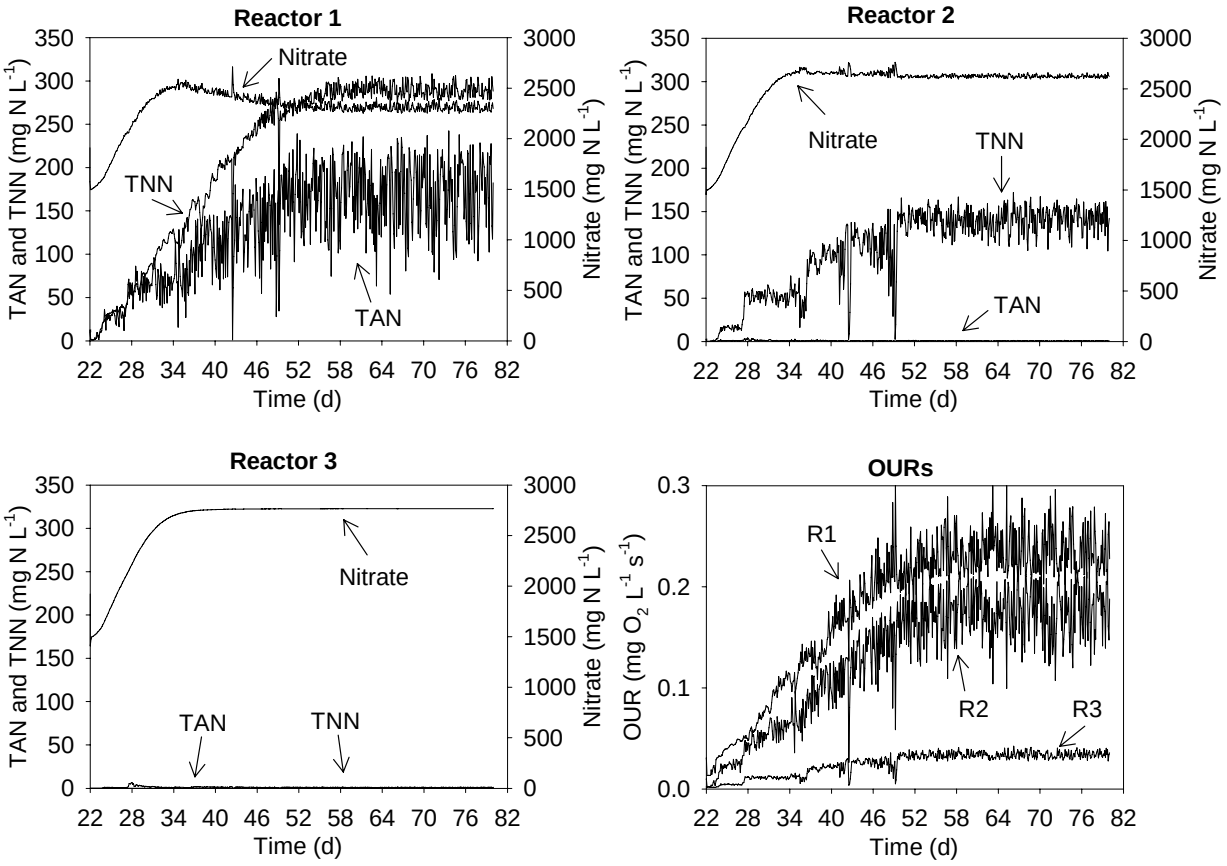

Figure 6.19 TAN, TNN, nitrate and OUR prediction in each reactor from day 22 to 80 in the start-up simulation with on-off control.

4.4 EXPERIMENTAL START-UP WITH AUTOMATIC PI CONTROL (START-UP III)

This section has a similar structure than section 4.3. Firstly, the experimental results for the start-up with automatic PI control are presented. Secondly, the model prediction is compared to the experimental data for TAN, TNN, nitrate, OUR, total biomass concentration and specific bacteria fractions by using experimental initial conditions and experimental inflow profile as input variables in the model. Finally, the PI controller is introduced in the simulator, the control strategy is simulated again and results are compared to the experimental data. The last simulation is used for long-term prediction.

4.4.1 EXPERIMENTAL RESULTS

The pilot plant was inoculated for the third time with sludge from the WWTP of Manresa (Barcelona). Operational conditions for start-up III are described in Table 6.5. Again, SRT was high at the beginning and was decreased to around 15 d on day 34.

Table 6.5 Operational conditions in start-up III.

pH	Temperature (ºC)	DO (mg O_2 L^{-1})	SRT (d)	HRT (d)	F_{IR} (L d^{-1})	F_{ER} (L d^{-1})
7.6 ± 0.3	R1: 22 ± 2 R2: 27 ± 4 R3: 25 ± 3	3.0 ± 1	15	40 - 5	346	22

TAN and COD concentrations in the influent were 2800 mg N L^{-1} and 100 mg COD L^{-1}, respectively. COD concentration was changed to 300 mg COD L^{-1} on day 42 in order to improve the settling characteristics of the sludge (Çeçen and Orak 1996; Gupta and Sharma 1996).

At the beginning, the pilot plant was fed with a NLR_s of 0.05 g N g^{-1} VSS L^{-1} (the same NLR_s than in the full-scale WWTP) and a very low OLR (0.002 g COD g^{-1} VSS $d)^{-1}$). After a week of operation, inflow was stopped for 7 days to perform batch experiments with this non-acclimated sludge. Later, inflow was changed manually until day 42, when automatic inflow control was activated (see Figure 6.20.A). Controller parameters optimized in the model-based start-up simulation were initially used (Kc = 0.035 (L d^{-1}) (mg O_2 L^{-1} $d^{-1})^{-1}$ and τ_I = 0.142 d) but it was soon detected that Kc was too high. So, it was decreased to 0.002 (L d^{-1})(mg O_2 L^{-1} $d^{-1})^{-1}$.

As Figure 6.20.B shows, temperature was very low at the beginning (winter time) and soon the heater system in R2 was activated. The lack of temperature control in R1 and R3 was the responsible for the different temperatures among reactors. Temperature set point in the controlled reactor was slowly increased up to 32 ºC to avoid temperatures below 20 ºC in the

whole system. These low temperatures, together with the fact that the inoculated sludge could contain low amount of nitrifying bacteria, provoked that the automatic inflow control could only be activated after 35 days of low NLR_s operation (day 42 if the 7 days of batch experiments are included) compared to the 22 days in start-up II.

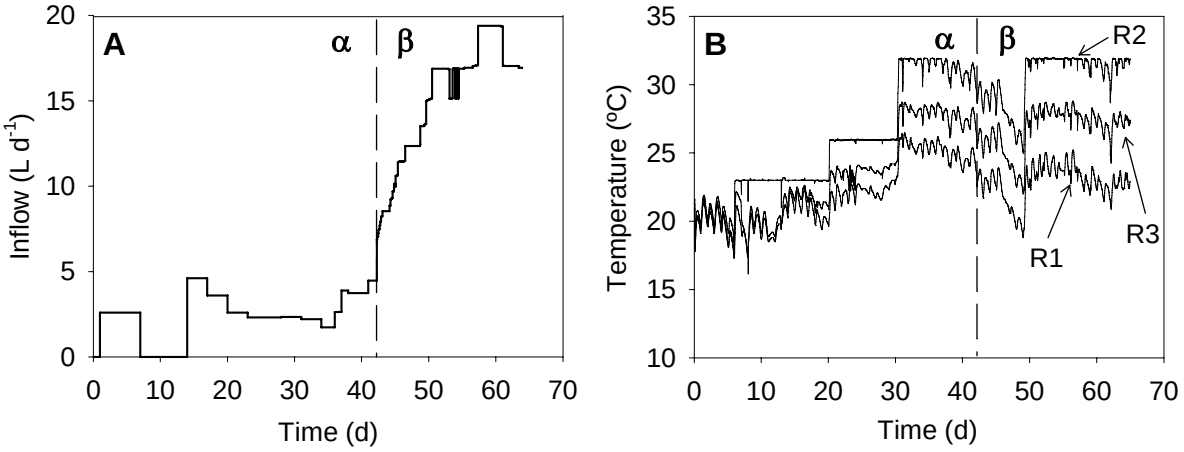

Figure 6.20 Start-up III. **A.** Inflow profile **B.** Temperature in each reactor. (**Period α**: manual inflow increases. **Period β**: automatic inflow control).

Figure 6.21 shows the results obtained in start up III with respect to nitrogenous compounds and OUR. In period α, some TAN and TNN accumulated because the applied NLR_s was higher than the nitrifying capacity of the system. It did not happen again when the inflow control was activated. In period β, TAN and TNN concentrations behaved similarly than in start-up II. TAN was totally depleted in R2 and TNN built up in R1 and R2 but it was almost entirely consumed in R3. In order to avoid high TNN concentrations in the effluent, the OUR_{sp} fixed on day 42 ($1.4 \cdot 10^{-3}$ mg O_2 L^{-1} s^{-1}) was used until the end. In this experiment, low TNN was preferred to variable OUR_{sp}, which could had sped up the start-up but it could also had caused TNN accumulation in R3. OUR profiles shown in Figure 6.21 are similar to the ones in Figure 6.9 except for the oscillatory behavior of the on-off controller.

Biomass also decreased in the first period (α) and increased again when the automatic controller was activated (period β) (see Figure 6.22). Biomass concentration was 1300 mg VSS L^{-1} at the end of period β and the VSS/TSS ratio was around 0.70 in the whole experiment. Biomass settling characteristics changed with time: SVI decreased from 86 to 37 mL g^{-1} but TSS in the effluent of the settler increased from 40 to 200 mg TSS L^{-1} indicating disperse growth.

Figure 6.22 also shows the NLR_s profile. The fast NLR_s increase during the first days of the automatically controlled period indicated that the controller forced the system to work at its maximum capacity. After these days, the NLR_s continued to increase but with a slower rate. Since this value was calculated with respect to the biomass concentration, this moderate NLR_s raise indicated that the sludge was being enriched with nitrifying bacteria at the same time as

the total biomass concentration was increasing. The maximum nitrification capacity of this system turned out to be around 0.5-0.6 g N g^{-1} VSS d^{-1}

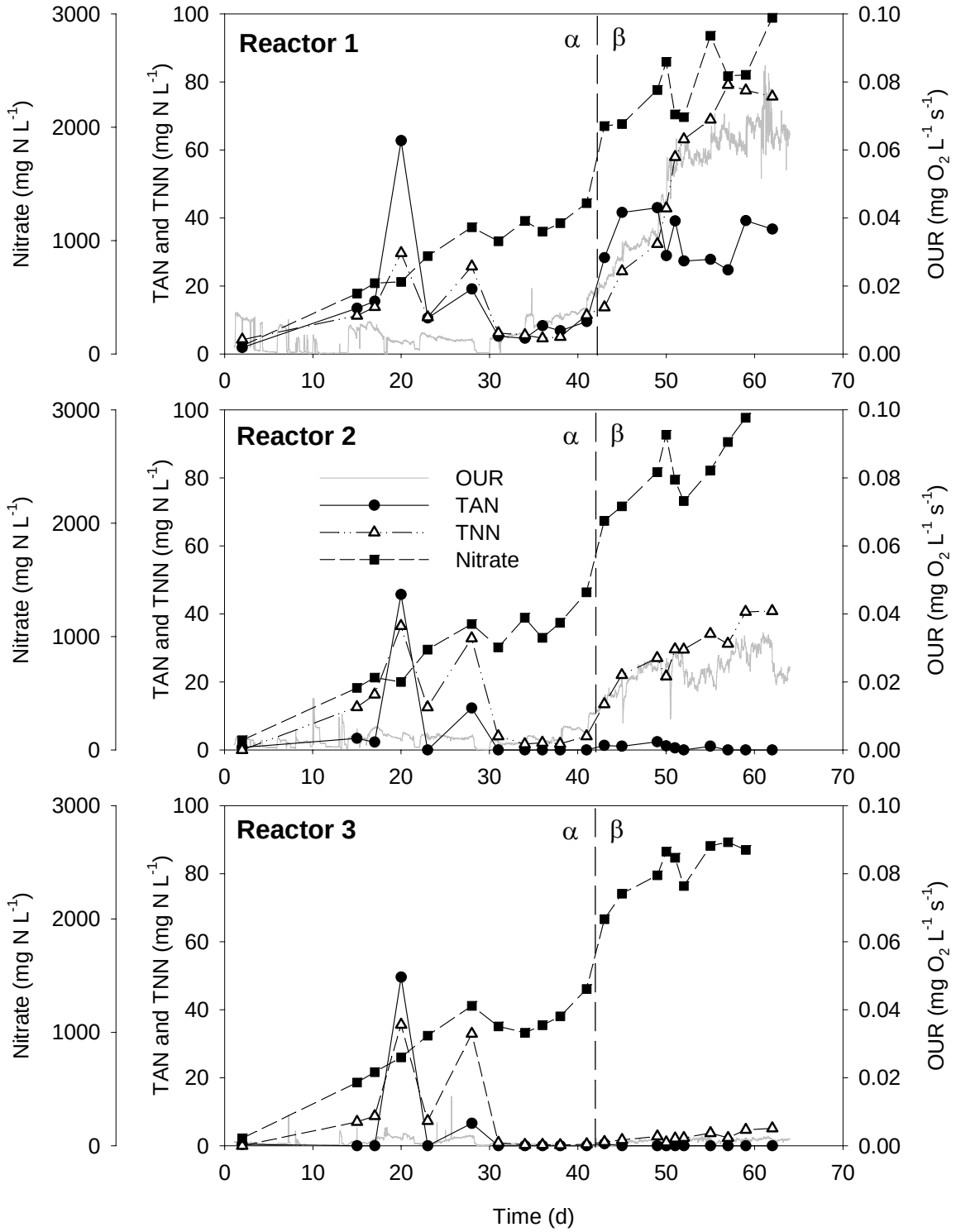

Figure 6.21 Nitrogenous compounds concentrations and OUR profile in each reactor during start-up III (period α: manual inflow increases; period β: automatic inflow control).

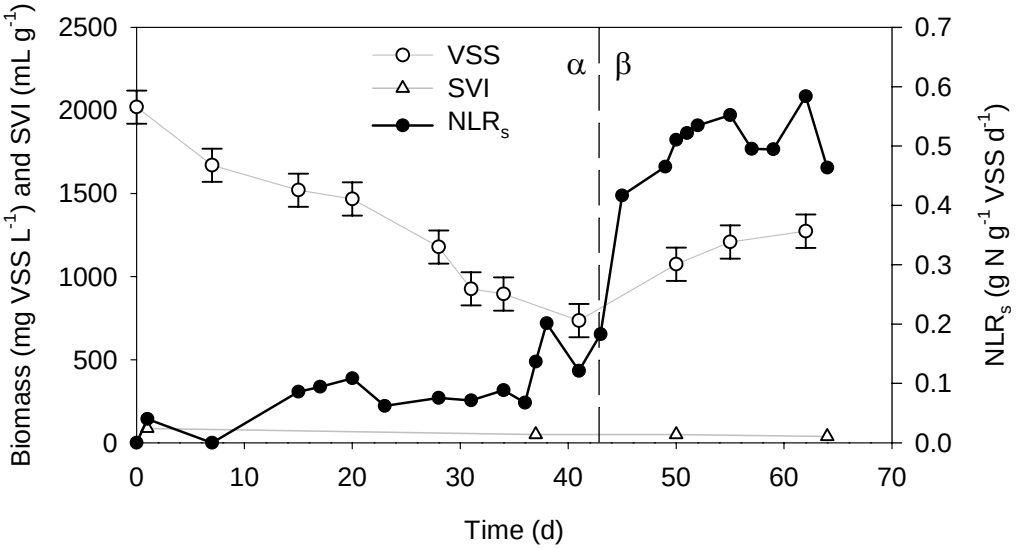

Figure 6.22 Biomass concentration, SVI and NLR_s during start-up III (period α: manual inflow increases; period β: automatic inflow control).

FISH was performed with samples taken on days 0 (beginning of the experiment), 42 (control activation) and 63 (end of the experiment). Results are depicted in Figure 6.23. AOB was detected only with probe Nso190. Negative results were obtained with probes Nso1225, Nsv443, Nsm156 and Nmo218. NOB was detected as *Nitrobacter* since NIT3 hybridized positively and Ntspa662 gave negative results. FISH results clearly indicated that both AOB and NOB populations increased and that AOB were more abundant than NOB. At the beginning of the experiment, AOB and NOB fractions were lower than 1 %, which demonstrates the difficulty of starting up a nitrifying system with activated sludge from municipal WWTPs. However, at the end of the experiment AOB and NOB fractions had increased to 21 % and 5 %, respectively. Figure 6.24 shows six representative images corresponding to the three samples analyzed and the two specific probes that gave positive results.

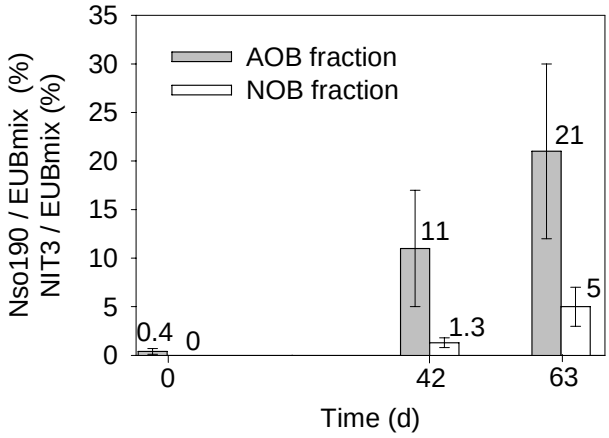

Figure 6.23 AOB and NOB fractions in start-up III.

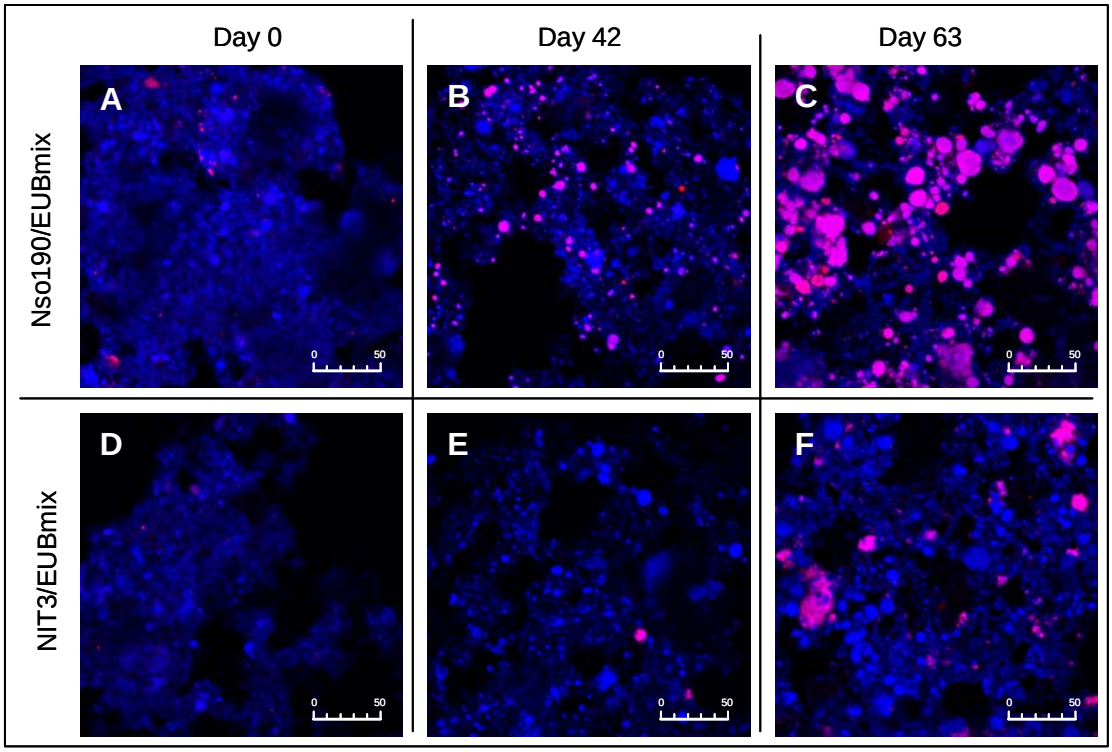

Figure 6.24 FISH/CLSM representative images of the sludge in start-up III. Specific probe is shown in pink and EUBmix probes in blue. Nso190 and EUBmix on day 0 (**A**), on day 42 (**B**) and on day 63 (**C**). NIT3 and EUBmix on day 0 (**D**), on day 42 (**E**) and on day 63 (**F**). Bar = 50 μm.

4.4.2 DESCRIPTION OF THE START-UP EXPERIMENTAL RESULTS WITH SIMULATION TOOLS

In a parallel way than in start-up II, this experiment was also simulated. Again, two parameters had to be modified to have a better description of the experimental data. Heterotrophic decay rate was reduced to half the default value and the NOB inhibition coefficient for FA was changed to $K_{I,FA,N}$ = 0.4 mg FA L^{-1} (default value: $K_{I,FA,N}$ = 9.5 mg FA L^{-1}, see Chapter 3).

The experimental inflow profile and the temperature profiles of each reactor were introduced in the model. Initial conditions for particulate compounds were the same than in the simulation of start-up II (1 % of AOB, Y_N/Y_A % of NOB, 10 % of particulate inert products and the rest heterotrophs). The whole start-up experiment was simulated but only data from day 34 to day 63 (9 days of period α and all period β) are shown here to compare model prediction with experimental data because this is the period of interest due to the inflow rise.

Figure 6.25 shows TAN, TNN and nitrate experimental data and model prediction. All the model concentrations agreed well with the measured concentrations in R1. TAN and nitrate prediction also agreed properly with experimental data in R2 and R3, but TNN concentration

was lower in the simulation than the experimental data. As it happened in start-up II, TNN accumulated in R2 while model predicted lower concentrations.

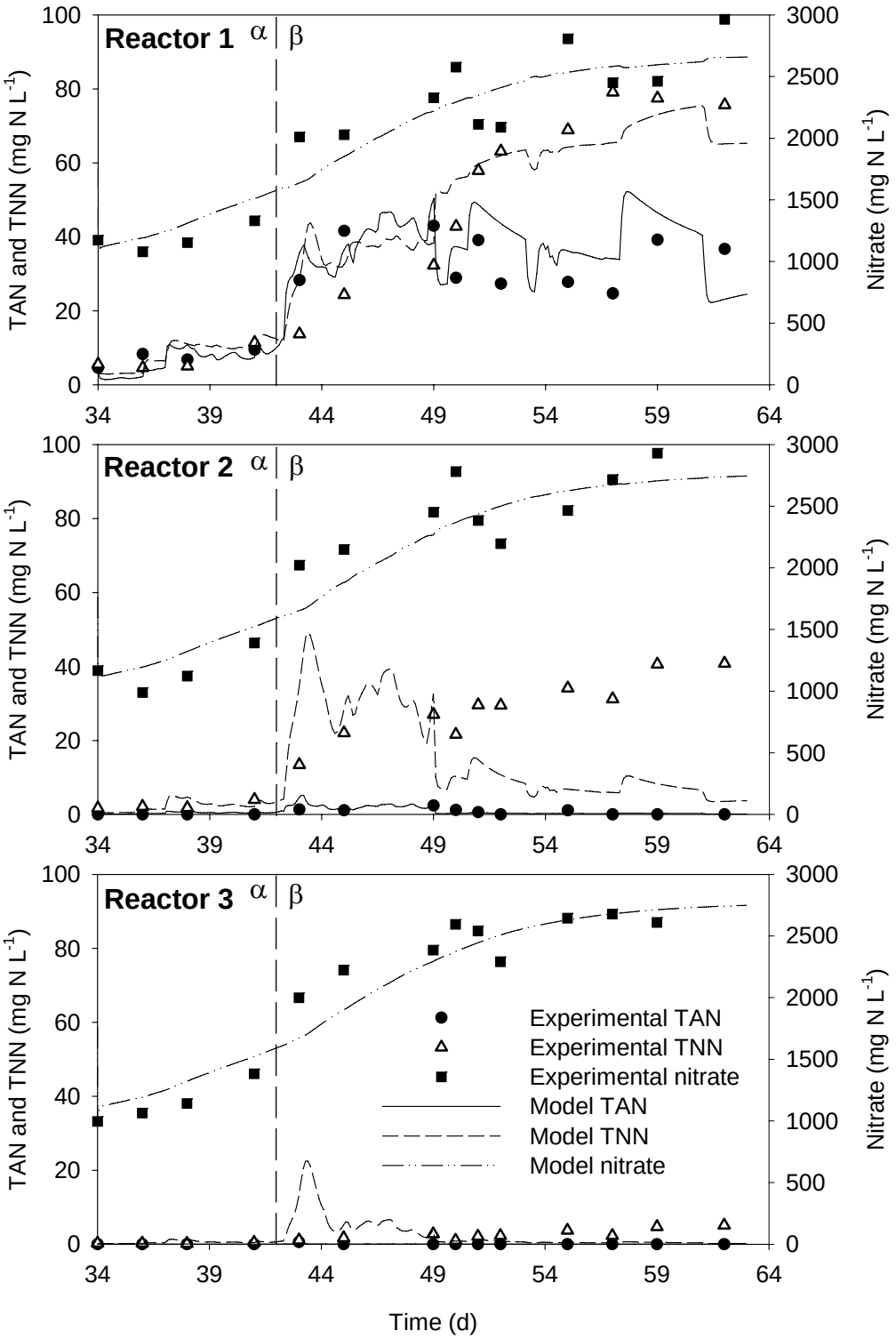

Figure 6.25 Nitrogenous compounds concentrations in each reactor during some days of period α (manual inflow increases) and period β (automatic inflow control) of start-up III.

OUR was also calculated and compared to experimental values. These results are shown in Figure 6.26. Model prediction and experimental results were very similar. The major difference

was in R2 where the model predicted higher values than experimental data although the tendency was similar.

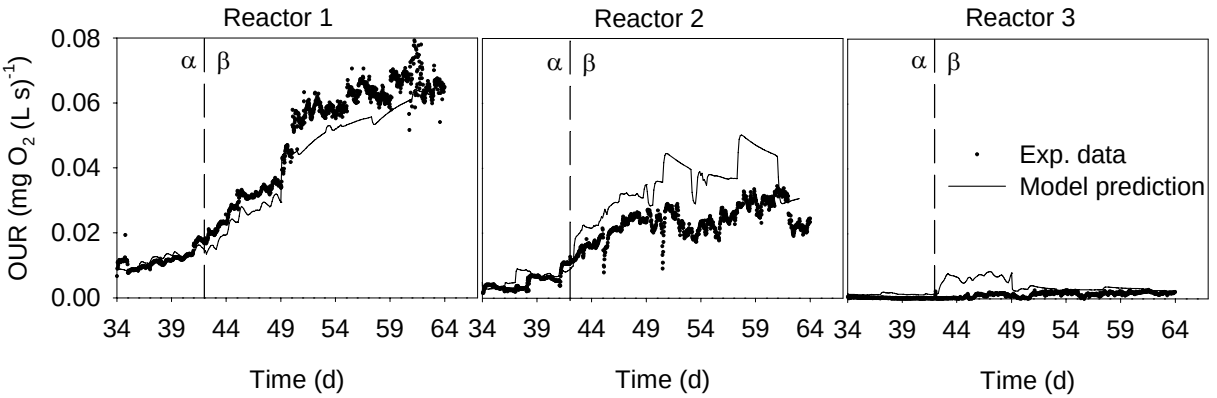

Figure 6.26 OUR experimental data and model prediction in each reactor during some days of period α (manual inflow increases) and period β (automatic inflow control) of start-up III.

Finally, if total biomass concentration is considered (see Figure 6.27.A), the predicted profile was similar to the experimental behavior. Figure 6.27.A also shows predicted AOB, NOB and heterotrophic biomass concentrations. In this case, compared to start-up II, heterotrophs are always more concentrated than AOB or NOB because the COD in the influent was higher in this start-up (300 mg COD L^{-1}) than in start-up II (100 mg COD L^{-1}). Figure 6.27.B shows the experimental AOB and NOB fractions determined with FISH and those predicted by the simulations, which were higher than the experimental ones.

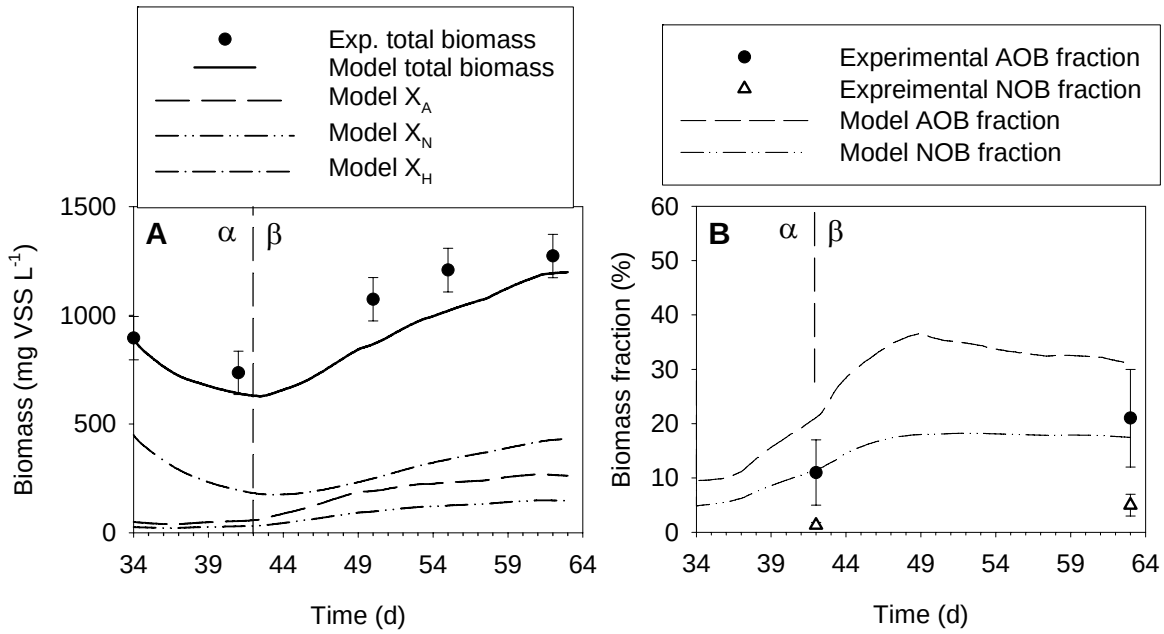

Figure 6.27 Experimental data and model prediction of biomass during some days of period α (manual inflow increases) and period β (automatic inflow control) of start-up III. **A.** Total biomass, X_A, X_N and X_H. **B.** Biomass fractions estimated with FISH and model prediction.

4.4.3 CONTROL LOOP SIMULATION AND LONG-TERM PREDICTION

As performed in section 4.3.3 for start-up II, start-up III was simulated again. Here, the experimental inflow profile was an input variable for the simulation of period α but not for the simulation of the automatically controlled period (β), in which the PI control loop was also simulated. Controller parameters for the simulation were the same as in the experimental system.

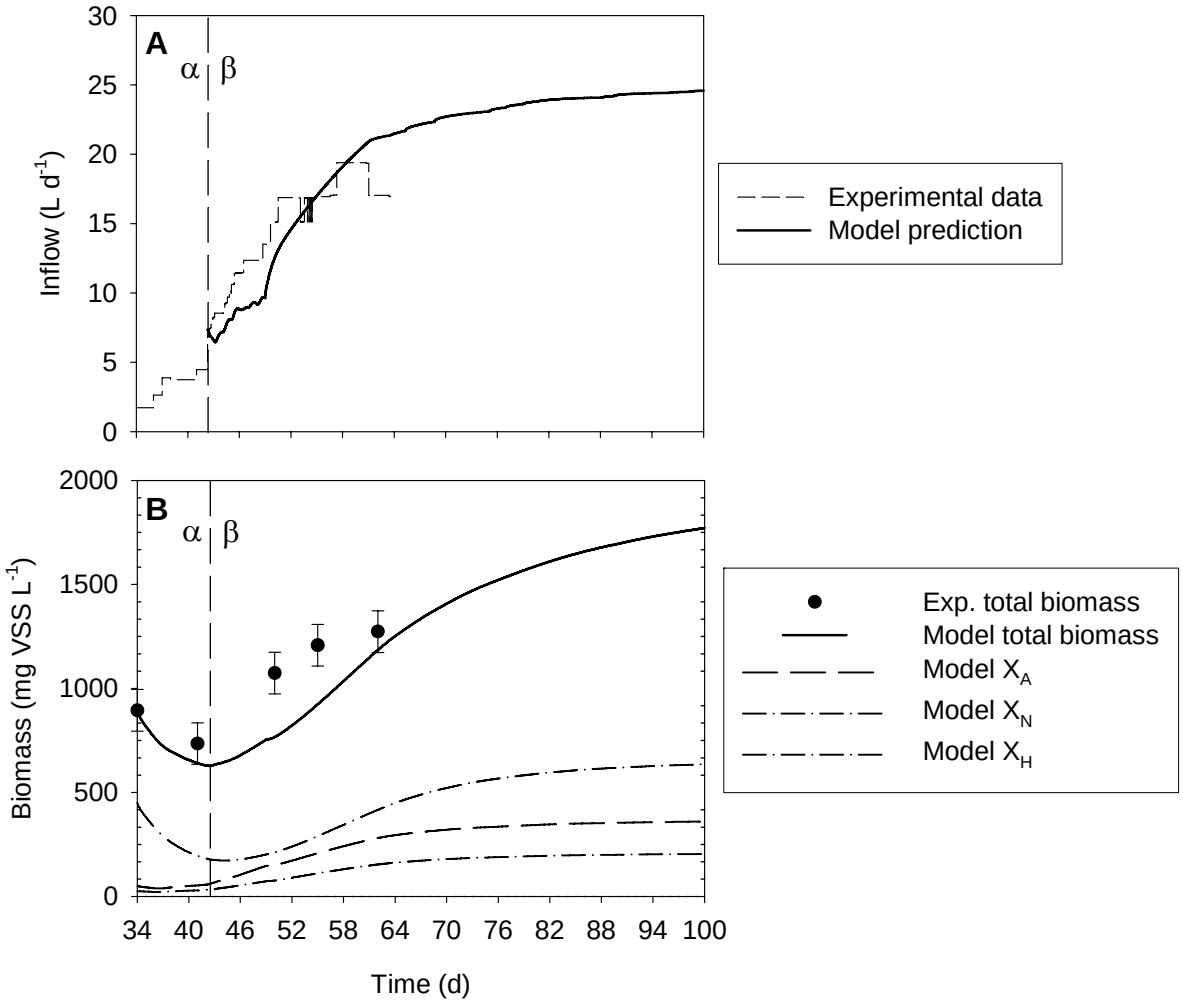

Figure 6.28 Model prediction and experimental data from day 34 to 100 in the start-up simulation with PI control. **A.** Inflow. **B.** Total biomass, X_A, X_N and X_H.

In the simulated PI controller, the OUR in R3 was compared with the OUR_{sp}. It is obvious that, if the calculated OUR was slightly different from the experimental value (see Figure 6.26), the set point used in practice could not be appropriate for the simulations. In fact, a slower inflow increase, compared with the experimental inflow increase, was obtained in the simulation when experimental OUR_{sp} was used ($1.4 \cdot 10^{-3}$ mg O_2 L^{-1} s^{-1}). Consequently, OUR_{sp} in the simulations was changed according to the OUR calculated in R3. Then, the value used in the simulations shown here was $4 \cdot 10^{-3}$ mg O_2 L^{-1} s^{-1}.

This new simulation was also used to study the system behavior in the long term (100 d). Figure 6.28 shows that steady state is almost reached on day 100. Inflow stabilized around 24.6 L d^{-1} and biomass concentration around 1770 mg VSS L^{-1}. NLR_s was calculated to be 0.53 g N g^{-1} VSS d^{-1} at the end of this simulation. Figure 6.28 also shows AOB, NOB and heterotrophs concentration predicted by the model.

TAN, TNN, nitrate and OUR profiles with time are shown in Figure 6.29. Model predicted total consumption of TAN and TNN in R2 and R3, respectively. OUR in R3 was steady around the OUR_{sp} which was constant for the whole simulated controlled period.

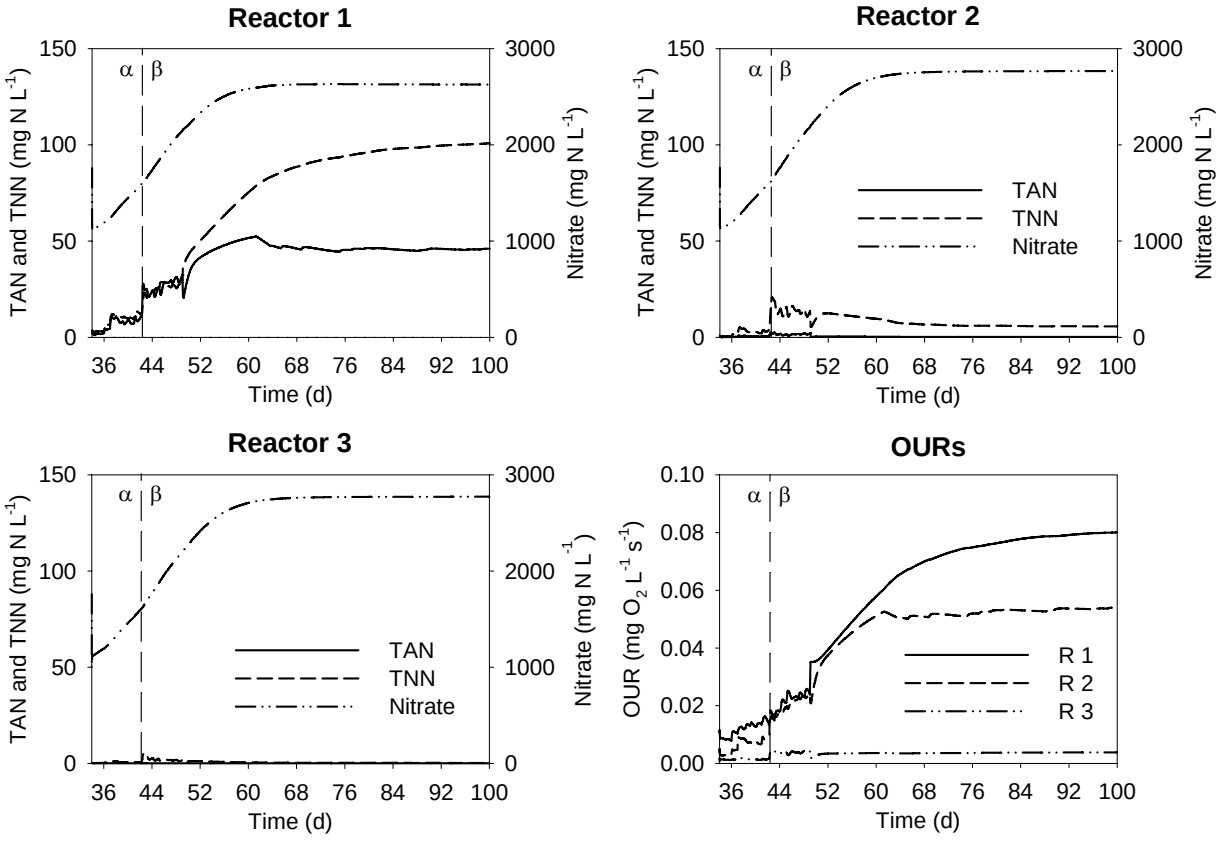

Figure 6.29 TAN, TNN, nitrate and OUR prediction in each reactor from day 34 to 80 in the start-up simulation with PI control.

5. DISCUSSION

Three start-up experiments were presented in this chapter. The inocula used in all them were grabbed from the sludge recirculation of municipal WWTPs, therefore, the nitrifying bacteria content was very low (< 1 %). The goal was to increase the nitrifying fraction in the sludge to raise its nitrification capacity in order to treat efficiently a high-strength ammonium

wastewater. Synthetic wastewater with high TAN concentration (≈ 3000 mg N L^{-1}) and low COD concentration (100 - 300 mg COD L^{-1}) was used. This low COD/TAN content can be found in a number of real wastewaters from several human activities as petrochemical, pharmaceutical, fertilizer and food industries, urban solid waste disposal, pig farms or sludge dewatering (Carrera et al. 2003; Doyle et al. 2001; Janus and Van Der Roest 1997; Mosquera-Corral et al. 2005; Salem et al. 2003).

Experimental start-up with automatic control (start-up I)

The first start-up experiment (start-up I) was performed with manual NLR_s increases after off-line MNR determination with OUR measures. Through the experiment the ratio between MNR/NLR_s was being decreased to take the maximum benefit of the entire volume of the plant, i.e. to have all the biomass working at the maximum removal rate. However, the system was working most of the time under suboptimal conditions and thus, 100 days were required to achieve a NLR_s around 0.4 g N g^{-1} VSS d^{-1}. This NLR_s was considered the target NLR_s because in Carrera et al. (2003) the MNR achieved with a similar system was 0.37 g N g^{-1} VSS d^{-1} at 25 ºC. A similar start-up was carried out in Ghyoot et al. (1999) with a membrane-assisted bioreactor (MBR) to remove nitrogen from sludge reject water. The strategy was also to conduct OUR measurements for the determination of the nitrifying capacity of the activated sludge and then adjust the nitrogen loading rate accordingly. In their work, the MNR/NLR_s was kept always close to one and as a consequence, any perturbation caused TAN and TNN accumulation which was not desired. It represents a good example of how difficult it is to manually start up a nitrifying system if MNR is wanted.

As already mentioned, the NLR_s of 0.4 g N g^{-1} VSS d^{-1} (or volumetric NLR: NLR_v = 0.24 g N L^{-1} d^{-1}) could be applied in the manual start-up experiment only after almost 100 days of operation. Start-up length can not be directly compared with other studies because inoculum, system and operational conditions are different in each case. For example, in Udert et al. (2003), the NLR_v was increased from 0.45 to 1.58 g N L^{-1} d^{-1} within 21 days in a pilot CSTR at 30 ºC. The goal in this study was to achieve an ammonium-nitrite solution for autotrophic denitrification, therefore, only half of the 7300 mg N L^{-1} of the influent were converted to nitrite. Another example can be found in Galí et al. (2006), where a SBR was inoculated with sludge from a municipal WWTP and fed with wastewater from anaerobic sludge digestion (800-1200 mg N L^{-1}) at 28 ºC. In this case, the NLR_s was increased up to 0.72-0.77 g N g^{-1} VSS d^{-1} in only 20 days and the effluent produced was a mixture of nitrite and nitrate. In both studies, the complete nitrification was not achieved and the temperature was higher than in start-up I, therefore the NLR_s applied were also higher.

As it was shown with simulations, and also other experimental works demonstrated (Pirsing et al. 1996; Shiskowski and Mavinic 1998; Vallés-Morales et al. 2004; Van Hulle et al. 2005), manual control of start-up or even operation of nitrifying systems with high-strength ammonium wastewater can lead to TAN and TNN accumulation. Hence, automatic control is

required in order to produce an effluent with TAN and TNN within the legal limits and, at the same time, to maximize the capacity of the system.

Model-based start-up optimization

Two control strategies were designed and optimized using simulations. The first strategy consisted of an on-off controller with successive inflow increases of 30%. The second one consisted of a PI controller with Kc = 0.5 L d^{-1} (mg N L^{-1})$^{-1}$ and τ_I = 0.25 d. Both strategies, simulated for 40 days, showed similar results as it was already discussed in section 4.2.4. The main difference was the oscillatory response of the on-off controller. Given that clear advantages of one of them were not found, both strategies were implemented.

In the model-based optimization of these controllers, TAN and TNN concentrations in the effluent of the system were the measured variables. Even though on-line analyzers for TAN and TNN are available and used for control purposes (Baeza et al. 2002a; Sorensen et al. 1994; Suescun et al. 2001), they need consistent maintenance and are expensive. Consequently, more researchers are exploring indirect in-line measurements (pH, ORP, DO, OUR) as measured variables to perform control (Casellas et al. 2006; Marsili-Libelli 2006). These sensors are cheaper, need less maintenance, give faster response and their profiles can be easily related to the biological processes occurring in the system. In-line OUR measurements were used in the present study to implement the optimized control strategies.

Experimental start-ups with automatic control (start-up II and start-up III)

Both designed controllers required an OUR_{sp} value. As depicted in Figure 6.10, this value should be higher than OUR_{end} but lower than OUR_{NOB}^{max}. However, Figure 6.10 is only valid for mainly nitrifying systems. This was not the case at the beginning of the start-up experiments because OUR_{end} was higher than OUR_{NOB}^{max}. This is the main drawback of using in-line OUR for control. Nevertheless, after some days of low NLR (22 in start-up II and 35 days in start-up III) heterotrophic biomass had decreased enough to do not interfere in the estimated OUR value and the automatic control could be initialized. On the other hand, a clear advantage of using OUR measurements and to set the OUR_{sp} value between OUR_{end} and OUR_{NOB}^{max} is that TAN and TNN concentrations in the effluent of the system will be always below the desired limits since the half saturation coefficient for TNN is very low. Therefore, the percentage of nitrification will be always close to 100%.

Strategies implemented in start-up II and III were different because of the controllers but also because OUR_{sp}s were different. In the on-off strategy (start-up II), the OUR_{sp} was being changed by an open loop supervisory control (manual control) taking into account TAN and TNN concentrations in the effluent to increase the set point at the same time as the nitrifying

biomass concentration was increasing. OURs in R1 and R2 were taken as a reference of the nitrifying biomass concentration increase (see equation 6.8). These OUR_{sp} changes were applied both manually and automatically, nevertheless this method did not work well for the entire experiment because nitrite accumulated in R3. As a result, OUR_{sp} was set at a fixed value in the third experiment (start-up III). In this case, although the set point was too much restrictive, it allowed a better performance because TNN never surpassed the fixed limit (10 mg N L^{-1}). In view of this results, the optimal strategy would be to periodically check the OUR profile in batch mode (off-line respirometry) in order to define the appropriate set point. However, the fast start-up obtained without OUR_{sp} tuning (start-up III) indicated that the improvement would be minimal.

Apart from these small differences, both implemented strategies resulted in fast start-ups with similar profiles of biomass concentration, OUR, TAN and TNN. Nitrogenous compounds concentrations in the effluent were lower than in the periods with manual control. It is interesting to point out that the biomass concentration decreased at the beginning of the experiments due to the heterotrophic decay but it increased again when the automatic controllers were activated. There was a decrease of approximately 1200 mg VSS L^{-1} and a following increase of 500 mg VSS L^{-1}, ending with 1800 and 1300 mg VSS L^{-1} in start-up II and III respectively. These results indicate that the biomass concentration must decrease approximately 50 % before the automatic control can be activated.

Observations must be done about the settling characteristics of the sludge which changed throughout the start-up experiments in a similar way. The SVI decreased from 100-200 to 40-60 mL g^{-1} if the three experiments are taken into account. Since 150 mL g^{-1} is considered the threshold of poor settleability (WEF 1992), the obtained nitrifying sludges were settling properly. Campos et al. (1999), Carrera et al. (2003) and Doyle et al. (2001) also experimented very low SVI values (<50 mL g^{-1}) and high settling velocity in their completely nitrifying systems. On the contrary, the TSS in the effluent of the settler increased along the start-ups reaching values of 150 – 200 mg TSS L^{-1}. This high concentration was not an excessive loss of biomass since the excess sludge waste was changed in order to have the desired SRT, however, this must be considered as an indicative of the disperse growth of nitrifyers. Figure 6.30 shows two representative images of the sludge in the pilot plant at the beginning (image A) and at the end (image B) of start-up III. Two main differences can be observed: first, the floc size was smaller at the end of the start up and second, the filamentous bacteria and higher organisms (protozoa, rotifers, nematodes, etc) were only present at the beginning of the experiment. Moussa et al. (2006) observed an increase in the floc diameter when the biomass was changed from fresh water conditions to high salt levels, which is in disagreement with the results of this study because salt concentration increased considerably during the start-up experiments (see below). They also reported that higher organisms disappeared immediately when salt concentration was 8.2 g NaCl as it happened in this study. Obviously, the size of the flocs and

the fraction of disperse growth depends on the bacterial and the growth conditions but other factors as shear stress are also decisive.

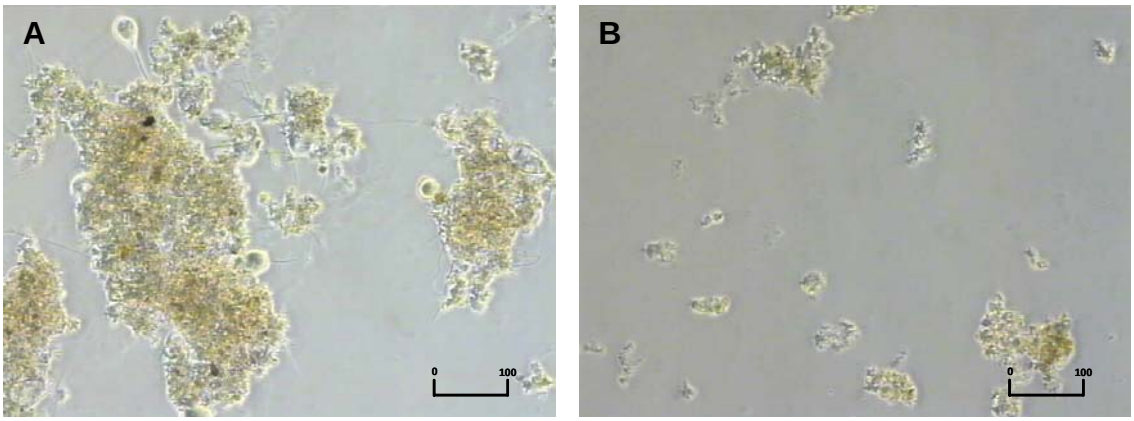

Figure 6.30 Microscopic images of sludge (x100). **A.** Beginning of the start-up III (day 1). **B.** End of the start-up III (day 39). Bar = 100 μm

Table 6.6 NLR at the end of each start-up experiment and from different completely nitrifying systems.

System	T	SRT	NLR or nitrification capacity		Reference
	(ºC)	(d)	(g N g^{-1} VSS d^{-1})	(g N L^{-1} d^{-1})	
Start-up I	28	25	0.4	0.24	This study
Start-up II	24	15	0.4	0.72	This study
Start-up III	26	15	0.5	0.65	This study
Immobilized biomass	35	≈ ∞	-	1.2 – 4.7	Bougard et al. (2006)
Suspended sludge	25	15	0.37	1.3	Carrera et al. (2003)
Suspended sludge	20	≈ ∞	0.2	4	Campos et al. (2002)
Suspended sludge	22	≈ ∞	0.88	5.9	Doyle et al. (2001)
Immobilized biomass	28-32	-	0.11 – 0.14	0.8 – 1	Arnold et al. (2000)
Suspended sludge	28-32	-	0.12 – 0.16	0.6 – 0.8	Arnold et al. (2000)
Suspended sludge	20	≈ ∞	0.5 – 0.7	7.7	Campos et al. (1999)
Suspended sludge	27	10	0.3	0.53	Gupta and Sharma (1996)

Applied NLR_s profiles were quite similar in both experiments. In start-up II, the automatic control was activated on day 22 and 8 days later (day 30) the target NLR_s (0.4 g N g^{-1} VSS d^{-1}) was obtained and surpassed. With respect to start-up III, the automatic control was activated after 35 days with low NLR_s (day 42) and after 8 days (day 50), the NLR_s was stabilized around 0.5 g N g^{-1} VSS d^{-1}. These time lengths are shorter than the 100 days required in start-up I to reach the same NLR_s. Considering both start-up II and III, the maximum NLR_s achieved without TNN accumulation in the effluent was 0.6 g N g^{-1} VSS d^{-1}. Table 6.6 shows the NLR_s and NLR_v reached at the end of each start-up compared to other studies found in the literature. NLR_v in start-up II and III were 2.7-3 times higher than in start-up I due to the higher attained

biomass concentration. These results clearly show that the automatic controllers implemented in the system sped up the start-up and enabled obtaining high biomass concentration. The obtained NLR_s is similar to values found in literature but the NLR_v is low when is compared to the systems with immobilized biomass or with high SRT because these systems have higher biomass concentration.

Microbial population

FISH results clearly demonstrated that the sludge was enriched in nitrifying bacteria. At the end of start-up III, AOB fraction was 21 % and NOB was 5 %, the rest were assigned to heterotrophs. The higher AOB fraction than NOB fraction was in agreement with the higher growth yield of AOB and it was also in agreement with the simulated results and with observations made by other researchers (Mota et al. 2005; Tsuneda et al. 2003).

AOB were detected only with probe Nso190. Probes Nso1225, Nsv443, Nsm156 and Nso218 did not hybridize to any cell. Although both Nso190 and Nso1225 are specific for all ammonia-oxidizers in the beta subclass of Proteobacteria (Mobarry et al. 1996; Mobarry et al. 1997), Nso190 gave positive results and Nso1225 gave negative results. Egli et al. (2003) observed that the fluorescence intensities obtained with Nso1225 were weaker than those obtained with Nso190 and thus decided not to use Nso1225 for quantitative FISH. However, this probe was successfully used elsewhere to detect and also quantify AOB (Kim et al. 2006; Mota et al. 2005). Therefore, these contradictory results may be due to differences in the bacterial population than due to hybridizations problems of this probe. Probably, the specific organisms targeted with each of these probes are not exactly the same. Since Nsv443, Nsm156 and Nso218 gave negative results; organisms detected with Nso190 were different from the *Nitrosomonas spp, Nitrosococcus mobilis, Nitrosospira spp* and *Nitrosomonas oligothropha* that would have been detected with these probes. Therefore cells exclusively stained with probe Nso190 did not correspond to AOB currently characterized by 16S rRNA sequencing, as suggested in Mobarry et al. (1996). A more comprehensive study of AOB community would have been possible if more specific probes were used, however, this was not the goal in this study. With respect to NOB, only *Nitrobacter* species were detected (probe NIT3) while no organisms from the genus *Nitrospira* was identified. Some researchers found that both populations coexisted in biofilm and activated sludge systems (Kim et al. 2006; Mota et al. 2005) whereas others could only detect one of them (Egli et al. 2003; Tsuneda et al. 2003).

Description of the start-ups experimental results with simulation tools

Start-up II and III were simulated with a model that included processes related to AOB, NOB and heterotrophs. Most of the kinetic and stoichiometric parameters were experimentally determined (see Chapter 3). The simulations of both experiments were not describing the experimental results accurately and thus, some modifications to the model parameters were

performed. Firstly, simulated experimental conditions (pH, T, DO, recirculation flows, etc) were changed within the logical limits but the improvement was minimal. Secondly, total biomass concentration was fitted by changing the heterotrophic biomass decay rate (b_H). This parameter had to be decreased to half its default value, which was found in the literature ($b_H=0.5\cdot b_H^{default}$).

Thirdly, another modification in the model parameters was done to describe the TNN build-up in R1 and R2 which appeared in both control strategies and were not described by the model (data not shown). Three parameters affecting NOB were modified separately: maximum specific NOB growth rate ($\mu_{max,N}$), NOB inhibition coefficient for FNA ($K_{I,FNA,N}$) and NOB inhibition coefficient for FA ($K_{I,FA,N}$). With all these parameters the outcome obtained was similar: the TNN accumulation in R1 was well described but not in R2. Finally, only $K_{I,FA,N}$ was changed. Maximum specific growth was considered constant and thus it was senseless to change it. With respect to the inhibition coefficients, NOB are always more sensitive to FA than to FNA (Anthonisen et al. 1976) and hence, the NOB inhibition for FA was decided to be changed. It was decreased from 9.5 mg FA L^{-1} to 1.3 mg FA L^{-1} in start-up II simulation and 0.4 mg FA L^{-1} in start-up III simulation. The fact that this parameter had been previously calibrated using a specific experiment with similar biomass and that TNN accumulation in the second reactor was not yet well described by the model indicated that another kind of inhibition was affecting the nitratation process. This "another" inhibition had to be a variable inhibition since it had different effect with time. Several reasons for this behavior can be postulated:

- Water conductivity increased from 10 to 38 mS cm^{-1} (5 to 22 g NaCl L^{-1} if all salt was NaCl) during the start-up experiments due to the increase of Cl^-, NO_3^- and $NaHCO_3$ concentration in the system. The effect of salts to the biomass is more likely due to the change in the osmotic pressure than due to the specific compounds (Campos et al. 2002; Hunik et al. 1992). However, several studies showed that nitrification efficiency was not affected when the salt concentration was progressively increased because biomass adapted. This acclimation consisted of a population change towards a less diverse community, but more adapted to high salt concentration (Chen and Wong 2004; Grommen et al. 2005). In spite of this acclimation, other studies found some inhibition due to increased salinity. Moussa et al. (2006) reported that AOB were more sensitive to short and long-term salt stress, while (Catalan-Sakairi et al. 1997) observed that NOB were the most sensitive. These contradictory results make it difficult to decide whether in this study the "unexpected" nitrite accumulation was because of salinity increase or not.

- As stated above, the change in the environmental conditions (i.e. salt concentration increase) has an effect on the biomass composition. Consequently, it makes sense that the same model did not explain the entire experiment (Sin et al. 2006).

- On the other hand, one of the main drawbacks of most models is that the activity does not depend on the "history" of the biomass and that the sudden changes in the conditions produce sudden changes in the behavior. For example, when biomass is under inhibitory conditions and it is rapidly changed to non-inhibitory conditions, the model will predict an immediate activity increase, while in practice it would need some time to recover from the adverse conditions. This phenomenon could happen in the studied system when the biomass was moved from R1 to R2. TAN concentration could inhibit NOB activity in R1 but not in R2 (where TAN concentration was almost zero). NOB activity in R2 was not as recovered as the model predicted.

Probably, the sum of all these effects produced the differences between model predictions an experimental data. However, the model and the simulations were useful to optimize the control strategies and the results for TAN, nitrate and OUR after implementation were not so different to the model prediction.

The COD/TAN ratio effect on the relative amount of each specific bacterium in the sludge can be observed in Figures 6.16 (start-up II) and 6.27 (start-up III). The simulations predicted similar concentration for X_A and X_H at the end of start-up II while higher concentration for X_H than for X_A were predicted at the end of start-up III. The only reason for this was that the COD/TAN ratio differed in both experiments: it was 0.033 in start-up II and 0.1 in start-up III. The higher COD concentration in the inflow of start-up III provoked that the increase in the biomass concentration when the automatic control was activated was not only due to the increase in the nitrifying biomass concentration but also due to the growth of heterotrophs.

Short-term prediction

In addition to prediction in a day-time scale, one on-off cycle in start-up II (hour-time scale) was also simulated. Model prediction for TAN, TNN and OUR agreed well with experimental data. The oscillatory behavior of this kind of controller was clearly reflected in the time course of TAN concentration because it decreased when the control position was *on* and increased when it was *off*. The same behavior was not observed in the TNN concentration because it depended on the activity of both AOB and NOB.

Control loop simulation and long-term prediction

Both control strategies were simulated again with a modification in the model: the inflow was no longer an input variable. The control loop was included in the model and the control action (inflow value) was calculated by the model with the same frequency than in the experiments. The behavior of both on-off and PI controllers was accurately predicted as shown in Figures 6.18A and 6.27A. In the on-off control simulation, the experimental OUR_{sp} was used but in the PI control, the OUR_{sp} had to be changed in order to get a similar inflow profile than the experimental one. This was because of the differences between the experimental and predicted

OUR in R3. Although these differences were small for both start-up experiments, they had more influence on the PI controller than in the on-off controller. Nevertheless, the results of these new simulations showed that the model was useful to simulate not only the pilot plant performance when the inflow was an input variable, but also the controllers.

Furthermore, this model was used to predict the steady state conditions for each different control strategy. The obtained steady states were different in terms of biomass concentration and NLR_s. In start-up II the biomass concentration was 4000 mg VSS L^{-1} and the NLR_s was 0.823 mg N g^{-1} VSS d^{-1} and in start-up III they were 1770 mg VSS L^{-1} and 0.53 mg N g^{-1} VSS d^{-1}, respectively. These disagreements can be explained with the used of different OUR_{sp}s because similar biomass concentration and inflow values than in start-up II simulation were obtained when variable OUR_{sp} (equation 6.8 with k=6) was simulated (data not shown) in start-up III. Although the biomass concentration predicted for start-up II (4000 mg VSS d^{-1}) seems quite high compared with the experimental biomass concentration reached in these experiments, this biomass concentration was experimentally obtained in similar conditions (Carrera et al. 2003).

The fact that start-up III was low-loaded can be demonstrated if TAN, TNN and nitrate concentrations predicted for both experiments are compared (Figures 6.19 and 6.29). TAN and TNN accumulation in R1 and R2 were lower in start-up III than in start-up II simulation. Furthermore, these accumulations and the predicted OUR in start-up III tended to decrease with time. This would have been avoided with OUR_{sp} changing according to biomass growth. OUR values in all reactors were also lower than in start-up II simulation due to lower biomass concentration. This fact corroborates the importance of the chosen OUR_{sp} in this kind of controllers.

Both control strategies were used to control the system not only in the start-up procedure but also in the "normal" operation to change the NLR when perturbations occurred (data not shown). Therefore, the optimized strategies were very useful for the operation of the pilot plant.

Full-scale implementation of the automatically controlled start-up and operation

The control strategies and the control loop itself could be used in a full-scale plant for both start-up and operation whatever its configuration was. For sure, the dynamics of the system would be different and the strategies should be optimized again. The equipment to determine the OUR would be minimal: a respiration chamber in the effluent of the aerobic reactor with a DO probe connected to a PC. Also a previous buffer tank and a variable-flow device for the inflow would be required.

6. CONCLUSIONS

- The start-up of a completely nitrifying system treating high ammonium concentration can be done with manual inflow increases provided that the NLR_s is lower than the MNR to avoid ammonium and nitrite build-up and system destabilization. 100 days were required to achieve sludge capable of treating a NLR_s of 0.4 g N g^{-1} VSS d^{-1} when sludge from municipal WWTP was used as inoculum.

- Two strategies were optimized by means of simulations tools to speed up the start-up while accomplishing the TAN and TNN requirements in the effluent (TAN+TNN<10 mg N L^{-1}): an on-off controller with successive inflow increases (30 %) and a PI controller with τ_I = 0.25 d and Kc = 0.5 L d^{-1} (mg N L^{-1})$^{-1}$.

- Although TAN and TNN were the measured variables in the controllers optimization, OUR measurements were used in the experimental implementation because the required equipment is cheaper, needs less maintenance and is more easily available. OUR_{sp} must be set in between OUR_{NOB}^{max} and OUR_{end} to allow the system control and to produce an effluent with very low TAN and TNN concentration.

- Experimental start-ups with both optimized controllers led to similar results in terms of TAN, TNN and VSS concentration, and OUR profiles. Settling characteristics also behaved similarly: the SVI decreased but the TSS in the effluent rose because the salinity content in the bulk liquid and the biomass composition changed. The start-up time was decreased from 100 days in the manual start-up experiment to 30-40 days in the experiments with automatic control. The maximum NLR_s achieved was 0.6 g N g^{-1} VSS d^{-1}.

- The model prediction described quite well the experimental results when two of the model parameters were changed (b_H and $K_{I,FA,N}$). However, some disagreements were detected which could be due to several reasons: the increase in the salt concentration, the fact that the same group of model parameters may not be appropriate to describe such changing conditions and/or the fact that the model did not consider the dependence of the biomass activity on the biomass history. Nevertheless, the model was very useful to make short- and long-term prediction.

- The simulation of both control strategies described the experimental data quite well and was further used to predict the steady state conditions. It was confirmed that the OUR_{sp} value is of great importance in the final biomass concentration. For an optimal operation (maximum NLR_s), the OUR_{sp} should be changed according to the biomass concentration in the system.

7. REFERENCES

Anthonisen AC, Loehr RC, Prakasam TBS, Srinath EG. 1976. Inhibition of nitrification by ammonia and nitrous acid. *Journal of the Water Pollution Control Federation* 48(5):835-852.

APHA. 1995. Standard methods for the examination of water and wastewater. 19th Ed. Washington DC, USA: American Publishers Health Association.

Arnold E, Böhm B, Wilderer PA. 2000. Application of activated sludge and biofilm sequencing batch reactor technology to treat reject water from sludge dewatering systems: A comparison. *Water Science and Technology* 41(1):115-122.

Baeza JA, Gabriel D, Lafuente J. 1999. An expert supervisory system for a pilot WWTP. *Environmental Modelling and Software* 14(5):383-390.

Baeza JA, Gabriel D, Lafuente J. 2002a. Improving the nitrogen removal efficiency of an A2/O based WWTP by using an on-line Knowledge Based Expert System. *Water Research* 36(8):2109-2123.

Baeza JA, Gabriel D, Lafuente J. 2002b. In-line fast OUR measurements for monitoring and control of WWTP. *Water Science and Technology* 45(4-5):19-28.

Bougard D, Bernet N, Dabert P, Delgenes JP, Steyer JP. 2006. Influence of closed loop control on microbial diversity in a nitrification process. *Water Science and Technology* 53(4-5):85-93.

Brouwer H, Bloemen M, Klapwijk B, Spanjers H. 1998. Feedforward control of nitrification by manipulating the aerobic volume in activated sludge plants. *Water Science and Technology* 38(3):245-254.

Campos JL, Garrido-Fernández JM, Méndez R, Lema JM. 1999. Nitrification at high ammonia loading rates in an activated sludge unit. *Bioresource Technology* 68(2):141-148.

Campos JL, Mosquera-Corral A, Sánchez M, Méndez R, Lema JM. 2002. Nitrification in saline wastewater with high ammonia concentration in an activated sludge unit. *Water Research* 36(10):2555-2560.

Carrera J, Baeza JA, Vicent T, Lafuente J. 2003. Biological nitrogen removal of high-strength ammonium industrial wastewater with two-sludge system. *Water Research* 37(17):4211-4221.

Casellas M, Dagot C, Baudu M. 2006. Set up and assessment of a control strategy in a SBR in order to enhance nitrogen and phosphorus removal. *Process Biochemistry* 41(9):1994-2001.

Catalan-Sakairi MAB, Wang PC, Matsumura M. 1997. Nitrification performance of marine nitrifiers immobilized in polyester- and macro-porous cellulose carriers. *Journal of Fermentation and Bioengineering* 84(6):563-571.

Çeçen F, Orak E. 1996. Nitrification of fertilizer wastewaters in a biofilm reactor. *Journal of Chemical Technology and Biotechnology* 65(3):229-238.

Corominas L, Sin G, Puig S, Traore A, Balaguer M, Colprim J, Vanrolleghem PA. 2006. Model-based evaluation of an on-line control strategy for SBRs based on OUR and ORP measurements. *Water Science and Technology* 53(4-5):161-169.

Chen GH, Wong MT. 2004. Impact of increased chloride concentration on nitrifying-activated sludge cultures. *Journal of Environmental Engineering* 130(2):116-125.

Chen SD, Chen CY, Shen YC, Chiu CM, Cheng HJ. 1996. Treatment of high-strength nitrate wastewater by biological methods - Operational characteristics study. *Water Science and Technology* 34(1-2):269-276.

Doyle J, Watts S, Solley D, Keller J. 2001. Exceptionally high-rate nitrification in sequencing batch reactors treating high ammonia landfill leachate. *Water Science and Technology* 43(3):315-322.

Egli K, Langer C, Siegrist HR, Zehnder AJB, Wagner M, Van der Meer JR. 2003. Community analysis of ammonia and nitrite oxidizers during start-up of nitritation reactors. *Applied and Environmental Microbiology* 69(6):3213-3222.

Galí A, Dosta J, Mace S, Mata-Alvarez J. 2006. Start-up of a biological sequencing batch reactor to treat supernatant from anaerobic sludge digester. *Environmental Technology* 27(8):891-899.

Galluzzo M, Ducato R, Bartolozzi V, Picciotto A. 2001. Expert control of DO in the aerobic reactor of an activated sludge process. *Computers and Chemical Engineering* 25(4-6):619-625.

Ghyoot W, Vandaele S, Verstraete W. 1999. Nitrogen removal from sludge reject water with a membrane-assisted bioreactor. *Water Research* 33(1):23-32.

Grommen R, Dauw L, Verstraete W. 2005. Elevated salinity selects for a less diverse ammonia-oxidizing population in aquarium biofilters. *FEMS Microbiology Ecology* 52(1):1-11.

Guisasola A, Pijuan M, Baeza JA, Carrera J, Lafuente J. 2006. Improving the start-up of an EBPR system using OUR to control the aerobic phase length: A simulation study. *Water Science and Technology* 53(4-5):253-262.

Gupta SK, Sharma R. 1996. Biological oxidation of high strength nitrogenous wastewater. *Water Research* 30(3):593-600.

Hunik JH, Meijer HJG, Tramper J. 1992. Kinetics of Nitrosomonas europaea at extreme substrate, product and salt concentrations. *Applied Microbiology and Biotechnology* 37(6):802-807.

Janus HM, Van Der Roest HF. 1997. Don't reject the idea of treating reject water. *Water Science and Technology* 35(10):27-34.

Katsogiannis AN, Kornaros ME, Lyberatos GK. 1999. Adaptive optimization of a nitrifying sequencing batch reactor. *Water Research* 33(17):3569-3576.

Kim DJ, Lee DI, Keller J. 2006. Effect of temperature and free ammonia on nitrification and nitrite accumulation in landfill leachate and analysis of its nitrifying bacterial community by FISH. *Bioresource Technology* 97(3):459-468.

Kishida N, Kim JH, Chen M, Tsuneda S, Sasaki H, Sudo R. 2004. Automatic control strategy for biological nitrogen removal of low C/N wastewater in a sequencing batch reactor. *Water Science and Technology* 50(10):45-50.

Krause K, Böcker K, Londong J. 2002. Simulation of a nitrification control concept considering influent ammonium load. *Water Science and Technology* 45(4-5):413-420.

Liu J, Olsson G, Mattiasson B. 2004. Monitoring and control of an anaerobic upflow fixed-bed reactor for high-loading-rate operation and rejection of disturbances. *Biotechnology and Bioengineering* 87(1):43-53.

Marsili-Libelli S. 2006. Control of SBR switching by fuzzy pattern recognition. *Water Research* 40(5):1095-1107.

Marsili-Libelli S, Giunti L. 2002. Fuzzy predictive control for nitrogen removal in biological wastewater treatment. *Water Science and Technology* 45(4-5):37-44.

MATLAB. 2002. User's guide. Version 6.5 (Release 13). Mathworks T, editor. Natick, USA.

Mobarry BK, Wagner M, Urbain V, Rittmann BE, Stahl DA. 1996. Phylogenetic probes for analyzing abundance and spatial organization of nitrifying bacteria. *Applied and Environmental Microbiology* 62(6):2156-2162.

Mobarry BK, Wagner M, Urbain V, Rittmann BE, Stahl DA. 1997. Erratum: Phylogenetic probes for analyzing abundance and spatial organization of nitrifying bacteria (Applied and Environmental Microbiology 62:6 (2157)). *Applied and Environmental Microbiology* 63(2):815.

Mosquera-Corral A, González F, Campos JL, Méndez R. 2005. Partial nitrification in a SHARON reactor in the presence of salts and organic carbon compounds. *Process Biochemistry* 40(9):3109-3118.

Mota C, Ridenoure J, Cheng J, De Los Reyes Iii FL. 2005. High levels of nitrifying bacteria in intermittently aerated reactors treating high ammonia wastewater. *FEMS Microbiology Ecology* 54(3):391-400.

Moussa MS, Sumanasekera DU, Ibrahim SH, Lubberding HJ, Hooijmans CM, Gijzen HJ, Van Loosdrecht MCM. 2006. Long term effects of salt on activity, population structure and

floc characteristics in enriched bacterial cultures of nitrifiers. *Water Research* 40(7):1377-1388.

Pirsing A, Wiesmann U, Kelterbach G, Schaffranietz U, Röck H, Eichner B, Szukal S, Schulze G. 1996. On-line monitoring and modelling based process control of high rate nitrification - Lab scale experimental results. *Bioprocess Engineering* 15(4):181-188.

Puig S, Corominas L, Vives MT, Balaguer MD, Colprim J, Colomer J. 2005. Development and implementation of a real-time control system for nitrogen removal using OUR and ORP as end points. *Industrial and Engineering Chemistry Research* 44(9):3367-3373.

Puñal A, Melloni P, Roca E, Rozzi A, Lema JM. 2001. Automatic start-up of UASB reactors. *Journal of Environmental Engineering* 127(5):397-402.

Puznava N, Thornberg D, Magnin P, Reddet E. 2000. Aeration control on a nitrifying biofilter system by using on-line analyzers. *Water Science and Technology* 41(4-5):369-374.

Pynaert K, Smets BF, Beheydt D, Verstraete W. 2004. Start-up of Autotrophic Nitrogen Removal Reactors via Sequential Biocatalyst Addition. *Environmental Science and Technology* 38(4):1228-1235.

Salem S, Berends DHJG, Heijnen JJ, Van Loosdrecht MCM. 2003. Bio-augmentation by nitrification with return sludge. *Water Research* 37(8):1794-1804.

Shiskowski DM, Mavinic DS. 1998. Biological treatment of a high ammonia leachate: Influence of external carbon during initial startup. *Water Research* 32(8):2533-2541.

Show KY, Wang Y, Foong SF, Tay JH. 2004. Accelerated start-up and enhanced granulation in upflow anaerobic sludge blanket reactors. *Water Research* 38(9):2292-2303.

Sin G, Villez K, Vanrolleghem PA. 2006. Application of a model-based optimisation methodology for nutrient removing SBRs leads to falsification of the model. *Water Science and Technology* 53(4-5):95-103.

Sorensen J, Thornberg DE, Nielsen MK. 1994. Optimization of a nitrogen-removing biological wastewater treatment plant using on-line measurements. *Water Environment Research* 66(3):236-242.

Stephanopoulos G. 1984. Chemical Process Control. An introduction to theory and practice: Prentice/Hall International, Inc. New Jersey.

Suescun J, Ostolaza X, Garcia-Sanz M, Ayesa E. 2001. Real-time control strategies for predenitrification - Nitrification activated sludge plants biodegradation control. *Water Science and Technology* 43(1):209-216.

Surmacz-Gorska J, Gernaey K, Demuynckz C, Vanrolleghem P, Verstraete W. 1995. Nitrification process control in activated sludge using oxygen uptake rate measurements. *Environmental Technology* 16(6):569-577.

Teichgräber B. 1993. Control strategies for a highly loaded biological ammonia elimination process. *Water Science and Technology* 28(11-12):531-538.

Teichgräber B, Stein A. 1994. Nitrogen elimination from sludge treatment reject water - Comparison of the steam-stripping and denitrification processes. *Water Science and Technology* 30(6):41-51.

Tsuneda S, Nagano T, Hoshino T, Ejiri Y, Noda N, Hirata A. 2003. Characterization of nitrifying granules produced in an aerobic upflow fluidized bed reactor. *Water Research* 37(20):4965-4973.

Udert KM, Fux C, Münster M, Larsen TA, Siegrist H, Gujer W. 2003. Nitrification and autotrophic denitrification of source-separated urine. *Water Science and Technology* 48(1):119-130.

Vadivelu VM, Yuan Z, Fux C, Keller J. 2006. Stoichiometric and kinetic characterisation of Nitrobacter in mixed culture by decoupling the growth and energy generation processes. *Biotechnology and Bioengineering* 94(6):1176-1188.

Vallés-Morales MJ, Mendoza-Roca JA, Bes-Pia A, Iborra-Clar A. 2004. Nitrogen removal from sludge water with SBR process: Start-up of a full-scale plant in the municipal wastewater treatment plant at Ingolstadt, Germany. *Water Science and Technology* 50(10):51-58.

Van Hulle SWH, Van Den Broeck S, Maertens J, Villez K, Donckels BMR, Schelstraete G, Volcke EIP, Vanrolleghem PA. 2005. Construction, start-up and operation of a continuously aerated laboratory-scale SHARON reactor in view of coupling with an Anammox reactor. *Water SA* 31(3):327-334.

Verstraete W, Vanstaen H, Voets JP. 1977. Adaptation to nitrification of activated sludge systems treating highly nitrogenous waters. *Journal of the Water Pollution Control Federation* 49(7):1604-1608.

Villaverde S, Fdz-Polanco F, García PA. 2000. Nitrifying biofilm acclimation to free ammonia in submerged biofilters. Start-up influence. *Water Research* 34(2):602-610.

WEF. 1992. Design of municipal wastewater treatments plants. Water Environment Federation. Alexandria, USA: Water Environment Federation.

Wyffels S, Van Hulle SWH, Boeckx P, Volcke EIP, Van Cleemput O, Vanrolleghem PA, Verstraete W. 2004. Modeling and simulation of oxygen-limited partial nitritation in a membrane-assisted bioreactor (MBR). *Biotechnology and Bioengineering* 86(5):531-542.

Yu RF, Liaw SL, Chang CN, Cheng WY. 1998. Applying real-time control to enhance the performance of nitrogen removal in the continuous-flow SBR system. *Water Science and Technology* 38(3):271-280.

PART IV - Chapter 7

CONTROLLED START-UP AND OPERATION OF A PARTIAL NITRIFICATION SYSTEM WITH HIGHLY CONCENTRATED AMMONIUM WASTEWATER

Parts of this chapter are being prepared for publishing as:

Jubany I, Baeza JA, Carrera J, Lafuente J. Strategy for the optimal start-up of a partial nitrification system with automatic control to treat highly concentrated ammonium wastewater. Water Research

Jubany I, Baeza JA, Carrera J, Lafuente J. Expert control for the operation of a partial nitrification system to treat highly concentrated ammonium wastewater. Process Biochemistry.

Three attempts were performed to achieve partial nitrification under different conditions. It was finally obtained at 25 ºC, 1.1 mg O_2 L^{-1} and pH of 8.3 using an automatic inflow controller to permanently keep stressing conditions to NOB. With the three-reactor configuration, high free ammonia (FA) concentration was maintained in the first two reactors to inhibit NOB while an ammonium-free effluent was obtained. Steady partial nitrification was run for 120 days with an averaged specific nitrogen loading rate (NLR_s) of 0.5 g N g^{-1} VSS L^{-1}. NOB were completely washed out after 100 days of operation. Two expert rules were added to the inflow control system when only nitritation took place in order to prevent FA build-up and automatically adjust the set point of oxygen uptake rate (OUR_{sp}) to the AOB activity. A model-based study under different conditions showed that partial nitrification could be achieved even at 15 ºC if pH was 8.3 and dissolved oxygen was 1.1 mg O_2 L^{-1} with the three-reactor configuration and the automatic inflow controller.

1. INTRODUCTION

Partial nitrification has gained a lot of interest among researchers in the last years, especially in the field of highly nitrogenous wastewater treatment. Turk and Mavinic (1987) demonstrated that this shortcut in the ammonium removal process has several advantages with respect to the complete nitrification: (1) a 40 % reduction of COD demand during denitrification; (2) 63 % higher rate of denitrification and (3) 300 % lower biomass production during anoxic growth. Furthermore, partial nitrification can save up to 25 % of the oxygen demand for nitrification due to the suppression of the nitratation and reduce the CO_2 emissions by 20 % due to the denitrification from nitrite instead of nitrate (Peng and Zhu 2006).

The effluent composition of a partial nitrification process can vary significantly according to the degree of ammonium removal and nitratation inhibition; it can range from basically nitrite (Ciudad et al. 2005) to a mixture of ammonium and nitrite (Fux et al. 2002) and also a mixture of nitrite and nitrate with low ammonia concentration (Ruiz et al. 2003). These variations are due to the different configurations and operational conditions which were chosen depending on the following treatment (denitrification).

Denitrification is the most widely used biological process to remove nitrate after nitrification and it can be even more convenient to remove nitrite after partial nitrification. Abeling and Seyfried (1992) and Chung and Bae (2002) found 1.8 and 4.3 times faster denitrification rates with nitrite than with nitrate although both pointed out the fact that free nitrous acid (FNA) could inhibit the process if the biomass was not acclimated. In addition, FNA can also have negatively influence on the activity of heterotrophs (Abeling and Seyfried 1992; Weon et al. 2002). However, the choice of an appropriate reactor configuration or the acclimation of the biomass to FNA can solve this problem. On the other hand, the heterotrophic denitrification is

not the only available process to be used after partial nitrification. A completely new microbial group was discovered on the mid-1990s due to the observed loss of N in nitrifying reactors (Siegrist et al. 1998; Strous et al. 1998): anaerobic ammonium oxidizers or anammox-bacteria. They oxidize ammonia to dinitrogen gas with nitrite as the electron acceptor under anaerobic conditions in the absence of any organic C-source. The main characteristics of these bacteria are the low biomass yield and low maximum specific growing rate: doubling time of 11 days at 32-33 ºC (Strous et al. 1998) compared to around 7-8 hours of doubling time of nitrifiers (Blackall and Burrell 1999). The first characteristic is advantageous in terms of excess sludge production but both provoke a slow and difficult start-up of any system, specially full-scale installations which can take months even under favorable conditions (Fux and Siegrist 2004). These bacteria need a very specific ammonium/nitrite ratio in the influent of 1-1.5 (Fux et al. 2002; Gut et al. 2006) because if FNA is not totally depleted in the reactor, it has severe inhibitory effect on them causing permanent loss of activity (Dapena-Mora et al. 2006; Van Loosdrecht and Salem 2006). Therefore, any ANAMMOX reactor requires a previously very well controlled process to produce the optimal effluent without composition oscillations.

Because of the new opportunities emerging with the new processes (nitrification/denitrification via nitrite and ANAMMOX process), a number of studies were performed to identify the optimal operation conditions to obtain partial nitrification. The key point is to favor the nitritation process and at the same time to inhibit or suppress the nitratation process in order to have a biomass enriched in AOB and poor in NOB. The main factors affecting AOB and NOB activities in a different degree and useful to achieve partial nitrification are:

Temperature: both AOB and NOB populations increase their activity with temperature but their maximum growth rates intersect around 20 ºC (see Chapter 3). For temperatures above 20ºC, maximum growth rate of AOB is higher than maximum growth rate of NOB. This characteristic is used in the SHARON process (single reactor high activity ammonia removal over nitrite), in which a chemostat is operated at a hydraulic retention time (HRT), equal to the sludge retention time (SRT), of 1 day and 30-35 ºC (Hellinga et al. 1998). Under these conditions NOB can be washed out while AOB are retained in the reactor. The SHARON process was designed for the separate treatment of reject water from digested sludge dewatering. This wastewater has a temperature of 30-35 ºC, contains 600-1000 g $N\text{-}NH_4^+$ L^{-1}, low chemical oxygen demand (COD) content and enough alkalinity to convert 50-60 % of its ammonium to nitrite. Therefore a mixture of 50 % ammonium and 50 % nitrite can be easily obtained without pH control. This effluent contains also suspended solids typically in concentrations well below 1 g L^{-1} (Hellinga et al. 1998). If this effluent is stable, this process can be successfully coupled with the ANAMMOX process (Dapena-Mora et al. 2006; Fux et al. 2002; Van Dongen et al. 2001; Van Loosdrecht and Salem 2006). Other studies have taken advantage of the temperature influence on the nitrifying populations to achieve partial nitrification (Bougard et al. 2006; Mace et al. 2006).

Dissolved oxygen (DO): As shown in Chapter 3 and also in Hellinga et al. (1998) and Wiesmann (1994), NOB have lower affinity for DO than AOB, therefore nitrite accumulation is favored at low DO concentration. Ciudad et al. (2005) found that in a nitrifying activated sludge reactor operating at 25 ºC and pH of 7.8, the optimal DO was 1.4 mg O_2 L^{-1} and the achieved accumulation was 75 % with 95 % of ammonia removal. A lower DO concentration (<1 mg O_2 L^{-1}) was required in Chung et al. (2007) to maintain stable nitrite accumulation for more than 1.5 years with a hybrid reactor containing both biofilm and suspended-growth biomass. Therefore, considering ammonia oxidation rate and nitrite accumulation, DO concentration should be maintained about 1.0-1.5 mg O_2 L^{-1} (Peng and Zhu 2006).

pH: The pH influences in the equilibrium of NH_4^+/NH_3 and NO_2^-/HNO_2 and the non-ionized forms can inhibit both AOB and NOB population in different extent. Usually, NOB are more influenced than AOB (Anthonisen et al. 1976). Since in the nitrification process it is easier to have high free ammonia (FA) concentration than FNA, this parameter was used in numerous studies to achieve nitrite accumulation. For example, Yun and Kim (2003) stated that nitrite accumulation was obtained in a packed biofilm reactor because of the FA level in the reactor (0.3-5 mg N- NH_3 L^{-1}) and Chung et al. (2006) found that the optimal FA concentration was 5-10 mg N- NH_3 L^{-1} for maximum ammonium removal and nitratation suppression. On the other hand, Villaverde et al. (2000) detected NOB acclimation to FA because the threshold level moved from 0.2 to 0.5-0.7 mg NH_3-N L^{-1} after four months of operation and Turk and Mavinic (1989) could not either sustain nitrite build-up using FA as the sole NOB inhibiting factor in a long-term experiment. The differences in the optimal FA concentration and the fact that some researches have found acclimation of NOB to this compound indicate that this parameter is quite dependent on the bacterial population and history. A similar situation can be described for FNA inhibition because the acclimation can also change the inhibitory effect (Chapter 3). In Kim and Seo (2006) both FA and FNA were responsible for the washout of the NOB in a sequencing batch airlift reactor.

Free-hydroxylamine (FH): Yang and Alleman (1992) suggested that hydroxylamine, which is an intermediate in the nitritation process, inhibited NOB population, specifically in the form of free-hydroxylamine (NH_2OH). It appeared likely to accumulate in a nitrifying system with high ammonium concentration, deficient DO and high pH (Peng and Zhu 2006).

Operational and aeration pattern: Turk and Mavinic (1986) observed a lag time in nitratation when bacteria changed from the anoxic to the aerobic cell that resulted in a temporary, but significant, accumulation of nitrite. They also reported that the extension of aeration time alleviates stress on the NOB and results in loss of nitrite build-up. These concepts were used in Yoo et al. (1999) and Antileo et al. (2006). Moreover, intermittent aeration was proved to be more favorable than continuous aeration in SBRs to convert ammonium to nitrite (Pollice et al. 2002).

The reactor type or configuration will determine which of these parameters can be successfully used. For example, FA can not be chosen as the key parameter in a CSTR if low ammonia effluent is required but it can be used in a SBR treating high ammonium concentration wastewater. Although it is possible to implement nitrite accumulation only through regulation of one of the factors, most of the studies used at least two of them to gain in process stability (Lai et al. 2004; Terada et al. 2003; Yoo et al. 1999). Besides, several studies have been performed to find the optimal parameter combination. As an example, Lu et al. (2006) carried out an orthogonal experiment to study the combined effects of operation parameters on the performance of shortcut nitrification of an internal-loop fluidized bed reactor. The found optimal parameters were: temperature of 35 ºC, pH of 8.0, DO of 1.0 mg O_2 L^{-1}, FA concentration of 68 mg FA L^{-1} and HRT of 16 h. In this case, the nitratation suppression was due to high pH, high FA and low DO.

If the nitratation process is inhibited in an extent that the minimum retention time required for NOB growth is higher than the current SRT of the system, they will be washed out and the effluent will not contain nitrate. This has been achieved using both suspended solids (Fux et al. 2002) and immobilized biomass (Kim and Seo 2006). On the contrary, if the NOB population is not inhibited enough, nitratation will take place and the system would be able to easily turn to complete nitrification. In many of the studies to accumulate nitrite, nitrate is also produced and often, problems to stably maintain the nitrite build-up are found (Fux et al. 2004; Van Hulle et al. 2005; Villaverde et al. 2000; Yun and Kim 2003). It is obvious that, like in all the systems which require very specific conditions, the process control appears as the best option in order to achieve successful results. There are not too many studies applying real-time-control strategies in partial nitrification systems. Usually, only the basic environmental parameters like pH, T and DO are controlled around the optimal values by using simple and independent control loops (Lu et al. 2006; Ruiz et al. 2003) but no extra control is supplied to prevent biomass acclimation or to act in front of external disturbances. Some applications of advanced control systems are found in Li et al. (2004) and Poo et al. (2006) were SBR operation was optimized by step-feed and on-line control with pH, ORP and DO measurements. In these studies, the phases of each cycle were controlled and high nitrogen removal efficiencies were obtained. In Antileo et al. (2006), a supervisory pH control for maintaining optimal ammonia concentration and an automatic interruption of aeration when the endpoint of ammonia oxidation was detected was experimentally tested in a sequencing batch rotating disk reactor. Bernet et al. (2005) optimized the O_2/NH_4^+ ratio and used on-line regulation of this parameter in a two-step control scheme to oxidize up to 80 % of the inflow ammonium into nitrite. This was performed in an inverse turbulent bed reactor even when disturbances on the nitrogen loading rate (NLR) were applied. A similar reactor was used in Bougard et al. (2006) to achieve partial nitrification by maintaining low DO concentration (around 2 mg O_2 L^{-1}) and low ammonia concentration (less than 300 mg FA L^{-1}) acting on the

input feed flow. Some research was also directed to the control of the SHARON process with the aim to successfully couple it with the ANAMMOX process. For example, Volcke et al. (2005) tested two control strategies by means of simulation and found that the optimal one consisted on a cascade feedback control of the effluent ammonium/nitrite ratio through setting a DO set point tracked by adjusting the air flow rate.

In this study, simple control strategies are used to achieve partial nitrification at 25 ºC in an activated sludge system with high biomass concentration. Since the FISH technique has been recently used to demonstrate the complete washout of NOB in partial nitrification systems and to study the bacterial community of AOB under the applied conditions (Egli et al. 2003; Kim et al. 2006; Kim and Seo 2006), it was also used in this work. Partial nitrification and denitrification or Anammox can take place in the same reactor or in the same biofilm and thus, take advantage of the competition of NOB and denitrifiers or Anammox bacteria for nitrite (Fux et al. 2006; Hao et al. 2002; Pynaert et al. 2004). Nevertheless, in this study, separation of both processes was chosen for a better process control. Particularly, only partial nitrification is studied. Moreover, a continuous system is used because few literature is found using continuous-flow processes (Peng and Zhu 2006).

2. OBJECTIVES

The objective of this chapter is threefold. The first objective is to start-up a partial nitrification system from a completely nitrifying system with the help of automatic control. The second objective is to maintain the partial nitrification with the best control strategy to achieve stable operation. And the last objective is to use the simulation tools to test the control strategy under different environmental conditions and different reactor configurations.

3. MATERIALS AND METHODS

This section points out the main characteristics of the system and conditions used in the experiments. It also describes the determination of the maximum ammonium and nitrite oxidation rates and the chemical analyses carried out. Furthermore, references to the previous chapters are given to describe the system modeling and the choice of the used set of parameters.

3.1 EXPERIMENTAL SYSTEM

All the experiments shown in this chapter were carried out in the pilot plant described in Chapter 4. Temperature was controlled in R1 by an electric heating device, pH was controlled

in R1 and R2 by the addition of solid $NaHCO_3$ or Na_2CO_3 and DO was controlled in each reactor by a PID controller acting over the aeration valves. Different set-points for these parameters were used depending on the nitrite accumulation strategy (see Table 7.1). The strategy followed in Run 1 was to increase the volumetric nitrogen loading rate (NLR_v). In Run 2, the same strategy was applied but the DO in the reactors was lower. Finally, in the last run, the increase of NLR and low DO were applied together with an increase in the pH.

Table 7.1 Nitrite accumulation strategies and parameter set points in each run.

Experiment	Strategy	T	DO	pH
Run 1	NLR_v	23	3	7.5
Run 2	NLR_v+DO	23	1.25	7.5
Run 3	NLR_v+DO+pH	25	1.25	8.4

3.1.1 EXPERIMENTAL INFLOW CONTROL LOOP

The inflow control loop with the PI controller optimized and implemented in Chapter 6 was also used in these experiments. This control loop consisted of a feedback controller where the measured variable was the OUR in R3. Every 10 minutes, the averaged OUR value from the last 30 minutes was calculated and compared with the set point of OUR (OUR_{sp}). The final control action, performed every 30 minutes, was a change in the inflow value. This inflow control loop was implemented in a supervisory expert control system. For a more detailed explanation see section 3.1.2 in Chapter 6.

OUR_{sp} was changed throughout the experiment depending on the biomass activity. Each new set point value was determined in R3 with the addition of a total ammonia nitrogen (TAN) pulse (40 mg N L^{-1}). TAN pulse was completely depleted in a few hours and therefore it did not have much effect on the overall performance of the system. The study of the OUR profile of this TAN pulse enabled the determination of the suitable OUR_{sp} under the existing conditions. This will be extensively explained below.

3.1.2 MAXIMUM NITRIFICATION RATE DETERMINATION

The maximum ammonium oxidation rate (MAOR) and the maximum nitrite oxidation rate (MNOR) were periodically determined to check the activity of each kind of biomass. These activity assays were performed off-line in the respirometer, with biomass from the pilot plant, using LSS respirometry and specific inhibitors (ATU and azide) and under the same conditions than in the pilot plant.

Biomass was placed in the respirometer and the DO drop was measured (OUR_1), then, ATU (final concentration 10 mg L^{-1}) was added and the DO drop was measured again (OUR_2). Finally, sodium azide (final concentration 1.56 mg L^{-1}) was injected and OUR was measured (OUR_3). All OUR measurements were performed in triplicate and the average value was used. MAOR and MNOR were calculated as shown in equations 7.1 and 7.2, respectively,

$$MAOR = \frac{OUR_1 - OUR_2}{[VSS]\cdot(3.43 - Y_A)} \quad (7.1)$$

$$MNOR = \frac{OUR_2 - OUR_3}{[VSS]\cdot(1.14 - Y_N)} \quad (7.1)$$

where, [VSS] is the VSS concentration, 3.43 and 1.14 are the stoichiometric coefficients for oxygen in the nitritation and nitratation processes, respectively, and Y_A and Y_N are the growth yield coefficients for AOB and NOB, respectively.

3.2 MODELING

The kinetic and stoichiometric model built in Chapter 3 and the pilot plant model described in Chapter 4 were used for modeling purposes in this chapter. Parameters determined for acclimated sludge and the ones modified in Chapter 6 were used.

All simulations were performed with Matlab 6.5® (2002). The ode15s function, a variable order solver based on the numerical differentiation formulas, was used to solve the differential equations of the system balances.

3.3 ANALYSES AND FISH

TAN was analyzed by means of a continuous flow analyzer (CFA) based on potentiometric determination of ammonia (Baeza et al. 1999). Total nitrite nitrogen (TNN) and nitrate were measured with capillary electrophoresis using a WATERS Quanta 4000E CE. The used electrolyte solution was a WATERS commercial solution and the conditions of the analyses were 20ºC, 15 kV from a negative source, indirect UV detection at 254 nm and 6 min of analysis (Carrera et al. 2003). Volatile suspended solids (VSS), total suspended solids (TSS) and sludge volumetric index (SVI) were determined according to Standard Methods (APHA 1995).

Fluorescence *in situ* hybridization (FISH) technique coupled with confocal microscopy was used to determine the predominant nitrifying species. A Leica TCS SP2 AOBS confocal laser scanning microscope (CLSM) at a magnification of x63 (objective HCX PL APO ibd.B1 63x1.4 oil) equipped with two HeNe lasers with light emission at 561 and 633 nm was used for biomass quantification. The FISH technique and the quantification method were described in

Chapter 5 (section 3.3.4 and 4.1.2, respectively). Hybridizations were carried out using, at the same time, a Cy3-labeled specific probe and Cy5-labeled EUBmix probes. Specific probes used for AOB detection were Nso190, Nmo218, Nsv443 and NEU; and for NOB detection, were Ntspa662 and NIT3.

4. RESULTS

The experiments and simulations performed to achieve the proposed objectives are shown here. First of all, the experimental results of three start-ups of a partial nitrification system are shown. In each new experiment the environmental conditions were changed to improve the start-up strategy but in all of them the inflow control was activated to always apply the maximum NLR_v. Then, several disturbances were provoked to test the robustness of the controller and improve it with expert control rules. Finally, simulation tools were used to test the strategy of the partial nitrification system start-up under different environmental parameters and reactor configurations.

4.1 RUN 1: NITRITE ACCUMULATION BY CHANGING THE NLR_V

The first attempt to convert a complete nitrifying system into a partial nitrifying system was performed by increasing NLR_v without changing the environmental conditions. The idea was to get an effluent with low TAN and nitrate concentration and maximum TNN concentration.

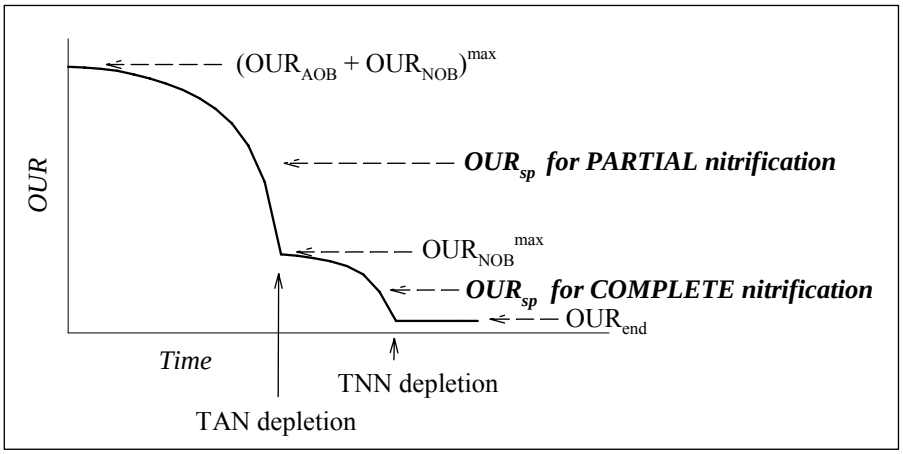

Figure 7.1 OUR profile of a theoretical batch ammonium pulse. Theoretical optimum OUR_{sp} for complete and partial nitrification.

The NLR_v rise was not based on a specific reduction of the HRT; it was based on increasing the OUR_{sp} and let the inflow control loop increase the inflow accordingly. The key point of this strategy was the choice of an appropriate OUR_{sp}. When a completely nitrifying system was

preferred, the OUR_{sp} was fixed at a value in between the endogenous OUR (OUR_{end}) and the maximum OUR of the nitratation process (OUR_{NOB}^{max}) (see Chapter 6). In order to change the conditions and get an effluent composition of low TAN and nitrate concentrations but high TNN concentration, the OUR_{sp} was fixed to a value in between the maximum OUR of the whole process ($(OUR_{AOB}+OUR_{NOB})^{max}$) and the maximum OUR of the nitratation process (OUR_{NOB}^{max}). Figure 7.1 shows a simulated OUR profile of a TAN pulse in one reactor in batch mode and the theoretical optimal set points to achieve complete or partial nitrification.

The experiment shown in this section was performed 2 months after the end of start-up III (shown in Chapter 6, section 4.4). During the first of these two months, several ammonium and nitrite pulses were added to the reactors to determine some kinetic parameters in batch mode. During the second month, the system was continuously operated for complete nitrification with the automatic inflow control activated and a very low OUR_{sp} ($8 \cdot 10^{-4}$ mg O_2 L^{-1} s^{-1}). Then, a new OUR_{sp} ($1.35 \cdot 10^{-2}$ mg O_2 L^{-1} s^{-1}) was determined with a batch experiment similar to the one shown in Figure 7.1 and the experiment called Run 1 began. Operation conditions in this experiment are shown in Table 7.2. pH, temperature and DO were steady during the experiment. The same internal recirculation flow (F_{IR}) as in Chapter 6 was used to increase the system dynamics in order to be able to perform inflow control. The averaged inflow composition was 3600 mg N-TAN L^{-1} and 360 mg COD L^{-1}.

Table 7.2 Experimental operation conditions in Run 1.

pH	Temperature	DO	SRT	HRT	F_{IR}	F_{ER}
7.6 ± 0.2	23 ± 1 ºC	3.0 ± 0.2 mg O_2 L^{-1}	30 d	5 d	300 L d^{-1}	53 L d^{-1}

In all the figures of this section, the previous week to the beginning of the nitrite accumulation strategy was also shown. The beginning of the strategy took place on day zero and is indicated with a dashed line.

Figure 7.2.A shows the OUR profile of each reactor and the OUR_{sp} in R3 recorded during Run 1. The new set point was quickly reached due to the fast response of the controller which increased the inflow from 5 to 15 L d^{-1} (see Figure 7.2.B). If the OUR values before and after the beginning of the nitrite accumulation strategy are compared, it can be seen that the system was under-loaded for time < 0 d because the OUR values in R1 and R2 were below the maximum value. For time > 0 d, the OURs in R1 and R2 were maxima and the OUR in R3 was half the maximum. Figure 7.2.B shows the specific nitrogen loading rate (NLR_s), the inflow and the VSS concentration. In both OUR and inflow profiles, eight periods with zero inflow can be identified from day 0 to day 40. They correspond to the system stops which occurred at night or in the weekend because of pump failures or dampness detection errors and could not be solved immediately. The stops length added up to 3.6 d (9 % of the entire experiment length). The NLR_s increased at the same rate than the inflow, to be exact, from 0.2 to an averaged value of 0.5 g N g^{-1} VSS L^{-1}. Both parameters remained quite constant during the

experiment. On the other hand, the biomass concentration was 1020 ± 80 mg VSS d^{-1} and the TSS concentration in the effluent were 230 ± 90 mg TSS L^{-1}.

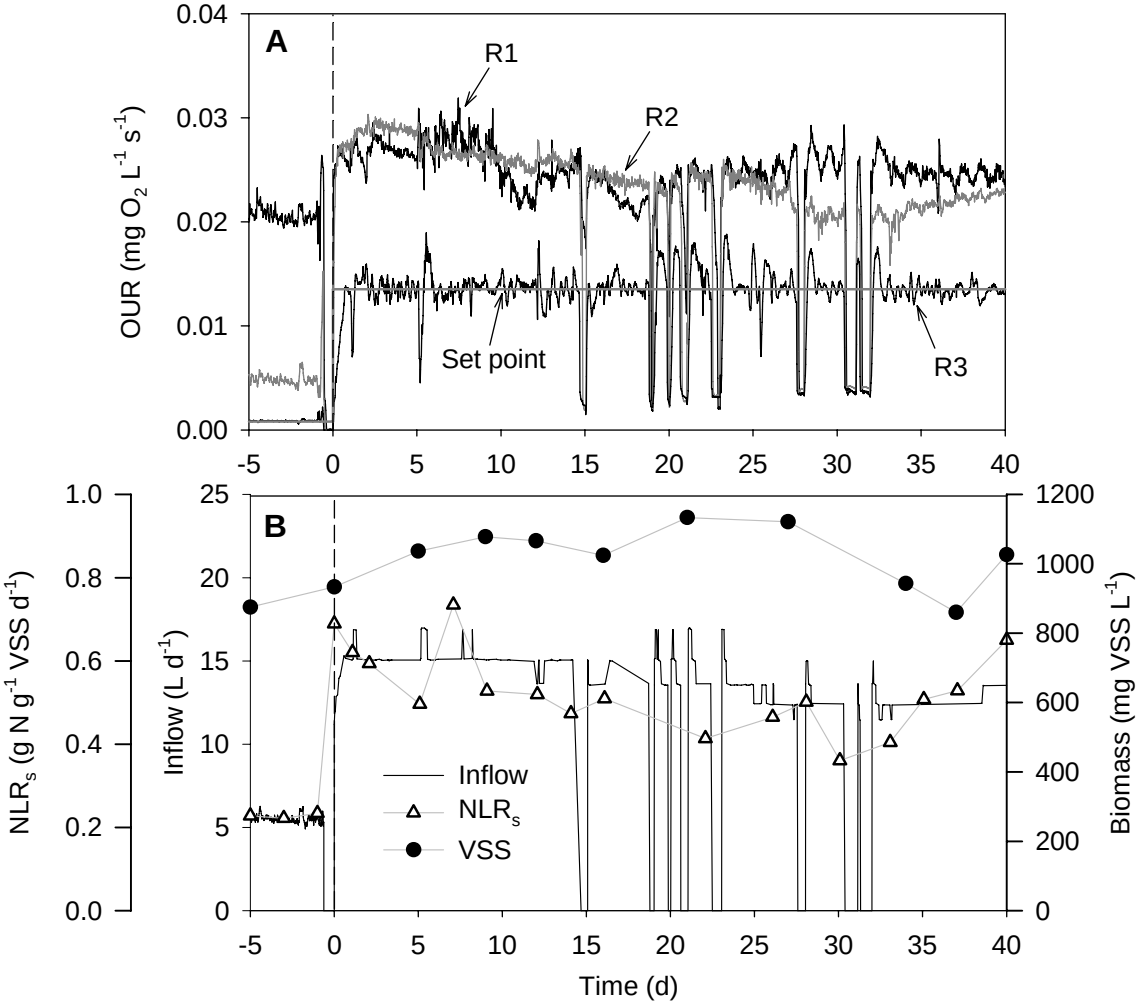

Figure 7.2 Run 1. **A.** OUR profile in each reactor and OUR_{sp}. **B.** NLR_s, inflow and VSS concentration. Dashed line indicates the beginning of the nitrite accumulation strategy.

Time course of TAN, TNN and nitrate are shown in Figure 7.3. TAN concentration in each reactor was shown (Figure 7.3.A) but TNN and nitrate concentrations were only shown for R3 (Figure 7.3.B) since they were similar in the all reactors. The system was completely nitrifying at the beginning but when the new OUR_{sp} was reached, TNN immediately started to build-up. TNN accumulation rate was steady until day 15 when it started to slow down until day 33; then, TNN concentration remained stable at around 1350 mg N L^{-1}. The maximum TNN/NO_x ratio (TNN/(TNN+nitrate)), reached on day 22, was 0.57 and it was 0.4 at the end of the experiment. The reactors configuration (in series) provoked a gradient of TAN concentration through the reactors. Therefore, FA concentration was also different, with averaged values of 1.7 ± 0.5, 0.5 ± 0.1 and 0.04 ± 0.02 mg FA L^{-1} for R1, R2 and R3, respectively. The maximum FNA concentration was 0.44 mg FNA L^{-1}, corresponding to 2220 mg N-TNN L^{-1}.

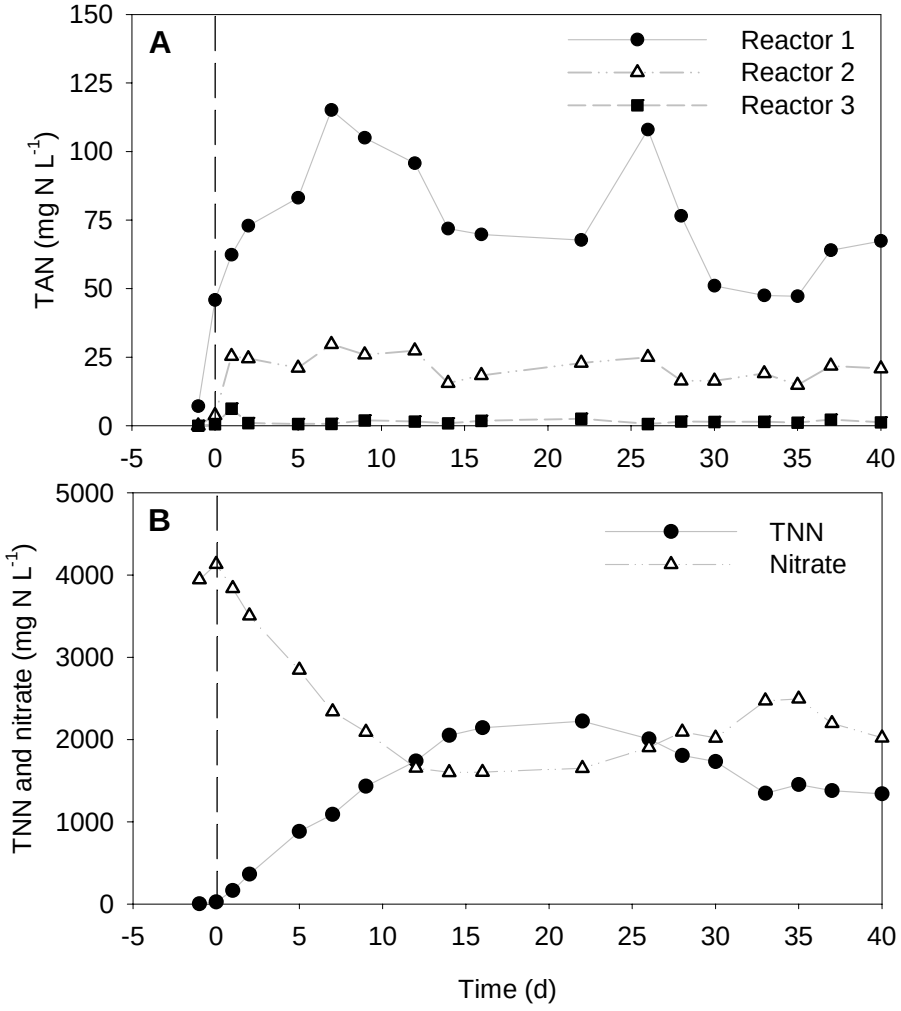

Figure 7.3 Nitrogenous compounds concentration in Run 1. **A.** TAN in each reactor. **B.** TNN and nitrate in R3 (the same concentrations existed in R1 and R2). Dashed line indicates the beginning of the nitrite accumulation strategy.

Table 7.3 MAOR and MNOR obtained with off-line LSS respirometry in Run 1.

Day	MAOR (g N-TAN g^{-1} VSS d^{-1})	MNOR (g N-TNN g^{-1} VSS d^{-1})	MAOR / MNOR	TNN/NO_x
14	0.49 ± 0.09	0.12 ± 0.01	4.1	0.57
34	0.47 ± 0.03	0.19 ± 0.01	2.5	0.40

MAOR and MNOR were determined on days 14 and 34 (Table 7.3) when the TNN accumulation rates were positive and zero, respectively (see Figure 7.3). Both rates were calculated under the same conditions than in R2 (pH, DO, temperature, TNN and TAN concentrations) to avoid FA inhibition to AOB and NOB and also to avoid low nitritation rate due to low TAN. The MAOR did not change significantly from day 14 to day 34, whereas the MNOR increased in a 58 %. The ratio between them decreased from 4.1 to 2.5 and as a result, the nitrite accumulation rate slowed down.

The experiment was stopped on day 40 because the goal of total partial nitrification was not achieved under the studied conditions, although a significant nitrite accumulation occurred.

4.2 RUN 2: NITRITE ACCUMULATION AT LOW DO BY CHANGING THE NLR_V

The second strategy to achieve nitrite accumulation was the operation under low DO concentration and the use of the automatic inflow control with the appropriate OUR_{sp}. Thus, this strategy was called NLR_v +DO.

The new DO concentration was chosen in accordance with the experimentally determined affinity constants for DO: $K_{O,A}$ = 0.74 mg O_2 L^{-1} and $K_{O,N}$ = 1.75 mg O_2 L^{-1} (see Chapter 3). The percentages of MAOR and MNOR achieved at different DO concentrations using these values and assuming no other limitations were simulated (see Figure 7.4). This figure shows that the optimal point for nitrite accumulation would be the DO concentration in which both rates are more different. The optimal point corresponds to 1.1 mg O_2 L^{-1} which is indicated in the figure with a double arrow. Because of this theoretical study, the DO set point was fixed at 1.1 mg O_2 L^{-1} in R1 and R2, and the in-line OUR determination was deactivated in these reactors since the applied methodology was not reliable under these conditions. However, as the in-line OUR estimation was needed in R3 for the automatic inflow control, it was not deactivated in this reactor and the DO was set to 2 mg O_2 L^{-1} for a properly OUR assessment. From the same simulation, it can be predicted that the nitritation and nitratation rates will diminish in 25 and 38 %, respectively if the DO is changed from 3 to 1.1 mg O_2 L^{-1}.

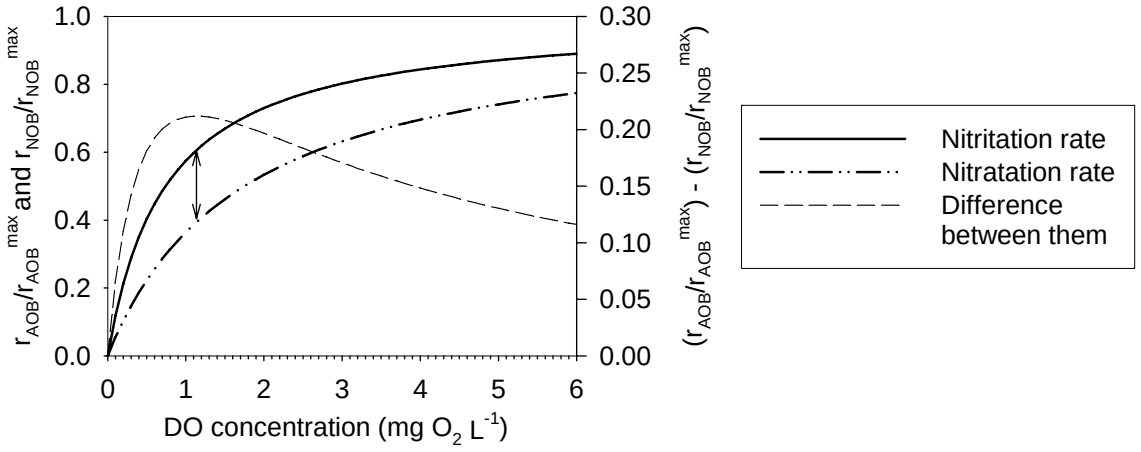

Figure 7.4 Simulation of the nitritation and nitratation rates as a function of DO concentration and the calculated difference between them. The double arrow indicates the largest difference.

When the nitrite accumulation strategy NLR_v +DO (experiment named Run 2) started, the pilot plant had been operating for a month as a complete nitrification system with an OUR_{sp} of

$7.3 \cdot 10^{-3}$ mg O_2 L^{-1} s^{-1} and DO set points of 1.1, 1.1 and 2 mg L^{-1} in each reactor. On day zero, the OUR_{sp} was increased to $1.8 \cdot 10^{-2}$ after the analysis of a batch OUR profile. Experimental operation conditions in Run 2 are shown in Table 7.4. Temperature, pH and DO were steady during the experiment and the averaged inflow composition was 2720 mg N-TAN L^{-1} and 270 mg COD L^{-1}.

Table 7.4 Experimental operation conditions in Run 2.

pH	Temperature	DO	SRT	HRT	F_{IR}	F_{ER}
7.5 ± 0.3	22 ± 1 ºC	R1: 1.2 ± 0.1 mg O_2 L^{-1} R2: 1.2 ± 0.1 mg O_2 L^{-1} R3: 1.9 ± 0.3 mg O_2 L^{-1}	30 d	3 - 5 d	300 L d^{-1}	58 L d^{-1}

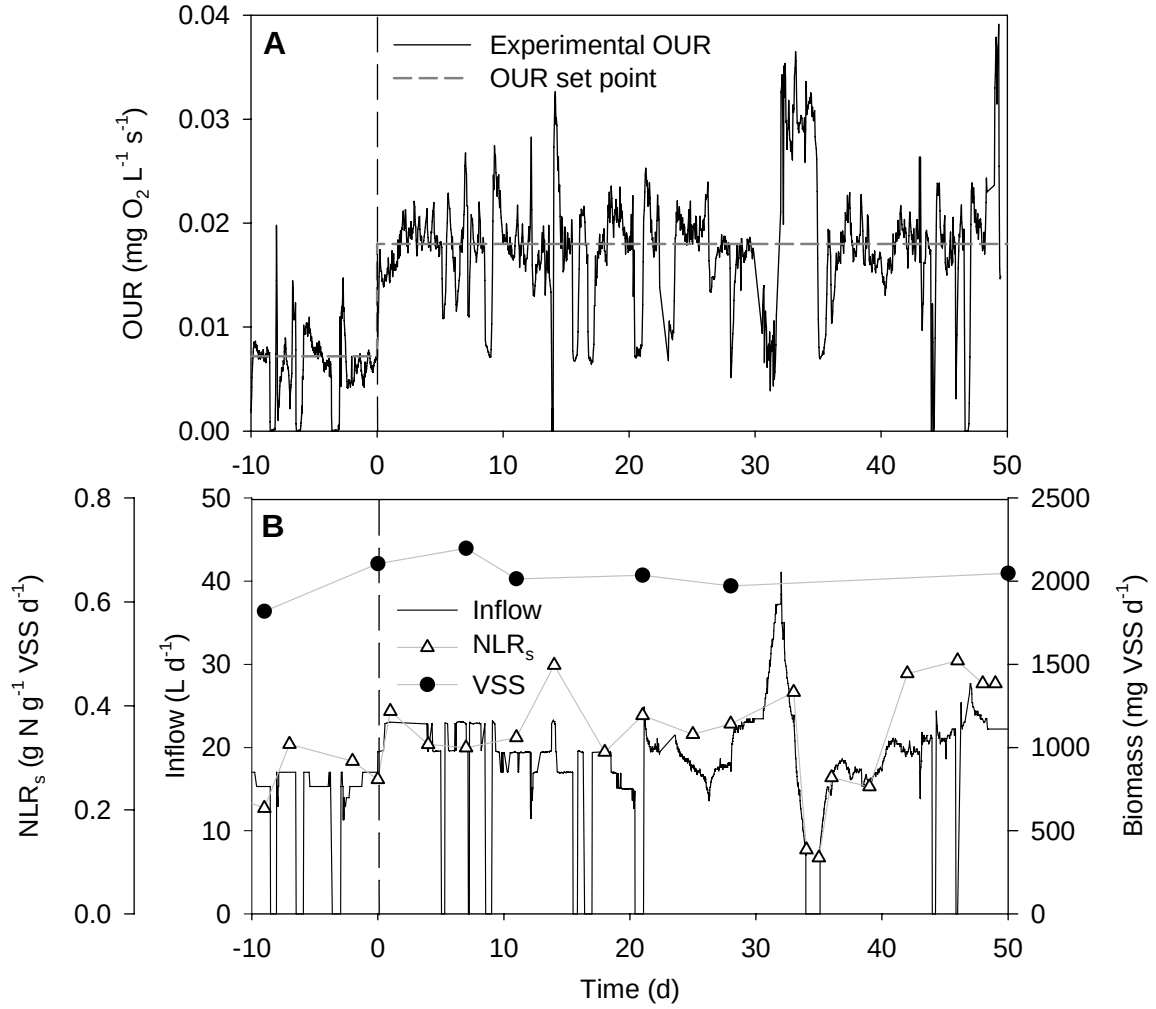

Figure 7.5 Run 2. **A.** OUR profile and OUR_{sp} in R3. **B.** NLR_s, inflow and VSS concentration. Dashed line indicates the beginning of the nitrite accumulation strategy.

Figure 7.5.A shows the OUR measurements and OUR_{sp} in R3 through the experiment. In Figure 7.5.B, inflow, NLR_s and biomass concentration are depicted. Biomass concentration

was quite steady, with an averaged value of 2050 ± 90 mg VSS L^{-1}. TSS in the effluent were 180 ± 40 mg TSS L^{-1}. The inflow profile shows 3 stops for time < 0 d and 9 stops for time > 0 d. Except for the long stop around day 35, the others were due to system failures like the ones explained in the previous section. The stops occurred from day 0 to day 34 added up to 1.7 d, which was a 5 % of the total time. All these stops can also be detected in Figure 7.5.A because they look like sharp valleys in the OUR profile. The minimum OUR reached when the system stopped depended on the presence or absence of TNN in the system (see also Figure 7.6.B). If there was not TNN, the minimum OUR was almost zero (OUR_{end}), but if TNN was present, the minim value was OUR_{NOB}^{max}.

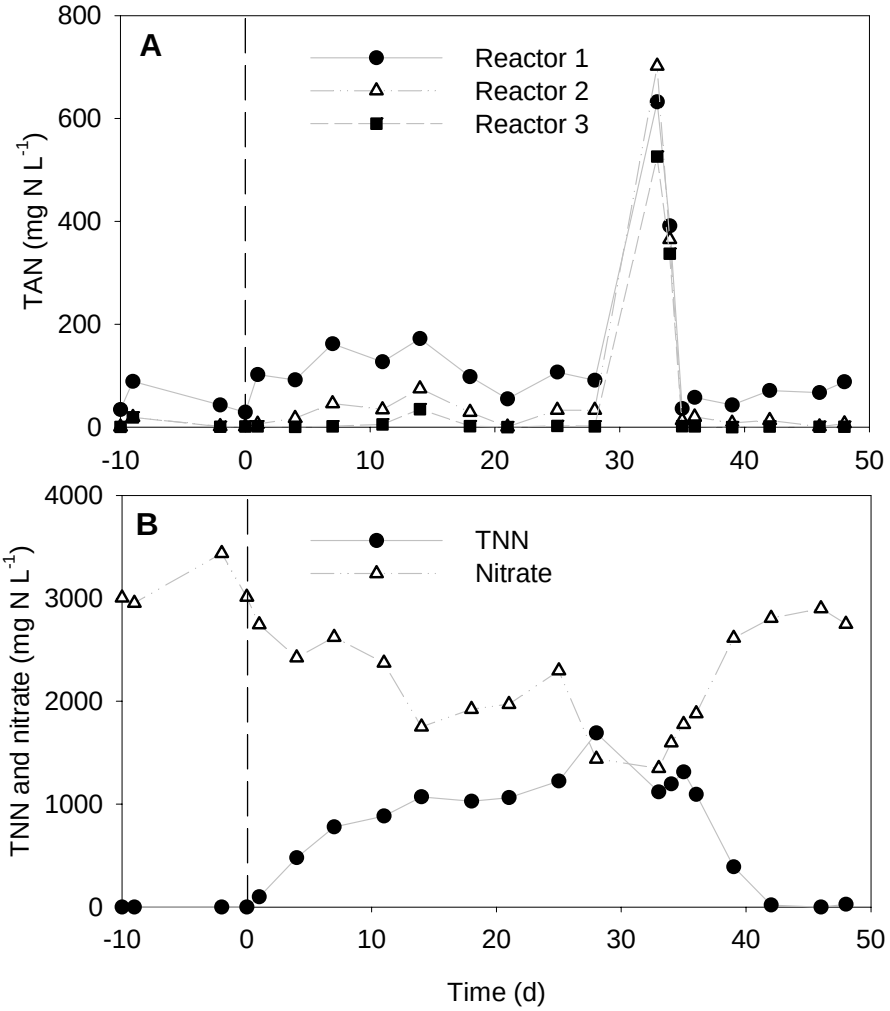

Figure 7.6 Nitrogenous compounds concentration in Run 2. **A.** TAN in each reactor. **B.** TNN and nitrate in R3 (the same concentrations existed in R1 and R2). Dashed line indicates the beginning of the nitrite accumulation strategy.

Time course of TAN, TNN and nitrate are shown in Figure 7.6. Figure 7.6.A shows TAN concentration in each reactor and Figure 7.6.B shows TNN and nitrate concentrations only in

R3 since they were similar in the three reactors. Nitrogenous compounds before the beginning of the nitrite accumulation strategy indicated that the pilot plant was operating as a completely nitrifying system. When OUR_{sp} was changed, TNN started to build-up and it accumulated until day 28 when it reached 1700 mg N L^{-1}. On day 30 (Saturday morning), the DO probe of R3 stopped working properly and the in-line OUR measurements were underestimated. This provoked that the automatic controller increased dramatically the inflow value and that TAN built up. One and a half days latter, the DO probe was replaced and the inflow was decreased by the automatic controller. Since the inflow reduction rate was too slow, it was decided to stop feeding the system to accelerate TAN depletion. The highest TAN measurement (700 mg N L^{-1}) was detected on day 33 in R2 but it was totally consumed on day 35. After this incident, the system was operated under the same conditions as it was being operated previously but the accumulated TNN started to decrease until complete nitrification was reached again. The capacity of nitrite build-up was lost after the incident. In this experiment, the maximum TNN/NO_x ratio was 0.54 and the maximum FNA concentration was 0.44 mg FNA L^{-1}. With respect to FA concentration, the averaged values in R1, R2 and R3 before the incident were 1.8 ± 0.8, 0.5 ± 0.4 and 0.1 ± 0.2 mg FA L^{-1}, respectively. The maximum FA concentration during the incident was 12.5 mg FA L^{-1}.

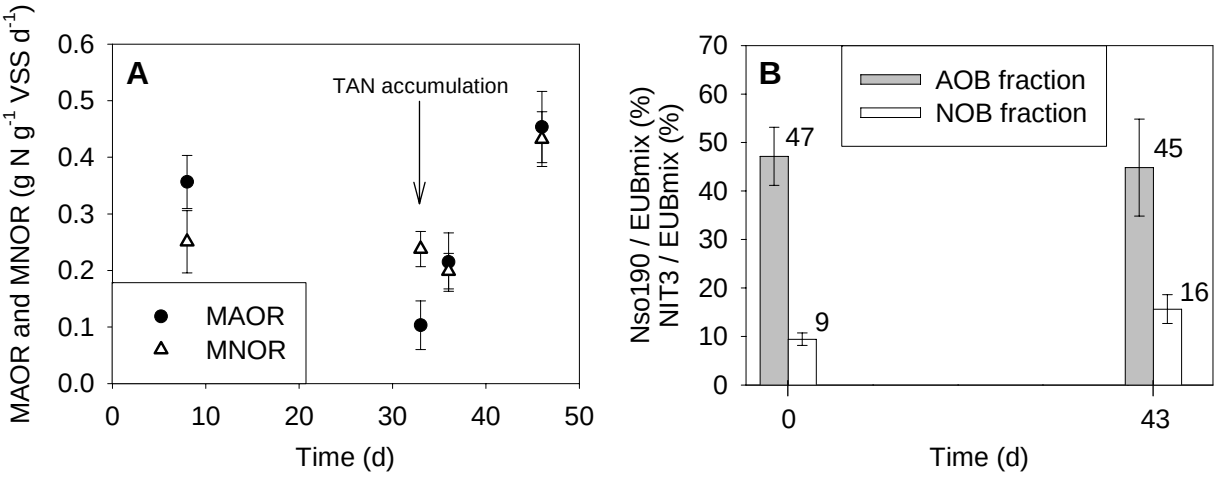

Figure 7.7 Run 2. **A.** MAOR and MNOR obtained with off-line respirometry. The arrow indicates the samples withdrawn when high TAN accumulation occurred. **B.** AOB and NOB fractions determined with FISH.

MAOR and MNOR were determined throughout the experiment by using off-line respirometry. These determinations were performed at the same pH and temperature than in the pilot plant and at 1.1 mg O_2 L^{-1}. The TNN was the same than it the system but the ammonium was around 30-60 mg N L^{-1} for MAOR determination (similar to the TAN concentration in R2) and less than 10 mg N L^{-1} for MNOR determination (similar to the TAN concentration in R3) to avoid FA inhibition. On day 33, both MAOR and MNOR were determined with the same TAN concentration than it was in the pilot plant (≈ 600 mg N L^{-1}) to ascertain the influence of TAN build-up on both populations. These results are shown in Figure 7.7.A. At the beginning

of the experiment MAOR was higher than MNOR and thus nitrite accumulated. On day 33, when TAN was accumulated, AOB were more inhibited than NOB. Even when TAN was completely depleted (day 35) both rates were lower than they were at the beginning, showing some inhibitory effect on their activities. As a consequence, the admitted inflow was less than it was before the incident. At the end of the experiment, both activities recovered and increased with respect to the beginning of the experiment and thus the inflow was also increased by the automatic controller. However, both rates were similar and thus nitrite accumulation did not occur.

Figure 7.7.B shows AOB and NOB fractions estimated by using FISH of samples withdrawn on days 0 and 43. AOB were detected with probe Nso190 while negative results were obtained with probes Nmo218 and Nsv443. AOB fraction with respect to biomass detected with probe EUBmix did not change significantly throughout the experiment. NOB were detected with probe NIT3 and not with probe Ntspa662. The obtained NOB fraction at the end was almost twice the fraction at the beginning.

On day 0, the fixed sample was hybridized also with proves NEU and EUBmix. The calculated fraction of biomass was 46 ± 7 %. If this value is compared with the 47 ± 6 % obtained with proves Nso190 and EUBmix, it can be concluded that all the existing AOB corresponded to the halophilic and halotolerant members of the genus *Nitrosomonas* together and/or to *Nitrosococcus mobilis* (Wagner et al. 1995).

4.3 RUN 3: NITRITE ACCUMULATION AT LOW DO AND HIGH pH BY CHANGING THE NLR_V

The last strategy applied to the system was based on the previous strategies and furthermore it included the rise of the pH to increase the FA concentration and thus inhibit NOB activity. Therefore, the DO was maintained low (≈ 1.1 mg O_2 L^{-1} in R1 and R2 and ≈ 2.0 mg O_2 L^{-1} in R3), the pH was increased (from 7.5 to 8.3) and the inflow controller was activated with the appropriate OUR_{sp}. The increase in the pH was performed stepwise to avoid AOB inhibition. In this case, the strategy was called NLR_v +DO+pH.

Table 7.5 Experimental operation conditions in Run 3.

Temperature	SRT	HRT	F_{IR}	F_{ER}
25 ± 1 ºC	30 d	1.6 – 9.0 d	300 L d^{-1}	58 L d^{-1}

This experiment (Run 3) began just after the end of Run 2, i.e. day 50 in Run 2 corresponds to day 0 in Run 3. On that day, a new OUR_{sp} ($2.3 \cdot 10^{-2}$ mg O_2 L^{-1} s^{-1}) was determined and applied. The experimental operation conditions in Run 3 are shown in Table 7.5 and Table 7.6. The averaged inflow composition was 2870 mg N-TAN L^{-1} and 290 mg COD L^{-1}.

Table 7.6 Experimental pH and DO in Run 3.

pH				DO (mg O_2 L^{-1})			
Period (d)	Reactor 1	Reactor 2	Reactor 3	Period (d)	Reactor 1	Reactor 2	Reactor 3
0 - 20	7.5 ± 0.2	7.6 ± 0.2	7.5 ± 0.3	0 -137	1.2 ± 0.2	1.4 ±0.2	1.9 ± 0.4
20 – 38	7.9 ± 0.1	8.4 ± 0.1	8.2 ± 0.2	137 - 223	1.9 ± 0.1	2.0 ± 0.2	1.9 ± 0.3
38 -223	8.3 ± 0.2	8.3 ± 0.4	8.3 ± 0.4				

In the 223 days that this experiment lasted, partial nitrification was achieved and maintained. Furthermore, on day 160, several disturbances were applied to the system in order to test and improve the automatic control. Although the disturbances will be extensively explained in section 4.4, the results are also shown here to demonstrate the achieved stability of the partial nitrification sytem.

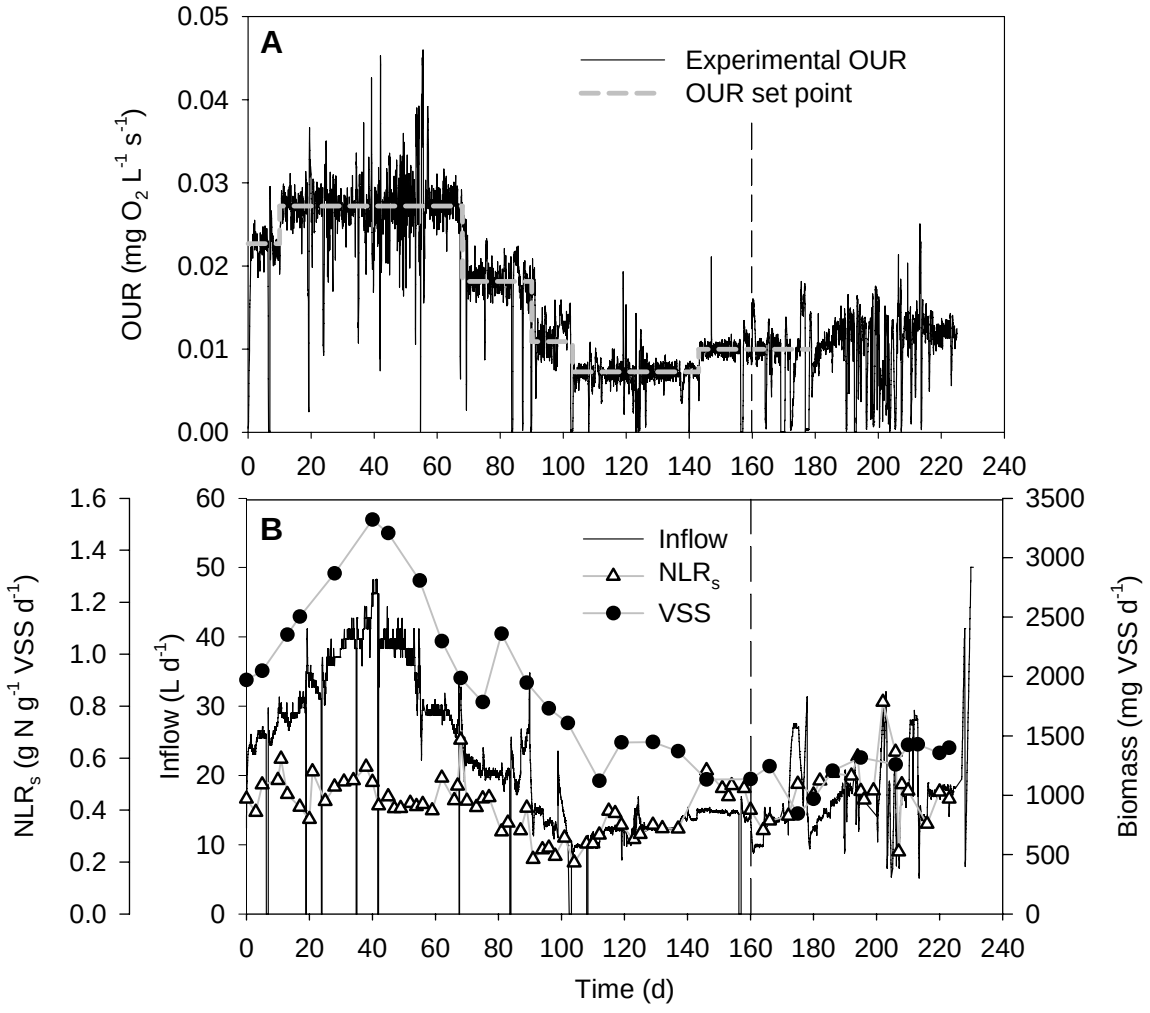

Figure 7.8 Run 3. **A.** OUR profile and OUR set point in R3 **B.** NLR_s, inflow and VSS concentration. Dashed line indicates the beginning of the period with provoked disturbances.

Figure 7.8.A shows the time course for the OUR in R3 and the OUR_{sp} which changed between $7 \cdot 10^{-3}$ and $2.7 \cdot 10^{-2}$ mg O_2 L s^{-1}. This wide range was due to two main reasons. The first one is related to the biomass concentration because the OUR is proportional to its value. Figure 7.8.B

shows that the biomass concentration increased from 2000 to 3500 and then it decreased to 1500 mg VSS L^{-1}. These changes provoked the need of variable OUR_{sp}. The second reason is the achievement of the partial nitrification and NOB inhibition that changed the contribution of AOB and NOB in the measured OUR. This will be explained below. Figure 7.8.B also shows that while the inflow profile followed the same trend as the biomass concentration, the NLR_s remained quite steady: 0.4 ± 0.1 g N g^{-1} VSS d^{-1}. The TSS concentration in the effluent was 130 ± 30 mg TSS L^{-1}. Also in Run 3, some problems occurred which provoked ten short stops in the system in the first 160 days of operation (2.7 % of the time).

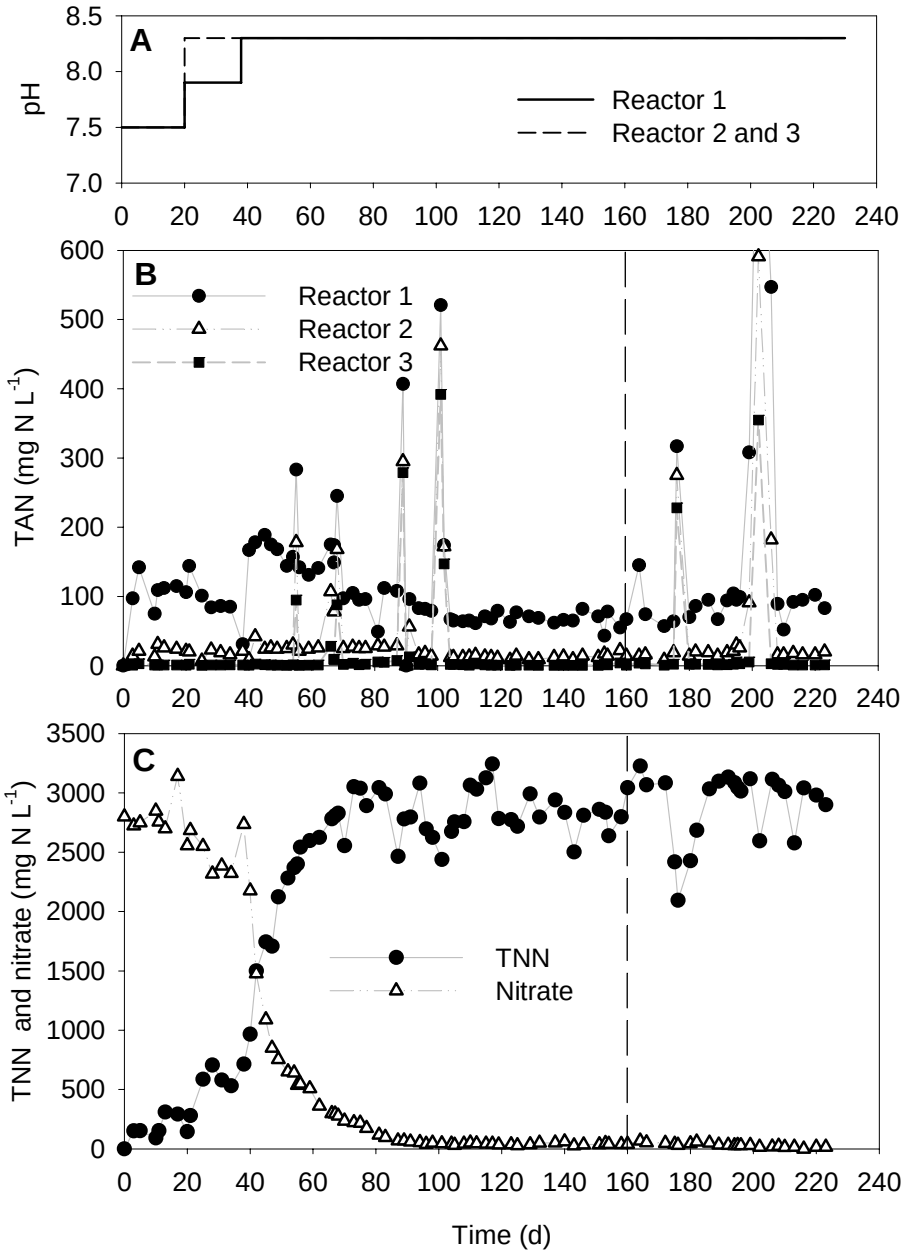

Figure 7.9 Run 3. **A.** pH profile in each reactor. **B.** TAN concentration in each reactor. **C.** TNN and nitrate concentrations in the third reactor (the same concentrations existed in R1 and R2). Dashed line indicates the beginning of the period with provoked disturbances.

Time course for TAN in each reactor is depicted in Figure 7.9.B. TAN was totally depleted in the system except for the periods with accumulation. Figure 7.9.C shows the TNN and nitrate concentrations in R3 (data for R1 and R2 are not shown because they were similar to those in R3). TNN build-up was totally related to the pH increases (see Table 7.6 and Figure 7.9.A). On day 0, OUR_{sp} was changed and TNN increased up to 300 mg N L^{-1}. On day 20, the pH was raised to 8.3 in R2 and R3 and to 7.9 in R1. This pH change did not affect TAN concentration but TNN concentration in the system increased to 700 mg N L^{-1}. However, TNN tended to decrease and therefore, pH in R1 was also raised to 8.3 mg N L^{-1}. This last change provoked an increase in the TAN in R1 and was the definitive change to inhibit NOB activity and achieve total partial nitrification. On day 100, TNN/NO_x ratio was 0.99, and it was maintained unchanged until the end of the experiment (day 223). TAN concentration on day 40 reached 190 mg N L^{-1} (23.5 mg FA L^{-1}) and it progressively decreased to 60-70 mg N L^{-1} (7.4 – 8.7 mg FA L^{-1}), however, it did not cause the recovery of NOB activity.

On the other hand, DO concentration in R1 and R2 was increased up to 2 mg O_2 L^{-1} on day 137. This caused a slight increase of the applied NLR_s but it did not diminish the degree of nitrite build-up.

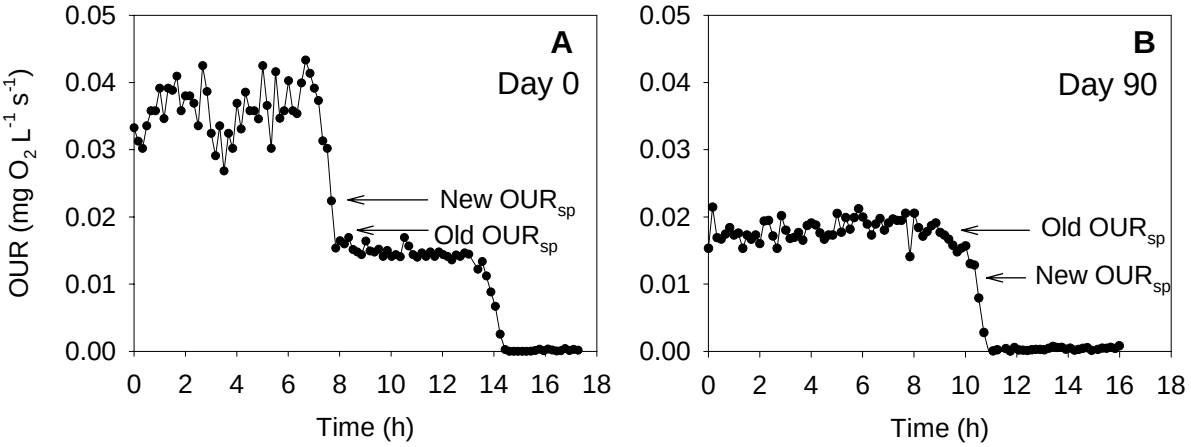

Figure 7.10 OUR profile in R3 in several OUR_{sp} determinations. Arrows indicate the current OUR_{sp} (Old OUR_{sp}) and the newly determined value (New OUR_{sp}). **A.** Day 0. **B.** Day 90.

Figure 7.10.A shows the experimental profile of the OUR in R3 before the beginning of Run 3 (day 0). At that time, some TAN had build-up and the system had been stopped until it was totally depleted. The OUR profile was used to determine a better OUR_{sp} to be used from that moment onward. As previously explained and showed in Figure 7.1, the set point should be in between $(OUR_{AOB}+OUR_{NOB})^{max}$ and OUR_{NOB}^{max} if nitrite accumulation is desired. Therefore, on day 0, the OUR_{sp} was increased from $1.8 \cdot 10^{-2}$ mg O_2 L^{-1} s^{-1} to $2.3 \cdot 10^{-2}$ mg O_2 L^{-1} s^{-1}. Since the biomass concentration changed considerably in the first 80 days of the experiment, the OUR_{sp} had to be changed accordingly. For example, on day 68, the biomass concentration had decreased in a way that the current OUR_{sp} was not longer suitable and TAN accumulated (see Figure 7.9.B). The feeding was stopped until TAN was depleted and the obtained OUR profile

was used to set another value. On day 90, even though the biomass concentration was similar than that on day 68, TAN built up. On this occasion, the OUR profile of the TAN depletion in R3 showed a completely different shape (Figure 7.10.B) because NOB activity was negligible. Therefore, OUR_{sp} was set in between OUR_{AOB}^{max} and the minimum OUR experimentally measurable; it was set to $1.1 \cdot 10^{-2}$ mg O_2 L^{-1} s^{-1}. TAN accumulation periods which occurred before day 160 demonstrated the need of a systematic and periodic OUR_{sp} determination.

Figure 7.11 shows a different way of determining the OUR_{sp} (corresponding to day 143) for the case when the system is operating under steady conditions with very low TAN concentration in the effluent. In this case, a pulse of 100 mg N-TAN L^{-1} was added to the third reactor that enabled the measurement of OUR_{AOB}^{max}. This amount of TAN was quickly depleted and did not affect too much the overall performance of the system. The automatic controller rapidly actuated and the current OUR_{sp} (old OUR_{sp}) was immediately reached. After analyzing the OUR profile, a new OUR_{sp} was determined and then it was manually introduced in the controller.

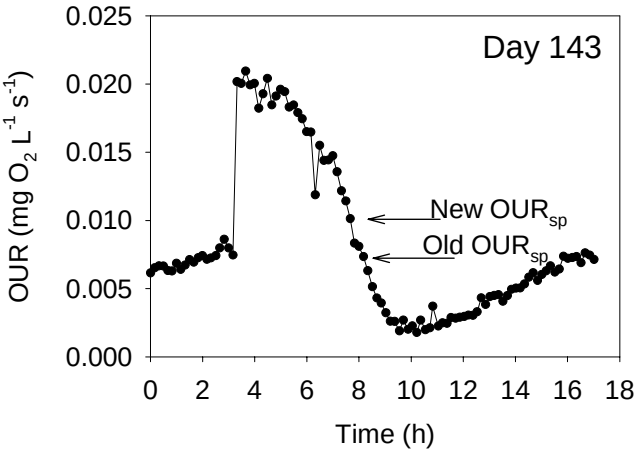

Figure 7.11 OUR profile in R3 for a new OUR_{sp} determination on day 143. Arrows indicate the current OUR_{sp} (Old OUR_{sp}) and the newly determined value (New OUR_{sp}).

The NLR_v +DO+pH strategy was useful to achieve and maintain nitrite build-up for more than 100 days. The key factor was the high inhibition of NOB activity and the following decrease in the NOB concentration. Figure 7.12.A shows the time course for MAOR and MNOR. MNOR was really impaired when the pH was increased and it declined until day 90, when it was negligible. Figure 7.12.B shows the results obtained with the FISH technique. Quantification results using probes NIT3 and EUBmix demonstrated that the washout of the NOB took place from the beginning of the experiment. From day 110 on, NOB were undetectable using this technique. On the other hand, AOB activity also decreased due to the raise in the pH but their activity remained around 0.2 – 0.3 mg N mg^{-1} VSS d^1 when the partial nitrification was achieved. AOB fraction, detected with proves Nso190 and EUBmix, increased due to the

decrease of NOB fraction. The averaged amount of nitrifiers until day 160 was 65 ± 3 %. The AOB fraction measured on day 194 was lower than the averaged fraction probably because of the severe disturbances affecting the system.

On day 153, the reactor sample was hybridized also with proves NEU and EUBmix. The fraction was calculated as 69 ± 10 %. If this value is compared with the 65 ± 13 % obtained with proves Nso190 and EUBmix, it can be concluded that all the AOB detected with Nso190 were also detected with probe NEU which is specific for halophilic and halotolerant members of the genus *Nitrosomonas* together with *Nitrosococcus mobilis* (Wagner et al. 1995).

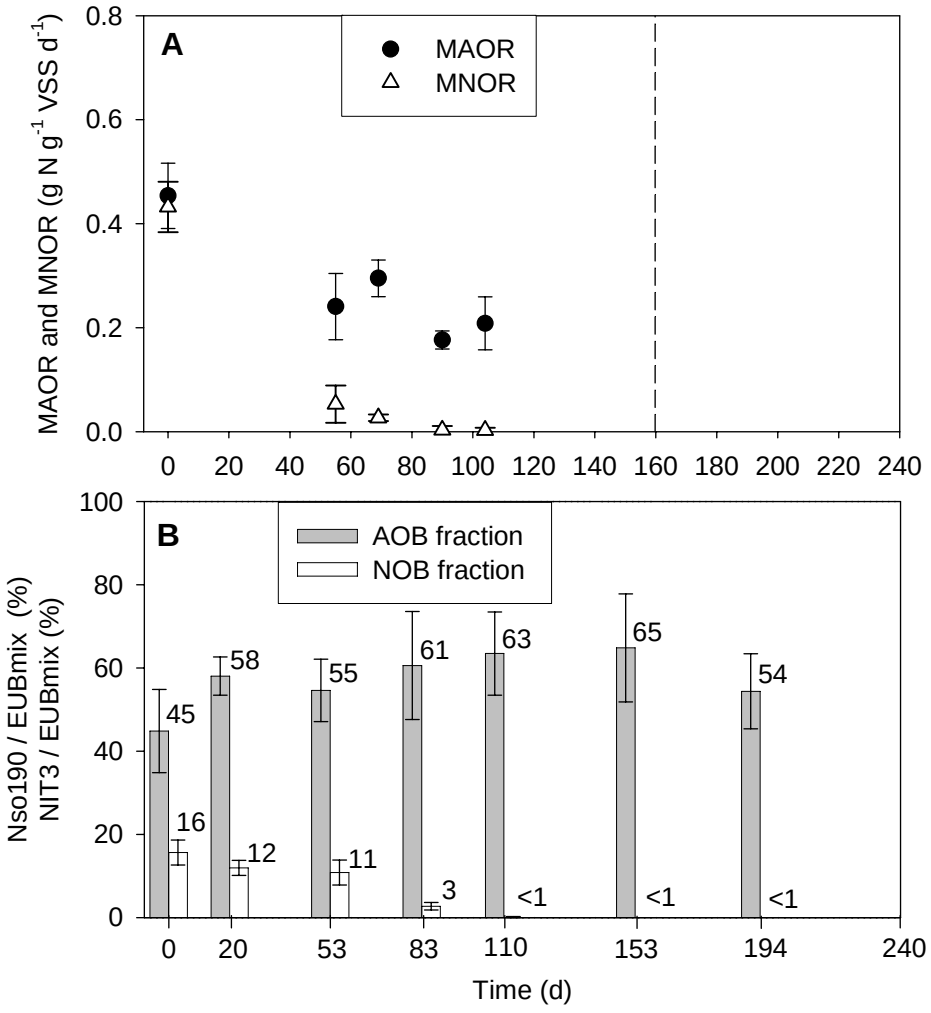

Figure 7.12 Run 3. **A.** MAOR and MNOR measured with off-line respirometry. Dashed line indicates the beginning of the period with provoked disturbances. **B.** AOB and NOB fractions determined with FISH.

Figure 7.13 shows representative images of the changes of the biomass composition in which it is clearly demonstrated that the NOB were washed out.

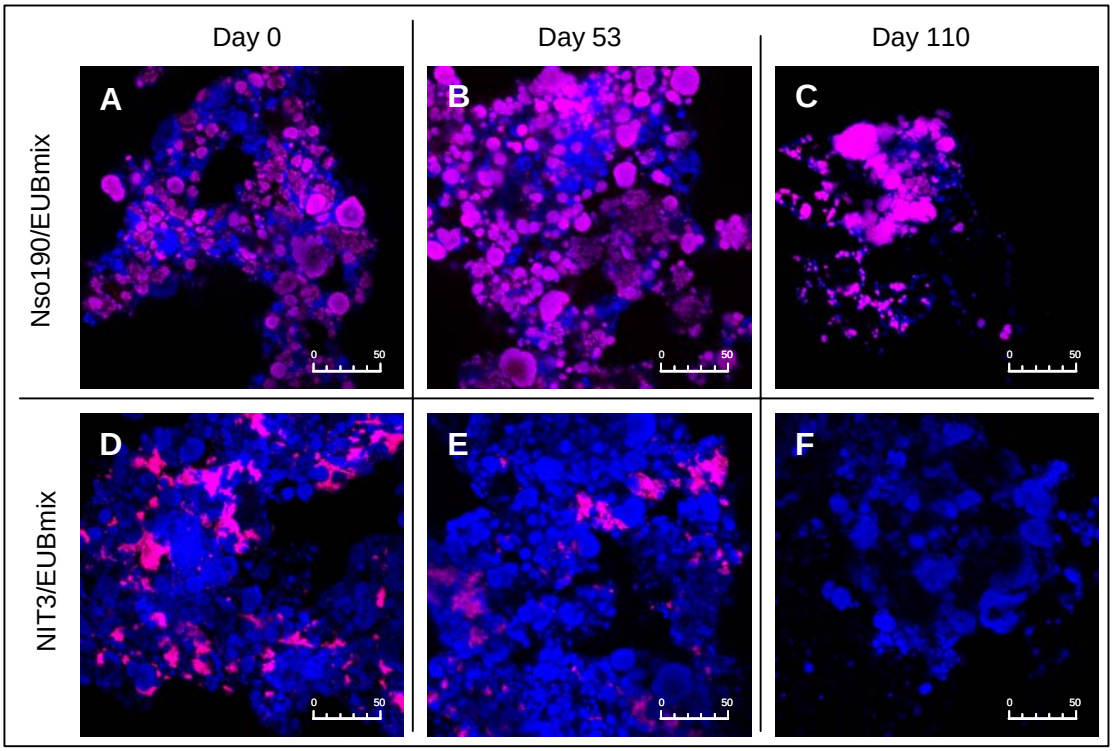

Figure 7.13 FISH/CLSM representative images of the sludge in Run 3. Specific probe is shown in pink and EUBmix probes in blue. Nso190 and EUBmix on day 0 (**A**), on day 53 (**B**) and on day 110 (**C**).NIT3 and EUBmix on day 0 (**D**), on day 53 (**E**) and on day 110 (**F**). Bar = 50 μm.

4.4 CONTROL LOOP RESPONSE IN FRONT OF EXTERNAL DISTURBANCES AND IMPROVEMENT OF THE CONTROL SYSTEM

Until day 160, the pilot plant had been operating in a very stable way as a partial nitrification system with an effluent free of TAN and a TNN/NO_x around 0.99. From that day onward, five external disturbances where applied to test the robustness of the automatic inflow controller and to improve it, if necessary. Table 7.7 summarizes the main characteristics and results of the disturbances.

Table 7.7 Description of the applied disturbances, experiment length and controller performance.

#	Disturbance	Length	Result
1	Aerobic volume reduction	7 d	Good control
2	Oscillatory influent TAN concentration: 3000 → 1500 → 3000 mg N L^{-1}	8.5 d	TAN build-up: need of controller improvement
3	Oscillatory influent TAN concentration: 3000 → 2000 → 4000 → 3000 mg N L^{-1}	10 d	Good control*
4	Variable temperature	4 d	Good control*
5	Variable temp. and biomass concentration	9 d	Good control*

* Using the controller improvements designed after disturbance 2.

4.4.1 DISTURBANCE 1: AEROBIC VOLUM REDUCTION

The first disturbance applied to the partial nitrification system was a reduction of the aerobic volume to ⅔ of its total volume by setting the DO set point in R2 to 0 mg O_2 L^{-1}. This disturbance was designed to simulate a failure of the aeration in one reactor and the lost of aerobic volume which could cause a significant TAN accumulation and the system performance deterioration.

Figure 7.14 shows the experimental results for OUR and TAN concentration in each reactor and the inflow behavior with time set to zero when the disturbance started. pH and temperature were constant through the experiment. On day 0, OUR in R2 suddenly dropped due to the decrease of the DO concentration. TAN in this reactor and in R3 increased up to 60 and 10 mg N L^{-1}, respectively, since no nitrification could take place in R2. As a result, the inflow was decreased from 14.6 to 8.8 L d^{-1}. One and a half days later, the system had reached steady conditions with respect to the inflow and the TAN concentration. The inflow stabilized at 9.9 L d^{-1}, approximately ⅔ of the inflow on day 0. On day 4, R2 was aerated again with a DO set point of 2 mg O_2 L^{-1}, the automatic controller increased the inflow again and the earlier steady state was reached in 1-2 days. The implemented control loop could successfully control this significant disturbance.

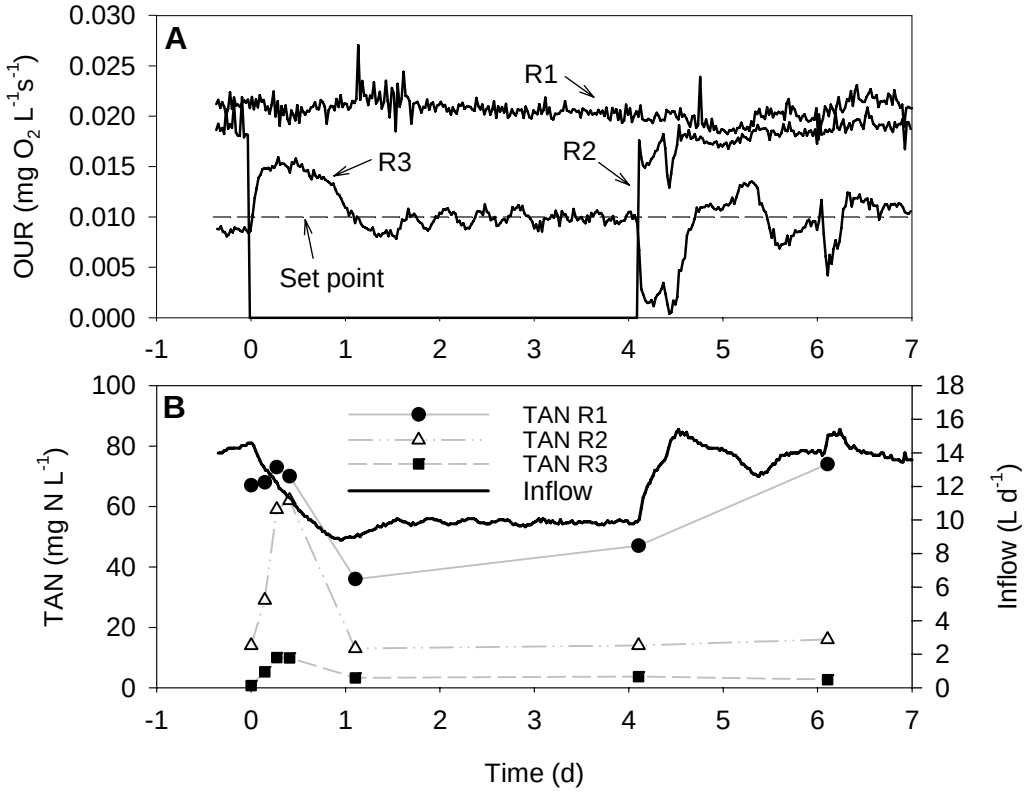

Figure 7.14 Disturbance 1: Aerobic volume reduction **A.** OUR profile in each reactor and OUR_{sp}. **B.** Time course for TAN in each reactor and inflow profile.

4.4.2 DISTURBANCE 2: OSCILLATORY INFLUENT TAN CONCENTRATION

The second disturbance was an oscillatory pattern of the influent TAN concentration. It was changed from the typical value in this study (3000 mg N L^{-1}) to half its value (1500 mg N L^{-1}) and then to the former value again (3000 mg N L^{-1}). This disturbance was designed to study the response of the controller in front of a non steady inflow load.

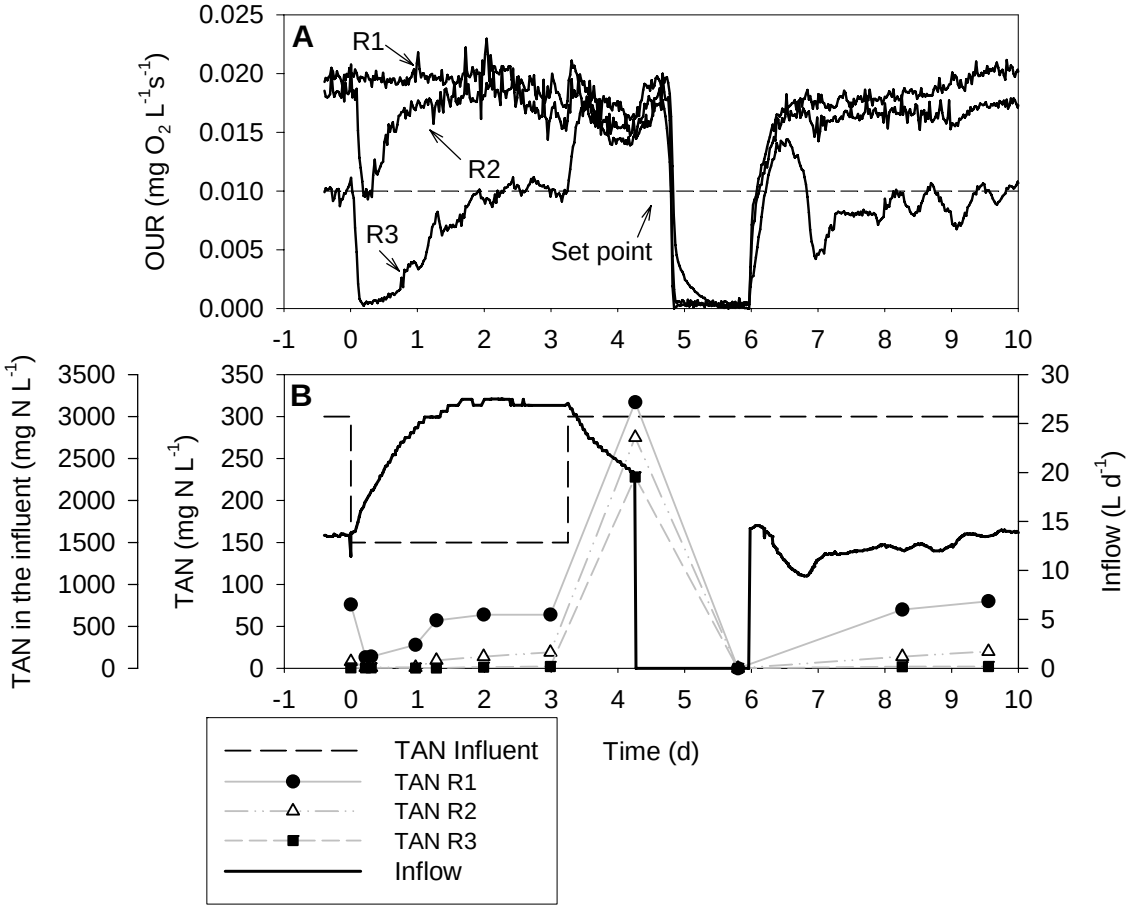

Figure 7.15 Disturbance 2: oscillatory influent TAN concentration **A.** OUR profile in each reactor and OUR_{sp}. **B.** Time course for TAN in each reactor and in the influent; and inflow profile.

Figure 7.15.A shows the in-line OUR measurements in each reactor and the OUR_{sp} in R3 and Figure 7.15.B shows the influent TAN concentration changes, the TAN concentration in each reactor and the inflow through the experiment. On day 0, TAN concentration in the influent was decreased to 1500 mg N L^{-1} and a quickly reaction of the automatic inflow control was detected. Two days later, the inflow was steady at 16.8 L d^{-1}, OUR_{sp} had been achieved again and the TAN concentration in each reactor was the same than it was at the beginning of the experiment. The only problem was that the conductivity of the bulk liquid had decreased from 33 to 25 mS cm^{-1} and the settling properties started to deteriorate. Therefore, on the third day, influent TAN concentration was re-established and the automatic controller decreased the

inflow again. On day 4, analyses demonstrated that the inflow decrease was too slow because TAN had built up to 320 mg N L^{-1} (40 mg FA L^{-1} at pH = 8.3), and thus the influent was manually stopped until all TAN was exhausted. On day 8, the stability of the system was recovered even though the overall activity had decreased (see the lower OUR in R2 and R3 and the lower inflow on day 8 compared to day 0).

The existing automatic control loop could not properly solve the high nitrogen load and therefore two improvements were designed. The first one consisted on a supervisory rule that actuated when fast inflow diminution was needed. This rule was preferred to the change of the PI controller parameters because the current parameters were appropriate for the control of slight disturbances, which occurred more often than considerable disturbances. This rule (see Table 7.8) was activated when the averaged value of the OUR in R3 (OUR_{R3}) for the last 3 hours was higher than 1.2 times the OUR_{sp}, and the final actuation was a sudden decrease of the inflow value of 15 %.

Table 7.8 New supervisory rules for the automatic inflow controller.

Rule		
1	If OUR_{R3} (3 h) > 1.2·OUR_{sp}	Then $F_{in}^{new} = 0.85 \cdot F_{in}^{old}$
2	Every 3 h	$OUR_{sp} = 0.5 \cdot \max[OUR_{R1}(3h), OUR_{R2}(3h)]$

The second rule was designed to continually change OUR_{sp} according to the biomass activity. Previous experience (see Chapter 6) and the fact that only AOB were present in the system were used to define this rule. It consisted of a cascade control to change the OUR_{sp} every 3 hours. Averaged values of OUR in R1 and R2 in the last 3 hours (OUR_{R1}(3h) and OUR_{R2}(3h)) were used as reference because each new value was set to half the maximum of these values. Considering the maximum OURs evaluated in R1 and R2 as the OUR_{AOB}^{max}, this rule would assure low TAN concentration in the effluent. Both strategies were applied in the following provoked disturbances.

4.4.3 DISTURBANCE 3: OSCILLATORY INFLUENT TAN CONCENTRATION

One month after disturbance 2 finished, a similar disturbance was provoked to test the supervisory rules. In this case the changes of the TAN concentration were slightly different to avoid the big variations of the conductivity that impaired the biomass settleability.

Figure 7.16 shows the response of the system in front of this disturbance. Figure 7.16.A shows the in-line OUR measurements in R1 and R3 and the variable OUR_{sp} (OUR in R2 was not available due to DO probe failure). Figure 7.16.B shows the applied influent TAN concentration pattern. On day 0, TAN concentration was decreased to 2000 mg N L^{-1} and the automatic controller increased the inflow until the OUR in R3 reached the OUR_{sp}.. Later, on day 3, TAN concentration was increased to 4000 mg N L^{-1} and the inflow was quickly reduced.

On day 4, steady conditions were reached with respect to inflow and TAN concentration in the bulk liquid. The maximum measured TAN concentration in the effluent of the system was 36 mg N L^{-1}. Compared to disturbance 2, the automatic control avoided TAN build-up and the system destabilization. Finally, on day 6, the initial influent TAN concentration was applied and the system came back to the initial state. This experiment showed the appropriateness and usefulness of the supervisory rule number 1 for the good performance of the system in front of such disturbances.

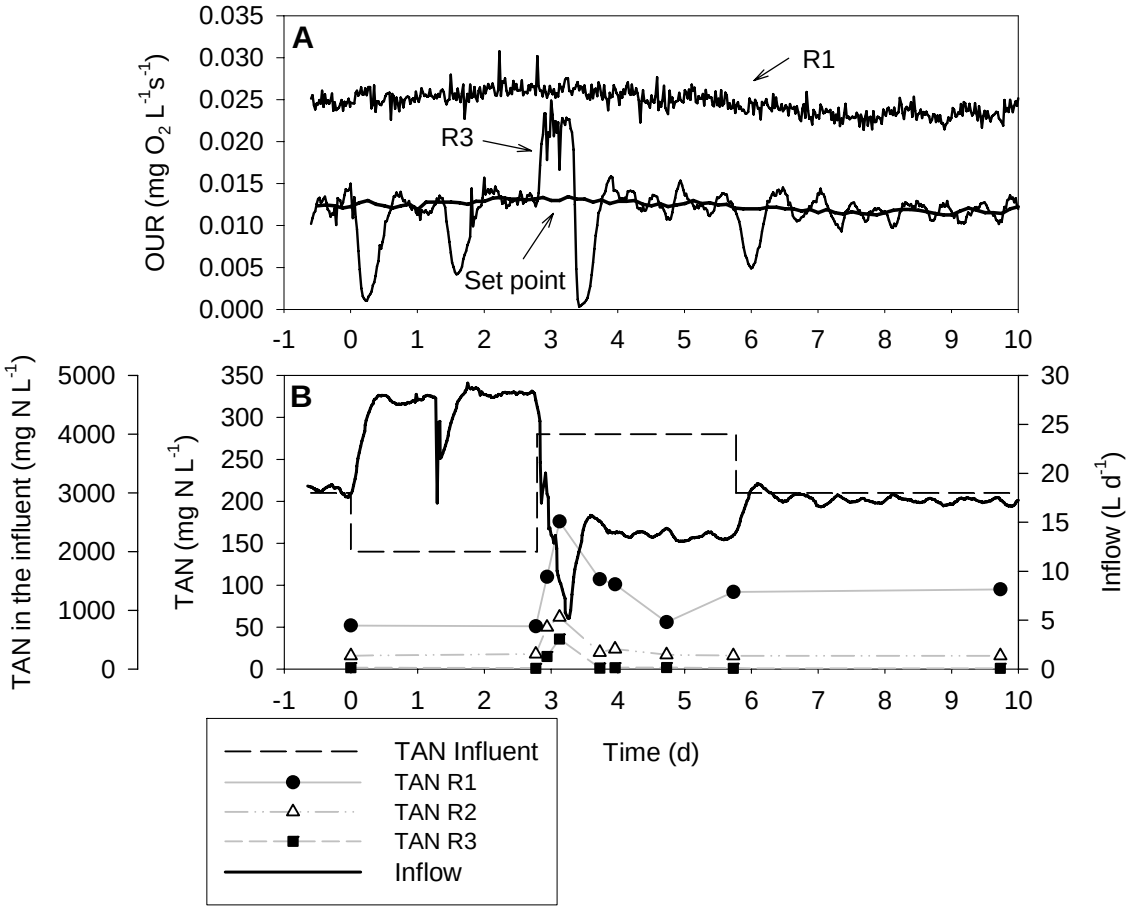

Figure 7.16 Disturbance 3: oscillatory influent TAN concentration **A.** OUR profile in R1 and R3 and OUR_{sp}. **B.** Time course for TAN in each reactor and in the influent; and inflow profiles.

4.4.4 DISTURBANCES 4 AND 5: VARIABLE BIOMASS ACTIVITY

Finally, two experiments are shown to verify the second rule introduced in the supervisory system. In both experiments the temperature control was deactivated and furthermore, in the second one, the biomass concentration increased due to the change in the purge flow. These disturbances caused variable biomass activity through the experiments.

Figure 7.17 shows the OUR measurements in R1 and R3, the variable OUR_{sp}, the temperature and the inflow in each of the experiments. In the experiment corresponding to disturbance 4, the temperature oscillations produced the same fluctuation in the biomass activity as it can be seen in the OUR measurements of R1 (Figure 7.17.A). Therefore, the supervisory rule number 2 changed the OUR_{sp} and the inflow controller changed the inflow value. Moreover, the temperature drop that occurred on day 3 provoked a decrease in the biomass activity that required a rapid decrease of the inflow (supervisory rule number 1). In the experiment corresponding to disturbance 5 (see Figure 7.17.B), apart from the temperature oscillations, the biomass concentration also changed. It was 970 mg VSS L^{-1} at the beginning and it increased up to 1200 mg VSS L^{-1} at the end. The inflow control system increased the inflow value at the same rate than the biomass activity was increasing. In both cases, the NLR_v was successfully modified accordingly to the nitrifying capacity.

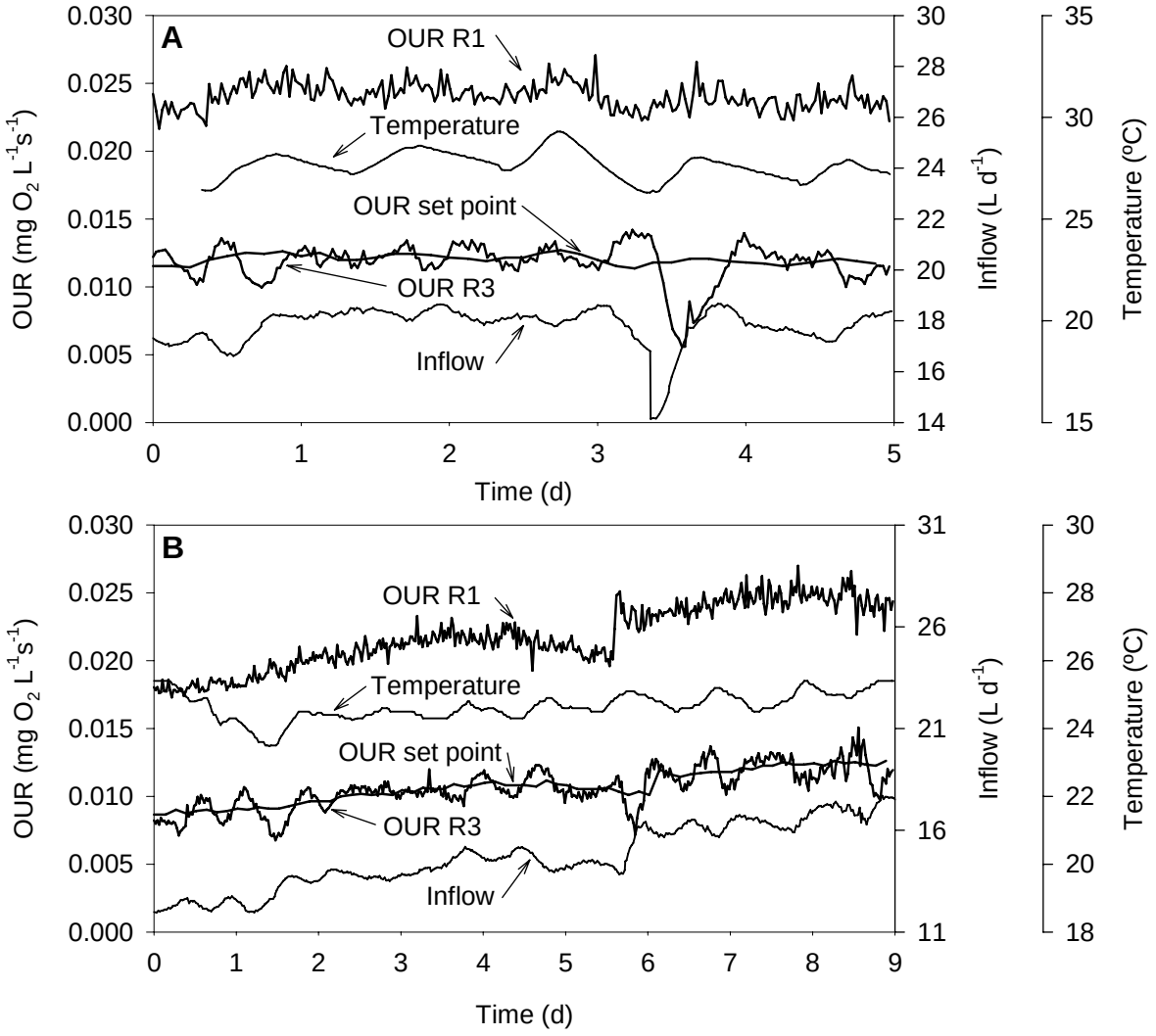

Figure 7.17 Variable biomass activity. OUR in R1 and R3, OUR_{sp}, temperature and inflow. **A.** Disturbance 4. **B.** Disturbance 5.

4.5 MODEL-BASED STUDY OF NITRITE ACCUMULATION

In this section, simulation tools will be used with several purposes: firstly, to describe the experimental results of Run 3; secondly, to study different conditions and configurations; and finally, to study the influence of an external disturbance on the nitrite build-up capacity.

4.5.1 DESCRIPTION OF THE EXPERIMENTAL RESULTS WITH SIMULATION TOOLS

Simulation tools were used to describe the experimental data of Run 3.

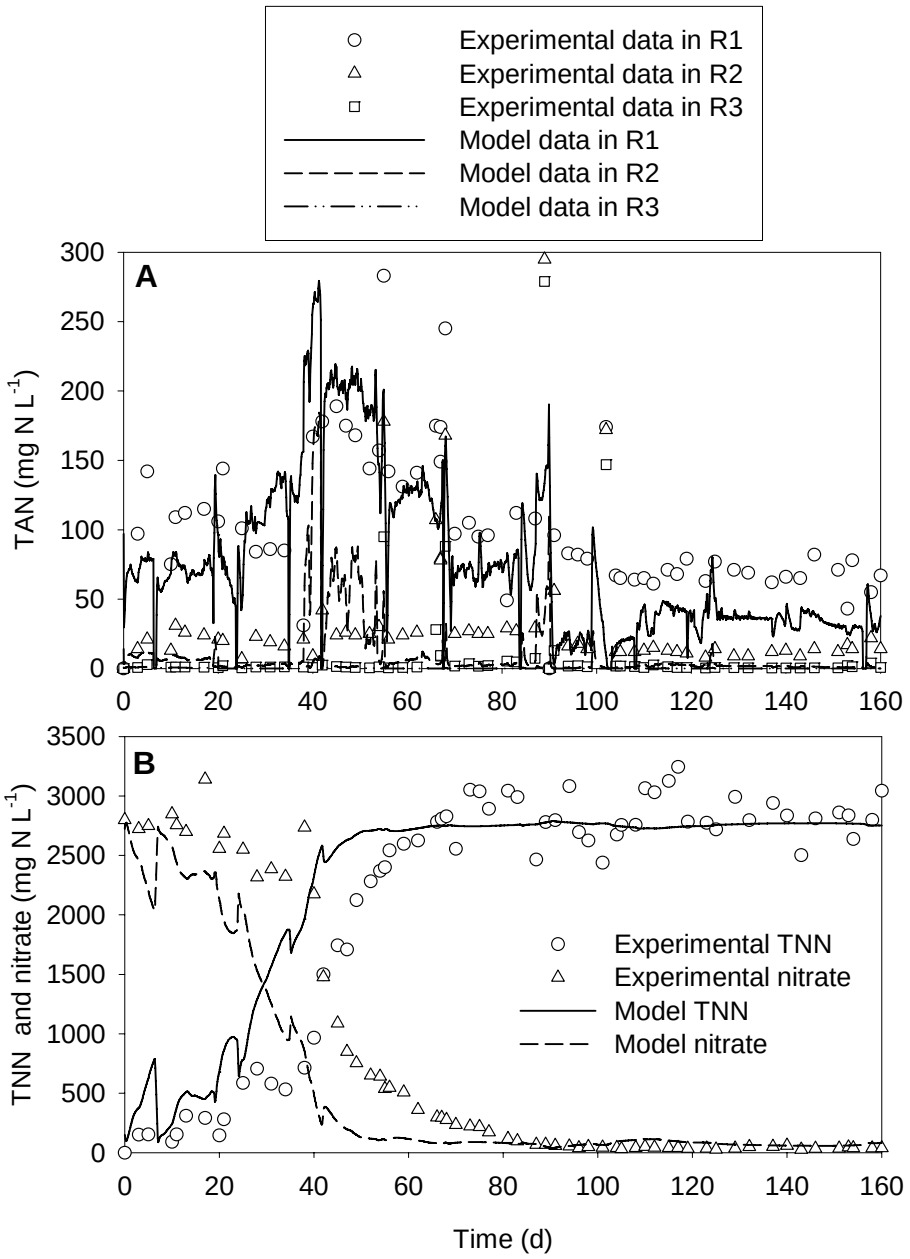

Figure 7.18 Experimental data and model prediction in Run 3. **A.** TAN in each reactor. **B.** TNN and nitrate in R3.

The inflow profile and the operation conditions (pH, T and DO) were introduced in the model as input variables. Initial values for the biomass composition were obtained from the simulation of the steady state under the initial conditions. TAN, TNN and nitrate profiles obtained by simulation did not agree well with experimental data and therefore some parameters had to be changed. After several simulations with different values for the inhibition coefficients it was found that by changing only two of them, a good estimation of the experimental results was obtained. $K_{I,FA,A}$ was changed from 93 to 15 mg FA L^{-1} and $K_{I,FA,N}$ from 9.5 to 0.32 mg FA L^{-1}. Experimental results and model prediction for TAN concentration in each reactor are shown in Figure 7.18.A and TAN and nitrate concentration in R3 in Figure 7.18.B. TAN predicted by the simulation was lower than the experimental data in all the reactors and TNN build-up started earlier in the simulated data than in the experimental data. Even though there are some differences between model prediction and experimental data, the general trend of these compounds are in good agreement and the steady state is well described.

Figure 7.19.A shows the experimental data and model prediction for the biomass concentration and the OUR in R3. The biomass concentration profile was very well described by the model but the experimental OUR was higher than that predicted by the model. This disagreement is in accordance with the differences between the experimental and predicted TAN concentration in R3. In Figure 7.19.B, the AOB and NOB fractions obtained by FISH are compared with the simulated fractions, which were calculated using equation 7.3, where X_i stands for each kind of biomass (X_A, X_N and X_H).

$$X_i = \frac{X_i}{X_A + X_N + X_H} \tag{7.3}$$

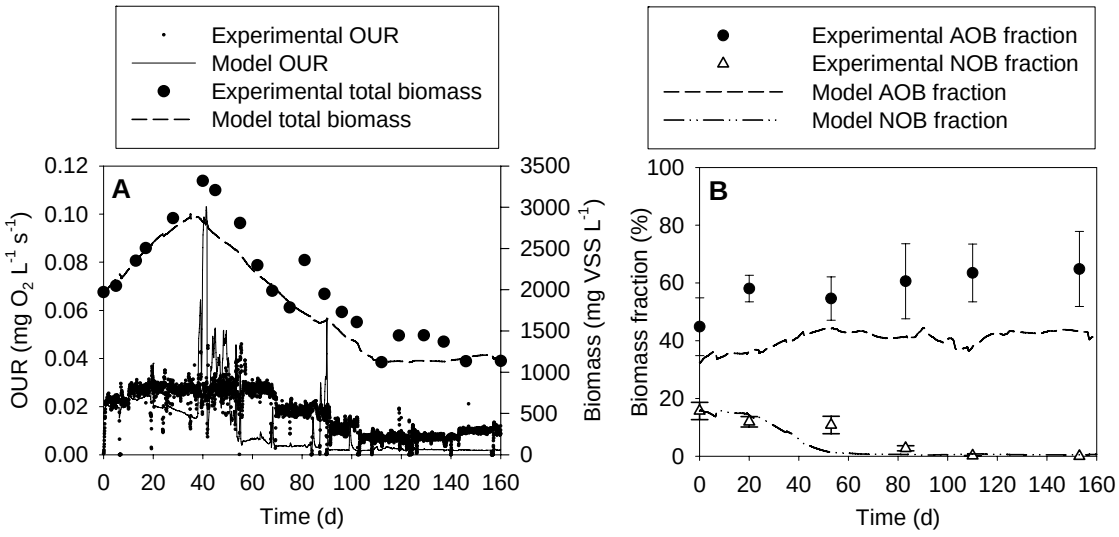

Figure 7.19 Experimental data and model prediction for Run 3. **A.** Biomass concentration and OUR in R3. **B.** Biomass fractions estimated with FISH and model prediction.

Since the model predicted an earlier TNN accumulation, the NOB fraction also decreased earlier than the experimental one did. Even though, good agreement between experimental and simulated data was obtained for NOB fraction. With respect to AOB fraction, the general trend of this parameter was well described by the model but the experimental values were higher.

4.5.2 MODEL-BASED STUDY OF NITRITE ACCUMULATION UNDER SEVERAL CONDITIONS AND CONFIGURATIONS

In this section, the results of several simulations are shown. The model parameters used in the previous section were used to simulate the pilot plant and the inflow controller under different conditions of pH, T and DO to see the effect of these factors on the degree of TNN accumulation and thus to go deeply into the comprehension of the accumulation phenomenon. Moreover, another reactor configuration consisting of a sole CSTR, with the same total volume than the experimental 3-reactor configuration, was studied.

All the previously described nitrite accumulation experiments started from a completely nitrifying system whose conditions and OUR_{sp} were changed in order to achieve partial nitrification. Therefore, the simulations were performed following the same scheme: first of all, the steady state for complete nitrification with the appropriate OUR_{sp} in the inflow controller was determined and then, the conditions and the OUR_{sp} were changed.

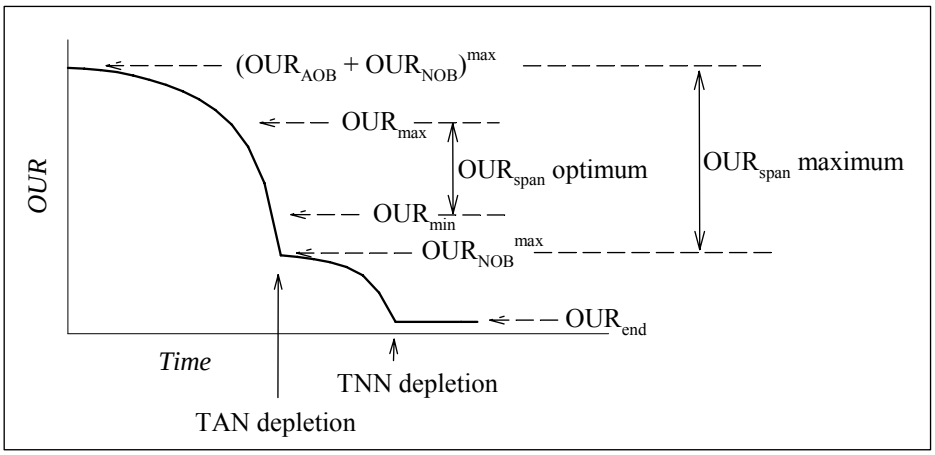

Figure 7.20 OUR profile of a theoretical batch ammonium pulse. Maximum and optimum OUR_{span} to achieve nitrite accumulation.

According to Figure 7.20 and as already explained, the OUR_{sp} for partial nitrification should be between the maximum OUR of the whole process ($(OUR_{AOB}+OUR_{NOB})^{max}$) and the maximum OUR of the nitratation process (OUR_{NOB}^{max}). By means of simulations, it was observed that there is a minimum value of OUR_{sp} (OUR_{min}) from which the total nitrite accumulations takes place and a maximum value (OUR_{max}) to avoid TAN build-up (see Figure 7.20). An OUR_{sp} below the OUR_{min} leads to negligible nitrite build-up or low TNN/NO_x when the steady state is

reached. This analysis is true if the same OUR_{sp} is used for the whole simulation, which is the case of this study. The OUR span in which TNN/NO_x is equal to 1 (OUR_{span} optimum) with respect to the maximum OUR span determined with a batch experiment (OUR_{span} maximum) was used to compare the different strategies (equation 7.4).

$$OUR_{ratio} = \frac{OUR_{span}\,optimum}{OUR_{span}\,maximum} \cdot 100 \qquad (7.4)$$

The conditions used to calculate the steady state for complete nitrification in the simulations were: DO = 3 mg O_2 L^{-1}, pH = 7.5, SRT = 25 d and T = 25, 20, 15 ºC depending on the case. When the steady state was reached, pH and/or DO were suddenly changed and with the new conditions OUR_{min} and OUR_{max} were determined and OUR_{ratio} was calculated. With these conditions and OUR_{sp} equal to OUR_{min} the system was simulated until the new steady state was reached. Another simulation was run with OUR_{sp} equal to OUR_{max}. In order to compare all the simulation, VSS concentration, TAN concentration in the effluent, NLR_v and NLR_s at the steady state were used (VSS^{SS}, TAN^{SS}, NLR_v^{SS} and NLR_s^{SS}, respectively). Furthermore, the time needed to reach TNN/NO_x = 0.99 was also determined for each conditions. All these results are summarized in Table 7.9.

The simulations at 25 ºC, pH of 7.5 and 3 mg O_2 L^{-1} showed that stable partial nitrification is feasible under these conditions. It was also possible when only DO or pH was modified to 1.1 mg O_2 L^{-1} and 8.3, respectively and obviously also when both parameters were modified simultaneously. It must be pointed out that the effluent of the simulation with low DO contains the highest amount of TAN (40-47 mg N L^{-1}). If OUR_{ratio} is compared, the best conditions are DO = 1.1 mg O_2 L^{-1} and pH = 8.3 because there is a higher optimum OUR_{span} in which partial nitrification is possible and therefore, it would be easier to reach it in practice. However, if the NLR_v^{SS} is compared, the optimal conditions are DO = 3 mg O_2 L^{-1} and pH = 8.3; but if a fast start-up is required, working at DO = 3.0 and pH = 7.5 is the best option. These simulations show the importance of the chosen OUR_{sp} because the start-up time and the applied NLR_v really depend on it. For example, if 25 ºC, 3.0 mg O_2 L^{-1} and a pH of 8.3 were applied to the system the start-up time would be either 108 days using OUR_{sp} equal to OUR_{min} or 53 days using OUR_{max} as a set point. When the simulation temperature was decreased to 20 or 15 ºC, the nitrite build-up was also possible and the best conditions in terms of NLR_v^{SS} were again DO = 3 mg O_2 L^{-1} and pH = 8.3. The three-reactor configuration takes advantage of the different conditions in the reactors.

Table 7.9 Results from several simulations under different conditions and configurations. "OUR_{ratio}" refers to (OUR_{span} optimum/OUR_{span} maximum)*100. "^{SS}" stands for steady state. "time" is the time required to reach $TNN/NO_x = 0.99$.

System configuration: 3 reactors of 26 L each									
T	DO	pH	OUR_{ratio}	OUR_{sp}	VSS^{SS} (mg L^{-1})	time (d)	TAN^{SS} (mg N L^{-1})	NLR_v^{SS} (mg N L^{-1} d^{-1})	NLR_s^{SS} (mg N mg^{-1} VSS d^{-1})
25	3.0	7.5	30	OUR_{min}	1884	45	4.0	1.1	0.57
				OUR_{max}	3015	25	3.5	1.7	0.57
25	1.1	7.5	29	OUR_{min}	285	162	47	0.2	0.57
				OUR_{max}	730	33	40	0.4	0.58
25	3.0	8.3	26	OUR_{min}	4741	108	0.06	2.9	0.61
				OUR_{max}	5446	53	0.08	3.2	0.59
25	1.1	8.3	57	OUR_{min}	517	94	0.02	0.3	0.57
				OUR_{max}	1852	27	0.4	1.1	0.57
20	3.0	7.5	18	OUR_{min}	914	51	25	0.4	0.48
				OUR_{max}	1137	40	23	0.6	0.49
20	3.0	8.3	41	OUR_{min}	3586	137	0.1	1.8	0.49
				OUR_{max}	5029	37	0.2	2.5	0.50
20	1.1	8.3	69	OUR_{min}	252	145	0.85	0.1	0.49
				OUR_{max}	1690	35	0.6	0.8	0.48
15	3.0	7.5	Not possible						
15	3.0	8.3	33	OUR_{min}	1982	107	0.3	0.8	0.43
				OUR_{max}	2950	50	0.4	1.2	0.42
System configuration: 1 reactor of 78 L									
T	DO	pH	OUR_{ratio}	OUR_{sp}	VSS^{SS} (mg L^{-1})	time (d)	TAN^{SS} (mg N L^{-1})	NLR_v^{SS} (mg N L^{-1} d^{-1})	NLR_s^{SS} (mg N mg^{-1} VSS d^{-1})
25	3.0	7.5	22	OUR_{min}	630	71	18	0.4	0.59
				OUR_{max}	720	25	18	0.4	0.59
25	1.1	7.5	129	OUR_{min}	90	348	55	0.05	0.56
				OUR_{max}	497	49	57	0.3	0.57
25	3.0	8.3	Not possible						
25	1.1	8.3	129	OUR_{min}	50	513	2.0	0.03	0.54
				OUR_{max}	450	74	2.0	0.3	0.56

Finally, the same controller was tested with a different system configuration. It consisted of a single reactor with the same volume than the three-reactor configuration (26 L · 3 = 78 L). In this case, FA and FNA inhibitions depend only on the effluent composition. Partial nitrification was achieved under all the simulated conditions except for DO = 3 mg O_2 L^{-1} and pH = 8.3 because the increase of the OUR_{sp} provoked TAN accumulation instead of TNN build-up. The

best conditions in terms of low TAN concentration in the effluent were DO = 1.1 mg O_2 L^{-1} and pH = 8.3 even though the NLR_v^{SS} was quite low compared to the NLR_v^{SS} reached when 3 reactors were simulated. Because of the characteristics of the CSTR, the nitrite accumulation with low TAN concentration in the effluent is only possible when DO is low.

4.5.3 MODEL-BASED STUDY OF PARTIAL NITRIFICATION START-UP WITH DISTURBANCES

Simulations were used to study the influence of the system stops on the continuous nitrite accumulation to explain the failure of the TNN build-up in Run 1 (section 4.1). For this purpose, the system was simulated using the following conditions: DO = 3 mg O_2 L^{-1}, pH = 7.5, and T = 25 ºC; and two different OUR_{sp}: OUR_{min} and OUR_{max} (according to Figure 7.20). A 24-hour stop on the 6th day of the simulations was provoked in both cases and was compared with simulations without this stop. Figure 7.21 shows the time courses for TNN and X_N in R1 when the set point was OUR_{min} (7.21.A) and OUR_{max} (7.21.B).

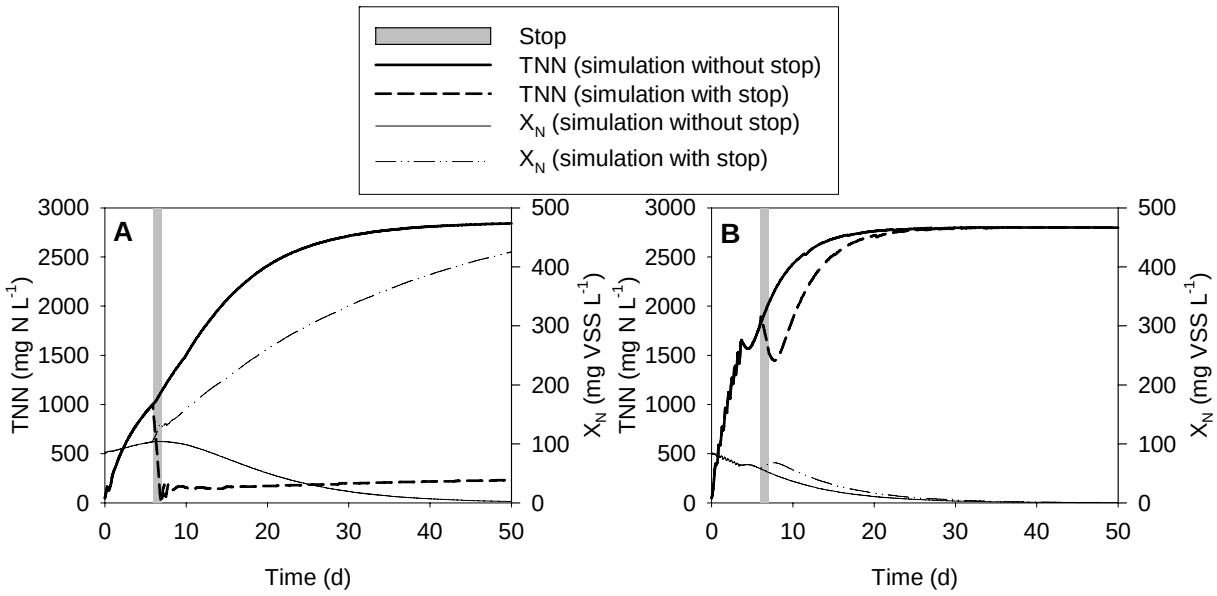

Figure 7.21 Time course for TNN and X_N in R1 in the simulation of two nitrite accumulation start-ups (with and without 24-hour stop on day 6). **A.** Using OUR_{min} as the set point in the controller. **B.** Using OUR_{max} as the set point in the controller

Using both OUR_{sp}s and without any stop in the inflow, nitrite completely built up and NOB decreased until they were washed out. Their activity decreased due to the FA inhibition in the first reactor and the increasing FNA concentration. In the simulation in which the minimum OUR_{sp} was used, the 24-hour stop on day 6 caused TAN depletion (data not shown) and thus activation of NOB, which grew enough to remove almost all TNN. A different result was obtained when the OUR_{sp} used in the controller was the maximum value. In this case, the NOB concentration raise produced during the inflow stop was not enough to reach a steady state

without biomass washout. Similar results than the ones showed in Figure 7.21.B were obtained with simulation under more severe conditions: DO = 1.1 mg O_2 L^{-1}, pH = 8.3, and T = 25 ºC.

Although these simulations are not accurately representing Run 1, they were helpful to demonstrate that the combination of moderate conditions (OUR_{min}, low DO and moderate pH) and inflow stops could provoke the failure of nitrite accumulation and the attainment of a new steady state with TNN/NOx ratio lower than 1. They also showed that as much higher the OUR_{sp} is, faster the nitrite accumulation is and more resistant to stops the system is because there exist a higher difference between nitritation and nitratation effective rates.

5. DISCUSSION

Three experimental start-ups of partial nitrification were performed starting from complete nitrification systems which were treating 3000 mg N L^{-1} with a removal efficiency of 100 %. In the first and second start-ups, partial nitrification with an effluent TNN/NOx ratio around 0.5 was achieved. However, an effluent free of nitrate (TNN/NOx =1) was achieved in the third start-up. The experimental results presented in the previous section are compared and discussed here. The model-based study is also considered to argue about the best start-up strategy. Improvements in the automatic control system are also discussed.

Strategy for partial nitrification start-up

The main strategy used in all the previously shown start-ups was the control of the inflow to work always at the minimum HRT required to remove all TAN and thus treat the maximum admissible flow. Working under these stressing conditions with the three-reactor configuration allowed the permanent existence of TAN in the first two reactors which was helpful to inhibit NOB and favor nitrite accumulation. This approach was similar to the strategy used in other works with SBRs in which the length of the aerobic phase (aerobic HRT) was determined by the end of the ammonium oxidation using pH or OUR measurements (Li et al. 2004; Pambrun et al. 2006; Poo et al. 2006). In these systems, the initial high ammonium concentration (and thus high FA) inhibited the NOB activity which provoked nitrite build-up. The following denitrification took place from nitrite instead of nitrate. When this strategy was combined with low DO and high FA, NOB could be washed out; however, if aeration periods were extended, nitratation would had taken place and NOB would had not been eliminated (Arnold et al. 2000). In the three-reactor configuration, high FA concentrations were achieved in the two first reactors and at the same time a continuous flow was treated.

The higher OUR_{AOB} than OUR_{NOB} was used to switch from complete nitrification to partial nitrification by only changing the OUR_{sp} in the inflow controller (Figure 7.1). It must be also considered that FA inhibits also AOB and provokes a decrease in their activity. This fact would probably cause problems in the control action especially if the applied OUR_{sp} was close to the OUR_{AOB}^{max}. In this case, the system could easily evolve to the inhibition area where the response of the system is the opposite, that is, higher concentration results in lower OURs. Therefore, if the system was working in this area, the OUR decrease would provoke an inflow increase by the control system and the subsequent increase of the FA concentration. This would lead to FA build-up and system destabilization. In that case, the right control action would be to decrease the inflow. Figure 7.22 shows the OUR profile of a batch ammonium pulse with FA inhibition of AOB and an example of an unsuitable OUR_{sp} due to its proximity to the inhibition area.

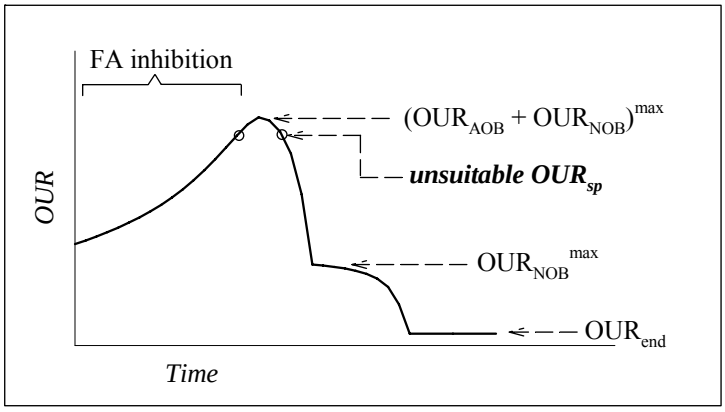

Figure 7.22 OUR profile of a theoretical batch ammonium pulse with FA inhibition of AOB. An example of an unsuitable OUR_{sp} due to its proximity to the $(OUR_{AOB}+OUR_{NOB})^{max}$ is indicated.

Run 1: nitrite accumulation by changing NLR_v

In the first attempt, the operation conditions were moderate (T = 25ºC, pH = 7.5 and DO = 3.0 mg O_2 L^{-1}) and similar to the conditions in the start-ups of the complete nitrification (see Chapter 6). When OUR_{sp} was increased, nitrite started to build-up immediately at a rate of 146 mg N L^{-1} d^{-1} until a TNN/NO_x ratio of 0.57 was reached. Then, the ratio decreased to 0.4 because the NOB activity had increased in a 58% with respect to the beginning of the experiment even though the OUR_{sp} was maintained steady (Table 7.3). The reasons for the change of the nitrite accumulation rate and the increase of the NOB activity could be several. On the one hand, NOB acclimation to FA could be one of the reasons since this phenomenon was already observed in other systems as described in Turk and Mavinic (1989) and Villaverde et al. (2000). On the other hand, it could also be postulated that FA concentrations in R1 and R2 were not high enough to produce significant NOB inhibition to provoke their washout and therefore, in the reached final state, both AOB and NOB populations survived. This option was demonstrated with simulations. It was shown that OUR_{sp} was the key point in order to either achieve partial nitrification with a low or high TNN/NO_x or even to build-up ammonium (see

section 4.5.3). In this case, probably a too low OUR_{sp} was applied and the partial nitrification was achieved with a TNN/NO_x ratio of 0.4. Finally, the last approach is that the numerous non-feeding periods which occurred when the TNN/NO_x was the highest, caused the alleviation of the inhibition conditions for NOB and they could grow and thus remove more nitrite than they did before the system stops. As a result, nitrite accumulation rate decreased and a steady state with lower TNN/NO_x was achieved. This approach seems the most feasible one since the changes of the nitrite accumulation rate were clearly related to the periods without feeding. Even though, NOB acclimation to FA and too low OUR_{sp} can no longer be undervalued. The fact that NOB are favored when the inhibition conditions are temporary alleviated was also demonstrated by simulations (section 4.5.3). It was also shown that the effect of the non-feeding periods depends on the applied OUR_{sp}: as much higher the OUR_{sp} is, less probable is the decrease of nitrite accumulation. In this experiment, a higher OUR_{sp} in the controller would have probably favored the achievement of TNN/NO_x ratio close to 1.

During the entire experiment the applied NLR_s was always between 0.4 and 0.6 mg N mg^{-1} VSS d^{-1} and the measured MAOR was around 0.5 mg N mg^{-1} VSS d^{-1}. This indicates that the system was optimized with respect to the ammonium removal capacity.

Run 2: nitrite accumulation at low DO by changing NLR_v

Low DO was chosen as the stressing factor for NOB in order to increase the difference between MAOR and MNOR and achieve partial nitrification with a high TNN/NO_x ratio. DO was shown to be decisive when using CSTR with biomass retention (Chung et al. 2007; Ruiz et al. 2003). Optimal DO concentration was obtained from experimental data since data in literature are quite scattered. The analysis of the nitritation and nitratation rates as a function of DO revealed that when DO was 1.1 mg O_2 L^{-1} the difference between these rates was the highest and therefore NOB activity lessening was produced with the minimal reduction on AOB activity. This result is similar than the optimal DO obtained in Ruiz et al. (2003) where nitrification performance was studied in an activated sludge unit at different DO concentrations. They concluded that a concentration of 0.7 mg O_2 L^{-1} produced the maximum nitrite accumulation ($TNN/NO_x = 0.65$) while maintaining high ammonia conversion (98 %).

The decrease of the DO concentration and the change in the OUR_{sp} provoked that TNN built up at rate of approximately 61 mg TNN L^{-1} d^{-1}. This rate was 60 % lower than in Run 1 therefore, the lower DO concentration did not seem to favor partial nitrification. With respect to FA, its concentration was similar in all reactors in both Run 1 and Run 2, producing similar inhibition to NOB. Two reasons can be postulated to explain the lower nitrite accumulation rate. On the one hand, it must be observed that several stops occurred when the TNN was accumulating (from day 5 to day 20) while in Run 1 the higher accumulation rate was calculated in a period of continuous feeding (from day 0 to day 15). It was clearly shown in Run 1 and by simulations

that it negatively affects the nitrite build-up. On the other hand, the MAOR and MNOR determined at the beginning of Run 2 (0.36 and 0.35 g N g^{-1} VSS d^{-1}, respectively) were not as much different as the ones determined at the beginning of Run 1 (0.5 and 0.12 g N g^{-1} VSS d^{-1} respectively) despite the DO concentration was lower. This could be explained by the different history of the biomass before the experiment. Despite the lower nitrite accumulation rate, high TNN/NO_x ratio would probably have been reached if the ammonium accumulation incident would not have occurred. The high TAN build-up had a negative effect on both nitrifying populations even though AOB were more influenced (Figure 7.7). This result is not in accordance with observations done by Anthonisen et al. (1976) because they found severest influence of FA to NOB than to AOB. Any clear explanation was found for this result. After the incident, nitrite accumulation decreased and complete nitrification was achieved. Both nitrification rates and FISH analyses showed that NOB were no longer washed out because their active fraction increased in 77 %.

The applied NLR_s was lower than in Run 1 because of the lower DO concentration. It was between 0.3 and 0.5 mg N mg^{-1} VSS d^{-1}.

These two experiments demonstrated that total nitrite accumulation is only possible if the conditions to achieve high effective nitritation rate and low effective nitratation rate are continually supplied to the system. This could be the reason why TNN/NO_x ratio lower than 1 was found in some works (Bae et al. 2002; Fux et al. 2004; Ruiz et al. 2003) and why nitrite accumulation failed in other published studies (Turk and Mavinic 1986; Yun and Kim 2003).

Run 3: nitrite accumulation at low DO and high pH by changing the NLR_v

In the last run, pH was increased to raise FA concentration in R1 and R2 and thus increase the FA inhibition to NOB. The pH increase was performed stepwise to avoid the inhibition of AOB which caused high TAN build-up in Run 2. When pH was 8.3 in all the system, FA was 24 and 3 mg FA L^{-1} in R1 and R2, respectively; and TNN started to steadily build up at a rate of 94 mg N L^{-1} d^{-1}. These FA concentrations were higher than those during both Run 1 and Run 2 which were approximately 2 mg FA L^{-1} in R1 and 0.5 mg FA L^{-1} in R2. At the same time that nitrite was building up, FNA concentration was also increasing. In spite of the fact that the pH was high, FNA concentration reached 0.11 mg FNA L^{-1} and this probably favored NOB inhibition. With respect to AOB activity, it was also impaired because a decrease in the applied NLR_s was observed from day 60 to day 100 (see Figure 7.8). Using the FNA inhibition coefficient for AOB determined on day 145 ($K_{I,FNA,A}$ = 0.55 mg FNA L^{-1}), a 17 % decrease in the AOB activity can be calculated. However, NLR_s increased again from day 100 onward. The high TNN concentration reached in this system makes it very sensitive to the pH because a failure in its control could cause a pH drop to, for example, 7.0 and suddenly increase the FNA concentration to 2.3 mg FNA L^{-1}. This could reduce the AOB activity to almost zero.

With respect to the system stops, they did not have negative effect on the nitrite accumulation rate because either they were less frequent or the more severe conditions did not allow NOB recovery. The sporadic TAN accumulation periods did not cause nitrite accumulation failure even though FA reached higher values than in Run 2: 36, 31, 52 and 66 mg FA L^{-1} in Run 3 and 12.5 mg FA L^{-1} in Run 2. It is obvious that high pH helped to quickly and steadily achieve nitratation suppression.

Off-line determination of MAOR and MNOR (Figure 7.12.A) showed that both rates were similar at the beginning of Run 3 (MAOR/MNOR = 1.05). On day 55, both rates were lower but the difference between them increased (MAOR/MNOR = 4.5). On the one hand, AOB activity decreased because of FA and FNA inhibition (as previously explained). On the other hand, NOB activity did not only decrease due to these inhibitions; they were washed out in 60 days as FISH analyses demonstrated (Figure 7.12.B).

From day 100 onward, when TNN/NO_x ratio was already 1 and NOB were negligible, the system was maintained in a very stable conditions for 60 days even though DO was increased to 2.0 mg O_2 L^{-1} on day 137. This DO change, together with the appropriate OUR_{sp} rise, provoked and increase of the applied NLR_s of a 50 %. The final applied NLR_s (before external disturbances were tested) was 0.5 g N g^{-1} VSS d^{-1} and the NLR_v was 0.57 g N L^{-1} d^{-1}. Table 7.10 compares these results with those obtained from the literature. Most of these works were performed at high temperature (above 30 ºC). Only in Ciudad et al. (2005) a CSTR was operated at 25 ºC treating a higher NLR_v but a similar NLR_s than in the three-reactor configuration. However, these authors did not achieve a TNN/NOx ratio of 1. In some of the references shown in this table, only half of the influent TAN was removed since a suitable effluent for an ANAMMOX reactor was desired. In order to compare their NLR_v with the obtained in the present work, the last should be doubled ($2 \cdot NLR_v$ = 1.14 g N L^{-1} d^{-1}). It means that if an effluent with half ammonium and half nitrite was needed, an inflow bypass should be added to the system and the treated inflow would be twofold. The new calculated NLR_v is in the same range than the values found in literature. Table 7.10 also shows that, as a general trend, biofilm reactors result in higher NLR_v.

Table 7.10 Summary of experimental results for partial nitrification treating high-strength ammonium wastewaters found in literature.

System	T	pH	DO	TAN removed	TNN/NO_x	NLR_v	NLR_s	Reference
	ºC		mg O_2 L^{-1}	%		g N L^{-1} d^{-1}	g N g^{-1} VSS d^{-1}	
3 CSTRs in series with settler	25	8.3	1.1 - 2	100	1	0.57	0.5	This work
CSTR with settler	25	7.8	1.4	95	0.75	1.5	0.6	Ciudad et al. (2005)
CSTR with settler	31	6.5 - 7.8	1.1	≈ 50	1	0.012	-	Gut et al. (2006)
CSTR with membrane	30	7.9	0.1	≈ 50	≈ 1	0.84	-	Wyffels et al. (2004)
CSTR without sludge retention	30 - 32	< 8.4	2 - 4	67	-	0.49	0.86	Fux et al. (2006)
SHARON	30	< 8	2 - 5	≈ 50	high	0.7	1.2	Fux et al. (2002)
SBR	30	7.4 – 8.6	0.4 – 0.5	100	high	0.37	0.11	Mace et al. (2006)
SBR	30 - 32	< 8.4	1 – 1.5	87	-	1.2	0.11	Fux et al. (2006)
SBR	35	< 8.0	-	≈ 50	high	2.6	-	Lai et al. (2004)
Upflow biofilm reactor	18 - 22	7.4	> 3	> 90	0.95	2.0	-	Yun and Kim (2003)
Inverse turbulent bed biofilm reactor	35	7.2	low	100	1	1.92	-	Bougard et al. (2006)
Granular sludge bed reactor	35	8.0	1.0	100	0.9	0.63	-	Lu et al. (2006)
Moving bed biofilm reactor	30	7.6	7.0	≈ 50	high	1.3	-	Fux et al. (2004)
Trickling filter	30	7.5 – 8.1	0 - 1	48	0.92	1.6	0.42	Chuang et al. (2007)

Automatic inflow control for partial nitrification

a) Partial nitrification start-up

The automatic inflow control designed and implemented in Chapter 6 was used also in the partial nitrification start-up. It consisted of a PI controller and was very useful to make the system work at its maximum capacity. The key point of this controller is the OUR_{sp} that can be chosen to achieve complete or partial nitrification. If partial nitrification is the goal, OUR_{sp} must be set in a value between OUR_{NOB}^{max} and $(OUR_{AOB}+OUR_{NOB})^{max}$. It was tested by simulations that there is only a range of OUR_{sp} inside these limits (OUR_{span} optimum) in which nitrite accumulation takes place with TNN/NO_x close to 1 and 100 % ammonium removal. Lower OUR_{sp} leads to an effluent with both TNN and nitrate and higher OUR_{sp} causes ammonium removal deterioration. The optimum OUR_{span} is wider when the operation conditions are more negatively affecting NOB activity. This means that it is easier to achieve nitratation suppression when pH is high and DO is low. A safe rule to set the OUR_{sp} is to choose the averaged of OUR_{NOB}^{max} and $(OUR_{AOB}+OUR_{NOB})^{max}$. With this automatic inflow control based on the OUR in R3, the effluent of the system will always contain low TAN concentration.

OUR_{sp} must be often refitted because the changes in the total biomass concentration and the specific bacteria fractions make the system dynamic. If the set point is not changed, the system works either underloaded or overloaded. A weekly OUR_{sp} tuning should be enough. It could be done by adding some extra TAN in R3 (40-70 mg N L^{-1}), analyzing the OUR profile of its consumption, detecting $(OUR_{AOB}+OUR_{NOB})^{max}$ and OUR_{NOB}^{max} and finally setting the OUR_{sp} to their averaged value. The disturbance provoked by this extra TAN would quickly be eliminated by the automatic inflow controller.

b) Partial nitrification maintenance

The automatic inflow controller was suitable for the slow dynamics of the system and also to control some external disturbances. On the contrary, it could not handle big external disturbances such as large oscillations of the inflow concentration. This was solved with an expert rule which suddenly diminished the inflow if the inflow decreases produced by the PI controller were not enough. Furthermore, a second expert rule was proposed in order to automatically fit OUR_{sp} to AOB activity. It consisted of fixing OUR_{sp} to half OUR_{AOB}^{max} which occurred in R1 and R2. This rule is only valid when nitratation does not longer occur. It was designed to actuate when the temperature or biomass concentration changed considerably or when any harmful compound entered the system (possible when dealing with industrial wastewater).

The design and implementation of automatic control for partial nitrification maintenance considering external disturbances is one of the novel achievements of this research. Some works can be found that use on-line control to optimize the phase length of SBR (Antileo et al.

2006; Li et al. 2004; Poo et al. 2006; Puig et al. 2005) or to control the process in front of changing inflow composition (Bernet et al. 2005), but non of them considered other external disturbances.

Microbial population

FISH analyses demonstrated that about 61 % of the detectable cells were nitrifiers when complete nitrification occurred (beginning of Run 3). The amount of AOB and NOB at that time was 45 and 16 % which were detected as *Nitrosomonas*-like bacteria and *Nitrobacter*-like bacteria respectively. The rest of the bacteria should probably be heterotrophs which grew from the influent COD and the COD resulting from biomass decay. Liebig et al. (2001) found a total amount of 45 % of nitrifiers in a chemostat and only a 23-28 % in a membrane-assisted bioreactor due to the higher SRT which favored biomass decay. With respect to AOB, they only found *Nitrosomonas*-like bacteria, like in our study. However, with respect to NOB, both *Nitrobacter* sp. and *Nitrospira* sp. were detected in comparable amounts (0.5 – 2.5 %) while in our research only *Nitrobacter*-like bacteria were found. Based on the substrate affinities and maximum reaction rates of all these species of bacteria, *Nitrosomonas* and *Nitrobacter* were classified as r-strategists while *Nitrosospira* and *Nitrospira* were regarded as K-strategists (Schramm et al. 1999). The r-strategists are characterized as having a low substrate affinity but a high reaction rate under high substrate concentrations while K-strategists have a high substrate affinity and a relatively low reaction rate under high substrate concentrations. This is in accordance with the obtained results: since two thirds of the aerobic volume was working under non-limiting TAN and TNN concentration, *Nitrosomonas* and *Nitrobacter* were more favored than *Nitrosospira* and *Nitrospira*.

The activity of nitrifiers is not directly coupled to their cellular rRNA content since they are capable of maintaining a high cellular ribosome content (and thus can also be detected by FISH) after inhibition (Wagner et al. 1995). Hence, the decrease of the NOB fraction detected by FISH clearly indicated that they were washed out of the system. Also Kim and Seo (2006) and Egli et al. (2003) demonstrated the NOB disappearance using FISH in the start-up of partial nitrification systems.

FISH was not useful to study the possible change of the community of AOB within the NEU-targeted bacteria because more specific probes were not used. Egli et al. (2003) showed that different reactors at pH 7.5 and 25 ºC formed communities that were indistinguishable by the applied FISH probes but differing in *amoA* RFLP types (restriction fragment length polymorphism analyses of the amoA gene encoding the active-site subunit of the ammonium monooxigenase). They also proved that feeding with sludge digester supernatant instead of synthetic wastewater produced a higher diversity in the bacterial communities because of the constantly reinoculation with AOB from the supernatant. Bougard et al. (2006) showed that different start-up strategies of partial nitrification led to different species of AOB. Particularly, it was shown that the combined oxygen and ammonia control strategy was more appropriate

than the shift in the temperature set point because a more diverse microbial ecosystem was obtained. Both Egli et al. (2003) and Bougard et al. (2006) stated that, from a perspective of performance stability, it would be preferable to choose conditions favoring a more complex community of ammonia oxidizers.

Model-based study of nitrite accumulation

The model was used to simulate the behavior of the system under the conditions of Run 3. When using the model parameter calibrated in Chapter 3, the model predictions did not agree well with experimental data. Since the goal was to get a good combination of parameters to be able to describe the experimental results and use it for system optimization, it was out of the scope to carry out an accurate study of the sensitivity of each of the model parameters. It was decided that only the inhibition coefficients would be modified because it is known that they can change depending on the biomass acclimation. The result was that only by changing $K_{I,FA,A}$ and $K_{I,FA,N}$, a good estimation of the experimental data was found. Probably, if other parameters were changed, a similar good description of experimental data would be obtained. However it is not possible to calibrate all the model parameters under the same exact conditions and at the same time. It is quite usual to obtain most of the them from literature and calibrate only a few of them (usually the most sensitive ones) with specific experiments (see for example Bernet et al. 2005; Wyffels et al. 2004). In this work, most of them were calibrated using similar biomass and under similar conditions than in Run 3.

Although the default value of $K_{I,FA,A}$ (93 mg FA L^{-1}) was obtained during Run 3 (day 145), it was modified to 15 mg FA L^{-1} to explain the high TNN concentrations in R1 and R2. On day 145, AOB had been working for several days at high FA concentration and probably the inhibition coefficient had changed with respect to the beginning of the experiment due to biomass acclimation. With respect to the $K_{I,FA,N}$, a value of 0.32 mg FA L^{-1} was needed to fit TAN accumulation. This value (lower than the default value of 9.5 mg FA L^{-1}) was close to the values obtained in the model-based study of start-up II and III (Chapter 6): 1.3 and 0.4 mg FA L^{-1} respectively. The final model prediction of nitrogenous compounds, OUR and biomass fractions was really accurate if these facts are considered: (1) the biomass composition changed considerably; (2) the inhibitions coefficients were considered constant even though they could change along the experiment due to FA and FNA acclimation; (3) both dynamic and steady state conditions were described and (4) not only the effluent composition was described but also the nitrogenous compounds in R1 and R2.

The final model was used to study several conditions and system configurations. Some of the results were already discussed above because the simulations were used to understand the experimental results obtained in Run 1 and Run 2. Other results are discussed here.

It was shown that the three-reactor configuration was appropriate when the working conditions favored high FA concentration in R1 and R2 because NOB were inhibited and quickly washed out. This occurred at high pH (8.3) and at a wide range of temperature (from 15 to 25 ºC). Hence, the proposed strategy is useful to treat highly concentrated ammonium wastewater at low or high temperature in contrast to the SHARON process which was designed to treat only sludge reject water at a temperature of 30-35 ºC (Hellinga et al. 1998). Furthermore, the automatic control allows working always with the maximum NLR_s. Low DO concentration also favored nitrite accumulation but it was not as crucial as it was in the configuration with only one reactor. In this last configuration, stable nitrite accumulation with low TAN in the effluent could only be obtained by working under high pH and low DO but treating very low NLR_v. As a result, larger volume would be required when using a sole CSTR than when using the three-reactor system to treat the same flow of wastewater.

6. CONCLUSIONS

- Partial nitrification start-up from complete nitrification must be done by changing the environmental conditions to such that nitritation and nitratation rates became as much different as possible (provided that MAOR > MNOR)

- A three-reactor configuration (CSTRs in series) allowed continuous treatment of high-strength wastewater with high FA in the first two reactors and TAN-free effluent. High FA concentration was required to inhibit NOB.

- In order to quickly achieve partial nitrification and maintain it with time, the stressing conditions for NOB had to be constantly supplied. Otherwise, NOB grew and the nitratation rate increased to an extent that the TNN/NO_x decreased and finally nitrite build-up capacity was lost.

- The automatic control system, based on OUR measurement in the last reactor and acting over NLR_v, was needed to permanently maintain the stressing conditions over NOB. Partial or complete nitrification was obtained depending on the chosen OUR_{sp}. OUR_{sp} should be changed weekly because it depends on AOB and NOB activities which change with time.

- Using the automatic inflow controller with DO of 1.1 mg O_2 L^{-1} and pH of 8.3, partial nitrification was obtained at a temperature of 25 ºC. Final TNN/NOx was 1, TAN removal was 100 %, VSS were 1400 mg L^{-1} and NLR_s was 0.5 mg N mg^{-1} VSS d^{-1}. Steady stressing conditions provoked the NOB washout that was demonstrated by using FISH.

- An expert rule to suddenly decrease NLR_v was designed in order to be able to deal with big external disturbances such as large oscillations of the inflow concentration. This was required since it was proved that the PI automatic inflow controller alone could not cope with them.

Satisfactory results were obtained when the expert rule was implemented in the pilot plant. Another expert rule was designed an implemented for the maintenance of the partial nitrification. It consisted of OUR_{sp} changes in accordance with AOB activity which was measured as OUR in the first two reactors of the system.

- Modeling tools were useful to study partial nitrification start-up under different environmental conditions. It was shown that it could be achieved with the three-reactor configuration and the automatic inflow controller even at 15 ºC if pH was 8.3 and DO was 1.1 mg O_2 L^{-1}.

- Suitable effluent for an ANAMMOX system would be obtained bypassing half of the inflow.

7. REFERENCES

Abeling U, Seyfried CF. 1992. Anaerobic-aerobic treatment of high-strength ammonium wastewater - Nitrogen removal via nitrite. *Water Science and Technology* 26(5-6):1007-1015.

Anthonisen AC, Loehr RC, Prakasam TBS, Srinath EG. 1976. Inhibition of nitrification by ammonia and nitrous acid. *Journal of the Water Pollution Control Federation* 48(5):835-852.

Antileo C, Werner A, Ciudad G, Muñoz C, Bornhardt C, Jeison D, Urrutia H. 2006. Novel operational strategy for partial nitrification to nitrite in a sequencing batch rotating disk reactor. *Biochemical Engineering Journal* 32(2):69-78.

APHA. 1995. Standard methods for the examination of water and wastewater. 19th Ed. Washington DC, USA: American Publishers Health Association.

Arnold E, Böhm B, Wilderer PA. 2000. Application of activated sludge and biofilm sequencing batch reactor technology to treat reject water from sludge dewatering systems: A comparison. *Water Science and Technology* 41(1):115-122.

Bae W, Baeck S, Chung J, Lee Y-W. 2002. Optimal operational factors for nitrite accumulation in batch reactors. *Biodegradation* 12:359-366.

Baeza JA, Gabriel D, Lafuente J. 1999. An expert supervisory system for a pilot WWTP. *Environmental Modelling and Software* 14(5):383-390.

Bernet N, Sanchez O, Cesbron D, Steyer JP, Delgenès JP. 2005. Modeling and control of nitrite accumulation in a nitrifying biofilm reactor. *Biochemical Engineering Journal* 24(2):173-183.

Blackall LL, Burrell PC. 1999. The microbiology of nitrogen removal in activated sludge systems. In: Seviour RJ, Blackall LL, editors. *The microbiology of activated sludge*. Dordrecht: Kluwer Academic Publishers. p 203-226.

Bougard D, Bernet N, Dabert P, Delgenes JP, Steyer JP. 2006. Influence of closed loop control on microbial diversity in a nitrification process. *Water Science and Technology* 53(4-5):85-93.

Carrera J, Baeza JA, Vicent T, Lafuente J. 2003. Biological nitrogen removal of high-strength ammonium industrial wastewater with two-sludge system. *Water Research* 37(17):4211-4221.

Ciudad G, Rubilar O, Muñoz P, Ruiz G, Chamy R, Vergara C, Jeison D. 2005. Partial nitrification of high ammonia concentration wastewater as a part of a shortcut biological nitrogen removal process. *Process Biochemistry* 40(5):1715-1719.

Chuang H-P, Ohashi A, Imachi H, Tandukar M, Harada H. 2007. Effective partial nitrification to nitrite by down-flow hanging sponge reactor under limited oxygen condition. *Water Research* 41(2):295-302.

Chung J, Bae W. 2002. Nitrite reduction by a mixed culture under conditions relevant to shortcut biological nitrogen removal. *Biodegradation* 13:163-170.

Chung J, Bae W, Lee Y-W, Rittmann BE. 2007. Shortcut biological nitrogen removal in hybrid biofilm/suspended growth reactors. *Process Biochemistry* 42(3):320-328.

Chung J, Shim H, Park SJ, Kim SJ, Bae W. 2006. Optimization of free ammonia concentration for nitrite accumulation in shortcut biological nitrogen removal process. *Bioprocess and Biosystems Engineering* 28(4):275-282.

Dapena-Mora A, Campos JL, Mosquera-Corral A, Méndez R. 2006. Anammox process for nitrogen removal from anaerobically digested fish canning effluents. *Water Science and Technology* 53(12):265-274.

Egli K, Langer C, Siegrist HR, Zehnder AJB, Wagner M, Van der Meer JR. 2003. Community analysis of ammonia and nitrite oxidizers during start-up of nitritation reactors. *Applied and Environmental Microbiology* 69(6):3213-3222.

Fux C, Boehler M, Huber P, Brunner I, Siegrist H. 2002. Biological treatment of ammonium-rich wastewater by partial nitritation and subsequent anaerobic ammonium oxidation (anammox) in a pilot plant. *Journal of Biotechnology* 99(3):295-306.

Fux C, Huang D, Monti A, Siegrist H. 2004. Difficulties in maintaining long-term partial nitritation of ammonium-rich sludge digester liquids in a moving-bed biofilm reactor (MBBR). *Water Science and Technology* 49(11-12):53-60.

Fux C, Siegrist H. 2004. Nitrogen removal from sludge digester liquids by nitrification/denitrification or partial nitritation/anammox: Environmental and economical considerations. *Water Science and Technology* 50(10):19-26.

Fux C, Velten S, Carozzi V, Solley D, Keller J. 2006. Efficient and stable nitritation and denitritation of ammonium-rich sludge dewatering liquor using an SBR with continuous loading. *Water Research* 40(14):2765-2775.

Gut L, Plaza E, Trela J, Hultman B, Bosander J. 2006. Combined partial nitritation/Anammox system for treatment of digester supernatant. *Water Science and Technology* 53(12):149-159.

Hao X, Heijnen JJ, Van Loosdrecht MCM. 2002. Model-based evaluation of temperature and inflow variations on a partial nitrification-ANAMMOX biofilm process. *Water Research* 36(19):4839-4849.

Hellinga C, Schellen AAJC, Mulder JW, Van Loosdrecht MCM, Heijnen JJ. 1998. The SHARON process: An innovative method for nitrogen removal from ammonium-rich waste water. *Water Science and Technology* 37(9):135-142.

Kim DJ, Lee DI, Keller J. 2006. Effect of temperature and free ammonia on nitrification and nitrite accumulation in landfill leachate and analysis of its nitrifying bacterial community by FISH. *Bioresource Technology* 97(3):459-468.

Kim DJ, Seo D. 2006. Selective enrichment and granulation of ammonia oxidizers in a sequencing batch airlift reactor. *Process Biochemistry* 41(5):1055-1062.

Lai E, Senkpiel S, Solley D, Keller J. 2004. Nitrogen removal of high strength wastewater via nitritation/denitritation using a sequencing batch reactor. *Water Science and Technology* 50(10):27-33.

Li YZ, Peng CY, Peng YZ, Wang P. 2004. Nitrogen removal from pharmaceutical manufacturing wastewater via nitrite and the process optimization with on-line control. *Water Science and Technology* 50(6):25-30.

Liebig T, Wagner M, Bjerrum L, Denecke M. 2001. Nitrification performance and nitrifier community composition of a chemostat and a membrane-assisted bioreactor for the nitrification of sludge reject water. *Bioprocess and Biosystems Engineering* 24(4):203-210.

Lu G, Zheng P, Jin RC, Qaisar M. 2006. Control strategy of shortcut nitrification. *Journal of Environmental Sciences* 18(1):58-61.

Mace S, Dosta J, Gali A, Mata-Alvarez J. 2006. Optimization of biological nitrogen removal via nitrite in a SBR treating supernatant from the anaerobic digestion of municipal solid wastes. *Industrial and Engineering Chemistry Research* 45(8):2787-2792.

MATLAB. 2002. User's guide. Version 6.5 (Release 13). Mathworks T, editor. Natick, USA.

Pambrun V, Paul E, Spérandio M. 2006. Modeling the partial nitrification in sequencing batch reactor for biomass adapted to high ammonia concentrations. *Biotechnology and Bioengineering* 95(1):120-131.

Peng Y, Zhu G. 2006. Biological nitrogen removal with nitrification and denitrification via nitrite pathway. *Applied Microbiology and Biotechnology* 73(1):15-26.

Pollice A, Tandoi V, Lestingi C. 2002. Influence of aeration and sludge retention time on ammonium oxidation to nitrite and nitrate. *Water Research* 36(10):2541-2546.

Poo KM, Im JH, Jun BH, Kim JR, Hwang LS, Choi KS, Kim CW. 2006. Full-cyclic control strategy of SBR for nitrogen removal in strong wastewater using common sensors. *Water Science and Technology* 53(4-5):151-160.

Puig S, Corominas L, Vives MT, Balaguer MD, Colprim J, Colomer J. 2005. Development and implementation of a real-time control system for nitrogen removal using OUR and ORP as end points. *Industrial and Engineering Chemistry Research* 44(9):3367-3373.

Pynaert K, Smets BF, Beheydt D, Verstraete W. 2004. Start-up of Autotrophic Nitrogen Removal Reactors via Sequential Biocatalyst Addition. *Environmental Science and Technology* 38(4):1228-1235.

Ruiz G, Jeison D, Chamy R. 2003. Nitrification with high nitrite accumulation for the treatment of wastewater with high ammonia concentration. *Water Research* 37(6):1371-1377.

Schramm A, De Beer D, Van Den Heuvel JC, Ottengraf S, Amann R. 1999. Microscale distribution of populations and activities of Nitrosospira and Nitrospira spp. along a macroscale gradient in a nitrifying bioreactor: Quantification by in situ hybridization and the use of microsensors. *Applied and Environmental Microbiology* 65(8):3690-3696.

Siegrist H, Reithaar S, Koch G, Lais P. 1998. Nitrogen loss in a nitrifying rotating contactor treating ammonium-rich wastewater without organic carbon. *Water Science and Technology* 38(8-9 -9 pt 7):241-248.

Strous M, Heijnen JJ, Kuenen JG, Jetten MSM. 1998. The sequencing batch reactor as a powerful tool for the study of slowly growing anaerobic ammonium-oxidizing microorganisms. *Applied Microbiology and Biotechnology* 50(5):589-596.

Terada A, Hibiya K, Nagai J, Tsuneda S, Hirata A. 2003. Nitrogen removal characteristics and biofilm analysis of a membrane-aerated biofilm reactor applicable to high-strength nitrogenous wastewater treatment. *Journal of Bioscience and Bioengineering* 95(2):170-178.

Turk O, Mavinic DS. 1986. Preliminary assessment of a shortcut in nitrogen removal from wastewater. *Canadian Journal of Civil Engineering* 13(6):600-605.

Turk O, Mavinic DS. 1987. Benefits of using selective inhibition to remove nitrogen from highly nitrogenous wastes. *Environmental Technology Letters* 8(9):419-426.

Turk O, Mavinic DS. 1989. Stability of nitrite build-up in an activated sludge system. *Journal of the Water Pollution Control Federation* 61(8):1440-1448.

Van Dongen U, Jetten MSM, Van Loosdrecht MCM. 2001. The SHARON®-Anammox® process for treatment of ammonium rich wastewater. *Water Science and Technology* 44(1):153-160.

Van Hulle SWH, Van Den Broeck S, Maertens J, Villez K, Donckels BMR, Schelstraete G, Volcke EIP, Vanrolleghem PA. 2005. Construction, start-up and operation of a continuously aerated laboratory-scale SHARON reactor in view of coupling with an Anammox reactor. *Water SA* 31(3):327-334.

Van Loosdrecht MCM, Salem S. 2006. Biological treatment of sludge digester liquids. *Water Science and Technology* 53(12):11-20.

Villaverde S, Fdz-Polanco F, García PA. 2000. Nitrifying biofilm acclimation to free ammonia in submerged biofilters. Start-up influence. *Water Research* 34(2):602-610.

Volcke EIP, Van Hulle SWH, Donckels BMR, van Loosdrecht MCM, Vanrolleghem PA. 2005. Coupling the SHARON process with Anammox: Model-based scenario analysis with focus on operating costs. *Water Science and Technology* 52(4):107-115.

Wagner M, Rath G, Amann R, Koops HP, Schleifer KH. 1995. In situ identification of ammonia-oxidizing bacteria. *Systematic and Applied Microbiology* 18(2):251-264.

Weon SY, Lee CW, Lee SI, Koopman B. 2002. Nitrite inhibition of aerobic growth of Acinetobacter sp. *Water Research* 36(18):4471-4476.

Wiesmann U. 1994. Biological nitrogen removal from wastewater. *Advances in biochemical engineering/biotechnology* 51:113-154.

Wyffels S, Van Hulle SWH, Boeckx P, Volcke EIP, Van Cleemput O, Vanrolleghem PA, Verstraete W. 2004. Modeling and simulation of oxygen-limited partial nitritation in a membrane-assisted bioreactor (MBR). *Biotechnology and Bioengineering* 86(5):531-542.

Yang L, Alleman JE. 1992. Investigation of batchwise nitrite build-up by an enriched nitrification culture. *Water Science and Technology* 26(5-6):997-1005.

Yoo H, Ahn KH, Lee HJ, Lee KH, Kwak YJ, Song KG. 1999. Nitrogen removal from synthetic wastewater by simultaneous nitrification and denitrification (SND) via nitrite in an intermittently-aerated reactor. *Water Research* 33(1):145-154.

Yun HJ, Kim DJ. 2003. Nitrite accumulation characteristics of high strength ammonia wastewater in an autotrophic nitrifying biofilm reactor. *Journal of Chemical Technology and Biotechnology* 78(4):377-383.

PART V - Chapter 8

GENERAL CONCLUSIONS AND FUTURE PERSPECTIVES

This chapter gives an overview of the main achievements of this work and points out the topics for future research derived from this thesis.

Stable operation of partial nitrification was achieved for the treatment of highly concentrated ammonium wastewater at 25 ºC using automatic control. A complete study of the process was performed with modeling tools and microbiology techniques which were previously developed, calibrated and/or tested.

Modeling

The nitrification model calibrated with specific experiments was useful to optimize the control system for the start-up of a complete nitrification system and to study the start-up of a partial nitrification system.

Only some of the previously calibrated parameters had to be modified to accurately describe the experimental results with mathematical modeling and simulation. These parameters were basically inhibition coefficients, which depend on the acclimation of the biomass to the inhibitory compounds. The behavior of nitrogenous compounds and total biomass concentration of both short-term (hours) and long-term (months) experiments were accurately described with the developed model.

The inhibition coefficients should be frequently estimated in dynamic systems to investigate the rate and extent of the evolution of these parameters. This would allow the development of more accurate kinetic models that could maybe include an acclimation factor. The acclimation of biomass to inhibitory compounds should be also addressed from the point of view of the population composition in order to elucidate if the acclimation is due to the change of the bacteria metabolism or is due to the change of the bacterial population.

The calibration of the parameters describing the heterotrophic bacteria existing in an enriched nitrifying sludge should also be performed. This would allow better description of this population compared to the typical heterotrophic bacteria found in urban wastewater treatment plants (WWTPs).

Process operation and control

A control system based on the oxygen uptake rate (OUR) measurement in the last reactor and acting over the nitrogen loading rate (NLR) was useful for the optimal start-up of both a complete and a partial nitrification system. In the first case, the control system helped to decrease the start-up time while the discharge requirements were always satisfied. In the second case, the control system allowed maintaining the stressing conditions over NOB which was crucial for the achievement of partial nitrification at temperatures around 25 ºC. In this case, the ammonium and nitrate concentrations were always kept very low avoiding

ammonium accumulations that could have been harmful for the nitrifying population. NOB were washed out of the system as it was confirmed by using FISH.

Partial nitrification of high-strength ammonium wastewater was kept under optimal operation conditions even when external disturbances were applied. The key point was the addition of two expert control rules that adapted the NLR to the capacity of the system. Automatic control should be implemented in all processes because of the advantages regarding process stability in front of external disturbances.

The regular analysis of the AOB and NOB activities with LSS *off-line* respirometry and using specific inhibitors was very useful for the comprehension of the system behavior. This tool should be used when developing and testing new processes and strategies.

The control system developed for optimal start-up of a partial nitrification system from an enriched complete nitrification system should be tested for the same purpose but starting from an activated sludge with low nitrifying bacteria concentration like urban WWTP sludge.

Future research should be addressed to the combination of the developed partial nitrification with either denitrification or the ANAMMOX process. Furthermore, industrial wastewater instead of synthetic wastewater should be used.

Biomass fractions determination

FISH is an easy-to-implement methodology for routine analyses of the bacterial composition of enriched sludges. Several quantification techniques were optimized, tested and compared with respect to the accuracy and the analysis time.

The techniques that require aggregates disruption (cell counting with epifluorescence microscopy and flow cytometry) could not be proper due to the impossibility to obtain complete disruption without individual cell damage. Therefore, the obtained biomass fractions could not be completely representative of the original sample.

The technique based on the quantification of fluorescent area (confocal microscopy) does not need aggregates disruption but the differences in the aggregates density and cells size could lead to inaccuracies in the final result. However, FISH combined with confocal microcopy turned out to be the best technique for nitrifying biomass quantification when compared with the other studied techniques.

Biomass fractions results obtained experimentally and by mathematical simulation can not be directly compared. The reasons are basically two: the techniques restrictions and the definition of the simulated particulate compounds. With respect to the simulated compounds, they were created to describe the global behavior of the system and may not strictly correspond to the specific particulate compounds found in the sludge.

More efforts should be put on nitrifying bacteria quantification with flow cytometry because of the time saving that this technique would provide to the whole quantification method.

Research should also be focused on the transformation of the experimentally assessed fractions to simulated particulate compounds in order to use them for parameter calibration.

ANNEX

1. ACRONYMS

ANAMMOX	Anaerobic ammonia oxidation
AOB	Ammonium oxidizing bacteria
ATU	Allylthiourea
AUR	Ammonium uptake rate
BNR	Biological nitrogen removal
BOD	Biological oxygen demand
BOD_5	Five-day biological oxygen demand
CANON	Completely autotrophic nitrogen removal over nitrite
CFA	Continuous flow analyzer
CLSM	Confocal laser scanning microscope
COD	Chemical oxygen demand
COV	Covariance matrix
CSTR	Continuous stirred tank reactor
DO	Dissolved oxygen
FA	Free ammonia
FCM	Flow cytometer
FH	Free hydroxylamine
FI	Fluorescence intensity
FIM	Fisher information matrix
FISH	Fluorescent in situ hybridization
FNA	Free nitrous acid
FSC	Low angle or forward light scatter
GP	General probe
HRT	Hydraulic retention time
IN-FISH	In-solution fluorescent in situ hybridization
ISE	Integral of the square error
KBES	Knowledge based expert system
LFS	Liquid, flowing, static
LSS	Liquid, static, static
MAOR	Maximum ammonium oxidation rate
MBR	Membrane-assisted bioreactor
MNOR	Maximum nitrite oxidation rate
MNR	Maximum nitrification rate
MPN	Most probable number
NLR	Nitrogen-loading rate (in general)
NOB	Nitrite oxidizing bacteria
NUR	Nitrite uptake rate
OC	Oxygen consumption
OED/PE	Optimal experimental design for parameter estimation

OLAND	Oxygen-limited autotrophic nitrification-denitrification
OLR	Organic loading rate
ORP	Oxido-reduction potential
OS-FISH	On-slide fluorescent in situ hybridization
OUR	Oxygen uptake rate
PAO	Polyphosphate accumulating organism
PC	Process computer
PFR	Plug-flow reactor
PI	Proportional-integral
PID	Proportional-integral-derivative
R1	Reactor 1
R2	Reactor 2
R3	Reactor 3
RFLP	Restriction fragment length polymorphism
RGA	Relative gain analysis
SAI	Surface-averaged intensity
SBR	Sequencing batch reactor
SHARON	Single reactor high activity ammonia removal over nitrite
SISO	Simple input simple output
SP	Specific probe
SRT	Sludge retention time
SSC	Right angle or side light scatter
SVI	Sludge volumetric index
TAN	Total ammonium nitrogen
TKN	Total Kjeldahl nitrogen
TNN	Total nitrite nitrogen
TSS	Total suspended solids
UASB	Upflow anaerobic sludge blanket
VSS	Volatile suspended solids
WWTP	Wastewater treatment plant

2. NOMENCLATURE

ε	Deviation (error) of the measured variable from the desired set point
τ_I	Integral time constant in a PI controller
Δt	Control interval time / Data collection interval
A_{bA}	Arrhenius pre-exponential factor for b_A
A_{bN}	Arrhenius pre-exponential factor for b_N

AUR_{max}	Maximum AUR
$A_{\mu maxA}$	Arrhenius pre-exponential factor for $\mu_{max,A}$
$A_{\mu maxN}$	Arrhenius pre-exponential factor for $\mu_{max,N}$
b	Decay rate
b_A	AOB decay rate
b_H	Heterotrophic bacteria decay rate
b_N	NOB decay rate
C	Controller output variable
C_s	Controller output signal when the error is zero
d_{eq}	Equivalent diameter
det	Determinant of a matrix
Ea_A	Activation energy of AOB
Ea_N	Activation energy of NOB
F_{ER}	External recirculation flow
F_{in}	Inflow to the system
F_{in}^{step}	Fixed inflow in the on-off controller
F_{IR}	Internal recirculation flow
$f_N(0)$	Initial NOB fraction
f_P	Fraction of biomass leading particulate inert products
f_{sp}	Fraction of the target organisms obtained by FISH
I	Intensity
I_{thr}	Intensity threshold
I_{thr}^{GP}	Intensity threshold for general probes images
I_{thr}^{SP}	Intensity threshold for specific probes images
i_{XB}	Nitrogen content of biomass (X_A, X_N and X_H)
i_{XP}	Nitrogen content of particulate inert products (X_P)
J	Objective function
J_{min}	Minimum J value
J_{opt}	Objective function for the optimal parameters
k	Parameter to relate the OUR in the first and second reactors with the OUR_{sp}
k_a	Ammonification rate
K_a	Ionization constant of nitrous acid equilibrium
K_b	Ionization constant of ammonia equilibrium
Kc	Proportional gain in a PI controller
k_h	Maximum specific hydrolysis rate
K_I	Inhibition coefficient
$K_{I,FA,A}$	AOB inhibition coefficient for FA
$K_{I,FA,N}$	NOB inhibition coefficient for FA
$K_{I,FNA,A}$	AOB inhibition coefficient for FNA
$K_{I,FNA,N}$	NOB inhibition coefficient for FNA
$K_{I,TAN,A}$	AOB inhibition coefficient for TAN

$K_{I,TAN,N}$	NOB inhibition coefficient for TAN
$K_{I,TNN,A}$	AOB inhibition coefficient for TNN
$K_{I,TNN,N}$	NOB inhibition coefficient for TNN
k_La	Global oxygen transfer coefficient from the bubbles to the liquid phase
k_La_{FA}	Global FA transfer coefficient
k_La^{sup}	Global DO transfer coefficient from the superficial air and the liquid phase
K_O	Affinity constant for DO
$K_{O,A}$	AOB affinity constant for DO
$K_{O,H}$	Heterotrophic bacteria affinity constant for DO
$K_{O,N}$	NOB affinity constant for DO
K_S	Affinity constant for substrate
$K_{S,FA,A}$	AOB affinity constant for FA
$K_{S,FNA,N}$	NOB affinity constant for FNA
$K_{S,H}$	Heterotrophic bacteria affinity constant for readily biodegradable substrate (S_S)
$K_{S,TAN,A}$	AOB affinity constant for TAN
$K_{S,TNN,N}$	NOB affinity constant for TNN
k_t	"Start-up" time coefficient
K_w	Ionization constant of water
K_X	Affinity constant for slowly biodegradable substrate (X_S)
Mod 1	Model modification number 1
Mod 2	Model modification number 2
N	Amount of experimental data
N_{AOB}	N-TAN assimilated due to AOB to grow
NLR_s	Specific NLR (g N g^{-1} VSS d^{-1})
NLR_s^{SS}	Specific NLR at steady state
NLR_v	Volumetric NLR (g N L^{-1} d^{-1})
NLR_v^{SS}	Volumetric NLR at steady state
N_{max}	Maximum TAN plus TNN concentration allowed in the effluent of the system
N_{NOB}	N-TAN assimilated due to NOB to grow
$N_{ox,1}$	N-TAN oxidized to nitrite
$N_{ox,2}$	N-TNN oxidized to nitrate
np	Number of estimated parameters
$N_{set\ point}$	Nitrogen set point
N_{sum}	Sum of TAN and TNN concentration in the effluent of the system
NUR_{max}	Maximum nitrite uptake rate
$O2_{AOB}$	COD produced due to AOB growth
$O2_{NOB}$	COD produced due to NOB growth
$O2_{sto,1}$	Stoichiometric OC in the first step of nitrification
$O2_{sto,1+2}$	Stoichiometric OC in the whole nitrification process

$O2_{sto,2}$	Stoichiometric OC in the second step of nitrification
OUR_{AOB}	OUR due to nitritation process
OUR_{end}	Endogenous OUR
OUR_{ex}	Exogenous OUR
OUR_{max}	Maximum OUR / maximum OUR without limitation / maximum OUR_{sp} to achieve total partial nitrification
OUR_{max}^{*}	Maximum OUR at the DO concentration of S_O^{min}
OUR_{max}^{ref}	Maximum OUR in the reference experiment (without inhibitor)
OUR_{min}	Minimum OUR set point to achieve total partial nitrification
OUR_{NOB}	OUR due to nitratation process
OUR_{R3}	OUR in reactor 3
OUR_{ratio}	Ratio between OUR_{span} optimum and maximum
OUR_{sp}	OUR set point
OUR_{span}	Range of OUR_{sp}
pK1	Parameter for the pH effect on $\mu_{max,A}$ and $\mu_{max,N}$
pK2	Parameter for the pH effect on $\mu_{max,A}$ and $\mu_{max,N}$
Q	Measurement error covariance matrix
r	Parameter to define the inflow increases in the on-off control strategy / rate
R	Universal gas constant
r_{max}	Maximum rate
S	Substrate concentration
S_{FA}	FA concentration
$S_{FA}(0)$	Initial FA concentration
S_{FA}^{*}	FA saturation concentration in equilibrium with gas phase
S_{FNA}	FNA concentration
S_I	Inhibitory compound concentration
S_{ND}	Soluble biodegradable organic nitrogen concentration
S_{NO3}	Nitrate concentration
S_O	DO concentration
S_O^{*}	DO saturation concentration
S_O^{corr}	Corrected value of DO concentration
S_{OE}	DO concentration when endogenous respiration and superficial oxygen transfer are in equilibrium
S_O^{meas}	Measured DO concentration
S_O^{min}	Minimum DO in a respirometric experiment
S_S	Readily biodegradable substrate concentration
S_{TAN}	TAN concentration
S_{TNN}	TNN concentration
T	Temperature
t	Time
TAN_{pulse}	Initial TAN concentration of a pulse

TAN^{SS}	TAN in the effluent at steady state
TNN_{pulse}	Initial TNN concentration of a pulse
t_{out}	Percentage of the total simulated time in which the N_{sum} was above N_{max}
tr	Trace of a matrix
VSS^{SS}	VSS at steady state
X	Total biomass concentration
X(0)	Initial total biomass concentration
X_A	AOB concentration
$X_{autotrophic}$	Nitrifiers concentration
X_H	Heterotrophic bacteria concentration
X_N	NOB concentration
$X_N(0)$	Initial NOB concentration
X_{ND}	Particulate biodegradable organic nitrogen concentration
X_P	Particulate inert products concentration
$X_{P,A}$	Fraction of particulate inert products from the decay of AOB
$X_{P,H}$	Fraction of particulate inert products from the decay of heterotrophs
$X_{P,N}$	Fraction of particulate inert products from the decay of NOB
X_S	Slowly biodegradable substrate concentration
Y_A	AOB growth yield
Y_H	Heterotrophic bacteria growth yield
Y_N	NOB growth yield
Z_i^{GP}	Sum of "positive" pixels of a general probe image
Z_i^{SP}	Sum of "positive" pixels of a specific probe image
θ	Vector containing the calibrated parameters
θ_{opt}	Vector containing the optimal estimated parameters
λ_{max}	Largest eigenvalue
λ_{min}	Smallest eigenvalue
$\mu^*_{max,N}$	Maximum NOB specific growth rate under specific conditions of pH, T and DO
$\mu_{max,A}$	Maximum AOB specific growth rate
$\mu_{max,H}$	Maximum heterotrophic bacteria specific growth rate
$\mu_{max,N}$	Maximum NOB specific growth rate
σ	Estimated uncertainty of a parameter
τ	DO probe time constant

3. PUBLICATIONS

INTERNATIONAL JOURNALS

Carrera J, **Jubany I**, Carvallo L, Chamy R, Lafuente J. 2004. Kinetic models for nitrification inhibition by ammonium and nitrite in a suspended and an immobilised biomass systems. *Process Biochemistry* 39:1159-1165.

Guisasola A, **Jubany I**, Baeza JA, Carrera J, Lafuente J 2005. Respirometric estimation of the oxygen affinity constants for biological ammonium and nitrite oxidation. *Journal of Chemical Technology and Biotechnology* 80:388-396.

Jubany I, Baeza JA, Carrera J, Lafuente J. 2005. Respirometric calibration and validation of a biological nitrite oxidation model including biomass growth and substrate inhibition. *Water Research*, 39:4574-4584.

Jubany I, Baeza JA, Carrera J, Lafuente J. 2007. Model-based design of a control strategy for optimal start-up of a high-strength nitrification system. *Environmental Technology* 28(2):185-194.

ARTICLES IN PREPARATION

Jubany I, Baeza JA, Carrera J, Lafuente, J. Respirometric determination of NOB inhibition coefficient for free ammonia. *Environmental Technology.*

Jubany I, Baeza JA, Carrera J, Lafuente, J. Automatic method for biomass fraction determination with FISH and confocal microscopy. *Biotechnology letters*.

Jubany I, Baeza JA, Carrera J, Lafuente J. Optimal start-up of a nitrification system with automatic control to treat highly concentrated ammonium wastewater. *Chemical Engineering Journal*.

Jubany I, Baeza JA, Carrera J, Lafuente J. Strategy for the optimal start-up of a partial nitrification system with automatic control to treat highly concentrated ammonium wastewater. *Water Research.*

Jubany I, Baeza JA, Carrera J, Lafuente J. Expert control for the operation of a partial nitrification system to treat highly concentrated ammonium wastewater. *Process Biochemistry*.

INTERNATIONAL CONFERENCES

Jubany I, Carrera J, Baeza JA, Lafuente J. Modelling biological nitrite oxidation including biomass growth and substrate inhibition using only oxygen uptake measurements. 4th IWA Word Water Congress and Exhibition. Marrakech, Morocco, September 2004. Oral presentation

Jubany I, Carrera J, Baeza J, Lafuente J. Design and control strategy for optimal start-up of a high-strength nitrification system. 2nd IWA Conference on instrumentation, control and automation for water and wastewater treatment and transport systems. Busan, Korea, May-June 2005. Oral presentation.

Jubany I, Baeza JA, Carrera J, Casas C, Sternberg C, Smets B. Flow cytometric determination of biomass fractions in activated sludge: nitrification case study. International Symposium on Environmental Biotechnology. Leipzig, Germany, July 2006. Oral presentation.

NATIONAL CONFERENCES

Jubany I, Carrera JA, Baeza J, Lafuente J. Optimisation of the starting up of a nitrification system to treat high ammonium concentration wastewater. 9º Congreso mediterráneo de ingeniería química. Barcelona, octubre 2002. Poster.

Jubany I, Carrera J, Baeza JA, Lafuente J. Diseño y aplicación de una estrategia de control para la puesta en marcha óptima de un proceso de nitrificación en alta carga. Mesa Española de Tratamiento de Aguas. Valencia, March 2006. Oral presentation.